On high-Reynolds-number laminar flows through a curved pipe, and past a rotating cylinder

A thesis presented for the

Degree of Doctor of Philosophy

of The University of London

by

Shui Tim Lam

Department of Mathematics,

Imperial College

July 1988

Abstract

This thesis is concerned with the numerical solution of boundary-layer problems arising in high-Reynolds-number laminar flows.

We first consider impulsively started flow down a curved pipe of circular cross-section and constant curvature. At high Dean numbers this flow includes boundary layers around the pipe's surface. The dominance of the pressure gradient over the outward centrifugal force in the boundary layer sweeps fluid particles towards the inner, more curved wall, causing a boundary-layer collision there. The time-dependent boundary-layer flow is examined numerically using a Lagrangian coordinate system. Solutions are obtained up to the time when the normal velocity in the boundary layer becomes singular. The singularity may be interpreted as the genesis of unsteady boundary-layer separation. An asymptotic structure for the singularity is proposed and is shown to be consistent with the numerical results.

The second problem studied is a classical example of a two-dimensional, incompressible flow with lift. A circular cylinder of radius a is rotated with constant angular velocity Ω and translated with uniform velocity U. Given a circulation $K = 4\pi Ua\varepsilon$, such that $0 \leq \varepsilon \leq 1$ inviscid theory predicts a stagnation point in the middle of the flow, and a unidirectional slip-velocity at the cylinder's surface. For non-zero viscosity a periodic boundary layer exists on the cylinder's surface, for which solutions have been obtained for order one values of ε, so relating K to Ω and U.

A critical value of ε, denoted by ε_s, has been found for which a second stagnation point develops in the middle of the boundary layer. For $\varepsilon > \varepsilon_s$, no classical boundary-layer solution could be found, suggesting that there will be a qualitative change in the fluid flow structure. This is borne out in a comparison with Prandtl *et al.*'s (1934) experiments.

The aforementioned periodic boundary-layer problem also arises in a high-Reynolds-number, interactive formulation for high-frequency nonlinear Tollmien-Schlichting waves in a plane channel. In this case the solution provides a relationship between the wave speed and amplitude.

Acknowledgments

I am deeply grateful to my superviser, Dr. Stephen Cowley, for his patience, guidance and encouragement throughout this work. In particular, I am much indebted for his assistance with the work in sections 1.5, 2.2 and appendix 3.E.

I also wish to thank Prof. Susan Brown for her interest in the work and her encouragement throughout, and Prof. Derek Moore for many helpful discussions, one of which resulted in the most robust way of calculating y discussed in section 1.4.

Mr. Neil Readwin is thanked for the implementation of the NRK package on the Cray 1S. I also thank my parents, my brothers, and my friends at Imperial College and University College for support. This work was financially supported by the SERC, and the majority of computations were performed on the Cray 1S and Amdahl at the University of London Computer Centre.

Contents

Abstract 2

Acknowledgement 4

Chapter 0 General Introduction: Boundary-Layer Separation 11

Chapter 1 Unsteady Flows through Curved Pipes

§ 1.1 Introduction 16

§ 1.2 Formulation 40

§ 1.3 Numerical Method 55

§ 1.4 The Calculation of y and v 70

§ 1.5 The Separation Singularity 80

§ 1.6 Results 89

§ 1.7 Flow inside an Impulsively Rotated Curved Pipe 124

Appendix 1.A The Unsteady Flow over a Circular Cylinder 135

Appendix 1.B The Finite Difference Equations 138

Appendix 1.C The Evaluation of a Function on a Characteristic in a Two-dimensional Computational Domain 152

Appendix 1.D Constants for a Padé Approximant Integration Method 154

Chapter 2 Stability of Flow through Curved Pipes

§ 2.1 Introduction 156

§ 2.2 Instability Analysis for Flow away from a Symmetry Line 158

§ 2.3 Instability Analysis for Flow near a Symmetry Line 168

Chapter 3 Periodic Boundary-Layer Flows

§ 3.1 Introduction 173

§ 3.2 Formulation 177

§ 3.3 Numerical Methods 181

§ 3.4 Results 197

§ 3.5 Nonlinear Tollmien-Schlichting Waves 216

Appendix 3.A Keller-box Schemes 230

Appendix 3.B Spectral Methods 232

Appendix 3.C Fourth-order Defect Correction 261

Appendix 3.D The (X, ψ) Coordinate Method 263

Appendix 3.E Attempts to find the Separation Singularity Structure 266

References 298

List of Figures

Chapter 1

Figure 1.1:1 The configuration of the curved pipe 35

Figure 1.1:2 Results for $D \leq 5000$ 36

Figure 1.1:3 Smith's (1976a) flow structure 23

Figure 1.1:4 Soh and Berger's (1984) results 37

Figure 1.1:5 Lyne's (1970) result for large ω and large R_s 39

Figure 1.3:1 Flow chart 69

Figure 1.4:1 A characteristic of x in a typical grid 75

Figure 1.5:1 The singularity structure 84

Figure 1.6:1 $\min_{\xi,\eta} |\text{grad } x|$ against t for $W_o = 1$, $\delta = 0$ 105

Figure 1.6:2 Contours of x in (ξ, η) 106

Figure 1.6:3 Contours of the axial velocity in (x,y) 107

Figure 1.6:4 Contours of the streamfunction in (x,y) 109

Figure 1.6:5 (x,y) position of fluid particles 114

Figure 1.6:6 u, v velocities of fluid particles 114

Figure 1.6:7 $(y-y_o+5.5)(t_s-t)^{1/2}$ against $(\pi-x)(t_s-t)^{-3/2}$ for $W_o = 1$, $\delta = 0$, $\eta = 5$, 10 120

Figure 1.6:8 The circumferential and axial wallshear for $W_o = 1$, $\delta = 0$ 122

Figure 1.6:9 The circumferential and axial wallshear for $W_o = \frac{4t}{t_1}\left(1 - \frac{t}{t_1}\right)$ $0 \leq t \leq t_1$, $\delta = 0.2$, where $t_1 = 11.926$ 123

Figure 1.7:1 $\min_{\xi,\eta} |\text{grad } x|$ against t for $W_R = 1$, $\delta = 0$ 132

Figure 1.7:2 The circumferential and axial wallshear for $W_R = 1$, $\delta = 0$ 133

Figure 1.7.3 $(y-y_o+5)(t_s-t)^{1/2}$ against $x(t_s-t)^{-3/2}$ for $W_R = 1$, $\delta = 0$, $\eta = 5$ 134

Figure 1.C:1 A characteristic of x in a typical grid 152

Chapter 3

Figure 3.2:1 A schematic picture of the flow field 180

Figure 3.3:1 Flow chart 196

Figure 3.4:1 $1/U_w$ against δ 206

Figure 3.4:2 $\varepsilon/(4\pi)$ against δ 207

Figure 3.4:3 u_{min} against δ 208

Figure 3.4:4 $\min_x u$ against ψ 209

Figure 3.4:5 u_{min} against $(\varepsilon_s - \varepsilon)^{1/2}$ 210

Figure 3.4:6 β and v_∞ against x 211

Figure 3.4:7a $\max_x \beta$ against $-\ln(\varepsilon_s - \varepsilon)$ 212

Figure 3.4:7b $(\max_x v - \min_x v)^{-1}$ against $(\varepsilon_s - \varepsilon)^{1/2}$ 212

Figure 3.4:8 Wallshear against x 213

Figure 3.4:9 Torque against x 213

Figure 3.4:10 Contours of ψ in (x,y) 214

Figure 3.5:1 The configuration of the plane channel 228

Figure 3.5:2 α_1 against a_o 229

Figure 3.B:1 A typical part of the VM Jacobian matrix 245

Figure 3.E:1 $\min_x u$ against ψ and y for $\lambda = 0.426$ 291

Figure 3.E:2 $\min_x u$ against ψ and y for $\lambda = 0.42595$ 292

Figure 3.E:3 $\min_x u$ against ψ and y for $\lambda = 0.4259$ 293

Figure 3.E:4 $\min_\psi u$ against x for $\lambda = 0.42595$, 0.4259 294

Figure 3.E:5 u_{min} against λ and $x_d - x_o$ 295

Figure 3.E:6 $w(0)$ against B for $X > 0$, and 296

$w(0)$ and $w_\zeta(0)$ against B for $X < 0$

List of Tables

Chapter 1

Table 1.3:1 Results from a leap-frog scheme 64

Table 1.6:1a Extrapolated t_s for $W_o(t) = 1$, $\delta = 0$ 91

Table 1.6:1b Extrapolated t_s for $W_o(t)$ defined in equation (1,6:1a) 92

Table 1.6:1c Extrapolated t_s for $W_o(t)$ defined in equation (1,6:1b) 92

Table 1.7:1a Extrapolated t_s for $W_R(t) = 1$, $\delta = 0$ 129

Table 1.7:1b Extrapolated t_s for different $W_R(t)$ 131

Chapter 3

Table 3.4:1 A comparison of results obtained by different methods 203

Table 3.4:2 An approximation to the stagnation point structure 204

Table 3.4:3 A summary of the results 205

Table 3.B:1,2 The NRK Jacobian elements 238

Table 3.B:3,5 The VM Jacobian elements 246

Table 3.E:1 The results of the model problem for $\lambda \geq 0.42595$ 271

Chapter 0 General Introduction

Boundary-layer Separation

Under many conditions, but not all, a good mathematical model of fluid motion can be based on the Navier-Stokes equations. Solutions to these equations depend on the Reynolds number, defined as the multiple of a typical velocity and a typical length scale divided by the Newtonian kinematic viscosity. At high Reynolds numbers, fluid flows typically consist of extensive inviscid regions separated by thin viscous layers. Viscous layers next to a rigid body are known as boundary layers (Prandtl, 1904).

The equations governing flow in a boundary layer are derived from the Navier-Stokes equations by assuming that the boundary layer is very thin in comparison with the typical length scales of the inviscid flow. Obviously, then the boundary-layer equations are no longer valid when the boundary layer is not 'thin' (if indeed the boundary layer can be said to exist at all). Such a thickening of the boundary layer can result from the 'breakaway' of a thin layer of vorticity from the surface of the rigid body. This phenomenon is usually referred to boundary-layer separation (although certain authors use the term 'separation' to refer to the occurrence of any reversed flow in a boundary layer; this can be misleading in unsteady flow). This definition of separation is close to that of both Prandtl (1904), and Sears and Telionis (1975). In particular, Sears and Telionis speak only of separation when the penetration of the boundary-layer vorticity away from the

wall becomes too large to be described on the usual scale of $O(R^{-1/2})$. Unsteady boundary-layer separation is often associated with singularities in the boundary-layer solution, and these singularities will be referred to as separation singularities.

Moore (1958), Rott (1956) and Sears (1956) independentely proposed conditions for a *steady* flow to separate, i.e.

$$u = 0, \qquad \frac{\partial u}{\partial y} = 0,$$

which often reduces to the onset of flow reversal. However, *unsteady* separation is more difficult to characterise. It has been hypothesised as a generalisation of steady separation with the inclusion of time dependence (Sears and Telionis, 1975), however according to Van Dommelen and Shen (1981), the singularities associated with steady and unsteady separation are fundamentally different.

This thesis studies the steady and unsteady boundary-layer separation that occurs in two laminar, incompressible high-Reynolds-number flows. In both problems, numerical solutions have been obtained up the time/parameter values where separation occurs. Where possible, an asymptotic solution has been sought to describe the structure of the flows close to separation.

In chapter 1 we consider impulsively started flow down a curved pipe with constant curvature L and a circular cross-section of radius a. In the limit of high Dean number this flow generates a boundary layer around the surface of the pipe. Physical arguments predict that the dominance of the pressure gradient over the outward centrifugal force in the boundary layer sweeps fluid

particles towards the inner, more curved wall, eventually causing boundary-layer separation there. The time-dependent boundary-layer flow is examined numerically in a Lagrangian coordinate system. A solution is obtained up to the time when the normal velocity in the boundary layer becomes singular. This may be interpreted as the genesis of unsteady boundary-layer separation. At this point our calculation terminates due to the invalidity of the classical boundary-layer approximation. A structure of the singularity is proposed and is shown to be consistent with the numerical results. This boundary-layer separation is probably the source of the jet which in steady flow originates at the inner wall and crosses to the outer wall.

Section 1 of chapter 1 is an introduction and a review of relevent work on the problem. Sections 2, 3 and 4 discuss the Lagrangian formulation of an axially-independent flow and the numerical techniques used to solve the unsteady Lagrangian boundary-layer equations. A separation singularity structure is proposed in section 5 which is then compared with the numerical solutions in section 6; other results are also given in section 6. Next the time-dependent flow due to impulsive rotation of a curved pipe is examined in section 7. This problem is similar to that for impulsively started flow down a fixed pipe, but is possibly more amenable to experiment. Again, unsteady boundary-layer separation occurs within a finite time, but at the symmetry line of the outer wall. The structure of the separation singularity is shown to be qualitatively similar to that of an impulsively started flow down a curved pipe.

Chapter 2 examines the linear stablity of flows down a loosely coiled pipe. A local stability analysis is performed both away from and close to the inner wall. Linear instablity is found in the flow, although this is apparently *not* related to the unsteady boundary-layer separation at the inner wall (cf. Cowley, Hocking and Tutty, 1985).

Chapter 3 studies a classical example of a two-dimensional, incompressible flow with lift. A circular cylinder of radius a is rotated with constant angular velocity Ω and translated with uniform velocity U. Given a circulation K, such that $0 \leq \varepsilon \leq 1$, where $\varepsilon = \frac{4\pi Ua}{K}$, inviscid theory predicts a stagnation point in the middle of the flow, together with a unidirectional slip-velocity at the cylinder's surface. With the introduction of viscosity, the slip-velocity generates a boundary layer around the cylinder. The solution of the resulting periodic boundary layer has been found for order one values of ε, so relating K to Ω and U. A critical value of ε, denoted by ε_s, has been identified for which a second stagnation point develops in the middle of the boundary layer. For $\varepsilon > \varepsilon_s$, no classical boundary-layer solution could be found. This suggests that there will be a qualitative change in the fluid flow structure depending on whether ε is greater or less than ε_s. This appears to be borne out in a comparison with Prandtl *et al.*'s (1934) experiments. Moreover, the mathematical boundary-layer problem is closely analogous to a problem which arises in a high-Reynolds-number, interactive formulation for high frequency Tollmien-Schlichting waves in a plane channel. In this case the

boundary-layer solution provides a relationship between the wave speed and amplitude.

Sections 1 and 2 of chapter 3 contain an introduction and a formulation, respectively, of the rotating cylinder problem. Then in sections 3 and 4 we give a description of numerical methods used to solve the relevant equations, and the results. Section 5 demonstrates that an interactive formulation of slowly-varying high frequency Tollmien-Schlichting waves in plane channel flow results in the same mathematical problem (cf. Smith and Burggraf, 1985).

Finally, we note how the chapters, sections, equations and figures are numbered in this thesis. Each problem is described in one chapter, and each chapter is divided into a number of sections, each devoted to one aspect of the problem (note that section 2 of chapter 1 is referred as section 1.2. etc.). Within each section we number the equations, figures and tables afresh from 1, hence equation/figure/table (1.2:3) refers to the third equation/figure/table in section 2 of chapter 1. Related equations/figures/tables are labelled with the same number, but distinguished by a following letter. Appendices are included at the end of *each* chapter; they are labelled by the chapter number followed by a letter, e.g. appendix 1.A. Equations/figures/tables in an appendix are labelled in much the same manner to those in a section, e.g. (1.A:2) refers to the second equation in appendix A of chapter 1.

CHAPTER 1

Unsteady Flow Through Curved Pipes

§ 1.1 Introduction

Flows through curved pipes are of interest because of their many physical applications. For example, in engineering problems it is often important to know the pressure drop in coiled pipes, so that enough pumping power is available to maintain a specified flow. Moreover, an understanding of the flow through curved pipes is a necessary preliminary to finding the heat transfer rates which are required, for instance, in the design of efficient cooling systems and other heat exchangers (e.g. steam generators and superheaters in power plants, and continuous chemical reactors in the chemical industry). Curved pipes which are rotated about an axis through the centre of curvature are also used for fractionating fine particles (e.g. Papanu, Alder, Gorensek and Menon, 1986).

The flow pattern in curved tubes is also of physiological importance because the largest artery in the system, the thoracic aorta, is highly curved as it leaves the heart. The actual flow there is particularly difficult to understand because of the elastic structure of the artery wall, and the fact that the ascending artery branches to the brachio cephalic and the left subclavian (for example see p.10, Pedley 1980). It has been observed that fatty streaks, which are possibly the cause of

atherogenesis, are distributed preferentially at certain locations on this and other artery walls. Experimental results for animals (particularly rabbits and dogs) which have been fed a concentrated high-cholesterol diet for a few weeks, suggest that fatty streaks develop on the outside wall of the aortic arch (Fry 1968, Cornhill and Roach, 1976). On the other hand, Caro, Fitz-Gerald and Schroter (1971) found that a normal, or a slightly higher than normal, cholesterol diet leads to fatty streaks occurring at the inside wall of, for example, the aortic arch. It therefore appears that in *normal* human beings atherosclerotic lesions develop at those locations where the wall shear is known to be low in *steady* flow. Of course, blood flow is *unsteady*, with the result that there is a need to understand time-dependent flow through curved pipes, and in particular the unsteady behaviour of the wall shear, if a definite correlation is to be made between wall shear and atherosclerotic lesions.

The study of fluid flows through ducts with curvature dates back to Thomson's (1876) qualitative observation of secondary motion in open channel flow and Grindley and Gibson's (1908) experiments on curvature effects. Since then, much research has been devoted to many aspects of flows through curved pipes. Extensive analytical, numerical and experimental work has been undertaken to understand such flows - for example see the survey articles by Berger, Talbot and Yao (1983) and Itō (1987).

In this study we consider a Newtonian, incompressible laminar fluid with viscosity μ and density ρ (kinematic viscosity ν)

flowing through a curved pipe. The pipe is assumed to have a circular cross-section with radius a, and a constant radius of curvature L (although this is admittedly a very idealised model of, for example, the aorta); see figure 1.1:1. The ratio of curvature δ will be defined as

$$\delta = \frac{a}{L} , \qquad (1.1:1a)$$

and we denote by s the distance along the centre-line of the pipe from some reference point. We refer to the surface of pipe closest/furthest to the centre of curvature as the *inner/outer* wall. Also the line on the inner/outer wall closest/furthest to the centre of the curvature is referred to as the *symmetry line of the inner/outer wall.* The plane intersecting both the inner and the outer symmetry lines is referred to as the *symmetry plane.*

Much of the previous analytical and numerical work has been based on the assumption that flows through curved non-helical pipes of constant curvature are symmetrical about the symmetry plane. Winters (1987) points out that for steady, axially-independent flows, asymmetrical solutions can be found even with symmetrical boundary conditions. However, he found that these solutions were unstable, hence we too will assume that the solutions of interest are symmetrical.

Some of the first theoretical investigations of flow through curved pipes are those by Dean (1927, 1928). He studied the fundamental problem of *steady, axially-independent* flow, and showed that the flow driven by a constant axial pressure gradient of -G down a loosely curved pipe, i.e. $\delta \ll 1$, could be completely

characterised by a dimensionless number, later known as the Dean number. Many definitions of the Dean number have used in subsequent works, for a detailed survey see Berger, Talbot and Yao (1983). For convenience, we will only refer to two here, K and D:

$$K = \sqrt{2\delta}\,\frac{Ga^3}{\mu\nu}\,, \qquad D = \frac{Q_c}{\pi a^2}\,\frac{a\delta^{1/2}}{\nu}\,, \tag{1.1:1b}$$

where Q_c is the volume flux in the curved pipe.[1] Note that in boundary-layer instability theory the Görtler number is equivalent to the Dean number.

For small curvature ratios and Dean numbers, i.e. $\delta \ll 1$, $K \ll 1$, Dean obtained an asymptotic solution by a double perturbation expansion about Hagen-Poiseuille pipe flow in terms of the small parameters K and δ (this analysis has been extended to a helical pipe by Germano (1982) and Kao (1987)). Dean's axially-independent solution, which can only be applicable in regions where any entrance effects are negligible, seems to be valid for values of K up to approximately 100. For asymptotically

---

[1] For steady axially-independent flows, the dependence of Q_c on G is part of the solution. Also, from (1.1:1b)

$$Q_c K = 2^{7/2} Q_s D\,,$$

where $Q_s = \frac{Ga^4\pi}{8\mu}$ is the volume flux driven through a straight pipe by a pressure gradient -G. Hence the functional dependence of D on K is also part of the solution. This relationship is known analytically for asymptotically small Dean numbers, but has to be calculated numerically for larger Dean numbers.

small δ, McConalogue and Srivastava (1968) solved Dean's equations numerically via a spectral method for K up to 600, and Collins and Dennis (1975) and Dennis (1980) improved upon this by finding numerical solutions for K up to 5000 (see the reviews by Berger *et al.* (1983) and Itō (1987) for references to other calculations in a torus, and Kao (1987) for calculations in a helical pipe). To illustrate the effects of increasing the Dean number in steady, fully developed flow, the numerical results obtained by McConalogue *et al.* (1968) and Collins *et al.* (1975) for small δ are shown in figure 1.1:2 for K = 96, 606 and 5000 respectively. The letters I and O label the inner and outer walls respectively; we refer to the flow within a cross-section as the *secondary flow*.

Austin and Seader (1973) have also obtained solutions for Dean numbers, D, up to 504 for $0.01 \leq \delta \leq 0.2$. A grid refinment from 11x11 points to 21x21 points was was claimed to give 'excellent agreement' between the two numerical results for $K \simeq 6000$. However, results were also presented for $K \simeq 22300$[2], and at such large Dean numbers boundary layers exist which would require very fine grids if they were to be resolved adequately. Thus, the accuracy of these numerical results is doubtful.

Van Dyke (1978) extended Dean's perturbation solution for $\delta \ll 1$ to higher orders than previous authors, and then used series extension techniques to obtain solutions at large Dean numbers. The

---

[2] This value of K was estimated using the relationship between K and D in Footnote 1.

ratio of the flow resistence coefficent[3] of a curved pipe to that of a straight pipe was found to grow asymptotically as $D^{1/4}$, whereas fully numerical calculations based on the same assumptions of steady, axially-independent flow suggest $D^{1/2}$. The reason for the difference is unresolved.

Dennis and Ng (1982) demonstrated non-uniqueness in the numerical solution of a steady, axially-independent flow for $K > 956$. For $K < 956$ only one solution could be found in which the secondary flow consists of a symmetrical pair of counter-rotating vortices. The same type of solution could be found for $K > 956$, but in addition there was a second family of solutions in which the secondary flow has two symmetrical vortex pairs. Multiple solutions in curved-pipe flows with different cross-sectional geometries have been found by Nandakumar and Masliyah (1982), Yang and Keller (1986) and Winters (1987) (note that Winters' (1987) paper includes one of the few stability analyses of curved pipe flow).

In the limit of large Dean number, the one-vortex flow solution is thought to consist of a largely inviscid core and a viscous boundary layer generated by the non-zero, axial, inviscid, slip velocity at the pipe wall. Within the boundary layer a strong

---

[3] The flow resistence coefficient is defined as

$$\left[\frac{F}{\rho \bar{W}^2} \right]^{1/2}$$

where F is the skin friction integrated over the circumference of a cross-section and $\bar{W}$ is the mean axial velocity.

secondary flow sweeps fluid particles toward the inner wall. The physical reason for this follows from the fact that fluid particles travelling in the core with typical axial velocity $\bar{W}$ experience an outward lateral acceleration of order $\frac{\bar{W}^2}{\bar{L}}$ as a result of curvature effects. This is balanced by an inward pressure gradient of the same magnitude. However, the axial velocity decreases to zero rapidly in the boundary layer because of the no-slip boundary requirement at the pipe wall, whereas the pressure gradient is essentially unchanged throughout the layer. So within the boundary layer, this excess pressure gradient sweeps fluid toward the inner wall of the pipe. The accumulation of fluid particles there results in a thickening of the boundary layer. This is observed in numerical computations together with a drift in the position of the maximum axial velocity (which occurs in the core) towards the outer wall.

At very large Dean numbers the complex flow structure should be resolved by a close examination of the boundary layer, and a boundary-layer approach has been used by many authors for asymptotically large K and small δ, e.g. Itō (1969) and Smith (1976a). They assume a flow structure with a primarily inviscid core and viscous effects confined to thin boundary layers around the pipe. The secondary flow is taken to be strongest in the boundary layer, and it is assumed that the secondary motion in the core is driven by ejection of fluid from the boundary layer. The governing equations in both the core and the boundary layer are coupled at leading order. For a loosely coiled pipe with a circular cross-section Itō (1969) attempted to find a solution using a

Pohlhausen technique. His solution broke down in the vicinity of the symmetry line of the inner wall because the boundary-layer thickness increased rapidly, thus invalidating one assumption in his calculation. Further, unpublished calculations of Prof. N. Riley and Prof. S. Dennis, based on a finite-difference scheme which marches from the outer wall towards the inner one, encounter difficulties well before the inner wall is reached. This is due to the onset of weak backflow in the secondary flow at the outer edge of the boundary layer. As yet no complete numerical solution has been found, which possibly brings into question the proposed asymptotic structure.

In an attempt to circumvent these numerical difficulties Smith (1976a) examined flow down a loosely coiled pipe with a triangular cross-section consisting of a 'pitched' inner wall and a vertical 'flat' outer wall. He used an extended version of Itō's (1969) interactive theory for the flow in the core, and boundary layers around the pipe as shown below.

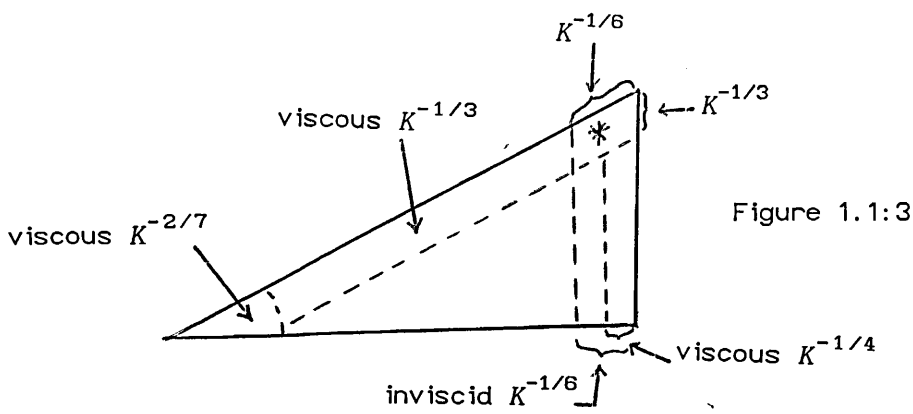


Figure 1.1:3

Similarity solutions of the leading-order equations were obtained on the walls, however, due to technical difficulties, the flow structure in the corners was not examined in detail. More

specifically, Smith (1976a) proposed a possible flow structure in which the flow from the invisicid core enters the inviscid $K^{-1/6}$ boundary layer and travels up to the corner (*), where it turns sharply in an anti-clockwise direction to enter the viscous $K^{-1/3}$ layer. The flow in this layer empties into a viscous $K^{-2/7}$ corner, which it leaves in form of a jet. Smith also considered a rectangular cross-section, and proposed that no attached boundary-layer solution could be found in that case.

Collins and Dennis (1976a,b) have obtained numerical Navier-Stokes solutions for steady, axially-independent flow through loosely coiled pipes of triangular cross-section with a 45° acute angle (where the lengthscale a is taken here to be the distance between the 'pitched' inner corner and 'flat' outer wall). They found that as K increases from 100 to 12000 there is evidence that the axial velocity becomes independent of the distance from the symmetry plane, as Smith (1976a) assumed in his analysis. Further, the numerical results for the axial velocity on the symmetry plane appear to be proportional to $x^{5/6}K^{2/3}$ as Smith (1976a) predicted, although the constant of proportionality is not accurate (x is the distance from the 'pitched' wall). A comparison between Smith's (1976a) theory and the numerical solution for the skin friction on the pitched wall is also not conclusively either in agreement or at variance.

In summary, while accurate numerical solutions for steady flow through uniformly curved pipes can be found for moderately large Dean numbers, there is no conclusive proof that the favoured high-Dean-number asymptotic structure is correct. In our

high-Dean-number calculations we side-step this problem by considering starting, rather than fully developed, flows (see section 1.2 and following).

Another aspect of curved pipe flow which has been studied is the flow *near the entrance* of a pipe. Here dependence on the distance down the pipe must be allowed for. Most work has concentrated on the *steady* transition of the flow from its inlet conditions to a *fully developed* state.

Singh (1974) examined *steady, entrance* flow down a curved pipe for asymptotically large Reynolds numbers and small δ (note that this scaling does not rule out order one Dean numbers). Near the entrance he assumed that the flow consists of an inviscid unidirectional core and a viscous boundary layer. A core flow consisting of the irrotational line-vortex solution was studied *inter alia*; this solution has been used as the starting velocity profile at the inlet by much of the subsequenent work (but see Smith 1976b). Singh (1974) showed that the shear maximum on the inner wall crosses over to the outer wall of the pipe at an O(a) distance downstream; the precise location depends on the inlet conditions. This asymptotic solution breaks down at a distance $s \sim O(\delta^{-1/2}a)$, i.e. at an angle $O(\delta^{1/2})$, from the entrance to the pipe. For order one Dean numbers the boundary layer then 'fills' the pipe, while at large Dean numbers extra terms must be included in the boundary layer equations due to curvature effects.

For $\delta \ll 1$ Stewartson, Cebeci and Chang (1980) have numerically examined the boundary-layer flow arising from the line-vortex core

velocity for distances $s \sim O(\delta^{-1/2}a)$ from the entrance (Yao and Berger (1988) have relaxed the $\delta \ll 1$ assumption). No numerical difficulty was experienced at the outer wall, but they found that the axial wall shear stress decreased to zero on the symmetry line of the inner wall at a distance $s \simeq 0.943\delta^{-1/2}a$, i.e. at an angle $\phi \simeq 0.943\delta^{1/2}$, from the entrance. This zero in the wall stress appears to be associated with boundary-layer separation since the axial boundary-layer displacement thickness increases to 'infinity'. To examine experimentally the behaviour of the flow near this point, Talbot and Wong (1982) measured the wall shear along the symmetry line of the inner wall in a curved pipe of $\delta = \frac{1}{7}$. They found that the wall shear dips to a minimum at a distance $s \simeq 0.96\delta^{-1/2}a$. Stewartson and Simpson (1982) extended the earlier numerical study and examined the flow in the neighbourhood of the separation point. They produced a detailed analysis of the singularity structure causing the boundary-layer separation and concluded that it has a global effect on the flow. They conjectured that the forward integration of the classical boundary-layer equations terminates at the point of zero wall shear. However, another possibility is that the assumed core flow is incorrect, and a grossly separated core flow must be assumed from the outset (but note the excellent agreement between Talbot and Wong's (1982) experiments and Yao and Burger's (1988) boundary-layer calculations for $\delta = \frac{1}{7}$).

An alternative approach to entrance flow is that of Smith (1976b) who considered flow through a pipe that starts bending uniformly after an initial straight section. The Dean number is

assumed to be finite, but the Reynolds number and curvature are assumed to be large and small respectively (cf. Singh 1974). The solution is valid an O(a) distance up- and down-stream of the start of the bend, and demonstrates upstream influence. The secondary motion within the boundary layer is comparable with that in the core. Bovendeerd, van Steenhoven, van de Vosse and Vossers (1987) report that their experiments are in fair agreement with this theory. The analysis breaks down when $s = O(a\delta^{-1/2})$, and results in a full numerical problem. The modifications necessary to Smith's (1976b) analysis at large Dean number have been considered by Bennett (1987).

In addition to the boundary-layer approach for entrance flow, numerical solutions to the Navier-Stokes equations at finite Dean number have been sought. Soh and Berger (1984) studied steady, developing flow in a loosely coiled pipe for $D \leq 340$ and $\delta = \frac{1}{7}, \frac{1}{20}$ [4]. They used the line-vortex solution as the inlet condition. The developing flow was found to have a more complex structure than the fully developed flow, see figures 1.1:4 for a typical flow with $D \simeq 340$. Figure 1.1:4a shows the development of the axial velocity on the symmetry plane. The position of the maximum axial velocity shifts towards the outer wall as the flow proceeds downstream, thus increasing the axial wall shear at the outer wall. Figures 1.1:4b,c illustrate the contours of constant

---

[4] Far downstream, this value of D corresponds to $K \simeq 14500$.

axial velocity on circular cross-sections in the developing and fully developed regions. The contours double back on themselves, thus indicating the development of double peaks in the velocity profile. Far downstream the solution is similar to the fully developed solutions obtained by Collins and Dennis for $K = 5000$ ($D \simeq 185$). Figure 1.1:4d displays a direction plot of the secondary flow at a downstream distance of $3.65\delta^{-1/2}a$ for $D \simeq 340$ which illustrates a recycling eddy near the inner wall. This may be evidence of a boundary-layer separation (cf. Stewartson, Cebeci and Chang (1980)). The eddy disappears further downstream. For $D \simeq 340$, the axial wall shear attains a non-zero minimum at approximately a downstream distance $2.22\delta^{-1/2}a$ where the eddy first occurs. However, this position is greater than $0.943\delta^{-1/2}a$, the postion of zero axial wall shear calculated by Stewartson *et al.* (1980).

Humphrey, Iacovides and Launder (1985) later reported qualitatively similar numerical results on entry flows down a curved pipe with $\delta = \frac{1}{20}$ or $\delta = \frac{1}{7}$ for D up to 1350. For large Dean numbers, the wall shear at the symmetry line of the inner wall attained a non-zero minimum, the position of which decreased as the Dean number increased; for $D \simeq 1350$, the minimum occured approximately a distance $1.8\delta^{-1/2}a$ downstream - again not that close to the figure reported by Stewartson *et al.* (1980). Moreover, experimental results obtained by Kluwick and Wohlfahrt (1986) using a hot-wire-anemometer technique showed that although the trend of axial velocity agrees qualitatively with Stewartson *et al.* (1980), the axial wall shear is not very close to zero even for Dean numbers D as large as 2530. Further experimental results have been

reported by Agrawal, Talbot and Gong (1978), and Snyder, Hammersley and Olson (1985), while other numerical results include those by Pratap Vanka (1985) and Shirayama and Kuwahara (1986). Kitoh (1987) has examined *inviscid* swirling motions at the entrance to circular curved pipes, while entrance effects in pipes with non-circular cross-sections have also been studied (for details see the aforementioned reviews).

Although steady flow through curved pipes is of interest, blood flow in the aorta is of course pulsatile. Hence a complete understanding of the flow pattern in blood vessels can be gained only by studying unsteady flows (although insights can *sometimes* be obtained by making a *loose* analogy between axially developing flows and unsteady axially independent flows).

Much of the work on time dependent flows has concentrated on unsteady flows through loosely curved pipes driven by *oscillatory* axial pressure gradients. To simplify the problem, it is often assumed that the flows are independent of the distance down the pipe, and that the pipes are of circular cross-section.

Under these assumptions Lyne (1971) studied the flow driven by a sinusoidal axial pressure gradient with frequency ω and *zero* mean. He showed that the flow can be characterised by two parameters: the Womersley parameter $\bar{\alpha} = a\left(\frac{\omega}{\nu}\right)^{1/2}$, and the secondary-streaming Reynolds number $R_s = \frac{\delta \bar{W}^2}{\omega\nu}$, where $\bar{W}$ is a typical axial velocity. R_s plays the role of a Reynolds number for the secondary flow. In the limit of high frequency oscillations, $\bar{\alpha} \to \infty$, a Stokes layer of $O\left(\sqrt{\frac{\nu}{\omega}}\right)$ in thickness develops next to the wall,

together with a secondary core flow which is *comparable* in magnitude to the secondary flow in the Stokes layers. For both large and small R_s Lyne found that the secondary-streaming in the core flow was from the outer to the inner wall, i.e. in the opposite direction to that for steady flow. Figure 1.1:5a illustrates the flow structure for *large* secondary-streaming Reynolds numbers, while the flow pattern is schematically represented in Figure 1.1:5b. This theoretical prediction has been experimentally verified by Lyne (1970). The stability of this flow has been examined by Papageorgiou (1987).

In a complementary approach based upon a small secondary-streaming number Zalosh and Nelson (1973), and Mullin and Greated (1980a), studied an unsteady flow driven by an oscillatory, zero mean, axial pressure gradient for small, intermediate and large frequencies. For asymptotically high frequencies Lyne's (1970) small secondary-streaming-number solution is recovered. For lower frequencies the secondary motion is in the same direction as that for low-Dean-number, steady, fully developed flows obtained by Dean (1927, 1928). Muson (1975) and Mullin and Greated (1980a) obtained experimental results consistent with these results.

Smith (1975) studied flows down a loosely curved pipe driven by an oscillatory axial pressure gradient with a *non-zero* mean. He examined axial-independent flows in a number of asymptotic limits of the Dean number K, the Womersley parameter $\bar{\alpha}$, and the secondary-streaming number R_s, e.g. $K \ll 1$; $K \ll 1$, $\bar{\alpha} \sim K^{-1/3}$, $R_s \sim 1$; $K \sim 1$, $\bar{\alpha} \ll 1$, $R_s \sim 1$; $K \sim 1$ $\bar{\alpha} \ll 1$, $R_s\bar{\alpha}^2 \sim 1$; $K \sim 1$, $\bar{\alpha} \gg 1$, $R_s \sim 1$; $K \gg 1$, $\bar{\alpha} \sim 1$, $R_s \sim 1$; $K \gg 1$, $\bar{\alpha} \sim K^{1/3}$, $R_s \sim 1$; $K \gg 1$,

$\bar{\alpha} \sim K^{2/3}$, $R_s \sim 1$; $K \gg 1$, $\bar{\alpha} \sim K^{1/6}$, $R_s \sim K$; $K \gg 1$, $\bar{\alpha} \sim K^{1/3}$, $R_s \sim K^{2/3}$, and prosposed various flow structures. Blennerhassett (1976) studied the flow for $K \sim 1$, $\bar{\alpha} \gg 1$, $R_s \sim 1$, performing the necessary numerical calculations.

Numerical solutions have been obtained for the unsteady, axially-independent Navier-Stokes equations by Rabadi, Simon and Chow (1980) and Chang and Tarbell (1985). In both studies the numerical integrations were started from some simple initial conditions and continued until a periodic solution was recovered. Rabadi *et. al.* (1980) examined an unsteady flow down a curved pipe driven by an oscillatory axial pressure gradient with a non-zero mean; the ratio of the amplitude of the oscillatory component of the pressure gradient to the steady component was denoted by k. Solutions were obtained for K approximately up to 212, $1 \leq \bar{\alpha} \leq 15$ and k = 0.5 or 1.0. Chang and Tarbell (1985) concentrated on parameter ranges more relevent to physiological flows such as blood flow in the aortic arch. Parameters were chosen to be compatible with the experiments by Talbot and Gong (1983)[5], Chandran and Yearwood (1981), and Yearwood and Chandran (1982)[6]. Numerical solutions were obtained for a range of parameters, e.g. $K \leq 300$,

---

[5] These results are in qualitative agreement with Smith's (1975) theory.

[6] Note that these experiments all included entrance effects, as did those by Mullin and Greated (1980b). Lin and Tarbell (1980) reported experiments where entry effects are negligible.

$\delta \leq 0.26$, $\bar{\alpha} \leq 21$, $R_s \leq 950$ and $k \leq 52$. Particularly for the flows with physiological parametric values a wide variety of flow phenomenon were observed (e.g. secondary flows consisting up to seven vortices). Qualitative agreement was observed between the numerical results and those regions in the experiments where the flow is fully developed.

Little research has been undertaken on unsteady axially-dependent curved pipe flows. Singh, Sinha and Aggarwal (1978) examined unsteady flow within an O(a) distance of the entrance of a curved pipe by similar boundary-layer techniques to those of Singh (1974). Shirayama and Kuwahara (1986) have reported numerical Navier-Stokes solutions for flows down an U-shaped pipe of circular cross-section. The flows consist of a Poiseuille velocity profile at the entry/exit in the straight inlet/outlet sections respectively. Steady solutions were obtained for small and medium Dean numbers, and unsteady solutions for high Dean numbers; the exact values of Dean numbers are unclear since no precise definition is given in the paper.

As indicated in the above review, one fundamental problem on which little work has been done is starting flow driven by an axial pressure gradient, although a number of the above Navier-Stokes solvers could be adapted to study this problem. *Inter alia*, such flows occur at the start of systole in humans, etc.. The only work we are aware of is Farthing's (1977) boundary-layer approach for unsteady, axially-independent, high-Dean-number, flows down a loosely curved pipe. Such flows consist of an inviscid core and a

viscous boundary layer adjacent to the pipe wall. In this chapter we will concentrate on the development of the secondary flow in the boundary layer. The analysis is based on classical boundary layer theory in which the only effect of the core flow is to impose a non-zero slip velocity at the edge of the boundary layer. However, rather than using the more conventional Eulerian co-ordinates (cf. Farthing 1977), we formulate and solve the boundary-layer problem in Lagrangian coordinates.

The Lagrangian approach was first used by Van Dommelen and Shen (1980) in the numerical solution of the classical, two-dimensional, unsteady boundary-layer problem for uniform flow past a horizontal circular cylinder. *Unsteady separation* of the boundary layer occurs after a *finite* time when the boundary layer next to the body thickens to 'infinity'. Van Dommelen and Shen showed that the two-dimensional Lagrangian boundary-layer formulation has the advantage of resulting in a momentum equation which both determines the motion and is independent of variables that become singular at the onset of unsteady boundary-layer separation. The analysis has been generalised to a three-dimensional study (Van Dommelen and Cowley, private communication). In general, Lagrangian numerical solutions will be more accurate than their Eulerian counterparts.

Similar *finite-time* boundary-layer separation also occurs in other unsteady problems, in particular, at the apex of a suddenly heated two-dimensional circular cylinder and at the equator of an impulsively rotated sphere (Van Dommelen, 1986). Both these unsteady boundary-layer problems have been examined on their

respective symmetry lines by Simpson and Stewartson (1982a, b) in Eulerian coordinates. The singularity structure due to unsteady boundary-layer separation in both problems are closely analogous to that occurring in the boundary layer driven by unsteady flow down a curved pipe. This will be discussed in detail in Section 1.5.

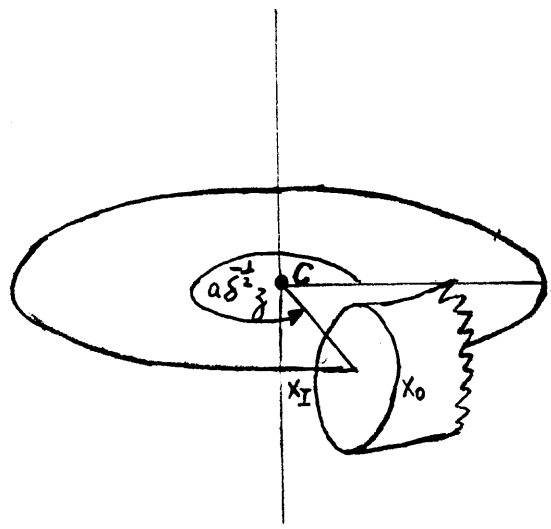


Figure 1.1:1a

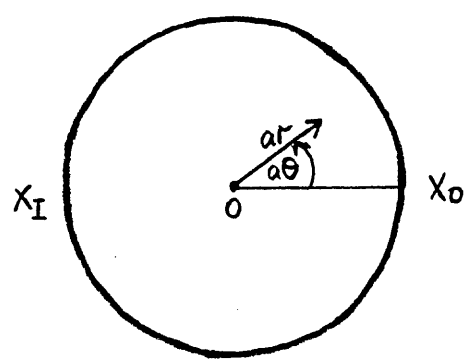


Figure 1.1:1b

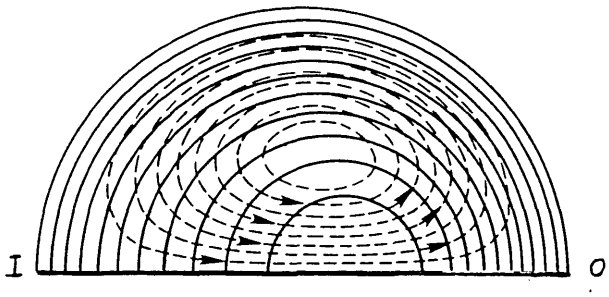


Figure 1.1:2a $K = 96$

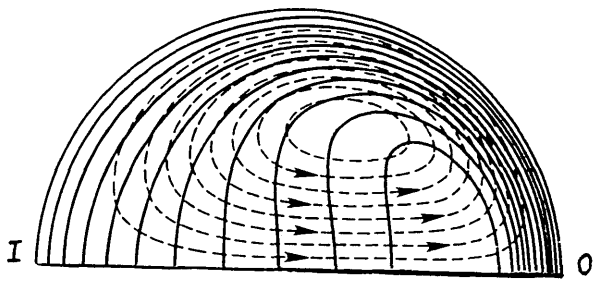


Figure 1.1:2b $K = 606$

Figures 1.1:2a,b McConalogue and Srivastava 1968

---------- Contours of the secondary streamlines

———— Contours of the axial velocity

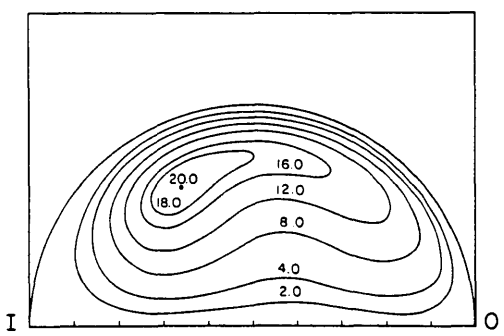


Figure 1.1:2c secondary streamlines

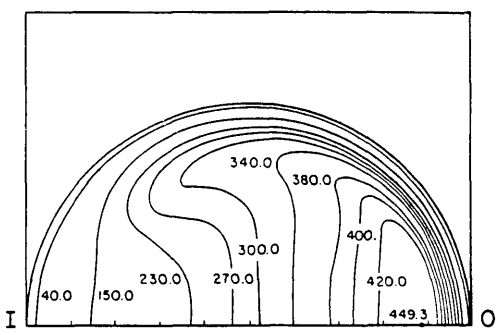


Figure 1.1:2d axial velocity

Figures 1.1:2c,d Collins and Dennis 1975, $K = 5000$

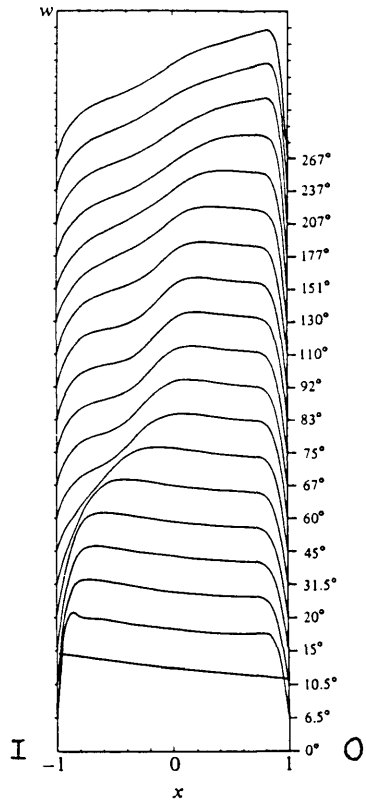
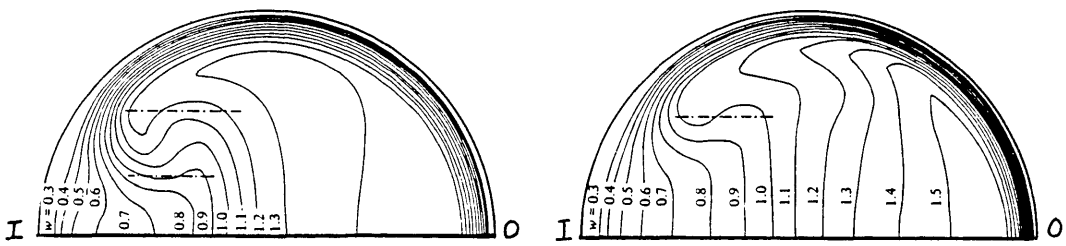


Figure 1.1:4a The development of the axial velocity on the symmetry plane.



$s = 3.83\delta^{-1/2}a$ $s = 12.33\delta^{-1/2}a$

Figures 1.1:4b,c Contour of constant axial velocity at at different s for D ≃ 340, $\delta = \frac{1}{7}$

Figures 1.1:4 Soh and Berger, 1984

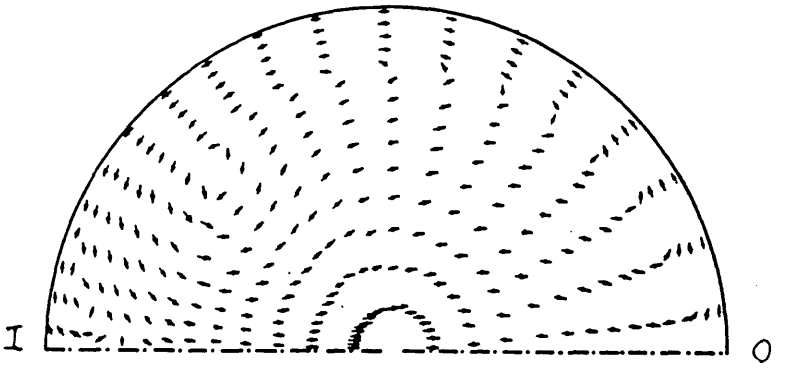


Figure 1.1:4d Direction plot of the secondary flow at a downstream distance of $s = 3.65\delta^{-1/2}a$

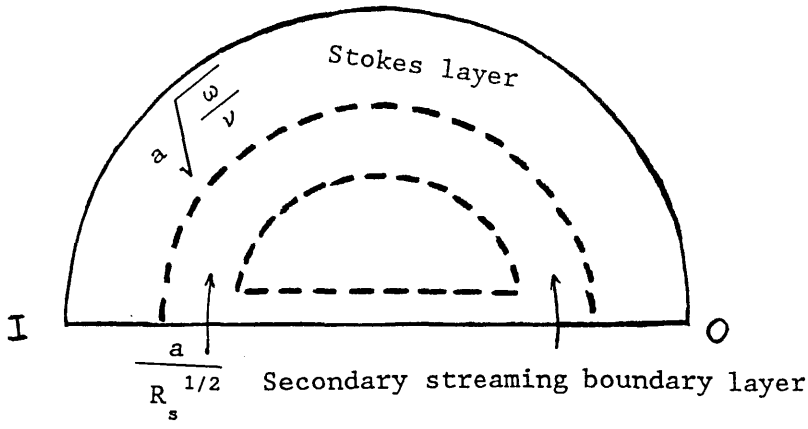


Figure 1.1:5a

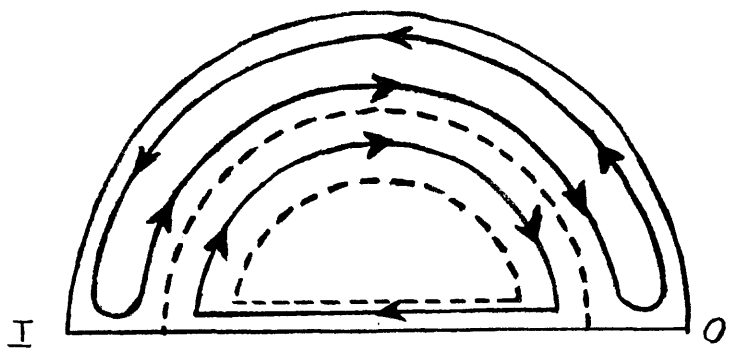


Figure 1.1:5b Velocity direction.

Figure 1.1:5 Lyne's (1970) result for large ω and large R_s.

§ 1.2 Formulation

In this section we consider the mathematical formulation of laminar flows down curved pipes. The fluid is assumed to be Newtonian and incompressible with kinematic viscosity ν and density ρ respectively. For simplicity, the pipe is assumed to have a circular cross-section with radius a and centre O, and to circle an axis C with constant radius of curvature L, see figure 1.1:1. We refer to the plane which contains O, and which is perpendicular to the axis, as the symmetry plane. The ratio of curvature δ is defined as

$$\delta = \frac{a}{L} . \qquad (1.2:1a)$$

The flow down the pipe is best described within a toroidal coordinate system $(ar, a\theta, a\delta^{-1/2}z)$ (i.e. $s = a\delta^{-1/2}z$) as illustrated in figure 1.1:1 (Dean 1927). Here ar measures the distance from the centreline of the pipe, $a\theta$ the angle from the intersection of the symmetry plane and the *outer* wall, and $a\delta^{-1/2}z$ the distance down the pipe from some reference point. We suppose a typical axial velocity is $\bar{W}$, and let the velocities in the $(ar, a\theta, a\delta^{-1/2}z)$ directions be $(\delta^{1/2}\bar{W}V, \delta^{1/2}\bar{W}U, \bar{W}W)$, and the time and pressure be $\frac{at}{\delta^{1/2}\bar{W}}$ and $\rho\bar{W}^2p$ respectively. For small curvature and low Reynolds numbers, Dean (1927) showed that flows down a curved pipe could be characterised by a dimensionless number, later known as the Dean number. Many versions of the Dean number have been defined and used in subsequent works, for a detailed survey see Berger, Talbot and Yao (1983). Here we follow the convention

used by Stewartson, Cebeci and Chang (1980) and define the Dean number D associated with the typical axial velocity as

$$D = \frac{\delta^{1/2}\bar{W}a}{\nu} . \qquad (1.2:1b)$$

The continuity equation for unsteady three-dimensional flow down the pipe is (e.g. Dean, 1927)

$$\frac{\partial V}{\partial r} + \frac{1+2\delta r\cos\theta}{1+\delta r\cos\theta}\frac{V}{r} + \frac{1}{r}\frac{\partial U}{\partial \theta} - \frac{\delta U\sin\theta}{1+\delta r\cos\theta} + \frac{1}{1+\delta r\cos\theta}\frac{\partial W}{\partial z} = 0 , \qquad (1.2:2a)$$

and the momentum equations in the r, θ and z directions are respectively

$$\frac{\partial V}{\partial t} + V\frac{\partial V}{\partial r} + \frac{U\partial V}{r\partial\theta} + \frac{W}{1+\delta r\cos\theta}\frac{\partial V}{\partial z} - \frac{U^2}{r} - \frac{W^2\cos\theta}{1+\delta r\cos\theta} = -\frac{1}{\delta}\frac{\partial p}{\partial r}$$

$$-\frac{1}{D}\left[\left(\frac{1}{r}\frac{\partial}{\partial\theta} - \frac{\delta\sin\theta}{1+\delta r\cos\theta}\right)\left(\frac{U}{r} + \frac{\partial U}{\partial r} - \frac{1}{r}\frac{\partial V}{\partial\theta}\right) - \frac{\delta}{(1+\delta r\cos\theta)^2}\frac{\partial^2 V}{\partial z^2}\right.$$

$$\left. + \frac{1}{1+\delta r\cos\theta}\left(\frac{\delta\cos\theta}{1+\delta r\cos\theta}\frac{\partial W}{\partial z} + \frac{\partial^2 W}{\partial r\partial z}\right)\right] , \qquad (1.2:2b)$$

$$\frac{\partial U}{\partial t} + V\frac{\partial U}{\partial r} + \frac{U\partial V}{r\partial\theta} + \frac{W}{1+\delta r\cos\theta}\frac{\partial U}{\partial z} + \frac{VU}{r} + \frac{W^2\sin\theta}{1+\delta r\cos\theta} = -\frac{1}{\delta r}\frac{\partial p}{\partial\theta}$$

$$+\frac{1}{D}\left[\left(\frac{\delta}{(1+\delta r\cos\theta)^2}\frac{\partial^2 U}{\partial z^2} - \frac{1}{r(1+\delta r\cos\theta)}\frac{\partial^2 W}{\partial\theta\partial z} + \frac{\delta\sin\theta}{(1+\delta r\cos\theta)^2}\frac{\partial W}{\partial z}\right.\right.$$

$$\left.\left. + \left(\frac{\partial}{\partial r} + \frac{\delta\cos\theta}{1+\delta r\cos\theta}\right)\left(\frac{U}{r} + \frac{\partial U}{\partial r} - \frac{1}{r}\frac{\partial V}{\partial\theta}\right)\right)\right] , \qquad (1.2:2c)$$

and

$$\frac{\partial W}{\partial t} + \frac{V\partial W}{\partial r} + \frac{U}{r}\frac{\partial W}{\partial \theta} + \frac{W}{1+\delta r\cos\theta}\frac{\partial W}{\partial z} + \frac{\delta VW\cos\theta}{1+\delta r\cos\theta} - \frac{\delta UW\sin\theta}{1+\delta r\cos\theta}$$

$$= -\frac{1}{(1+\delta r\cos\theta)}\frac{\partial p}{\partial z} + \frac{1}{D}\left[\left(\frac{\partial}{\partial r} + \frac{1}{r}\right)\left(\frac{\partial W}{\partial r} + \frac{\delta W\cos\theta}{1+\delta r\cos\theta}\right) + \frac{1}{r^2}\frac{\partial^2 W}{\partial \theta^2}\right.$$

$$- \frac{1}{r}\frac{\partial}{\partial \theta}\left(\frac{\delta W\sin\theta}{1+\delta r\cos\theta}\right) - \left(\frac{\partial}{\partial r} + \frac{1}{r}\right)\left(\frac{\delta}{1+\delta r\cos\theta}\frac{\partial V}{\partial z}\right)$$

$$\left. - \frac{1}{r}\frac{\partial}{\partial \theta}\left(\frac{\delta}{1+\delta r\cos\theta}\frac{\partial U}{\partial z}\right)\right] . \qquad (1.2:2d)$$

The boundary conditions on the surface of the pipe are the no-slip conditions,

$$U = V = W = 0 \qquad \text{on} \quad r = 1 \qquad (1.2:2e)$$

in addition there is the requirement that the flow be regular at $r = 0$ on the centreline of the pipe.[1]

One approach would be to solve the unsteady three-dimensional Navier-Stokes equations (1.2:2a-d) subject to boundary conditions (1.2:2e) and some initial velocity profile at $t = 0$, for various values of the Dean number. However, this can require significant computational effort, with possible limitations due to the

---

[1] Experiments are often performed on helical pipes, and the governing equations (1.2:2) must then be modified (e.g. Moore and Saffman (1972), Germano (1982)). However if the limit $\delta \ll 1$ is taken, in which case (1.2:2) simplify, the leading-order equations in δ are correct for a helical pipe if $\tau \ll \delta^{1/2}$, where τ is the torsion of the centre line. We also require $\pi\tau \geq \delta$ if the pipe is not to intersect itself.

availability of computer time and storage. This problem is particularly acute for large Dean numbers because of the boundary layers that develop and which require fine grids if they are to be adequately resolved.

One way forward is to simpify the Navier-Stokes equations (1.2:2a-d) by concentrating on different aspects of the flow. A number of these simplifications (e.g. axial independence, time independence) have been reviewed in the introduction. One of our aims is to gain a better understanding of aortic flow, so we will study high-Dean-number starting flows. In order to make the problem computationally more tractable, we will also assume axial-independence, (i.e. $\frac{\partial}{\partial z} \equiv 0$), although this makes our solution less directly applicable to flow through the aorta. We note that this is the same approach adopted by Farthing (1977).

Lyne (1971) showed that in the absence of viscosity, i.e. $D = \infty$, an exact solution of (1.2:2a-d) subject to the condition $V = 0$ in (1.2:2e), is (also see Singh, 1974)

$$V = U = 0, \qquad W = \frac{W_o(t)}{1 + \delta r \cos\theta} . \qquad (1.2:3)$$

Here W_o can be any function of t. This solution, which is that for a line vortex, has been used in a number of high-Dean-number problems mentioned previously, e.g. Stewartson, Cebeci and Chang (1980), Stewartson and Simpson (1982) etc.. It has a non-zero slip velocity at the wall of the pipe, $r = 1$, so generating a thin viscous boundary layer close to the wall. The boundary-layer solution satisfies the no-slip condition (1.2:2e) on the wall and matches to the inviscid slip velocity (1.2:3) at the edge of the

boundary layer.

Within the boundary layer the inertia terms must balance the viscous terms. A comparison of orders of magnitude of these terms suggests the thickness of the boundary layer is of order $D^{-1/2}$. Therefore, we define local boundary-layer co-ordinates (x, y) by

$$x = \theta , \qquad y = D^{1/2}(1 - r) . \tag{1.2:4a}$$

Here x measures the non-dimensional distance along the surface of the pipe from the symmetry line of the outer wall and lies in the range $-\pi$ to π. The coordinate y is the inward distance normal to the wall scaled by the conventional factor of $D^{1/2}$, and ranges from 0 to ∞. We define $(u, v, \bar{w})$, the scaled velocities in the boundary layer in the (x, y, z) directions respectively, as

$$u = (1 + \delta\cos x)U, \qquad v = -D^{1/2}V, \qquad \bar{w} = W(1 + \delta\cos x) . \tag{1.2:4b}$$

Note that the normal velocity v has also been scaled by the factor of $D^{1/2}$ to balance the normal variable y in the continuity equation. The classical boundary-layer hypothesis is that within the boundary layer the scaled y remains O(1) for large D. On taking the limit $D \to \infty$, (1.2:2a-d) are reduced to the unsteady boundary-layer equations (e.g. Farthing, 1977). The continuity equation is

$$(1 + \delta\cos x)v_y + u_x = 0, \tag{1.2:5a}$$

and the momentum equations in the x, y and z directions are respectively

$$u_t + vu_y + \frac{uu_x}{(1 + \delta\cos x)} + \frac{\sin x}{(1 + \delta\cos x)^2}\left(\delta u^2 + \bar{w}^2 - W_o^2 \right) = u_{yy} ,$$

(1.2:5b)

$$\frac{\partial p}{\partial y} = 0 , \qquad (1.2:5c)$$

and

$$\bar{w}_t + v\bar{w}_y + \frac{uw_x}{(1 + \delta\cos x)} = W_o'(t) + \bar{w}_{yy} .$$

(1.2:5d)

Equations (1.2:5a-d) are subject to the boundary conditions

$$u = v = \bar{w} = 0 \qquad \text{on } y = 0,$$

$$u \to 0, \qquad \bar{w} \to W_o(t) \qquad \text{as } y \to \infty.$$

(1.2:5e)

At the starting time $t = 0$, vorticity will not have had time to diffuse away from the wall, and hence, from (1.2:3),

$$u = v = 0, \qquad \bar{w} = W_o(0), \qquad \text{at } t = 0. \qquad (1.2:5f)$$

Equations (1.2:5) specify an initial value problem in time. The flow is periodic in x, and symmetrical about the plane where $x = 0$ and $x = \pi$; hence without loss of generality the problem can be restricted to the upper half of the pipe, i.e. $0 \le x \le \pi$.

As indicated in section 1.1, we expect a secondary motion to be generated in which fluid particles drift towards the inner wall. The continuous motion of fluid particles towards the inner wall means that the particles there are squashed azimuthally, and hence they elongate in the direction normal to the wall to conserve mass. This procedure forces fluid above the 'squashed' particles out of the boundary layer, thus increasing the thickness of the boundary

layer. This process is very similar to that generated when a sphere is impulsively rotated and a cylinder impulsively heated (Banks and Zaturska 1979, Simpson and Stewartson 1982a,b). In both these cases an equatorial particle collision occurs in which the boundary layer thickens to an 'infinite' thickness within a finite time, i.e. a 'separation singularity' develops.

As shown later, a similar singularity develops in the curved pipe problem. We interpret this as the *genesis* of an *unsteady* boundary-layer *separation* and refer to the particle squashed to infinitesimal thickness causing the separation as the 'separating' particle. In order to expel fluid particles out of the boundary layer within a finite time, the normal velocity at the edge of the boundary layer must become infinite. Therefore it is preferable to work in a coordinate system in which the governing equations are independent of both y and v.

Van Dommelen and Shen (1980) and Van Dommelen (1986) have successfully used Lagrangian coordinates to solve similar problems with unsteady boundary-layer separation. The approach was first applied to the classical two-dimensional problem of an unsteady, laminar flow over a stationary circular cylinder (Van Dommelen *et al.*, 1980). The flow was shown to develop an unsteady boundary-layer separation singularity after a finite time at about 111° from the front stagnation point. The same method has also been used on the impulsively rotated sphere (Van Dommelen, 1986). The most important advantage of the approach is that the momentum equations in Lagrangian coordinates are independent of y and v in each case. It has been shown that the resulting governing equations

can be integrated numerically up to (and sometimes even past) the separation time, predicting the position and the time of separation accurately.

Following Van Dommelen and Shen, the governing equations (1.2:5) are expressed in Lagrangian coordinates (ξ, η). We label a fluid particle by its position (ξ, η), at some fixed time, which we take to be t = 0 for convenience, i.e.

$$\xi = x, \qquad \eta = y \qquad \text{at} \qquad t = 0. \tag{1.2:6}$$

Applying the chain rule of differentiation, the tangential particle acceleration in the Lagrangian coordinates is related to Eulerian particle derivatives by

$$\left.\frac{\partial u}{\partial t}\right|_{\xi,\eta} = \left.\frac{\partial u}{\partial t}\right|_{x,y} + \left.\frac{\partial u}{\partial x}\right|_{y,t} \left.\frac{\partial x}{\partial t}\right|_{\xi,\eta} + \left.\frac{\partial u}{\partial y}\right|_{x,t} \left.\frac{\partial y}{\partial t}\right|_{\xi,\eta}.$$

From here onward we denote differentiation in Lagrangian coordinates by a subscript comma, so that

$$\left.\frac{\partial u}{\partial t}\right|_{\xi,\eta} = u_{,t}$$

whereas in Eulerian coordinates,

$$\left.\frac{\partial u}{\partial t}\right|_{x,y} = u_t .$$

From the definition of the toroidal coordinate system, the velocities (V, U, W) are related to their respective direction variables (r, θ, z) by

$$\delta^{1/2}\bar{W}V = ar_{,t}, \qquad \delta^{1/2}\bar{W}U = a\theta_{,t},$$

$$\bar{W}W = (1 + \delta\cos\theta)\delta^{1/2}z_{,t} .$$

Using equation (1.2:4) we may express these in terms of the local

boundary-layer velocities u, v, $\bar{w}$, and the Eulerian boundary-layer variables (x, y, z) by

$$u = (1 + \delta\cos x)\ x_{,t} , \tag{1.2:7a}$$

$$v = y_{,t} , \tag{1.2:7b}$$

$$\bar{w} = (1 + \delta\cos x)^2 z_{,t} . \tag{1.2:7c}$$

Therefore the tangential particle acceleration in Lagrangian coordinates is

$$\left.\frac{\partial u}{\partial t}\right|_{\xi,\eta} = \left.\frac{\partial u}{\partial t}\right|_{x,y} + \frac{u}{1+\delta\cos x}\left.\frac{\partial u}{\partial x}\right|_{y,t} + v\left.\frac{\partial u}{\partial y}\right|_{x,t} .$$

Similar expressions apply to the acceleration components in the other directions. Also we write

$$w = W_o(t) - \bar{w} .$$

Then the governing boundary-layer equations (1.2:5b,d) become, in Lagrangian coordinates,

$$u_{,t} = \frac{\sin x}{(1 + \delta\cos x)^2}\ (w(2W_o - w) - \delta u^2) + D^2 u \tag{1.2:8a}$$

$$w_{,t} = D^2 w . \tag{1.2:8b}$$

where the derivative operator D is given by

$$D = \frac{\partial}{\partial y} = \xi_y \frac{\partial}{\partial \xi} + \eta_y \frac{\partial}{\partial \eta} .$$

The purpose of the transformation is to obtain a system of governing equations independent of y and v. To achieve this, we seek an alternative expression for the operator D. First, we recall that the Eulerian spatial variables $x(\xi,\eta,t)$ and $y(\xi,\eta,t)$ are functions of the Lagrangian independent variables ξ and η. Hence, differentiation of x and y with respect to x gives

$$1 = x_{,\xi}\xi_x + x_{,\eta}\eta_x \,, \qquad 0 = y_{,\xi}\xi_x + y_{,\eta}\eta_x \,, \qquad (1.2:9a)$$

and similarly for x and y with respect to y

$$0 = x_{,\xi}\xi_y + x_{,\eta}\eta_y \,, \qquad 1 = y_{,\xi}\xi_y + y_{,\eta}\eta_y \,. \qquad (1.2:9b)$$

Equations (1.2:9) can be combined to give

$$x_{,\xi} = \frac{\eta_y}{\eta_y\xi_x - \xi_y\eta_x} \,, \qquad y_{,\xi} = \frac{-\eta_x}{\eta_y\xi_x - \xi_y\eta_x} \,, \qquad (1.2:10a)$$

$$x_{,\eta} = \frac{-\xi_y}{\eta_y\xi_x - \xi_y\eta_x} \,, \qquad y_{,\eta} = \frac{\xi_x}{\eta_y\xi_x - \xi_y\eta_x} \,. \qquad (1.2:10b)$$

The continuity equation (1.2:5a) can be expressed in Lagrangian coordinates as

$$(1 + \delta\cos x)(\xi_y v_{,\xi} + \eta_y v_{,\eta}) + (\xi_x u_{,\xi} + \eta_x u_{,\eta}) = 0 \,. \qquad (1.2:11)$$

Also we define

$$\frac{\partial(x, y)}{\partial(\xi, \eta)} = x_{,\xi}y_{,\eta} - x_{,\eta}y_{,\xi} \,, \qquad (1.2:12a)$$

and J, the Jacobian modified with curvature, as

$$J = \frac{1+\delta\cos x}{1+\delta\cos \xi}\frac{\partial(x, y)}{\partial(\xi, \eta)} \,. \qquad (1.2:12b)$$

From the definitions of u and v in (1.2:7a,b), the time derivative of $\left[(1+\delta\cos \xi)J\right]$ is

$$\left[(1+\delta\cos \xi)\, J\right]_{,t} = u_{,\xi}y_{,\eta} - u_{,\eta}y_{,\xi} + (1 + \delta\cos x)(x_{,\xi}v_{,\eta} - x_{,\eta}v_{,\xi}) \,.$$

Then by substitution of $x_{,\xi}$, $x_{,\eta}$, $y_{,\xi}$ and $y_{,\eta}$ from (1.2:10) into the above, and using equation (1.2:11), we obtain

$$\left[\left(1 + \delta \cos \xi \right) J \right]_{,t} = 0 \ . \qquad (1.2:12c)$$

Hence $(1+\delta\cos\xi)J$ is constant in time. The constant is obtained by applying the definition of ξ and η at $t = 0$ in (1.2:6); therefore

$$J = 1 \qquad (1.2:12d)$$

and from (1.2:12a,b)

$$\frac{\partial(x, y)}{\partial(\xi, \eta)} = x_{,\xi} y_{,\eta} - x_{,\eta} y_{,\xi} = \frac{1 + \delta\cos \xi}{1 + \delta\cos x} \ , \qquad (1.2:13a)$$

or alternatively,

$$\frac{\partial(\xi, \eta)}{\partial(x, y)} = \xi_x \eta_y - \xi_y \eta_x = \frac{1 + \delta\cos x}{1 + \delta\cos \xi} \ . \qquad (1.2:13b)$$

Using (1.2:13b), we may express (1.2:10) as

$$\xi_x = y_{,\eta} \frac{1 + \delta\cos x}{1 + \delta\cos \xi} \ , \qquad \xi_y = -x_{,\eta} \frac{1 + \delta\cos x}{1 + \delta\cos \xi} \ , \qquad (1.2:13c)$$

$$\eta_x = -y_{,\xi} \frac{1 + \delta\cos x}{1 + \delta\cos \xi} \ , \qquad \eta_y = x_{,\xi} \frac{1 + \delta\cos x}{1 + \delta\cos \xi} \ . \qquad (1.2:13d)$$

Therefore the differentiation operator D can be rewritten as

$$D = \xi_y \frac{\partial}{\partial \xi} + \eta_y \frac{\partial}{\partial \eta}$$

$$= \left[\frac{1 + \delta\cos x}{1 + \delta\cos \xi} \right] \left[-x_{,\eta} \frac{\partial}{\partial \xi} + x_{,\xi} \frac{\partial}{\partial \eta} \right] \ . \qquad (1.2:14)$$

The boundary-layer problem for $x(\xi,\eta,t)$, $u(\xi,\eta,t)$ and $w(\xi,\eta,t)$ is specified completely in Lagrangian coordinates by equations (1.2:7a) and (1.2:8) with the operator D defined in (1.2:14). The boundary conditions are

$$\begin{aligned} &u = w = 0, && && \text{for } t \le 0, \\ &u = 0, && w = W_o(t) \quad \text{on } \eta = 0 && \text{for } t \ge 0, \\ &u \to 0, && w \to 0 \quad \text{as } \eta \to \infty && \text{for } t \ge 0, \end{aligned} \qquad (1.2:15)$$

and the initial condition (1.2:6). Note that the equations for the velocities u and w are simplified because they include no curvature inertia terms, although the diffusive term expressed by the operator D^2 is complicated when expressed in full. However, the great advantage of working in the Lagrangian coordinate system is that the governing equations are independent of y and v. As shown below these are the quantities which become singular at the occurrence of the boundary-layer collision. Because the solutions for x, u and w remain regular up to the time of the collision, they can be calculated numerically with great accuracy.

With the problem specified in Lagrangian coordinates, we can now drop the subscript comma indicating Lagrangian differentiation, and assume all derivatives are with respect to the independent Lagrangian variables.

The Eulerian variable y and the normal velocity v can be calculated independently of the governing equations (1.2:6a, 8). An expression for the variable y follows from the identity

$$y(\xi,\ \eta,\ t) = \int_0^{y(\xi,\eta,t)} dy \ . \qquad (1.2:16)$$

This integral is to be evaluated on the path of constant x, which means

$$0 = \qquad dx = x_\xi d\xi + x_\eta d\eta \ , \qquad (1.2:17a)$$

$$d\xi = -\frac{x_\eta}{x_\xi}\, d\eta \qquad . \qquad (1.2:17b)$$

Since dy is given by

$$dy = y_\xi d\xi + y_\eta d\eta \ , \qquad (1.2:18a)$$

dy on constant x is given by (see (1.2:13a))

$$dy = (- y_\xi x_\eta + y_\eta x_\xi) \frac{d\eta}{x_\xi}$$

$$= \frac{1 + \delta\cos \xi}{1 + \delta\cos x} \frac{d\eta}{x_\xi} . \qquad (1.2:18b)$$

Therefore y can be expressed as

$$y(\xi, \eta, t) = \int_{\substack{0 \\ \text{constant } x}}^{\eta} \frac{1 + \delta\cos \xi}{1 + \delta\cos x} \frac{d\eta}{x_\xi} . \qquad (1.2:19a)$$

We define s, the arc length along any path of constant x, by

$$ds^2 = d\xi^2 + d\eta^2$$

$$= d\eta^2 \left(\frac{x_\eta^2}{x_\xi^2} + 1 \right) .$$

The function y from (1.2:19a) can then be expressed in terms of Lagrangian variables ξ, η and s as

$$y(\xi, \eta, t) = \int_{\substack{0 \\ \text{constant } x}}^{s} \frac{1 + \delta\cos \xi}{1 + \delta\cos x} \frac{ds}{\sqrt{(x_\xi^2 + x_\eta^2)}} . \qquad (1.2:19b)$$

Similarly the velocity normal to the wall can be expressed in terms of the arc length s along a path of constant x. From the continuity equation (1.2:5a) the velocity v normal to the wall is

$$v(\xi, \eta, t) = - \int_{\substack{0 \\ \text{constant } x}}^{y} \frac{u_x}{1 + \delta\cos x} dy . \qquad (1.2:20a)$$

Now u_x can be rewritten using (1.2:13) as

$$u_x = u_\xi \xi_x + u_\eta \eta_x$$

$$= (u_\xi y_\eta - u_\eta y_\xi)\,\frac{1+\delta\cos x}{1+\delta\cos \xi}\ ,$$

and dy is just as defined in (1.2:18b). Therefore, v can be expressed as

$$v(\xi,\ \eta,\ t) = -\int_{\substack{0\\ \text{constant } x}}^{\eta} \frac{1}{1+\delta\cos x}\,\frac{u_\xi y_\eta - u_\eta y_\xi}{x_\xi}\,d\eta\ . \qquad (1.2:20b)$$

Alternatively, using ξ, η and s as before, we obtain

$$v(\xi,\ \eta\ ,t) = -\int_{\substack{0\\ \text{constant } x}}^{s} \frac{(u_\xi y_\eta - u_\eta y_\xi)}{1+\delta\cos x}\,\frac{ds}{\sqrt{x_\xi^2 + x_\eta^2}}\ . \qquad (1.2:20c)$$

Let us define the Lagrangian gradient, grad x, as

$$\text{grad } x = (\ x_\xi,\ x_\eta\ ). \qquad (1.2:21)$$

It can be shown, see section 1.4, that the integrals in (1.2:19b) and (1.2:20c) become unbounded if at some time t_s, and some point $x_s(\xi_s,\ \eta_s,\ t_s)$,

$$|\ \text{grad } x\ |_s^2 = \left[\ (x_\xi)_s^2 + (x_\eta)_s^2\ \right] = 0\ , \qquad (1.2:22)$$

where $(x_\xi)_s^2$ is $(x_\xi)^2$ evaluated at $(\xi_s,\ \eta_s,\ t_s)$ and similarly for $(x_\eta)_s^2$. Hence the boundary-layer displacement thickness becomes infinite if a zero develops in grad x, and we interpret this as boundary-layer separation[2]. The critical time of the singularity t_s is easily located since it is associated with the zero of a

---

[2] Note that the Goldstein (1948) steady singularity has finite displacement thickness.

function in Lagrangian coordinates (cf. the singular quantity in Eulerian coordinates).

§ 1.3 Numerical Method

In this section we discuss the numerical schemes used to obtain the solution of the boundary-layer equations (1.2:7a, 8).

The flow is assumed symmetrical, so that the governing equations (1.2:7a, 8) need to be solved only for $0 \leq \xi \leq \pi$. In addition the axial independence means that it is only necessary to use a two-dimensional finite computational domain. Here we distribute, by means of 'stretch' functions, a total of N points over $0 \leq \xi \leq \pi$, and M points over $0 \leq \eta < \infty$.

The choice for the stretch function in the tangential direction was based on the physical reasoning presented in section 1.1, which suggests that boundary-layer separation may occur at the symmetry line of the inner wall; therefore a more refined grid is needed there. A stretch (cf. Van Dommelen and Shen, 1980) in the ξ direction was implemented by introducing the variable α such that

$$\xi(\alpha) = \lambda_1 \arctan(\lambda_2 \tan \tfrac{1}{2}\pi\alpha) - \lambda_3 \alpha , \qquad (1.3:1a)$$

where λ_1, λ_2 and λ_3 are constants to be chosen by test runs.

The matching conditions in (1.2:15) have to be applied at the edge of the boundary layer. Since we were limited to a finite computational domain, two ways were considered to impose the boundary conditions as $\eta \to \infty$. Either

i) the boundary conditions might be applied at a large but finite value of η,

or,

ii) a new variable could be introduced to map infinity to a finite value.

The second choice was that adopted, and a new coordinate β was introduced, defined by (cf. Van Dommelen and Shen, 1980)

$$\eta(\beta,t)= \lambda_4 \sqrt{\frac{4t}{1+4t}}\, \tan\tfrac{1}{2}\pi\beta \ . \qquad (1.3:1b)$$

The function $\sqrt{4t}$ in (1.3:1b) was included in order to obtain accurate answers for impulsively started flows. This is because when a flow is impulsively started, the boundary layer adjacent to the wall behaves like a Rayleigh layer with an $O(t^{1/2})$ thickness for small times, i.e.

$$y \sim t^{1/2} , \qquad \eta \sim t^{1/2} \qquad \text{for } t \ll 1 \ .$$

Consequently, in order to maintain accuracy it is necessary to stretch η with a factor of $t^{1/2}$. The denominator $\sqrt{1+4t}$ in (1.3:1b) is included to ensure that for fixed β, the function of η remains finite as $t \to \infty$ (although the integrations did not in general extend to large times).

In the new coordinates (α, β) the computational domain is $0 \le \alpha \le 1$, $0 \le \beta \le 1$. The choice for the constants λ_1, λ_2, λ_3, λ_4 will be discussed later in section 1.5.

The equations (1.2:7a,8) are *parabolic* in t and η, and *elliptic* in ξ and η. This initial value problem is only fully specified given an initial velocity profile at t = 0 and conditions at the boundaries of the domain. They have been fixed as follows.

We first consider the initial velocity profile in the boundary layer for small but positive time, t = 0+. When a core flow

consisting only of an axial velocity is started impulsively, very close to the start-up time the secondary transverse velocity will not have had time to develop; therefore

$$u = 0 \qquad \text{at } t = 0+ , \tag{1.3:2a}$$

and the spatial position x remains as given in equation (1.2:6). As indicated above, we would expect the axial velocity to have a Rayleigh layer solution. To see this in terms of Lagrangian coordinates, we note, from (1.2:6),

$$x_\xi = 1, \qquad x_\eta = 0 \qquad \text{at } t = 0+ .$$

The above equations and (1.3:2a) simplify (1.2:8b) to

$$w_t = w_{\eta\eta} \qquad \text{at } t = 0+ ,$$

which, when written in terms of the stretched variable β, is

$$w_{\beta\beta}\cos^3\frac{\pi}{2}\beta + \pi w_\beta\left(-\cos^2\frac{\pi}{2}\beta + \lambda_4^2\right)\sin\frac{\pi}{2}\beta = 0 .$$

This equation has a similarity solution,

$$w = W_o(0)\ \mathrm{erf}\left[\lambda_4 \tan\frac{\pi\beta}{2}\right] \tag{1.3:2b}$$

where erf is the error function, namely

$$\mathrm{erf}\ (\zeta) = \frac{2}{\sqrt{\pi}} \int_0^\zeta e^{-\vartheta^2}\, d\vartheta .$$

As a check on our numerical scheme, we also solved the above second-order, linear, ordinary differential equation for w numerically by second-order finite differences. This equation is independent of ξ, thus it needed to be discretized in the β direction only. At any column $\xi = \xi_i$ $(1 \le i \le N)$, this yielded M-2

implicit difference equations subject to two boundary conditions at $\beta = 0$ and 1. The difference equations were then represented in matrix form,

$$A \underline{f} = \underline{b} .$$

The $M \times M$ matrix A was a tridiagonal matrix. The vector $\underline{f}$ consisted of w at (ξ_i, η_j) for $1 \leq j \leq M$, and $\underline{b}$ was a known vector. Since A was not in general diagonally dominant, to minimize numerically induced instability it was inverted by Gaussian elimination with pivoting (Fox and Mayers, 1968). The differences between the analytical and numerical solutions were confirmed to be within the expected $O(h^2)$ truncation error, where h was the step size.

With the initial velocity profiles determined, we now describe how the boundary conditions were imposed. From (1.2:15) the boundary conditions for $\beta = 0$ and 1 are

$$u = v = 0, \qquad w = W_o(t), \qquad \text{on } \beta = 0 \qquad \text{for } t \geq 0,$$

$$u = 0, \qquad w = 0, \qquad \text{on } \beta = 1 \qquad \text{for } t \geq 0.$$

One boundary condition for the full problem, $-\pi \leq \xi \leq \pi$, would be periodicity of the flow. However, since the problem was reduced to $0 \leq \xi \leq \pi$, boundary conditions are needed on $\xi = 0$ and $\xi = \pi$.

The conditions for u and x on these planes follow directly from consideration of the geometry of the pipe. In particular, fluid particles on the symmetry planes must remain there, and the transverse velocity, u, must be zero

$$u = 0 \quad \text{on} \quad \xi = 0 \quad \text{and} \quad \xi = \pi \quad \text{for all } t\,, \tag{1.3:3a}$$

$$x = 0 \quad \text{on} \quad \xi = 0 \quad \text{and} \quad x = \pi \quad \text{on} \quad \xi = \pi \quad \text{for all } t. \tag{1.3:3b}$$

The condition on the axial velocity w requires more consideration.

The flow on the symmetry plane of the inner wall has been studied by Stewartson and Simpson (1982) for *steady entry* flow into a loosely coiled pipe. They examined the flow there by making an expansion in a neighbourhood close to $x = \pi$, and solved the simplified boundary-layer equations numerically. A similar approach for the flow in the symmetry planes can be used for our unsteady problem (note that we use Lagrangian coordinates where Stewartson and Simpson used Eulerian coordinates). Let us define new variables x^* and u^* as

$$x - x_f = (\xi - \xi_f)\, x^*, \qquad u - u_f = (\xi - \xi_f)\, u^*,$$

where $x = x_f$, $u = u_f$ at $\xi = \xi_f$.

Hence,

$$x_f = 0, \qquad u_f = 0, \qquad \text{at} \quad \xi_f = 0,$$

and $$x_f = \pi, \qquad u_f = 0, \qquad \text{at} \quad \xi_f = \pi.$$

Then substitution into the governing equations (1.2:7a, 8) gives

$$u^* = (1 \pm \delta) x^*_t , \qquad (1.3:4a)$$

$$u^*_t = \pm \frac{x^*}{(1\pm\delta)^2} w(2W_o - w) + x^{*2} u^*_{\eta\eta} - x^* x^*_\eta u^*_\eta + (x^{*2}_\eta - x^* x^*_{\eta\eta}) u^* , \qquad (1.3:4b)$$

$$w_t = x^{*2} w_{\eta\eta} + x^* x^*_\eta w_\eta , \qquad (1.3:4c)$$

subject to the conditions,

$$\begin{aligned} x^* = 1, \quad u^* = 0, \quad w = W_o(t) \quad & \text{at } \eta = 0 , \\ x^* = 1, \quad u^* = 0, \quad w = 0 \quad & \text{as } \eta \to \infty , \\ x^* = 1, \quad u^* = 0, \quad w = 0 \quad & \text{at } t = 0+, \ \eta \neq 0 , \end{aligned} \qquad (1.3:4d)$$

In the above, wherever there is a choice of sign, the - sign corresponds to the equation at the inner wall, and the + sign to that at the outer. Note that because of the difference in definitions of u^* and w, the derivative operator D applied on u and w results in extra terms on the right-hand side of equation (1.3:4b). Also, it turns out that δ can be scaled out of equations (1.3:4) altogether (see section 1.5).

Let us concentrate on one wall, for example $\xi_f = 0$; the solution procedure applies equally to the other wall $\xi_f = \pi$. In order to evaluate the velocity w at each time value $t = n\Delta t$, equations (1.3:4) were discretised by second-order finite differences in both t and η at points $(\xi = 0, \eta_j, (n-\frac{1}{2})\Delta t)$, for $1 \leq j \leq M$ and $n \geq 1$. Since the difference equations were nonlinear, they could be solved only by an iterative procedure, for example a Newton-Raphson procedure. Let $\underline{f}$ be a vector of length 3M, consisting of the true solution for x^*, u^* and w at points

$(\xi = 0, \eta_j, n\Delta t)$, and $\underline{f}^k$ be the kth iterate of $\underline{f}$ in the Newton-Raphson procedure and related to $\underline{f}^{k-1}$ by

$$\underline{f}^k = \underline{f}^{k-1} + \delta\underline{f} \ ,$$

where $\delta\underline{f}$ is a small correction vector. The iterate $\underline{f}^k$ was substituted to replace $\underline{f}$ in the nonlinear difference equations which were then linearised with respect to $\delta\underline{f}$ to give a system of 3(M-2) linear difference equations. These, when combined with the boundary conditions at $\eta = 0$ and $\eta \to \infty$, could be represented in matrix form as

$$L\ \delta\underline{f} = \underline{b} \ .$$

The 3Mx3M matrix L was a banded matrix with a band width of 9 and $\underline{b}$ was a known vector of length 3M. The equations were solved by Gaussian elimination with partial pivoting. The solution for the axial velocity was then updated, and the process repeated until the absolute value of the update was less than a small tolerance at each grid point. The solution for the axial velocity was then used as the boundary condition at the appropriate symmetry plane.

With the initial velocity profiles and the boundary conditions at the four boundaries of the computational domain determined, we now describe the procedure used to solve the governing equations for the full boundary-layer problem.

First, we introduce some notation. Let

$$x_{i,j,n} = x(\xi_i, \eta_j, n\Delta t) \ ,$$

and similarly for u and w. We also define the vectors $\underline{f}_{i,n}$, $\underline{f}_{j,n}$ and $\underline{f}_n$ as

$$\underline{f}_{i,n} = (x_{i,j,n}, u_{i,j,n}, w_{i,j,n}, \quad \text{for } 1 \le j \le M) ,$$

$$\underline{f}_{j,n} = (x_{i,j,n}, u_{i,j,n}, w_{i,j,n}, \quad \text{for } 1 \le i \le N) ,$$

$$\underline{f}_{n} = (x_{i,j,n}, u_{i,j,n}, w_{i,j,n}, \quad \text{for } 1 \le i \le N \text{ and } 1 \le j \le M).$$

Thus the vector $\underline{f}_{i,n}$ consists of elements of x, u and w at the column $\xi = \xi_i$ at time $t = n\Delta t$ and is of length 3M. The vector $\underline{f}_{j,n}$ consists of elements of x, u and w at the row $\eta = \eta_j$ at time $t = n\Delta t$ and is of length 3N. The vector $\underline{f}_{n}$ consists of elements of x, u and w at all points in the full computational domain (ξ_i, η_j, $n\Delta t$) and is of length 3MN.

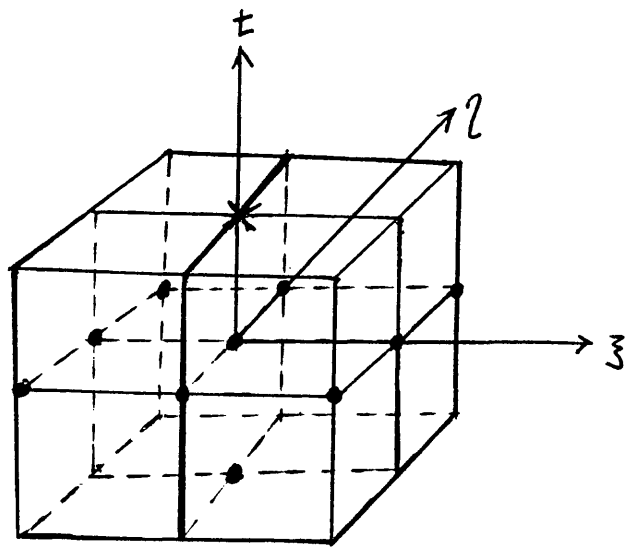
Let the superscript k denote the kth iterate in an iterative procedure. Hence the kth iterate to $x_{i,j,n}$ is $x^k_{i,j,n}$, and similarly for $\underline{f}_{i,n}$, $\underline{f}_{j,n}$ and $\underline{f}_{n}$.

All the equations were discretised using second-order central differences. The solution procedure for these nonlinear difference equations is illustrated in the flow chart in figure 1.3:1. Note that since equations (1.2:7a, 8) are parabolic, it is possible to march forward in time given the velocity profiles at an earlier time. At $t = 0$, the velocity profiles are determined by the initial conditions as discussed above. To march forward to $t = \Delta t$, the time-dependent boundary conditions at $\xi = 0, \pi$ and $\eta = 0, \infty$ are first calculated. Then the interior points are updated using an iterative scheme, which is essentially an Alternating Direction Implicit (ADI) method. The procedure at subsequent time steps is similar, but to improve convergence of the ADI iteration, an explicit leap-frog scheme is applied to yield an initial guess $\underline{f}^o_n$

for the solution at $t = n\Delta t$, $n \geq 2$. Note that for $n \geq 2$ the numerical solutions $\underline{f}_{n-1}$ and $\underline{f}_{n-2}$ are known. The procedure is repeated until a boundary-layer singularity is encountered in the form of a zero in grad x.

The Leap-Frog Scheme

The partial differential equations (1.2:7a,8) were discretized by second-order finite differences at points $(\xi_i, \eta_j, (n-1)\Delta t)$ for $2 \leq i \leq N-1$ and $2 \leq j \leq M-1$. The resulting finite difference equations are given in appendix 1.B. These equations relate the quantities x, u and w at the three time levels, $t = (n-2)\Delta t$, $(n-1)\Delta t$ and $n\Delta t$ as denoted by the 11 marked points below.



The dots denote the points at which the solution is known and the cross where it is to be calculated. The difference equations can be rearranged to express the unknown quantities x, u and w at $(\xi_i, \eta_j, n\Delta t)$ explicitly in terms of the solutions $\underline{f}_{n-1}$ and $\underline{f}_{n-2}$. The solution $\underline{f}^0$ can therefore be obtained point by point on the entire computational domain. This simple leap-frog scheme is unstable, for example test runs on a grid domain of 33x17 points

showed that as Δt was decreased, the time, t_b, at which $|\text{grad } x|$ decreased to zero also decreased (see table 1.3:1).

Δt	t_b
$\frac{1}{40}$	0.175
$\frac{1}{80}$	0.0875
$\frac{1}{120}$	0.05

Table 1.3:1

The variablity of these results suggests a numerical instability. In order to overcome this problem, an implicit scheme was therefore implemented. The solution $\underline{f}_{-n}^{0}$ served as an initial guess to the iterative solution $\underline{f}_{-n}$ at $t = n\Delta t$.

The implicit scheme selected was a second-order Crank-Nicolson scheme[1] in which the equations were discretised about the points $(\xi_i, \eta_j, (n-\frac{1}{2})\Delta t)$ for $2 \leq j \leq M-1$, $2 \leq i \leq N-1$ and $n \geq 1$. The resulting difference equations are given in appendix 1.B. These equations provide an implicit relationship between 18 neighbouring points, $(\xi_p, \eta_q, r\Delta t)$ for $i-1 \leq p \leq i+1$, $j-1 \leq q \leq j+1$ and $n-1 \leq r \leq n$. This discretisation yielded a system of difference equations which were nonlinear and could only be solved by an iterative procedure.

---

[1] A comparison of this discretisation with that used by Van Dommelen and Shen in a two-dimensional problem is given in appendix 1.A.

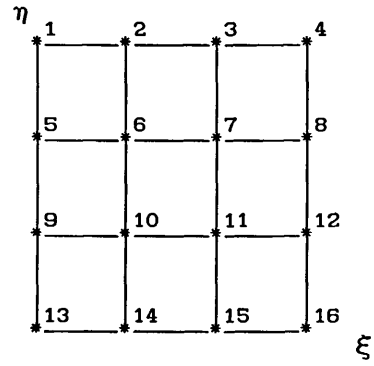
One approach would be a complete Newton-Raphson iteration, which would require linearization of the equations in the entire computational domain. This would be similar to the solution procedure for the flow in the symmetry planes with $\underline{f}$ replaced by $\underline{f}_n$ so that the linearised equation for the update would be

$$L\ \delta\underline{f}_n = \underline{b}\ . \qquad (1.3:5)$$

The $(3MN)^2$ matrix L would be a banded matrix with a band width of 8+min(6M, 6N), with $\delta\underline{f}_n$ the unknown vector, and $\underline{b}$ the known vector of residuals defined on the complete computational domain. To perform a Newton-Raphson iteration, the matrix L would have to be inverted and the solution for $\delta\underline{f}_n$ updated - a task which would require large amounts of computer memory. An alternative iterative scheme which involved less storage was therefore chosen.

Instead of performing a complete Newton-Raphson iterative procedure, a similar Alternating Direction Implicit iteration was used. This procedure consisted of applying a Newton-Raphson iteration along a line of unknowns within the computational domain, (e.g. for j=J, and $1 \le i \le N$), assuming that the variables in the rest of the domain were fixed, (i.e. $j \ne J$). This line iteration was performed for each j, and then a similar iteration was applied in the other direction for each i. We can illustrate the order of the applications of these line iterations by figure 1.3:2 below, assuming that the two-dimensional computational domain can be represented by 16 points, numbered 1 to 16. For example, when the iterations were applied on rows of constant η, the difference equations were first solved simultaneously on the row with points

13, 14, 15 and 16. Then we moved on to the next row containing the points 9, 10, 11 and 12, and so forth in the direction of increasing η. The line iterations in the other direction involved solving the difference equations for the column containing points 1, 5, 9 and 13 first, then for the column containing the points 2, 6, 10 and 14 etc. until all the points in the computational domain had been iterated.



To describe the linearisation in greater detail, we return to the full nonlinear governing equations (1.2:7a, 8). Let point 6 in figure 1.3:2 denote $(\xi_I, \eta_J, n\Delta t)$. Then discretisation of the governing equations at a point $(\xi_I, \eta_J, (n-\frac{1}{2})\Delta t)$ involved points 1, 2, 3, 5, 6, 7, 9, 10 and 11, and the known solution at the corresponding points for $t = (n-1)\Delta t$. Application of an 'ξ-line' iteration at the row $\eta = \eta_J$ involved solving for all points in the row, and was equivalent to writing the $(k+\frac{1}{2})^{th}$ iterate of $\underline{f}_{J,n}$ at $\eta = \eta_J$ as

$$\underline{f}_{J,n}^{k+1/2} = \underline{f}_{J,n}^{k} + \delta\underline{f}_{J,n}, \qquad (1.3:6a)$$

where $\delta\underline{f}_{J,n}$ was a small correction vector and the $\delta\underline{f}_{j,n}$ for $j \neq J$ were assumed to be zero. The iterate $\underline{f}_{J,n}^{k+1/2}$ was substituted into the full difference equations in place of $\underline{f}_{n}$, the equations

linearised with respect to $\delta\underline{f}_{J,n}$, and then solved with partial pivoting as discussed before when obtaining the solution on the symmetry line. Line iterations were applied over the full computational domain at all rows, $\eta = \eta_J$, for $2 \leq J \leq M-1$.

To complete the Alternating Direction Implicit procedure, 'η-line' iterations were then applied on a column $\xi = \xi_I$. This time

$$\underline{f}_{I,n}^{k+1} = \underline{f}_{I,n}^{k+1/2} + \delta\underline{f}_{I,n}, \qquad (1.3:6b)$$

where $\delta\underline{f}_{I,n}$ was a small correction vector, and $\delta\underline{f}_{i,n} = 0$ for $i \neq I$. As before, this was substituted into the full difference equations which were then linearised with respect to $\delta\underline{f}_{I,n}$. Again the linear equations were solved with partial pivoting. Line iterations were applied at all columns, $\xi = \xi_I$, for $2 \leq I \leq N-1$.

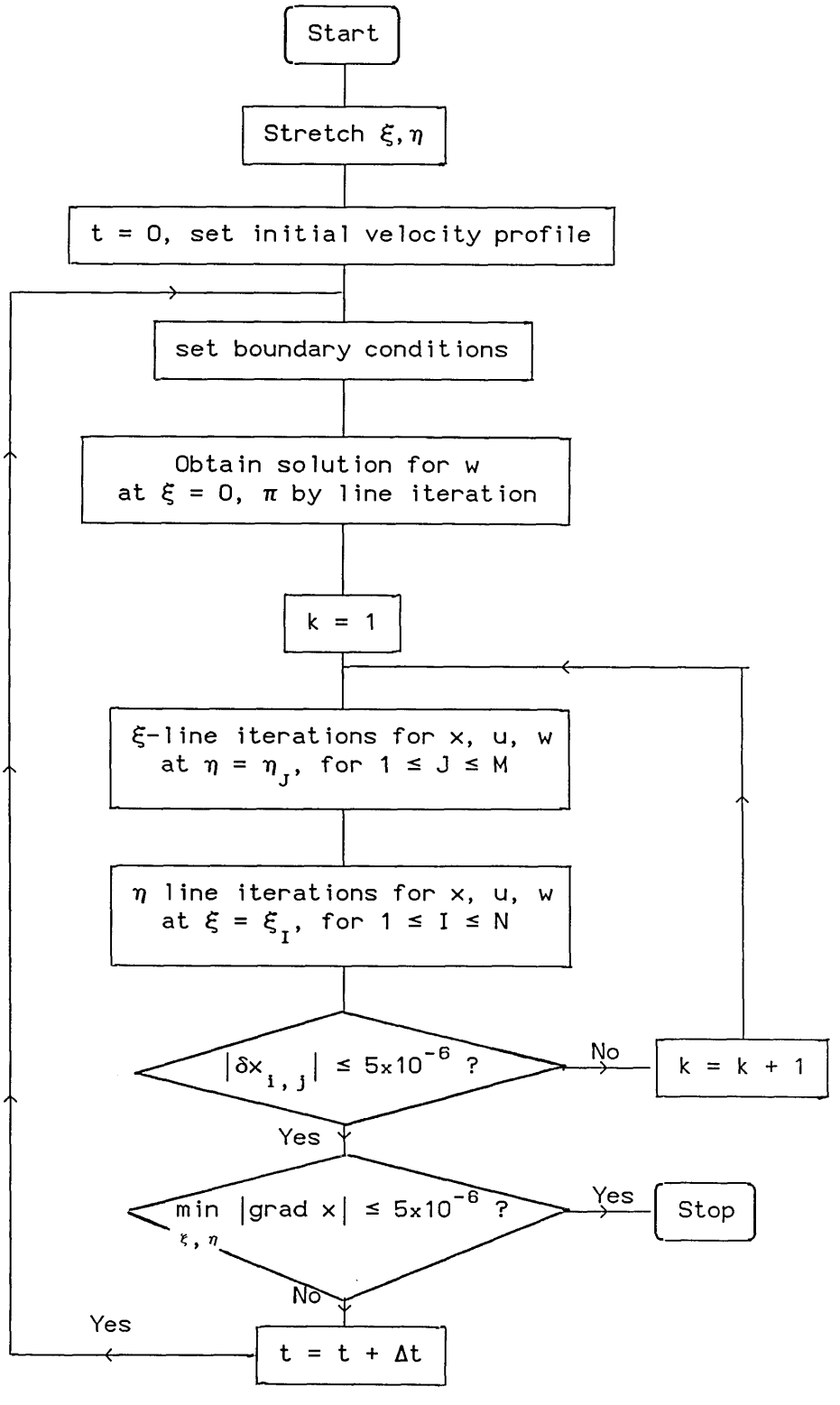
After each complete iteration of the Alternating Direction Implicit procedure the solution was tested against a convergence criterion which required that the update at each point was less than a specified small tolerance. If the test was unsuccessful, further complete iterations were performed.

At each time step a new set of boundary conditions for w at $\xi = 0$ and $\xi = \pi$ was calculated and the iteration procedure repeated. The calculation proceeded in time until a zero developed in grad x (thus indicating the development of a singularity in y).

After a few test runs the constants for the stretchings in (1.3:1) were chosen as: $\lambda_1 = 3$, $\lambda_2 = 2.5$, $\lambda_3 = \pi(\lambda_1 - 2)$ and $\lambda_4 = 1.5$. The convergence criterion was that the quantities x, u and w at each point in the domain changed by less than a tolerance of 5×10^{-6} at each point. The tolerance has been decreased to 5×10^{-9}

with no significant change in results, and no convergence difficulties have been experienced at times less than the singularity time. Grid sizes of 37x17, 73x33 and 145x65, and uniform time steps of $\frac{1}{40}$, $\frac{1}{80}$ and $\frac{1}{160}$ have been used. The accuracy of the scheme has been confirmed to be second-order. The program implementing these numerical schemes was run on a Cray 1S supercomputer and was fully vectorized.

Figure 1.3:1


Start
Stretch ξ, η
t = 0, set initial velocity profile
set boundary conditions
Obtain solution for w
at ξ = 0, π by line iteration
k = 1
ξ-line iterations for x, u, w
at η = η_J, for 1 ≤ J ≤ M
η line iterations for x, u, w
at ξ = ξ_I, for 1 ≤ I ≤ N
|δx_i,j| ≤ 5x10^-6 ?
No
k = k + 1
Yes
min |grad x| ≤ 5x10^-6 ?
ξ, η
Yes
Stop
No
Yes
t = t + Δt

§ 1.4 The Calculation of y and v

The most important advantage of the Lagrangian formulation is that both the variable y and the normal velocity v do not occur in the governing equations (1.2:7a, 8). Therefore, they can be calculated separately after the solutions for x, u and w have been obtained. In this section, we discuss various attempts to calculate y and v accurately.

There are two equivalent expressions for the Eulerian variable y, one written in the form of a partial differential equation in terms of ξ and η, i.e. from equation (1.2:13a)

$$x_\xi y_\eta - x_\eta y_\xi = \frac{1 + \delta\cos\,\xi}{1 + \delta\cos\,x}\,, \qquad (1.4:1a)$$

together with the initial/boundary condition

$$y = 0 \qquad \text{at} \qquad \eta = 0,$$

and one, from equation (1.2:19a), in the form of an integral along characteristics of constant x, i.e.

$$y(\xi,\ \eta,\ t) = \int_{\substack{0 \\ \text{constant } x}}^{\eta} \frac{1}{x_\xi}\,\frac{1 + \delta\cos\,\xi}{1 + \delta\cos\,x}\,d\eta\,. \qquad (1.4:1b)$$

The calculation for y can be conveniently divided into two parts, (a) one for early times of the boundary-layer development when the function is varying relatively slowly everywhere and (b) one after a finite time when the boundary layer is rapidly increasing in a small neighbourhood of the symmetry line on the *inner wall* due to the thickening associated with the convergence of

fluid particles there.

We first describe the relatively simple calculation of y for the early times when no difficulty has been experienced in obtaining numerically accurate results for either y or v. The calculation of the function y can be subdivided into two parts, that on the symmetry lines and that away from them.

On the symmetry lines where $x = \xi = 0$ or π, the path of constant x is also a path of constant ξ. The integral (1.4:1b) can thus be approximated by a simple application of the trapezium rule for $x = \xi = 0$ and π, i.e. for i = 1 and N:

$$y_{i,j} = y_{i,j-1} + \frac{1}{2}\left\{ \left[\frac{\Delta\eta}{x_\xi} \frac{1 + \delta\cos\xi}{1 + \delta\cos x} \right]_{i,j-1} + \left[\frac{\Delta\eta}{x_\xi} \frac{1 + \delta\cos\xi}{1 + \delta\cos x} \right]_{i,j} \right\} . \tag{1.4:2a}$$

Away from the symmetry lines, a number of methods to calculate y were tried. One was based on a discretization of equation (1.4:1a) using a second-order Crank-Nicolson approximation at $(\xi_i, \eta_{j-1/2})$ for $2 \le i \le N-1$ yielding a difference equation, namely

$$\frac{1}{2}\left[\frac{x_{i+1,j} - x_{i-1,j}}{2\Delta\xi} + \frac{x_{i+1,j-1} - x_{i-1,j-1}}{2\Delta\xi} \right]\left[\frac{y_{i,j} - y_{i,j-1}}{\Delta\eta} \right]$$

$$+ \frac{1}{2}\left[\frac{x_{i,j} - x_{i,j-1}}{\Delta\eta} \right]\left[\frac{y_{i+1,j} - y_{i-1,j}}{2\Delta\xi} + \frac{y_{i+1,j-1} - y_{i-1,j-1}}{2\Delta\xi} \right]$$

$$= \left[\frac{1 + \delta\cos\xi}{1 + \delta\cos\frac{1}{2}(x_{i,j} + x_{i,j-1})} \right] . \tag{1.4:2b}$$

This equation can then be rearranged with $y_{*,j}$ on the left-hand

side and $y_{*,j-1}$ on the right. Since the solution for x is available at all discrete grid points, this linear implicit equation can be represented as a matrix equation

$$L\,\underline{y} = \underline{b}\ .$$

The vector $\underline{y}$ consists of y at (ξ_i, η_j) for $1 \le i \le N$, and $\underline{b}$ is a known vector of length N. The NxN matrix L is a banded matrix with a band width of 3. The boundary conditions for (1.4:2b) are the values of y on the symmetry lines from equation (1.4:2a), and $y = 0$ on $\eta = 0$. Equation (1.4:2b) is solved by Gaussian elimination with partial pivoting. This can be repeated for the complete computational domain $2 \le j \le M$. Assuming that the step length $\Delta\eta$ is *small*, this method is suitable for a 'well-behaved' function $y(\xi, \eta, t)$. However, it must be stressed that this method can only be used for early times when the boundary layer remains thin (i.e. grad $x \neq 0$).

An alternative for an early-time calculation is to evaluate the integral expression (1.4:1b) for y directly over characteristics of constant x. This approach approximates the integral by a finite summation; therefore to give y at η_j along a path of constant x we have

$$y(x, \eta_j) = \sum_{k=2}^{j} \left[\frac{\Delta\eta}{x_\xi} \frac{1 + \delta\cos\,\xi}{1 + \delta\cos\,x} \right]_{\eta=\eta_{k-1/2}} \qquad \text{on constant x.} \tag{1.4:2c}$$

The summation requires the values of the integrand on characteristics of x at various level of η. The interpolation method used to obtain these is discussed in appendix 1.C.

Close to the onset of the boundary-layer separation fluid particles near the inner wall are 'squeezed', resulting in small values of x_ξ there. The squashed particles can only elongate in the direction normal to the wall, and thus as t tends to t_s there are increasingly large increases in y for moderate increases in η. The methods mentioned above have accuracy difficulties under such circumstances (essentially because the characteristics begin to develop a cusp point).

The first method by which we tried to overcome this problem used Padé approximants. Initially we restricted our attention to the flow at the symmetry line of the inner wall $x = \pi$. A plot of x_ξ against η suggested that here x_ξ was a regular function of η near its minimum, and that its minimum tended to zero monotonically as t tended to t_s. This suggested an approximation for its reciprocal (necessary in (1.4:1b)) of the form

$$\frac{1}{x_\xi} \simeq \frac{A}{\varepsilon+(\eta-\eta_o)^2} + \frac{B(\eta-\eta_o)}{\varepsilon+(\eta-\eta_o)^2} + C \ , \qquad (1.4:3a)$$

where A, B, C, ε and η_o are constants to be determined; in which case, to integrate $\frac{1}{x_\xi}$ from $\eta = \eta_L$ to η_U, we have

$$\int_{\eta_L}^{\eta_U} \frac{1}{x_\xi}\, d\eta \simeq \left[\frac{A}{\sqrt{\varepsilon}} \arctan \frac{(\eta-\eta_o)}{\sqrt{\varepsilon}} + B \ln \left(\varepsilon+(\eta-\eta_o)^2 \right) + C\eta \right]_{\eta_L}^{\eta_U} . \qquad (1.4:3b)$$

In the neigbourhood of a point $\eta = \eta_J$ the five constants were determined by the data values of $\frac{1}{x_\xi}$ at the five neighbouring points, $\eta = \eta_{J-2}$, η_{J-1}, η_J, η_{J+1} and η_{J+2}. The expressions for the

five constants are given in appendix 1.D.

We tried this approximation on a model problem with a known anaytical solution, i.e.

$$\int_0^{\pi} \frac{d\zeta}{f(\zeta)} = \sqrt{\frac{1}{\gamma(\gamma+1)}}\,\pi \ , \qquad (1.4:4)$$

where $f(\zeta) = \gamma + \cos^2\zeta$. The function $f(\zeta)$ is quadratic in ζ near the minimum γ at $\zeta = \frac{\pi}{2}$. The range $0 \le \zeta \le \pi$ was divided into a number of uniform intervals. The approximation (1.4:3b) was found to work well for small γ, giving a truncation error of within 0.67% with 65-grid points for $\gamma = 0.002203$ (this value of γ was specially chosen to correspond to the minimum of x_ξ at $t = 2.8$ for a uniform core velocity of $W_o(t) = 1$).

This method was then applied to the symmetry line problem over that range of η for which x_ξ was approximately quadratic. The improvement over the other methods is not as good as expected from the model problem, probably because x_ξ^{-1} can only be approximated by (1.4:3a) for a small region of η (plus the fact that the model problem is symmetric about the minimum of x_ξ). However, given enough grid points, this approximation is reasonably effective e.g. with 129 grid points, the answer appears to be within approximately 4%. While this is acceptable for the symmetry line problem, the greater complexity of the full problem prevents the use of such fine grids. A new approach was therefore required.

The next method is a characteristic method. In this approach a local Taylor expansion for x is formed about a grid point (ξ_i, η_j) and is used both to trace the path of constant x back to $\eta = \eta_{j-1}$

(see figure 1.4:1) and to approximate x_ξ in (1.4:1b).

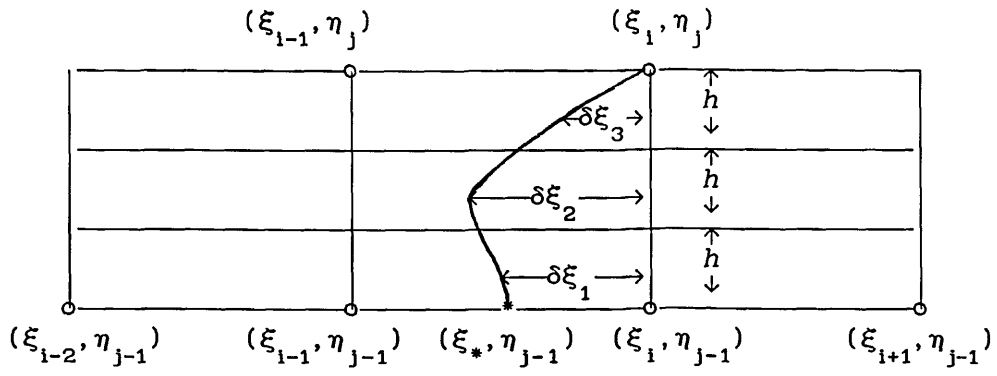


Figure 1.4:1

Specifically, the method is based on the Taylor expansion of $x(\xi, \eta)$ about a grid point $x_o(\xi_i, \eta_j)$:

$$x = x_o + x_{o,\xi}\delta\xi + x_{o,\eta}\delta\eta + \frac{1}{2}x_{o,\xi\xi}\delta\xi^2 + x_{o,\xi\eta}\delta\xi\delta\eta + \frac{1}{2}x_{o,\eta\eta}\delta\eta^2 + \ldots \qquad (1.4:5a)$$

where $\delta\xi = \xi - \xi_i$, $\delta\eta = \eta - \eta_j$ and $|\delta\xi| << 1$, $|\delta\eta| << 1$ (note that the subscript comma has been reintroduced to indicate differentiation). The coefficients in (1.4:5a) are evaluated by central differences about the point (ξ_i, η_j). The characteristic passing through (ξ_i, η_j) is given to second order in $\delta\xi$ and $\delta\eta$ by solving the equation

$$0 = x_{o,\xi}\delta\xi + x_{o,\eta}\delta\eta + \frac{1}{2}x_{o,\xi\xi}\delta\xi^2 + x_{o,\xi\eta}\delta\xi\delta\eta + \frac{1}{2}x_{o,\eta\eta}\delta\eta^2 \,. \qquad (1.4:5b)$$

At a specified value of $\delta\eta$ there exist two roots for $\delta\xi$; the root chosen is that of smallest magnitude since we are considering points close to x_o. The value of x_ξ is then obtained by substituting into

$$x_\xi = x_{o,\xi} + x_{o,\xi\xi}\delta\xi + x_{o,\xi\eta}\delta\eta + \ldots \,. \qquad (1.4:5c)$$

To approximate y accurately where x_ξ is small, it is necessary to make small steps in $\delta\eta$, since a small change in $\delta\eta$ could amount to a large change in y for t close to t_s. Therefore the step from η_{j-1} to η_j was divided into m smaller steps of length h, as shown in figure 1.4:1. With $\eta = \eta_{j-1} + \frac{1}{2}h$ for example, the procedure is to solve first (1.4:5b) for $\delta\xi_1$, in order to find the position of the characteristic of constant x which passes through (ξ_i, η_j). Then x_ξ at $(\xi_i - \delta\xi_1, \eta_{j-1} + \frac{1}{2}h)$ is evaluated from equation (1.4:5c). A similar proedure is followed at $\eta = \eta_{j-1} + (p-\frac{1}{2})h$ for $p \geq 2$. The *increment* in y along the characteristic x between η_{j-1} and η_j is then

$$\sum_{p=1}^{m} \left[\frac{h}{x_\xi} \frac{1 + \delta\cos\xi}{1 + \delta\cos x} \right]_{\eta=\eta_{j-1}+(p-1/2)h} . \qquad (1.4:6)$$

Suppose also the characteristic x intersects $\eta = \eta_{j-1}$ at the point (ξ_*, η_{j-1}), the value of y there is obtained by a cubic interpolant using the known values of y at four neighbouring horizontal points. Once $y(\xi_*, \eta_{j-1})$ has been calculated, $y(\xi_i, \eta_j)$ follows from the addition of (1.4:6) to it. This method works well for small x_ξ.

Finally among other attempted methods, the most successful and robust one was that obtained by rewriting equation (1.4:1b) as

$$\eta_y = \frac{1 + \delta\cos x}{1 + \delta\cos\xi} x_\xi \qquad \text{on constant } x . \qquad (1.4:7)$$

This is a first order ordinary differential equation for $\eta(y)$. The equation is well-behaved and can be integrated by a standard integration scheme along characteristics of x. In the region of small x_ξ, a large increment in y results in a small change in η.

The scheme chosen for the integration was a fourth-order

Runge-Kutta method from the NAG subroutine library. The right-hand side of equation (1.4:7) was required at various values of η on the characteristic of x; it was obtained by interpolation as described in appendix 1.C.

With y known at discrete values of x and η, y could then be approximated at the grid points (ξ_i, η_j) by cubic interpolation. This was required for the calculation of the normal velocity v.

The calculation for the function v is similar to that undertaken for y. For early times of the boundary-layer development, there are no difficulties in finding v. Therefore, from equation (1.2:20b),

$$v(\xi, \eta, t) = -\int_0^{\eta} \frac{1}{1 + \delta\cos x} \frac{u_\xi y_\eta - u_\eta y_\xi}{x_\xi} d\eta \qquad (1.4:8a)$$

constant x

is discretised by a second-order finite difference approximation, and the integrand summed by the trapezium rule on the symmetry lines. Away from the symmetry lines, v is calculated by a Crank-Nicolson approximation to the continuity equation as expressed in (1.2:12c)

$$(u_\xi y_\eta - u_\eta y_\xi) + (1 + \delta\cos x)(x_\xi v_\eta - x_\eta v_\xi) = 0 , \qquad (1.4:8b)$$

using the values of v at the symmetry lines as boundary conditions. Equation (1.4:8b) is discretized by the standard second-order finite difference at grid points $(\xi_i, \eta_{j-1/2})$ for $2 \le i \le N-1$, $2 \le j \le M$. The difference equation can be represented in matrix form. The matrix is solved by Guassian elimination with pivoting.

For later times when the boundary layer is rapidly increasing

near the inner wall, the calculation of v is slightly more complicated. Since the characteristics method works well for the calculation of y, it seems reasonable to try to apply the same technique to calculate v. As before, we express equation (1.2:20b) as an ordinary equation for η,

$$\eta_v = - \frac{x_\xi}{u_\xi y_\eta - u_\eta y_\xi} (1 + \delta \cos x) \qquad \text{on constant } x \ . \tag{1.4:8c}$$

However, this proves to be more difficult to integrate, the reason being that v is not monotonic throughout the computational domain (e.g. for intermediate values of η fluid particles are sucked into the boundary layer at the outer edge of the boundary layer, but are moving away from the wall for smaller values of η). This means it is difficult to decide on a v increment for the integration procedure.

Attempts have been made to combine the standard Crank-Nicolson scheme with the characteristic method. The characteristic method is used over the region in which the right-hand side in (1.4:8c) is close to zero. The integration proceeds as described before with a positive increment of v at every step. Once the solution has been found, cubic interpolation is used to approximate v at grid points $x(\xi_i, \eta_j)$ within the region where x_ξ is small. In the rest of the domain where v is nonsingular, the Crank-Nicolson scheme described above is used.

We conclude that both y and v, i.e. the variables which become singular as separation is approached, can be determined at times close to, but strictly less than, the time at which separation

occurs. However we emphasise that any inacuracy in the y and v does not affect the regular solutions x, u and w. The singularity structure for y and the results are presented in sections 1.5 and 1.6 respectively.

§ 1.5 The Separation Singularity

The unsteady axially-independent flow down a curved pipe of uniform curvature develops a boundary-layer singularity after a finite time t_s. This is caused by fluid particles trying to occupy the same tangential position at one part of the symmetry line of the inner wall, thus resulting in a stationary point in x, i.e. a point where grad x = 0. Due to conservation of mass, as fluid is swept towards the inner wall the particles there can only elongate in the direction normal to the boundary of the pipe, thus thickening the boundary layer and increasing both y and the normal velocity v, eventually without bound. We refer to the process by which fluid particles try to occupy the same tangential position, as a boundary-layer *collision* and interpret the formation of a singularity as the genesis of unsteady boundary-layer separation. It has been indicated, in section 1.2 equations (1.2:19-22), that the boundary layer *separates* in the sense that y and v can increase to infinity at a stationary point (ξ_s, η_s, t_s). This has been confirmed by our numerical results; graphs illustrating this phenomenon are presented and discussed in section 1.6. In this section, we are concerned with the analytical structure of the flow at time close to, but before, the time at which the singularity forms.

Van Dommelen and Cowley (private communication) showed that it is possible to examine the structure of a three-dimensional unsteady boundary-layer separation via a Taylor expansion in a small neighbourhood of the *separating fluid particle* (ξ_s, η_s, t_s).

The stationary point occurs along the symmetry line of the inner wall, i.e. $\xi_s = \pi$. Therefore, we define

$$X = x - x_s, \qquad \psi = \xi - \xi_s, \qquad \mathcal{N} = \eta - \eta_s, \qquad \tau = t_s - t,$$

and denote $x(\xi_s, \eta_s, t_s)$ by x_s (in fact $\xi_s = \pi$). It is hypothesised that the solution for x, u and w remains regular up to the separation time t_s; therefore for $t \leq t_s$ we seek a Taylor expansion for x in a close neighbourhood of (ξ_s, η_s, t_s), i.e. for

$$| X | \ll 1, \qquad | \psi | \ll 1, \qquad | \mathcal{N} | \ll 1, \qquad 0 < \tau \ll 1.$$

Note that the Taylor expansion is valid for all small values of X, ψ and $\mathcal{N}$, and for small and *positive* values of τ (i.e. times before the singularity forms).

The boundary layer around the complete circular cross-section is specified by $-\pi \leq \xi \leq \pi$; if a particle in the upper half is labelled as (ξ, η), the corresponding particle in the lower half is $(-\xi, \eta)$. The flow is symmetrical over the plane of symmetry, $\xi = 0$, therefore

$$x(\xi, \eta, t) = -x(-\xi, \eta, t), \qquad u(\xi, \eta, t) = -u(-\xi, \eta, t).$$

Hence the Eulerian tangential variable x is an odd function of ξ, and therefore all the even derivatives of x with respect to ξ are zero. Similarly using the symmetry about $\xi = \pi$, we have

$$\pi - x(\pi-\xi, \eta, t) = \pi + x(\pi+\xi, \eta, t),$$

$$u(\pi-\xi, \eta, t) = -u(\pi+\xi, \eta, t).$$

From the definition of the singularity point, we have

$$x_\xi(\xi_s, \eta_s, t_s) = x_\eta(\xi_s, \eta_s, t_s) = 0.$$

Thus the Taylor expansion for x in a close neighbourhood of

(ξ_s, η_s, t_s), $X \ll 1$, is

$$X = x_{s12}\psi\mathcal{N} + \frac{1}{6}x_{s111}\psi^3 + \frac{1}{2}x_{s122}\psi\mathcal{N}^2 + \ldots\ldots$$
$$- \tau\,(\,u_{s1}\psi + u_{s12}\psi\mathcal{N} + \ldots\ldots\,) + \ldots\ldots \quad . \qquad (1.5:1a)$$

The subscripts 1 and 2 denote derivatives with respect to ξ and η respectively, and x_{s12} is $x_{\xi\eta}$ evaluated at (ξ_s, η_s, t_s), etc.. Hence all the quantities x_{s12}, x_{s111}, x_{s122}, u_{s1} and u_{s12} are constants. Differentiation of (1.5:1a) with respect to ξ and η respectively gives

$$X_\xi = x_{s12}\mathcal{N} + \frac{1}{2}x_{s111}\psi^2 + \frac{1}{2}x_{s122}\mathcal{N}^2 + \ldots\ldots$$
$$- \tau\,(\,u_{s1} + u_{s12}\mathcal{N} + \ldots\ldots\,) + \ldots\ldots \quad , \qquad (1.5:1b)$$

$$X_\eta = x_{s12}\psi + x_{s122}\psi\mathcal{N} + \ldots\ldots$$
$$- \tau\,(\,u_{s12}\psi + \ldots\ldots\,) + \ldots\ldots \quad . \qquad (1.5:1c)$$

As x approaches the singularity point $X \to 0$, $\psi \to 0$, $\mathcal{N} \to 0$, $\tau \to 0+$; thus $x_\xi \to 0$ and $x_\eta \to 0$ (note that $x_\eta = 0$ on $X = 0$).

From (1.5:1) we see that $X_\xi = 0$ and $X_\eta = 0$ at

$$\mathcal{N} \approx \tau\frac{u_{s1}}{x_{s12}}, \qquad \psi \approx 0 \; . \qquad (1.5:2a,b)$$

Hence, from equation (1.5:2a), unless $x_{s12} = 0$ a stationary point exists for $\tau > 0$, which contradicts the assumption that $\tau = 0$ is the first time that a singularity develops. On assuming $x_{s12} = 0$, it follows that when ψ and $\mathcal{N}$ are small, $X_\xi = X_\eta = 0$ when

$$\frac{x_{s111}}{2u_{s1}}\psi^2 + \frac{x_{s122}}{2u_{s1}}\mathcal{N}^2 \approx \tau, \qquad \psi\mathcal{N} \approx 0 \; . \qquad (1.5:3a,b)$$

Since t_s is the *first* time at which a stationary point develops in

the flow, equation (1.5:3) must have no roots for $\tau > 0$. To exclude this possibility it follows that

$$\frac{x_{s111}}{u_{s1}} < 0 \qquad \text{and} \qquad \frac{x_{s122}}{u_{s1}} < 0 \ . \tag{1.5:4}$$

To describe the singularity structure in full, there should be variations in X etc. as both ψ and N change. To obtain this, the appropriate distinguished scaling must be, from (1.5:3),

$$\psi \sim N \sim \tau^{1/2} \ , \tag{1.5:5a}$$

which, on substitution into (1.5:1a) yields

$$X \sim \tau^{3/2} , \tag{1.5:5b}$$

and hence

$$| \text{ grad } x | \sim x_{\xi} \sim x_{\eta} \sim \tau \ . \tag{1.5:5c}$$

The scaling (1.5:5c) is confirmed by our numerical results which are discussed in section 1.6.

The variable $y(x, \eta)$ becomes singular at the stationary point (ξ_s, η_s, t_s). To examine the nature of the singularity as the flow approaches separation for times close to, but before t_s, an asymptotic approximation of y,

$$y(\xi, \eta, t) = \int_{\substack{0 \\ \text{constant } x}}^{\eta} \frac{1 + \delta\cos \xi}{1 + \delta\cos x} \frac{d\eta}{x_{\xi}} \qquad \text{(from (1.2:19a))} \ ,$$

is required. Now, if we assume that $\delta << 1$,

$$\frac{1 + \delta\cos \xi}{1 + \delta\cos x} \sim 1 \qquad \text{for all values of } x \text{ and } \xi,$$

and therefore, from equation (1.5:5),

$$y \sim \frac{\tau^{1/2}}{\tau} \sim \tau^{-1/2}, \qquad (1.5:6)$$

as $\tau \to 0+$. The scalings prosposed in equations (1.5:5,6) have been checked with our numerical results. Good agreement is observed. This is explained in detail in section 1.6.

From scaling (1.5:5b), we deduce

$$u \sim \tau^{1/2} \qquad (1.5:7)$$

and from (1.5:6),

$$\frac{u}{\tau} \sim \frac{u^2}{X} \gg \frac{u}{y^2}. \qquad (1.5:8)$$

Therefore the unsteady term is of the same order of magnitude as the inertia term, both of which dominate the viscous diffusion. The singularity is thus primarily *inviscid* in a region which is seen from equations (1.5:5b, 6) to be of width $\tau^{3/2}$ in the X direction and height $\tau^{-1/2}$ in the y direction - see figure 1.5:1.

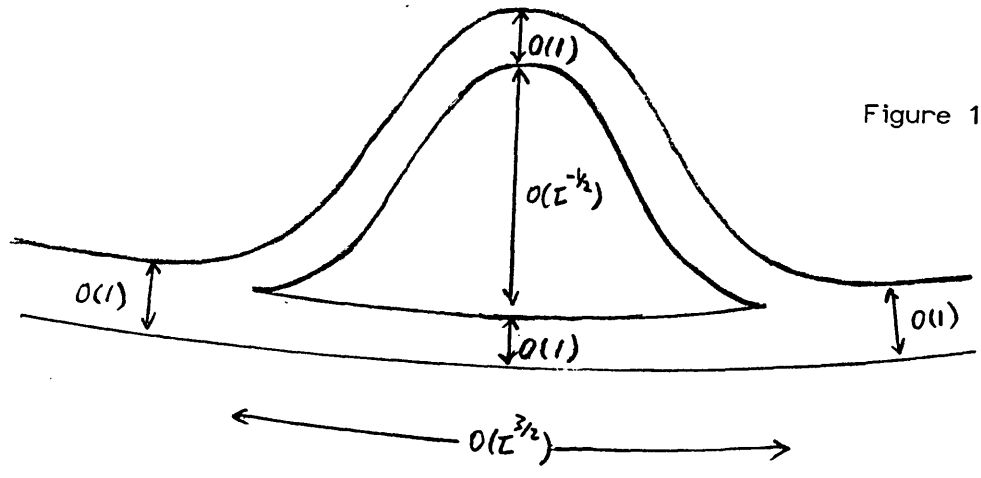


Figure 1.5:1

Two 'sandwich' layers exist at the bottom and on the top of this 'central' inviscid region. The transition layers are those regions where |grad x| is *not* small, and hence, from (1.2:19b), y

will vary by an O(1) distance across them. In these zones $X = O(\psi)$, $u = O(\psi)$, hence from (1.5:5b) $u = O(\tau^{3/2})$, i.e. the velocities in these zones are very much less than the velocity in the central region.

To obtain a more precise description of y as $\tau \to 0+$, the quantities X, ψ, N and y are rescaled as follows:

$$\tau^{3/2}\tilde{x} = X, \qquad \tau^{1/2}\tilde{\xi} = \psi, \qquad \tau^{1/2}\tilde{\eta} = N, \qquad \tau^{-1/2}Y = y \ . \tag{1.5:9}$$

Substitution of equations (1.5:9a,b,c) into (1.5:1), and evaluation of the resulting expressions correct to $O(\tau^{3/2})$, $O(\tau)$ and $O(\tau)$ respectively, yields (note that x_{s12} is assumed zero)

$$\tilde{x} = \frac{1}{6} x_{s111}\tilde{\xi}^3 + \tilde{\xi}\left(\frac{1}{2} x_{s122}\tilde{\eta}^2 - u_{s1} \right) \tag{1.5:10a}$$

$$\tilde{x}_{\tilde{\xi}} = \frac{1}{2} x_{s111}\tilde{\xi}^2 + \left(\frac{1}{2} x_{s122}\tilde{\eta}^2 - u_{s1} \right) , \tag{1.5:10b}$$

and

$$\tilde{x}_{\tilde{\eta}} = x_{s122}\tilde{\xi}\tilde{\eta} \ . \tag{1.5:10c}$$

For simplicity, we set δ to zero, then Y is given by

$$Y - Y_0 = \int_0^{\tilde{\eta}} \frac{d\tilde{\eta}}{\tilde{x}_{\tilde{\xi}}} \qquad \text{on constant } \tilde{x} \tag{1.5:11}$$

where Y_0 is Y evaluated at $\tilde{\eta} = 0$, i.e. $\eta = \eta_s$. We consider a particle above η_s (a similar argument applies to that below) such that $\tilde{\eta} \geq 0$. From the numerical calculations we expect $Y \geq Y_0$, and this can be so if and only if

$$\tilde{x}_{\tilde{\xi}} > 0 \ . \tag{1.5:12a}$$

From equation (1.5:10b) this condition can be expressed as

$$\frac{1}{2} x_{s111} \tilde{\xi}^2 + \left(\frac{1}{2} x_{s122} \tilde{\eta}^2 - u_{s1} \right) > 0 , \qquad (1.5:12b)$$

which implies

$$u_{s1} < 0 , \qquad (1.5:13a)$$

(by taking $\tilde{\xi} = \tilde{\eta} = 0$ in equation (1.5:12b)) and

$$x_{s111} > 0 \quad \text{and} \quad x_{s122} > 0 , \qquad (1.5:13b)$$

(by taking $\tilde{\xi} \to \infty$, $\tilde{\eta} \to \infty$).

To evaluate y it is necessary to identify the paths of characteristics of constant x in $(\tilde{\xi}, \tilde{\eta})$ space. For given $\tilde{x}$ and $\tilde{\eta}$, equation (1.5:10a) is a cubic equation for $\tilde{\xi}$, indicating that three roots exist. From (1.5:12b) (or equivalently (1.5:4)) it follows that the right-hand side of (1.5:10a) is a strictly monotonic function of $\tilde{\xi}$, and hence there is one *unique* real root for $\tilde{\xi}$ given $\tilde{x}$ and $\tilde{\eta}$. For convenience, we denote $\tilde{\xi}_0$ as the solution for $\tilde{\xi}$ at $\tilde{\eta} = 0$ on a characteristic $\tilde{x}$.

An alternative expression for Y is then

$$Y(\tilde{\xi}) - Y_0 = - \int_{\tilde{\xi}_0}^{\tilde{\xi}} \frac{d\tilde{\xi}}{x_{\tilde{\eta}}} \qquad \text{on constant } \tilde{x} \qquad (1.5:15a)$$

$$\approx - \int_{\tilde{\xi}_0}^{\tilde{\xi}} \frac{d\tilde{\xi}}{x_{s122}} \qquad \text{on constant } \tilde{x}, \qquad (1.5:15b)$$

from equation (1.5:10c). Substitution of $\tilde{\eta}$ from equation (1.5:10a) into (1.5:15b) and algebraic manipulation yields

$$Y(\tilde{\xi},\ \tilde{\eta}) - Y_0 \approx \frac{\pm 1}{2\sqrt{\frac{1}{12}\chi_{s111}\chi_{s122}}} \int_0^{\mu(\tilde{\xi})} \frac{d\zeta}{\sqrt{1 - m^2\sin^2\zeta}} \qquad (1.5:16a)$$

where the upper limit $\mu(\tilde{\xi})$ is

$$\mu(\tilde{\xi}) = 2 \arctan \sqrt{\frac{q(\tilde{\xi}_0 - \tilde{\xi})}{p\tilde{\xi}}},$$

and the constants q, p and m are

$$q = \sqrt{\frac{6\tilde{\chi}}{\chi_{s111}\tilde{\xi}_0}}, \qquad p = \sqrt{q^2 + 2\tilde{\xi}_0^2}, \qquad m = \sqrt{\frac{\tilde{\xi}_0^2 - (p-q)^2}{4pq}}.$$

Equation (1.5:16a) is an elliptical integral and can be expressed as

$$Y(\tilde{\xi},\ \tilde{\eta}) - Y_0 \approx \frac{\pm 1}{2\sqrt{\frac{1}{12}\chi_{s111}\chi_{s122}}} F\left(\mu(\tilde{\xi}) \mid m\right) \qquad (1.5:16b)$$

where F is an elliptic integral of the first kind. To fix the position, Y_0, of the 'separating' particle (ξ_s, η_s, t_s), note that as $\tilde{\eta} \to -\infty$ the position $Y(\tilde{\xi},\ \tilde{\eta})$ of the particles must match onto the position of the particles in the lower sandwich layer. Because of the scaling (1.5:9) this means that as $\tilde{\eta} \to -\infty$, we require $Y - Y_0 \to 0$. Also from (1.5:10a), $\tilde{\eta} \to -\infty$ implies $\tilde{\xi} \to 0$; hence from (1.5:16b)

$$Y_0 \approx \frac{1}{\sqrt{\frac{1}{12}\chi_{s111}\chi_{s122}}} F\left(\frac{\pi}{2} \mid m\right). \qquad (1.5:17a)$$

In terms of y, the position of the separating particle as the separation time is approached, $\tau \to 0+$, is thus

$$y_0 \approx \frac{\tau^{-1/2}}{\sqrt{\frac{1}{12} x_{s111} x_{s122}}} F\left(\frac{\pi}{2} \mid m\right) . \qquad (1.5:17b)$$

This singularity structure is shown to be consistent with our numerical results in section 1.6.

§ 1.6 Results

The governing equations (1.2:7a,8) for unsteady, axially-independent boundary-layer flow through a circular curved pipe of constant ratio of curvature δ have been successfully integrated in Lagrangian coordinates (ξ, η) for a number of inviscid core velocities $W_o(t)$, the choice of which is discussed later. We note that regular solutions for x, u and w can be obtained at times larger than that when $|\text{grad } x|$ first becomes zero, i.e. the separation time t_s, however, the validity of the solution at such times is unclear.

Singh (1974) showed that the slip velocity $W_o(t)$ can be any analytical function of t. To study different starting conditions a number of different time variations of the general form

$$W_o(t) = A + B\sin \omega t, \qquad (1.6:1a)$$

have been used. A = 1 and B = 0 corresponds to an impulsively started uniform flow, while A = 0 and B = 1 corresponds to an oscillating flow (cf. Lyne's (1970) large time analysis for the case when $\omega >> 1$). Numerical solutions have been obtained for a range of A, B and ω. In addition, we have tried a more physiologically relevant flow

$$\begin{aligned} W_o &= \frac{4t}{t_1}\left[1 - \frac{t}{t_1}\right] && \text{for } 0 \le t \le t_1 \\ &= 0 && \text{for } t < t \le t_2 \end{aligned} \qquad (1.6:1b)$$

where $t_1 \simeq 11.926$, $t_2 \simeq 35.777$ and $\delta = 0.2$[1]. This is a crude model for blood flow in the ascending aorta (e.g. see Pedley (1980)). However, unless specified otherwise, the numerical results presented here were obtained with $W_o(t) = 1$ and $\delta = 0$.

As indicated in earlier sections, one aspect of the flow which is of primary interest is whether there is a finite time, t_s, at which a zero develops in grad x. To determine the value of any separation time t_s we plot $\min_{\xi,\eta} |\text{grad } x|$ of the solution against t. For example, figure 1.6:1 is for the case $W_o = 1$. Note that a singularity time exists, and relatively close to it $|\text{grad } x|$ has the linear behaviour of (1.5:5c). Because of numerical difficulties in obtaining accurate values of grad x very close to zero, the separation time t_s is found by extending the portion of the curve which is straight through to its intersection with $|\text{grad } x| = 0$. The position of the 'separating' fluid particle is denoted by (ξ_s, η_s) where $\xi_s = \pi$ from our numerical results; however, η_s has to be approximated by applying a similar linear relationship to the η position at which $\min_{\xi,\eta} |\text{grad } x|$ occurs.

Standard numerical checks were performed. For example, the criterion for the convergence of the line iteration was varied between $0.5\text{x}10^{-4}$ and $0.5\text{x}10^{-9}$. This variation produced no

---

[1] Pedley (1980) examined a boundary-layer flow with this core velocity using an expansion in powers of $t^{1/2}$ ($t \ll 1$). His series solution is valid for $t \leq 4.025$, beyond which neglected higher-order terms appear to become important.

significiant convergence problems, and did not significantly change the results. The solution with $W_o(t) = 1$ has been obtained with three different grid sizes 37x17, 73x33 and 145x65 with $\Delta t = \frac{1}{40}$, $\frac{1}{80}$ and $\frac{1}{160}$ respectively (for the other choices of $W_o(t)$ only the first two grid sizes were used because of the lengthy computational time required). In addition the solutions were shown to be second-order accurate, thus allowing Richardson extrapolation to be applied to give improved results. With $W_o(t) = 1$ extrapolation was performed on the pairs of grids 37x17, 73x33 and 73x33, 145x65. Sample results are given in table 1.6:1a.

Table 1.6:1a $W_o(t) = 1$, $\delta = 0$

grid	t_s	Extrapolated t_s
37x17	2.828	
		2.813
73x33	2.817	
		2.813
145x65	2.814	

The position of the fluid particle (ξ_s, η_s) at which grad $x(\xi_s, \eta_s, t_s) = 0$, is $\xi_s = \pi$ and $\eta_s = 1.133$. By the time the flow separates at $\hat{t} = \frac{2.813a}{\delta^{1/2}\bar{W}}$, this particle has travelled approximately a dimensional distance $1.7031a\delta^{-1/2}$ down the pipe along the inner wall.

The extrapolated values of t_s from grid sizes 37x17 and 73x33 for other core velocities $W_o(t)$ with $\delta = 0$ are listed in table 1.6:1b.

Table 1.6:1b

$W_o(t)$	Extrapolated t_s
$1 + \sin 2t$	1.619
$1 + \sin t$	1.769
$1 + \sin \frac{1}{2}t$	2.0457
$1 - \sin t$	4.646

As might be expected from the physical arguments given earlier, all the boundary-layer collisions/singularities occur at the inner wall, $x_s = \pi$. Note that the addition of 'positive' pulsation to a non-zero mean leads to an earlier singularity time because in the period before the singularity forms the core flow velocity is effectively increased. For the same reason, a decreased core flow, e.g. $W_o = 1 - \sin t$, leads to a later separation time.

More detailed results have been obtained for the core velocity profile (1.6:1b) with $\delta = 0.2$ which Pedley (1980) used to model blood flow in the aorta. Solutions on three different grid sizes have been obtained: 37x17, 73x33 and 145x65 with $\Delta t = \frac{1}{40}$, $\frac{1}{80}$ and $\frac{1}{160}$ respectively, yielding the results listed in table 1.6:1c.

Table 1.6:1c

grid	t_s	Extrapolated t_s
37x17	4.1796	
		4.1789
73x33	4.1791	
		4.1787
145x65	4.1788	

This gives a dimensional separation time of $\frac{4.179a}{\delta^{1/2}\bar{W}}$ (cf. Pedley's estimate that the series solution is only valid for $t \leq 4.025$).

Detailed results for $W_o(t) = 1$ and $\delta = 0$

Figures 1.6:2-6 plot the flow resulting from the impulsively started motion, $W_o(t) = 1$, for t close to $t_s \simeq 2.813$. The left boundary represents the outer wall $\xi = x = 0$ and the right, the inner wall $\xi = x = \pi$. The bottom boundary similarly represents the surface of the pipe, $y = \eta = 0$, while the top boundary, $y = 10$, $\eta = 5$, is near the edge of the boundary layer. To produce the contour plots, the graphics package 'Tile, Solid and Conicon' was used to interpolate quantities (e.g. w) from the irregular mesh $(x_{i,j}, y_{i,j})$ to a regular grid. Contour plots were then produced from the regular grid. Each contour is labelled with a number, with the corresponding value being displayed in the key to the right of the plot for $t = 2.0$.

Figure 1.6:2 illustrates the characteristics of constant x in Lagrangian coordinates (ξ, η). As a rough guide, the greater distance between two characteristics, the smaller grad x, and hence the harder the fluid particles are being 'squashed'. The drift of the characteristics to the left between the boundaries indicates that fluid particles are being swept toward the inner wall by the excess pressure gradient.

Figure 1.6:3 displays lines of constant axial velocity $\frac{\bar{W}}{1+\delta\cos x}$ in the flow field (x, y) at different times. With $W_o(t) = 1$, the axial velocity ranges from 0 at $y = 0$ and to 1 as

$y \to \infty$. Contour 7, i.e. $\bar{w} = 0.9$, gives a rough indication of the position of the 'top' of the boundary layer. As t increases, there is an increase of the thickness of the boundary layer near the inner wall, indicated by the lifting-up of the contour lines there. Note that the anticipated thinning of the layer at the outer wall is not so obvious from the plots.

A streamfunction, ψ, can be introduced for the secondary motion, where

$$\psi_y = u, \qquad \psi_x = -(1 + \delta\cos x)v \ . \qquad (1.6:2a)$$

In Lagrangian coordinates (ξ, η), we obtain

$$\psi_\eta = \frac{1 + \delta\cos \xi}{1 + \delta\cos x} \frac{u}{x_\xi} \qquad \text{on constant } x \ . \qquad (1.6:2b)$$

Therefore ψ can be obtained by integrating η_ψ,

$$\eta_\psi = \frac{1 + \delta\cos x}{1 + \delta\cos \xi} \frac{x_\xi}{u} \qquad \text{on constant } x \ , \qquad (1.6:2c)$$

in a similar way to the calculation of y using a characteristic method last discussed in section 1.4. Figure 1.6:4 illustrates the contour plots of the instantaneous streamfunction ψ in the (x, y) flow field at different times (the arrows point in the direction of fluid motion). These graphs indicate the same phenomenon of fluid particles drifting from the outer wall to the inner. The increase in 'blowing velocity' on the inner wall as t_s is approached is indicated by the convergence of the streamlines near the inner wall.

Figures 1.6:5 are 'scatter' plots of fluid particles (ξ, η), illustrating their motion through (x, y) space. The data required for these plots was obtained by cubic interpolation from the

solutions of $x(\alpha,\beta,t)$ and $y(\alpha,\beta,t)$. Figure 1.6:5a gives the initial positions of the fluid particles at $t = 0$. Fluid particles starting at the same height, i.e. at the same y values, are joined by a solid line, and different markers are used to distinguish fluid particles at diffierent x positions. The boundary layer becomes thinner near the outer wall as time increases (e.g. the fluid particle at $x = 0$, $y \simeq 8.7$ at $t = 0$ ends up at $x = 0$, $y \simeq 7.0$, at $t = 2.8$), and thicker near the inner wall, this is indicated by the lifting up of the solid lines there. Note that a 'separating' particle must exist on the symmetry line of inner wall below which particles remain close to the boundary of the pipe, and above which particles shoot off to infinity. The first phenomonon is illustrated by the lowest solid line remaining completely within the boundary layer at $t = 2.8$, the second by all the lines above it disappearing out of the graphics window near the inner wall.

In a wide number of applications heat and mass transfer between the wall and the core flow is important. Clearly the ejection of fluid which has been relatively close to the boundary out into the core flow, as occurs in unsteady separation, will help this mixing process. However, we note that the unsteady separation phenomenon here, in which only the upper half of the boundary layer is ejected into the core, is possibly not as efficient as steady spearation in which the whole boundary layer, including particles which have been arbitrarily close to the wall, is lifted up and expelled into the core flow.

Figure 1.6:6 shows the direction and magnitute of the velocity $(\frac{u}{1+\delta\cos x}, v)$ of the fluid particles shown in Figure 1.6:5.

Initially, there is no secondary motion at $t = 0$ (Figure 1.6:6a). As secondary motion develops, we note that in agreement with the other graphs, the secondary velocity is from the outer wall to the inner. Fluid particles travel towards the boundary of the pipe near the outer wall, and away from it near the inner wall. We also note that the magnitude of the velocity at the inner wall increases significantly as it approaches separation.

In section 1.5 an asymptotic singularity structure was proposed for the times close to the separation time t_s. It was concluded that the singularity lengthscales behave like

$$(x_s - x) \sim (t_s - t)^{3/2}, \qquad y \sim (t_s - t)^{-1/2} \qquad (1.6:3a,b)$$

(see equations (1.5:5b, 6)). If this singularity structure is correct, and if the numerical results have adequate resolution, then a plot of $\left[y-y(t=0)\right](t_s-t)^{1/2}$ against $(x_s-x)(t_s-t)^{-3/2}$ for suitable fixed $\eta \geq \eta_s$ and different t should tend to a single curve as $(t_s-t) \to 0$. In figures (1.6:7a, b), graphs of $(y-\eta+c)(t_s-t)^{1/2}$ against $(x_s-x)(t_s-t)^{-3/2}$ have been plotted for $\eta = 5$ and $\eta = 10$ at times $t = 2.7$, 2.75 and 2.8. The value of t_s used was that given earlier, i.e. $t_s = 2.813$ and the constant $c = 5.5$ is included in an attempt to take into account the higher-order corrections in y (cf. equation (1.5:6)). The graphs collapse onto each other and the relationship seems independent of the position of $\eta > \eta_s$. The singularity structure thus appears to be confirmed. Note that other authors (e.g. Simpson and Stewartson (1982a,b)) who have worked on the similar problems of the impulsively rotated sphere and the impulsively heated circular cylinder, have previously obtained the

numerical behaviour of $y \sim (t_s - t)^{-1/2}$, however the confirmation of relevent $(x_s - x)$ scale appears to be new.

The axial displacement thickness $\mathcal{B}$ is defined as

$$\mathcal{B} = \int_o^\infty \left(1 - \frac{\bar{w}}{W_o} \right) dy \qquad (1.6:4a)$$

$$= \int_o^\infty \frac{w}{W_o} dy \, . \qquad (1.6:4b)$$

Since y can be approximately divided into three layers as discussed in section 1.5 (see figure 1.5:1), the displacement thickness can be expressed as

$$\mathcal{B} = \frac{1}{W_o} \left[\int_o^{\lambda_1} w \, dy + \int_{\lambda_1}^{2Y_o \tau^{-1/2} - \lambda_2} w \, dy + \int_{2Y_o \tau^{-1/2} - \lambda_2}^{\infty} w \, dy \right]$$

where

$$1 \ll \lambda_1, \lambda_2 \ll \tau^{-1/2} \, , \qquad (1.6:5)$$

$\tau = t_s - t$, and $Y_o \tau^{-1/2}$ is the y position of the 'separating' fluid particle (cf. equation (1.5:17a)). Throughout the central $O(\tau^{-1/2})$ region, including $y \sim \lambda_1$ and $y \sim 2Y_o \tau^{-1/2} - \lambda_2$, $w \sim w_s = w(\xi_s, \eta_s)$. In the two O(1) layers,

$$w \sim O(1) \, .$$

The leading order contribution of the first, second and third integrals are respectively,

(i) $O(1) + w_s \lambda_1$ (1.6:6a)

(ii) $2w_s Y_o \tau^{-1/2} - w_s(\lambda_2 + \lambda_1)$ (1.6:6b)

(iii) $O(1) + w_s \lambda_2$. (1.6:6c)

Therefore, the main contribution is from the second integral and

$$\mathcal{B} \sim \frac{2W_s}{W_o} Y_o \tau^{-1/2} + O(1) \ . \qquad (1.6:7a)$$

From our numerical results for $W_o = 1$,

$$\mathcal{B} \sim 0.963 Y_o \tau^{-1/2} + O(1) \ . \qquad (1.6:7b)$$

We note that both y and $\mathcal{B}$ have the same singularity structure at $\tau \to 0$, in particular,

$$\mathcal{B} \sim \frac{W_s}{W_o} y + O(1) \qquad (1.6:8)$$

at the top of the boundary layer. Therefore, figure 1.6:7 quantitatively represents the relationship between axial displacement thickness and x.

As discussed in secion 1.1, there may exist a correlation between the positions of distribution of atherosclerotic lesions and wall shear. Therefore, it is important to understand the development of wall shear with time. In figures 1.6:8 and 1.6:9 the circumferential and axial wall shear,

$$\frac{1}{1 + \delta \cos x} \frac{\partial u}{\partial y} \quad \text{and} \quad - \frac{1}{1 + \delta \cos x} \frac{\partial w}{\partial y} \qquad (1.6:9a,b)$$

respectively, are plotted against x for different values of $t < t_s$. Figures 1.6:8a and 1.6:8b correspond to $W_o(t) = 1$ with $\delta = 0$, while figures 1.6:9a and 1.6:9b are for the more physiologically relevent flow, as expressed in equation (1.6:1b) with $\delta = 0.2$. The secondary wall shear in both figures is qualitively similar. The steeper slopes near the inner wall in figiure 1.6:9a are due to the non-zero δ. Note that in figure 1.6:9b the axial wall shear has a

minimum at the outer wall and a maximum at the inner wall for small t, $t \leq 2$, whereas for larger times, the maximum wall shear is away from the symmetry lines, and the wall shear near the inner wall is less than that at the outer wall.

Both the physical reasoning and the numerical results suggest that the boundary-layer separation occurs at the inner wall, $x = \pi$. Therefore, if we assume that the separation occurs at the symmetry line at a finite time, we can restrict our attention to this line, where, as mentioned before in section 1.3, the flow can be examined by making a Taylor expansion.

To examine the precise dependence of the flow on δ, a parameter $\varepsilon = (1-\delta)$ is defined, and all the quantities defined in (1.3:4) are rescaled in terms of ε. New variables $\hat{t}$, $\hat{\eta}$, $\hat{x}$, $\hat{u}$ and $\hat{w}$ are introduced

$$t = \varepsilon^{3/2}\,\hat{t}, \qquad \eta = \varepsilon^{3/4}\hat{\eta},$$
$$x^{*} = \hat{x}, \qquad u^{*} = \varepsilon^{-1/2}\hat{u}, \qquad w^{*} = \hat{w}, \tag{1.6:10}$$

and then substituted into equations (1.3:9), yielding

$$\hat{u} = \hat{x}_{\hat{t}} \tag{1.6:11a}$$

$$\hat{u}_{t} + \hat{x}\,\hat{w}(2W_{o} - \hat{w}) = \hat{x}^{2}\,\hat{u}_{\hat{\eta}\hat{\eta}} - \hat{x}\,\hat{x}_{\hat{\eta}}\hat{u}_{\hat{\eta}} + (\hat{x}_{\hat{\eta}}^{2} - \hat{x}\,\hat{x}_{\hat{\eta}\hat{\eta}})\hat{u} \tag{1.6:11b}$$

$$\hat{w}_{t} = \hat{x}^{2}\,\hat{w}_{\hat{\eta}\hat{\eta}} + \hat{x}\,\hat{x}_{\hat{\eta}}\hat{w}_{\hat{\eta}} \tag{1.6:11c}$$

with boundary conditions,

$$\begin{aligned}
&\hat{x} = 1, \quad \hat{u} = 0, \quad \hat{w} = W_o(t) \quad \text{at } \hat{\eta} = 0 , \\
&\hat{x} \to 1, \quad \hat{u} \to 0, \quad \hat{w} \to 0 \quad \text{at } \hat{\eta} \to \infty , \\
&\hat{x} = 1, \quad \hat{u} = 0, \quad \hat{w} = 0 \quad \text{at } \hat{t} = 0+, \ \hat{\eta} > 0
\end{aligned} \tag{1.6:11d}$$

Equations (1.6:11) are the same as (1.3:4) with δ equal to zero. This implies that the boundary-layer flow at the symmetry line of the inner wall is self similar. The solution obtained with one value of δ, say $\delta = 0$, can easily be scaled to account for a different curvature effect. In particular the separation time t_s is modified with curvature by a factor of $(1-\delta)^{3/2}$, i.e. the larger the curvature, the earlier the singularity develops on the symmetry line.

Note that not all high-Dean-number flows down a curved pipe necessarily develop a boundary-layer separation at the inner wall, cf. Lyne's (1970) fast frequency analysis. Let us restrict our attention to

$$W_o(t) = \sin \omega t.$$

If flow down a curved pipe is started with a slow frequency core velocity, i.e. $\omega << 1$, the flow is similar to an impulsively started flow, and therefore, boundary-layer separation most probably occurs after a finite time. However with a fast frequency $\omega >> 1$, this need not be the case. In fact our calculations on the symmetry line of the inner wall, show that for small $\omega < 1.1$, unsteady boundary-layer separation occurs; for example as ω is increased from 0.001 to 1.1, t_s decreases from approximately 80.5

to 4.95. However, for $\omega > 1.2$ no boundary-layer separation was found at the symmetry line of the inner wall. For such values of ω, separation may occur off the symmetry line or at the outer wall, alternatively no separation may occur.[2] Indeed, in preliminary runs with larger values of ω there was evidence suggesting that unsteady boundary-layer separation might occur at the symmetry line of the outer wall at some large time, e.g. for $\omega = 1.2$, t_s was approximately 26. However, the accuracy of these results at such large time requires further investigation. An alternative for large ω is to seek a solution consisting of a Stokes layer at leading order. However we note that this cannot equal Lyne's (1971) high-frequency solution since with our scaling the secondary flow in the core is much less than in the boundary layer, whereas in Lyne's solution they are comparable. A high-frequency solution of our equations is therefore likely to include a 'diffusive wave', consisting of a non-zero secondary velocity, which slowly diffuses towards the core.

The mathematical formulation of our problem is applicable for O(1) values of δ, though an experiment is only possible for a loosely coiled pipe, i.e. $\delta \ll 1$. A more realistic model would be a pipe with variable curvature, but then the simplifying z-dependence

---

[2] In a test case with $\omega = 1.2$, a full calculation using a 145x65 grid suggested that no unsteady boundary-layer separation occurs for t up to 13.20 although this does not rule out separation at a later time.

could be lost. Alternatively a helical pipe might be considered (see e.g. Truesdell and Alder (1970), Snyder, Hammersley and Olson (1985), and Kao (1987)). However the simplifying symmetry assumptions could then be lost, and the separation singularity would most likely have the form studied by Van Dommelen and Shen (1982) as extended to three dimensions by Van Dommelen and Cowley (private communciation).

Summary

The unsteady boundary-layer problem of a starting flow down a curved pipe has been formulated in Lagrangian coordinates. Stable numerical solutions have been obtained using an Alternating Direction Implicit method which appears to be robust with no significant convergence difficulties. When the core flows are of slow frequency unsteady boundary-layer separation occurs at the symmetry line of the inner wall at finite times. A number of core flows have been studied. In particular, a crude model of blood flow in the aorta, suggested by Pedley (1980), has been used, and the resulting boundary-layer has been shown to develop unsteady boundary-layer separation at the inner wall relatively early in systole.

An asymptotic separation singularity structure has been proposed. Using numerical solutions for $W_o = 1$ as an example, this structure has been confirmed both on and off the symmetry line of the inner wall. This confirmation was possible since in Lagrangian coordinates the boundary layer momentum equations are independent of the variables y and v, that become singular at separation. These singular quantities can be calculated independently, and with good accuracy, once the solution for x, u and w has been obtained.

Although the governing equations can be integrated beyond separation times in Lagrangian coordinates, the validity of the solutions remain unclear since a singularity exists which contradicts the basic assumption that the boundary-layer thickness is O(1). Therefore, a new interactive theory is most probably

needed for flows at times greater than the separation time.

Figure 1.6:1 $W_o = 1$, $\delta = 0$

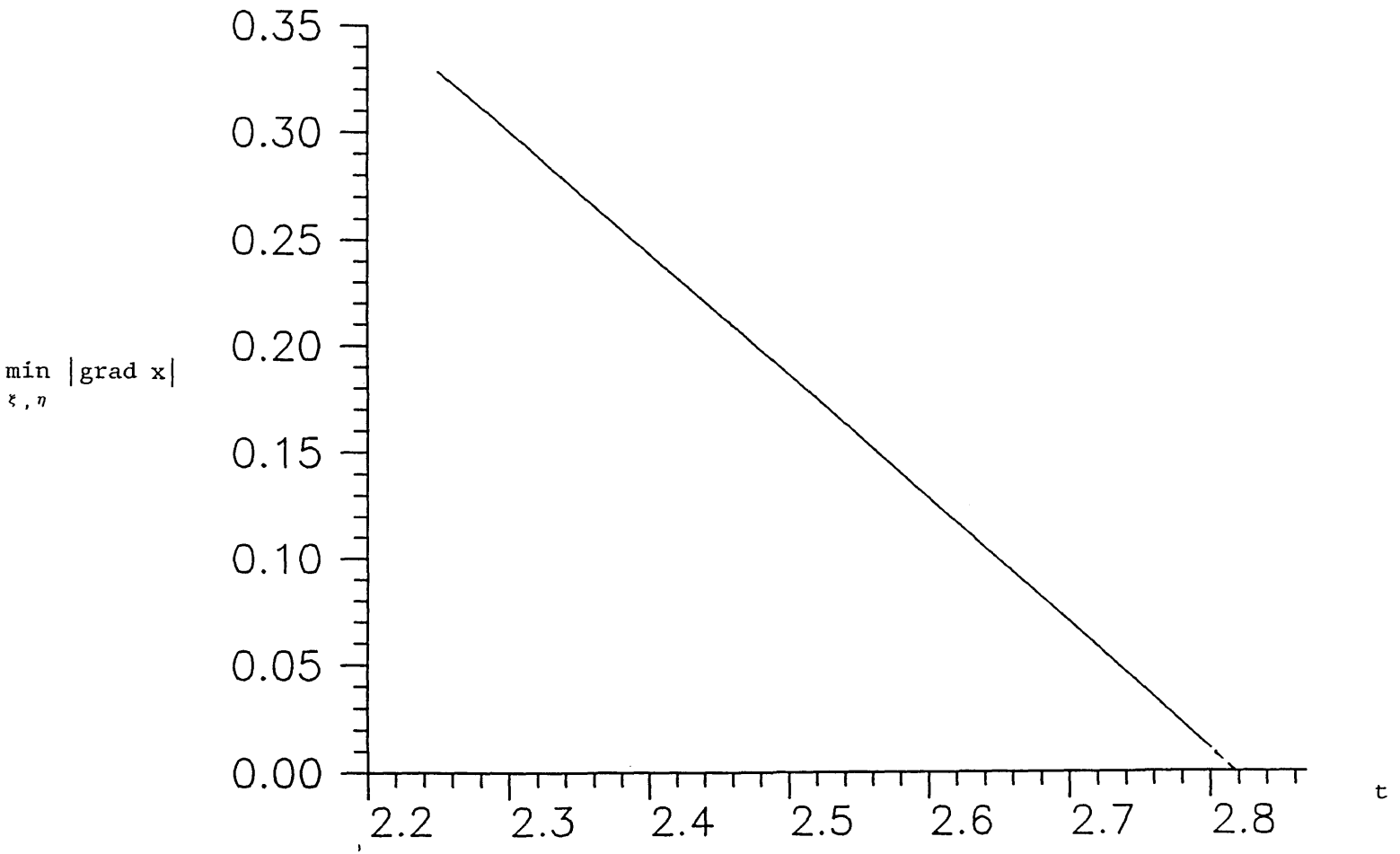


Figure 1.6:2a

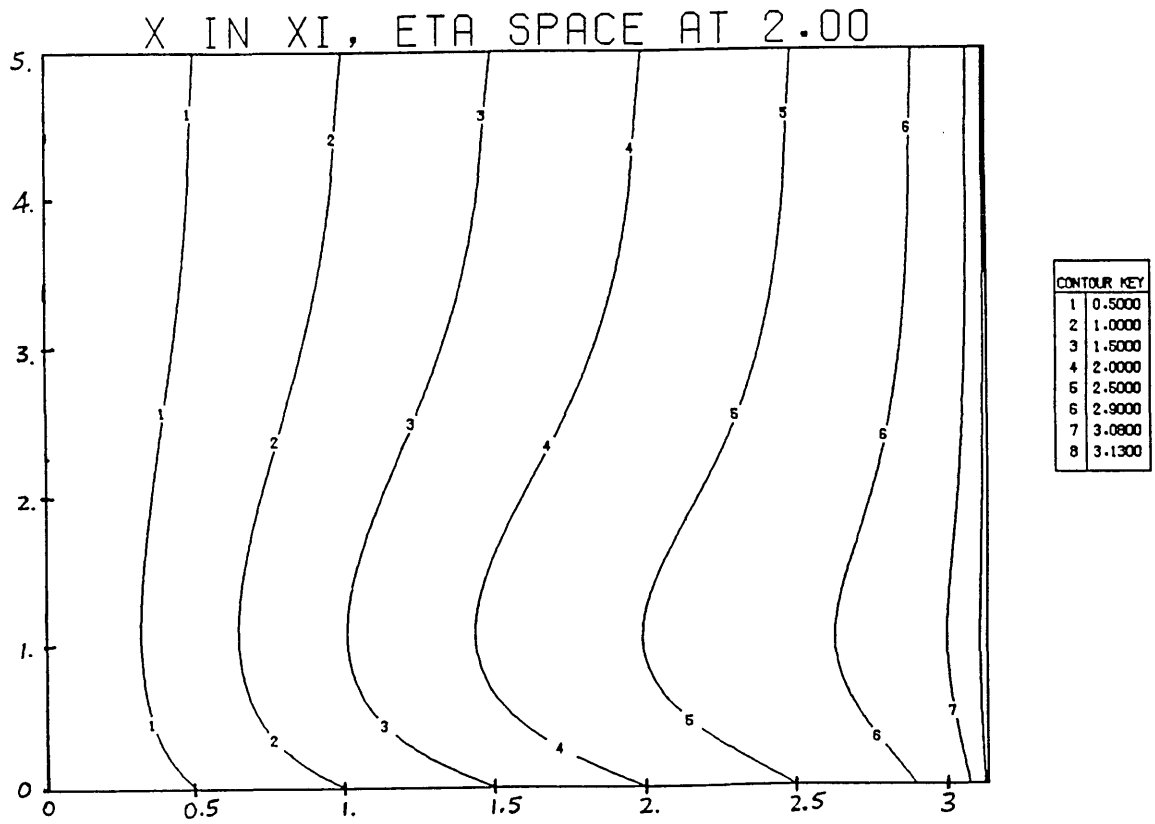


Figure 1.6:2b

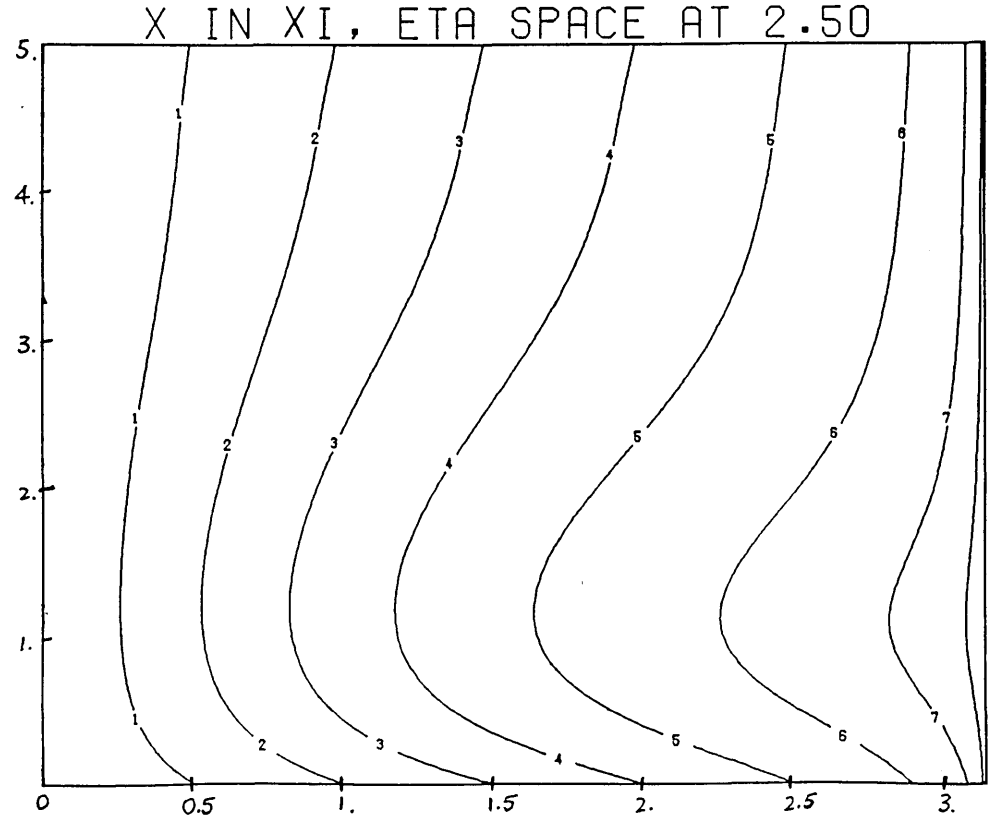


Figure 1.6:2c

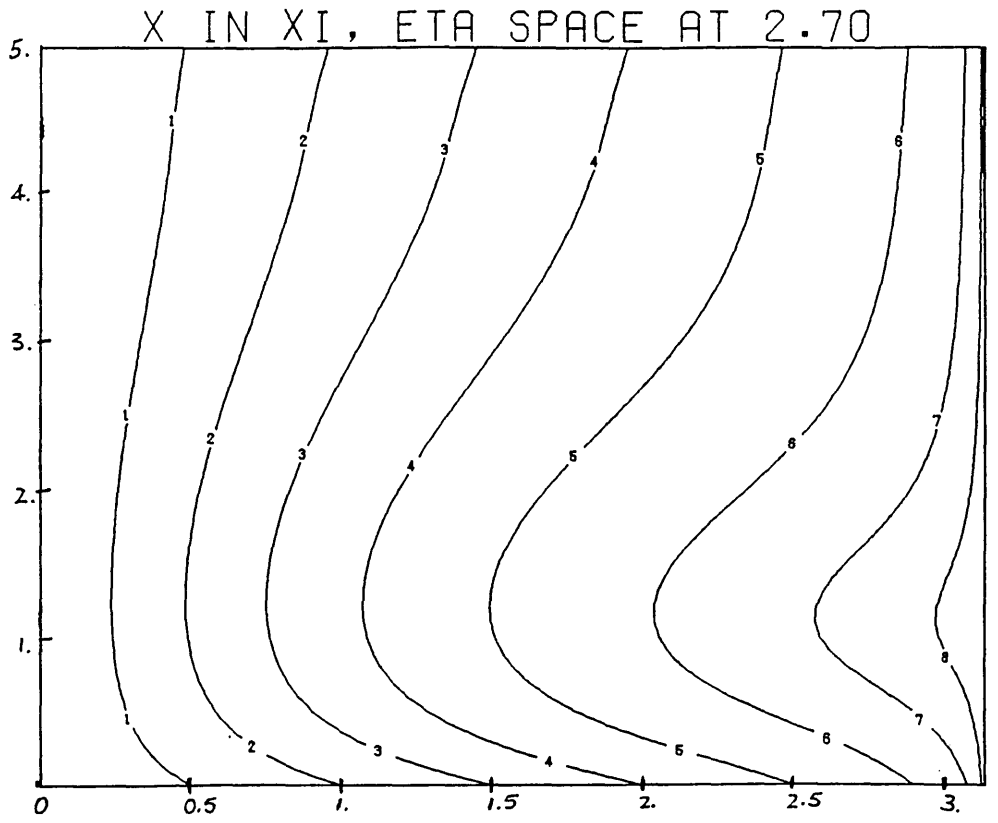


Figure 1.6:2d

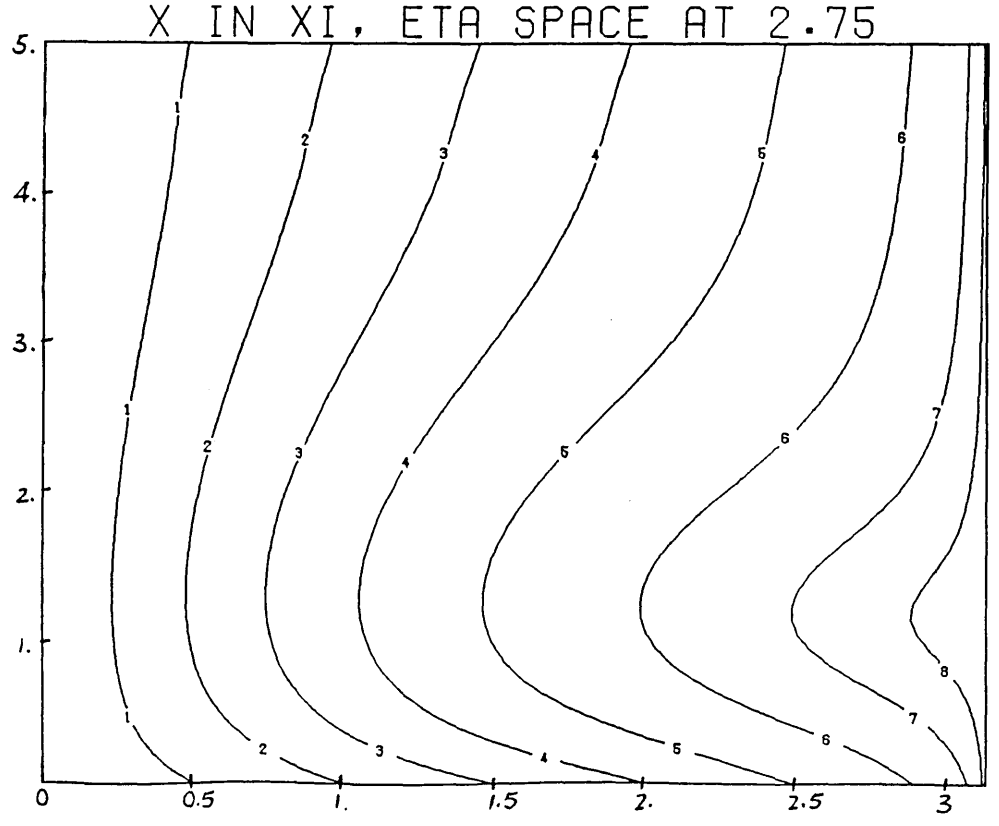


Figure 1.6:2e

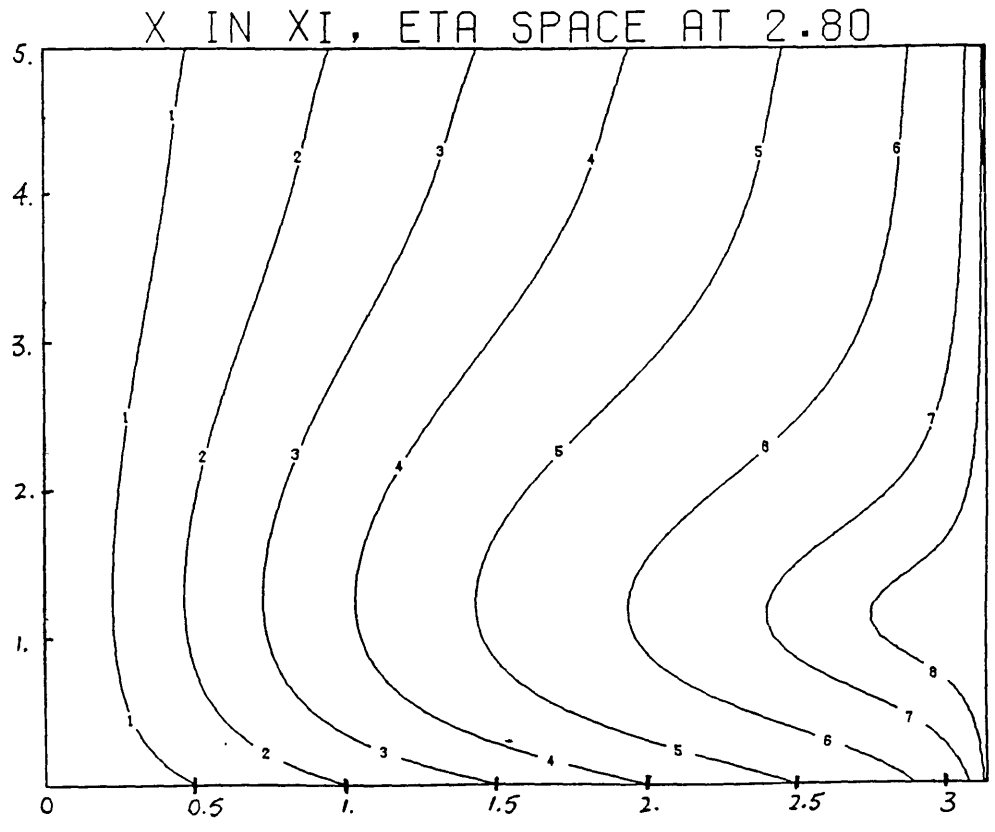


Figure 1.6:3a

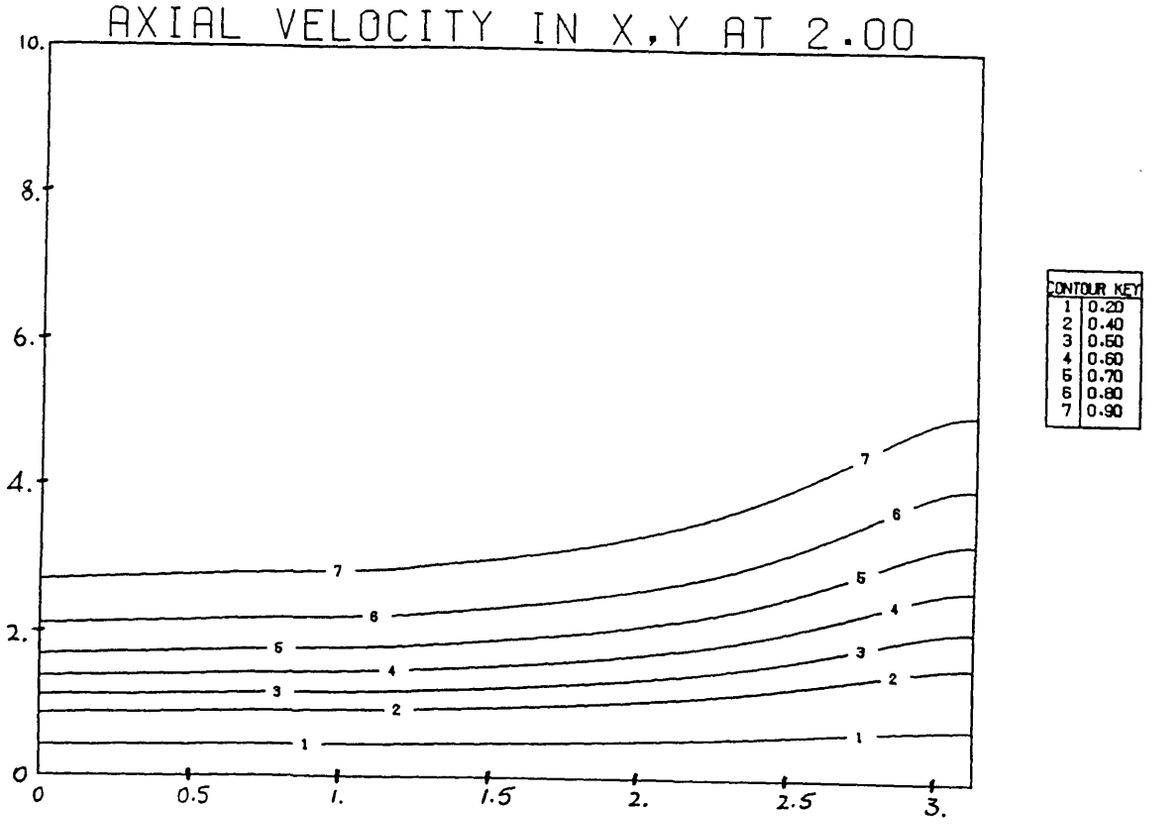


Figure 1.6:4a

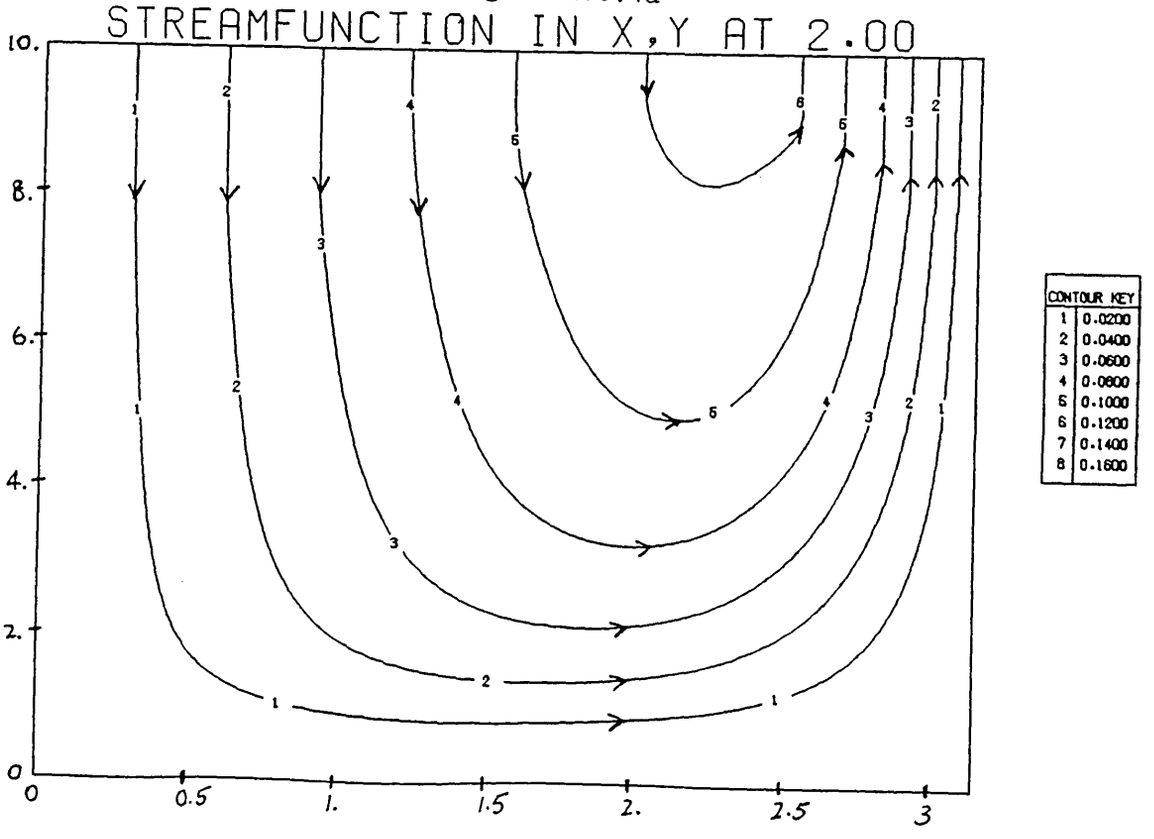


Figure 1.6:3b

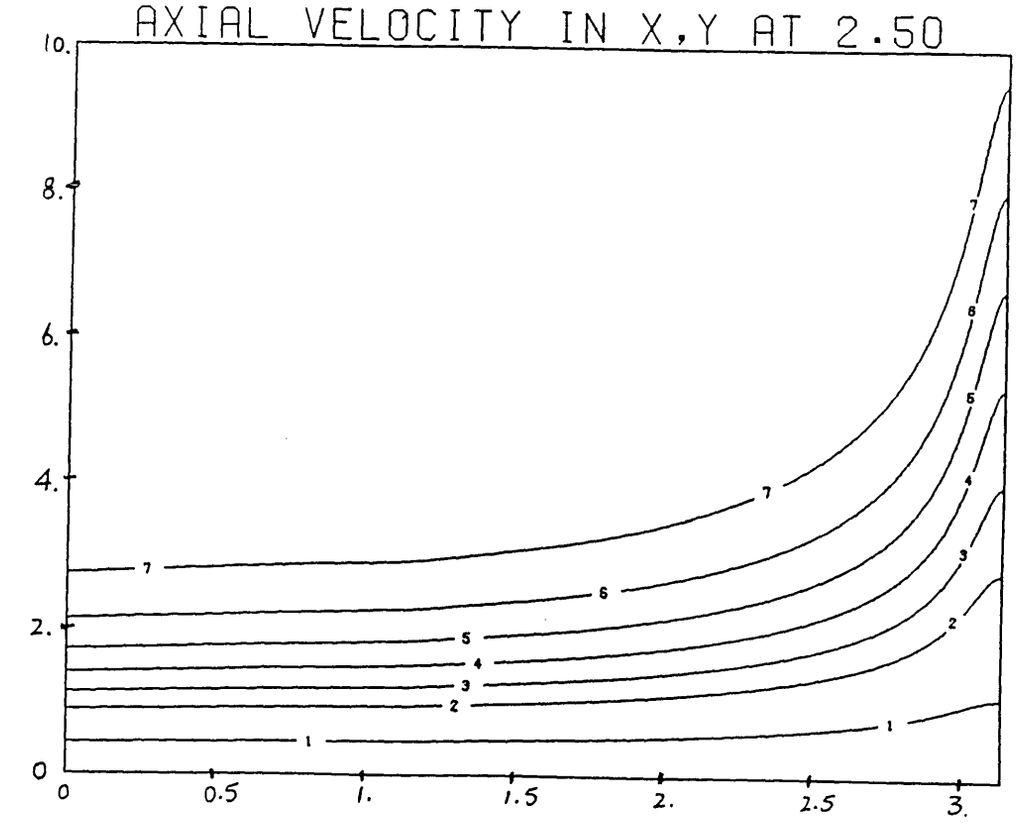


Figure 1.6:4b

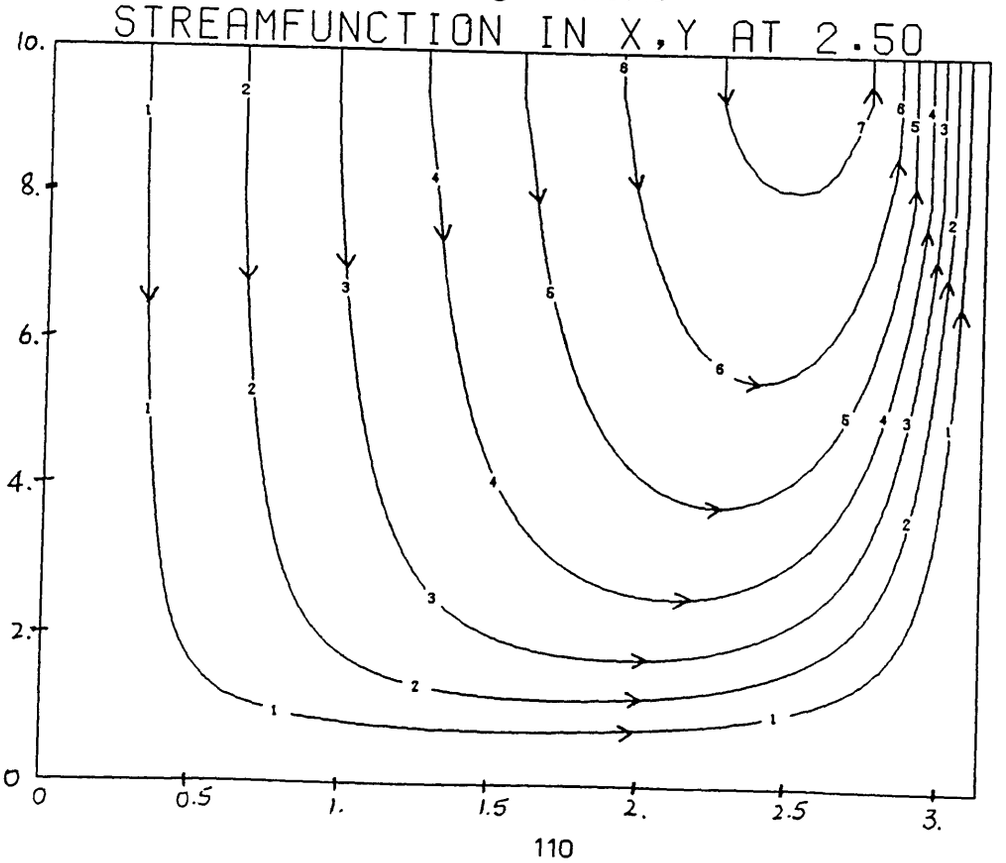


Figure 1.6:3c

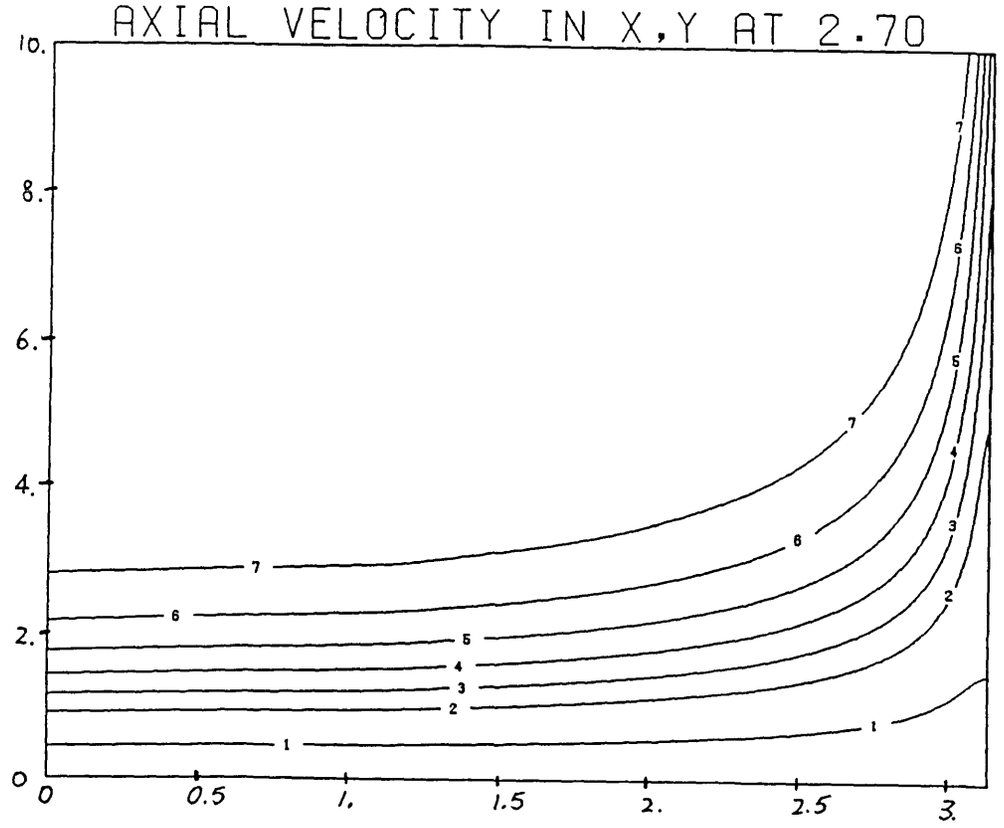


Figure 1.6:4c

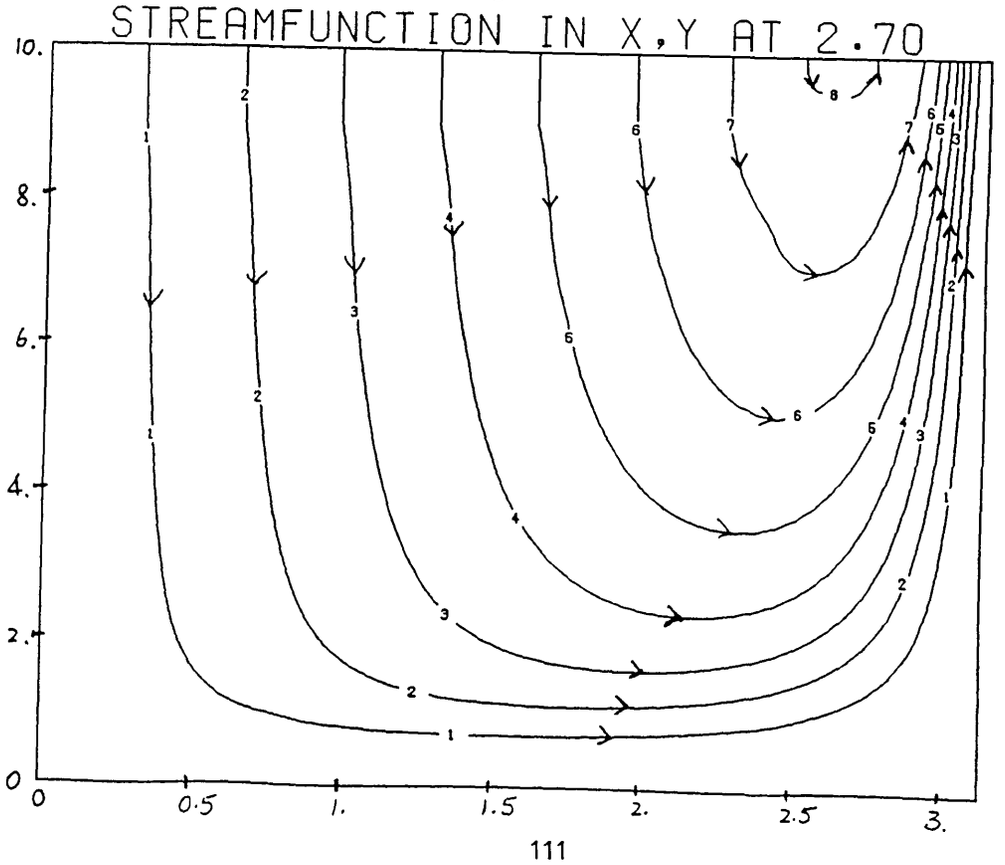


Figure 1.6:3d

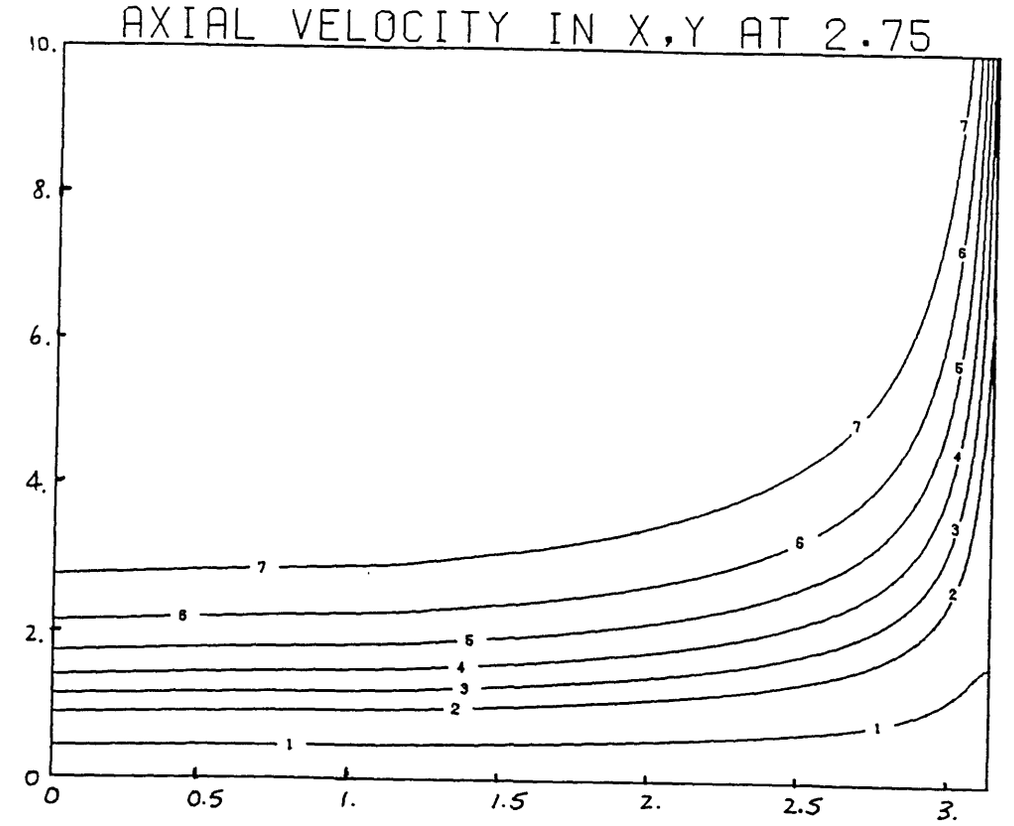


Figure 1.6:4d

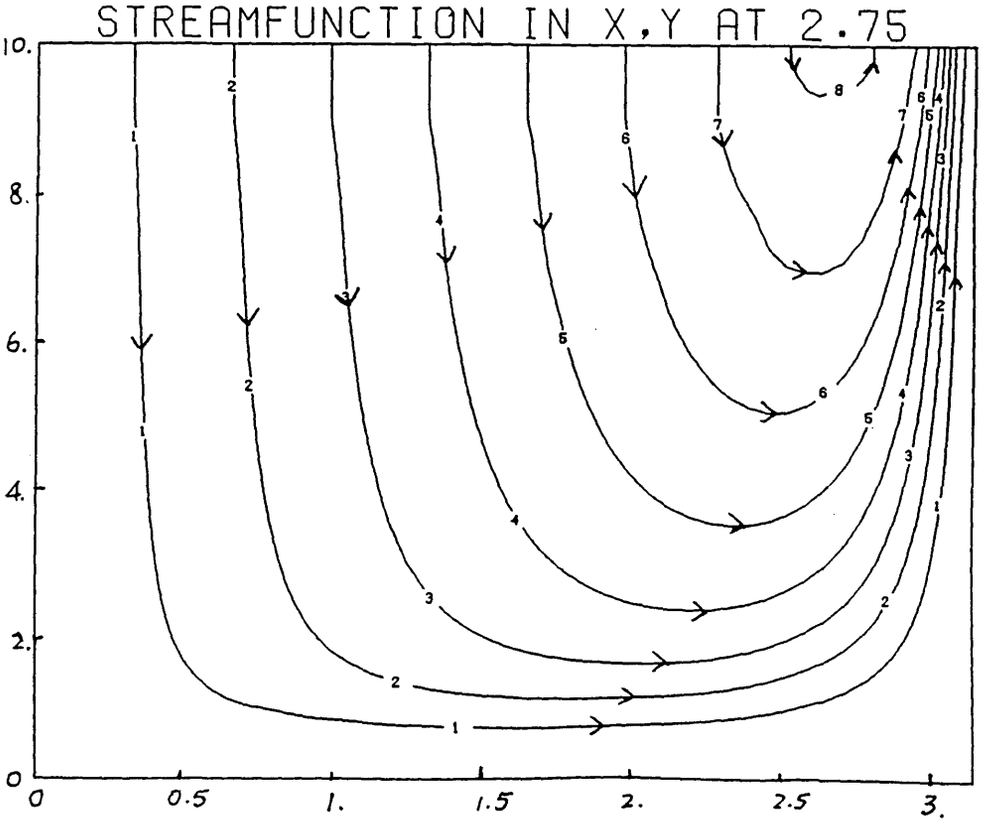


Figure 1.6:3e

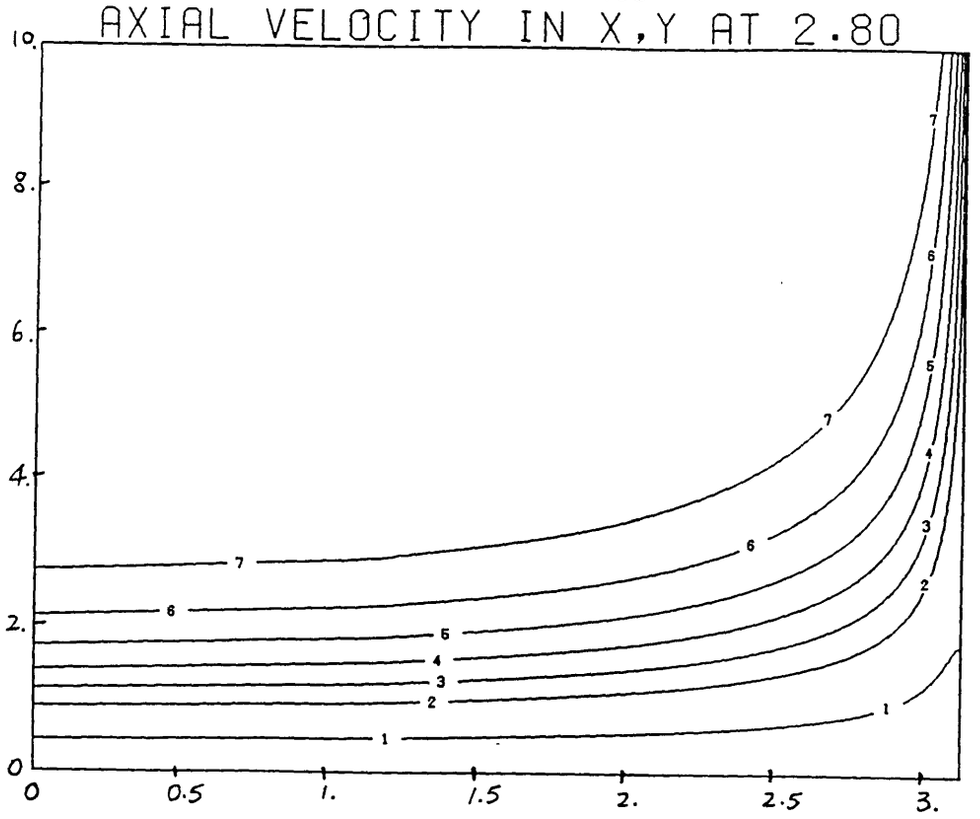


Figure 1.6:4e

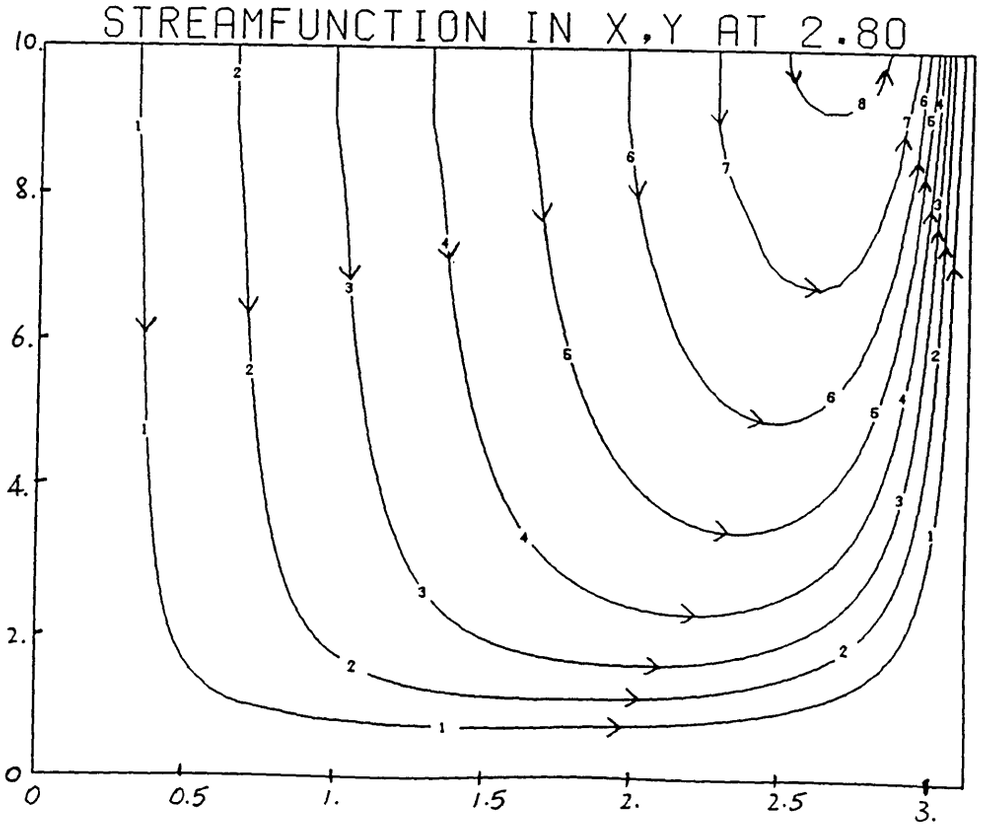


Figure 1.6:5a

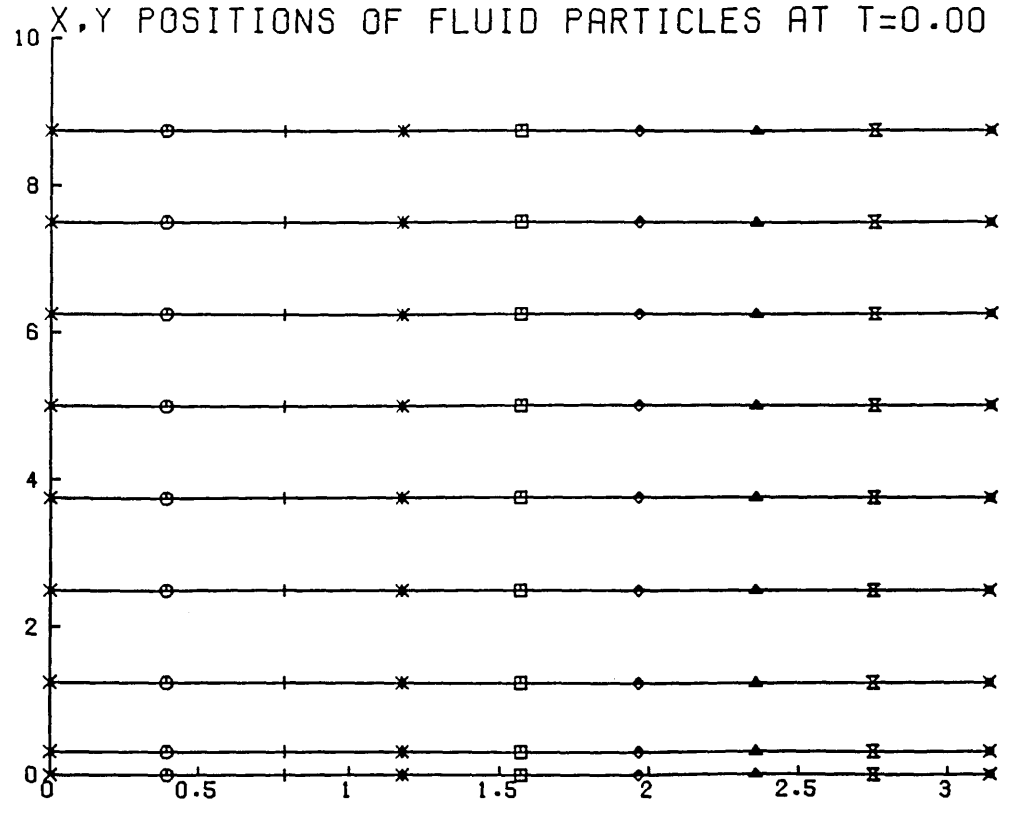


Figure 1.6:6a

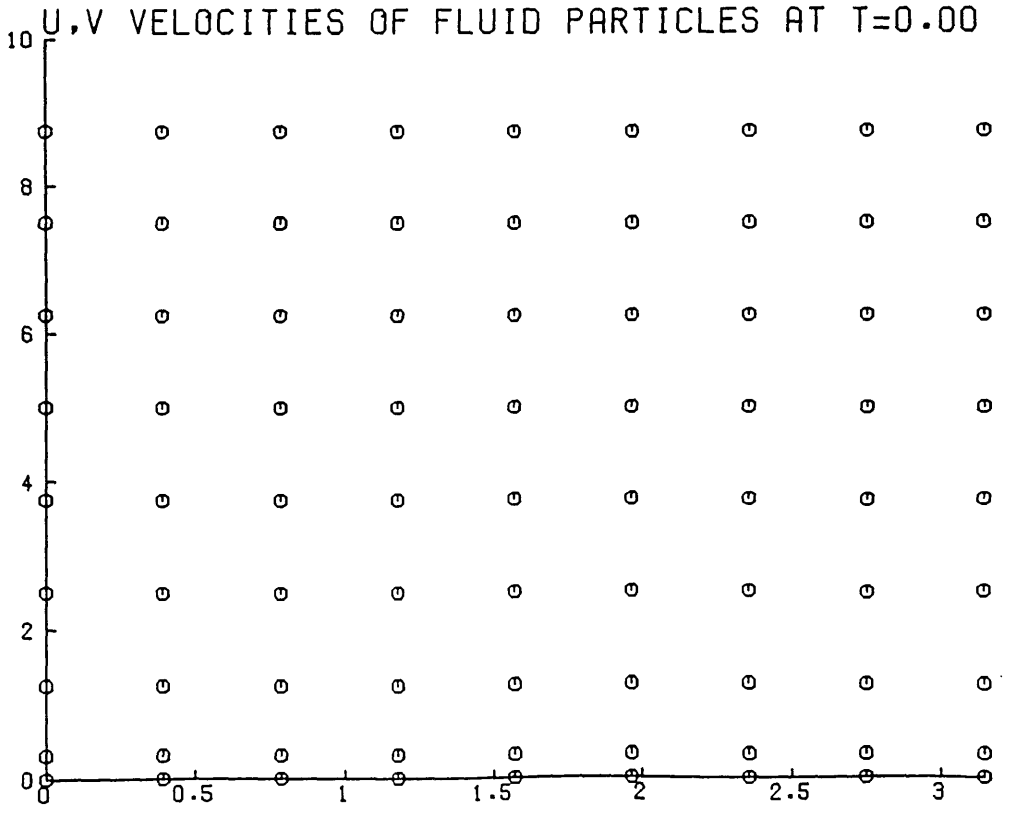


Figure 1.6:5b

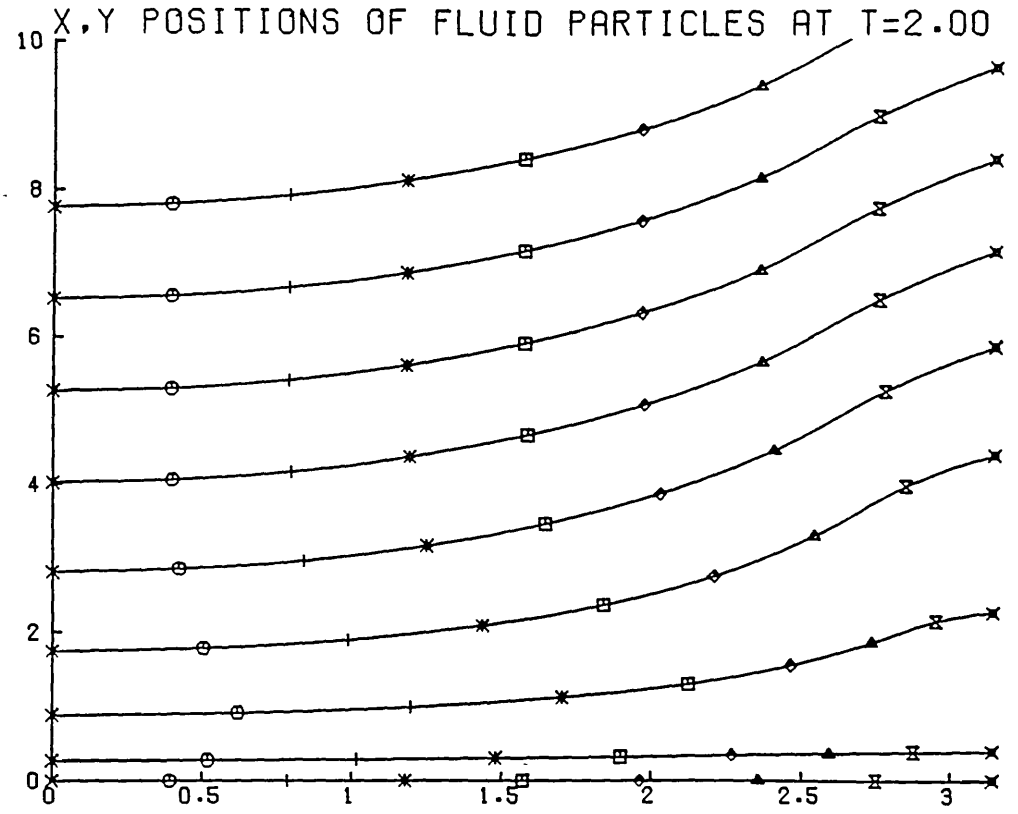


Figure 1.6:6b

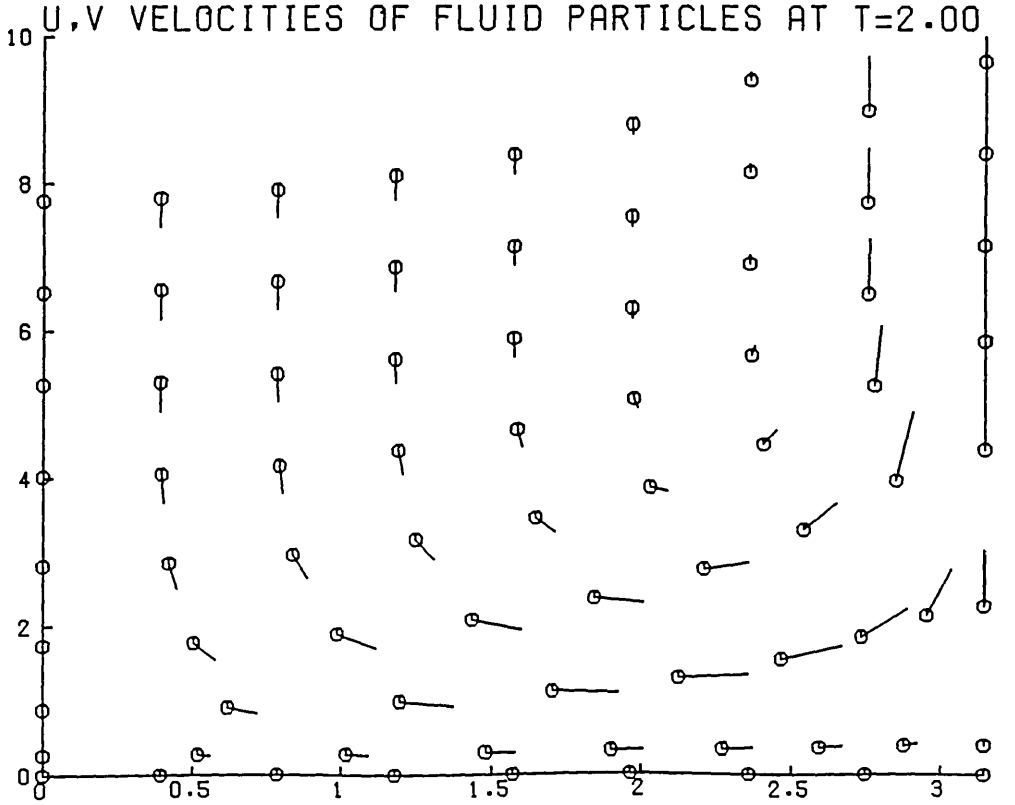


Figure 1.6:5c

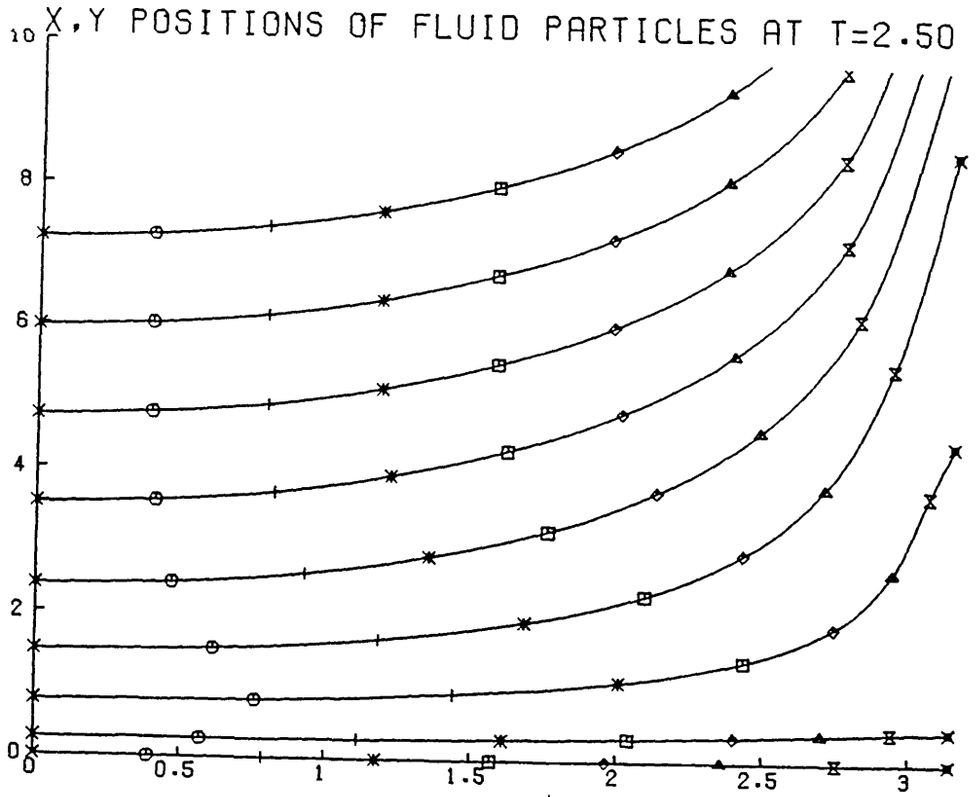


Figure 1.6:6c

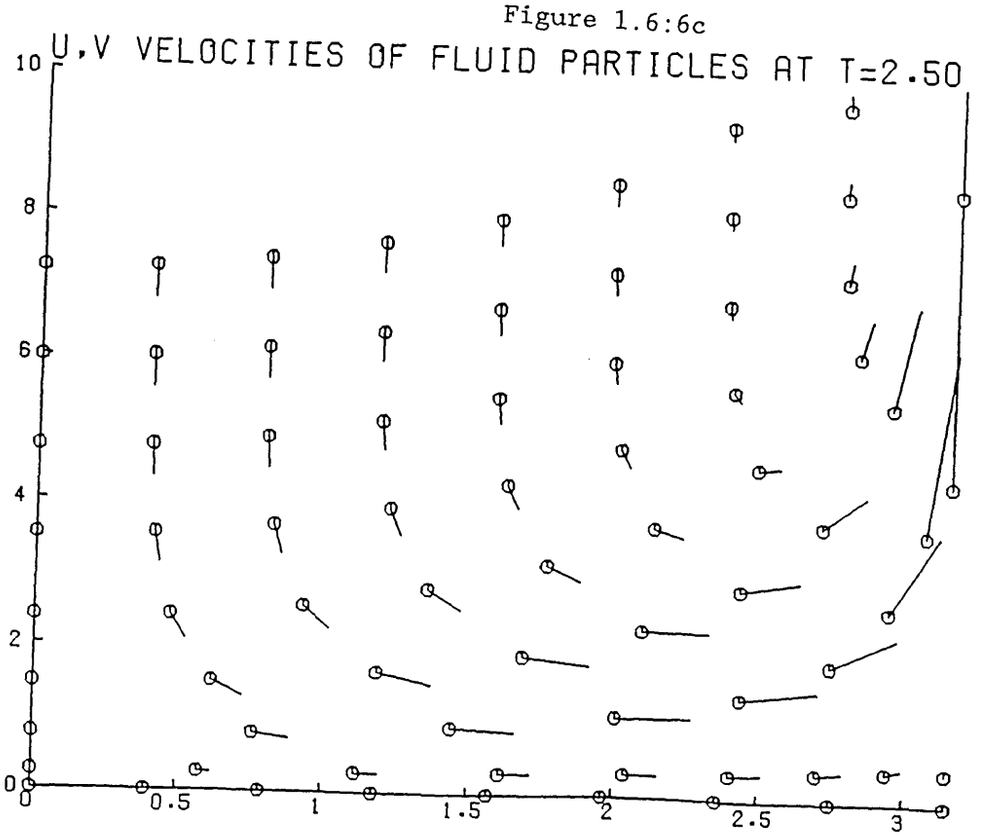


Figure 1.6:5d

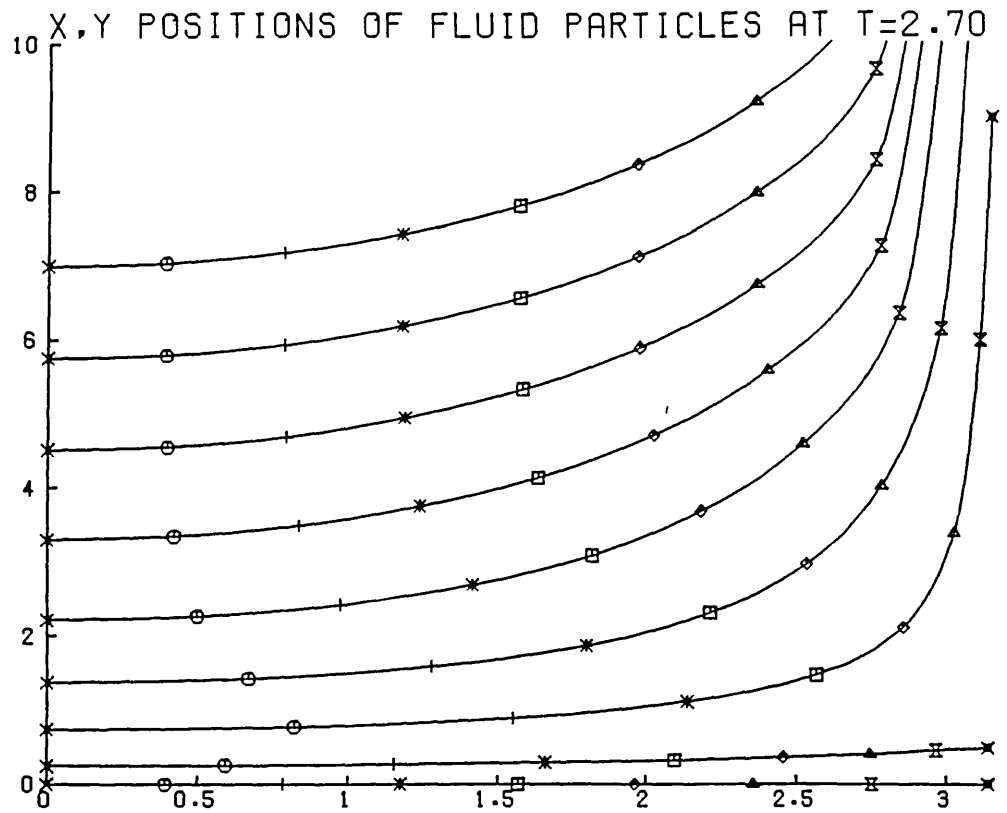


Figure 1.6:6d

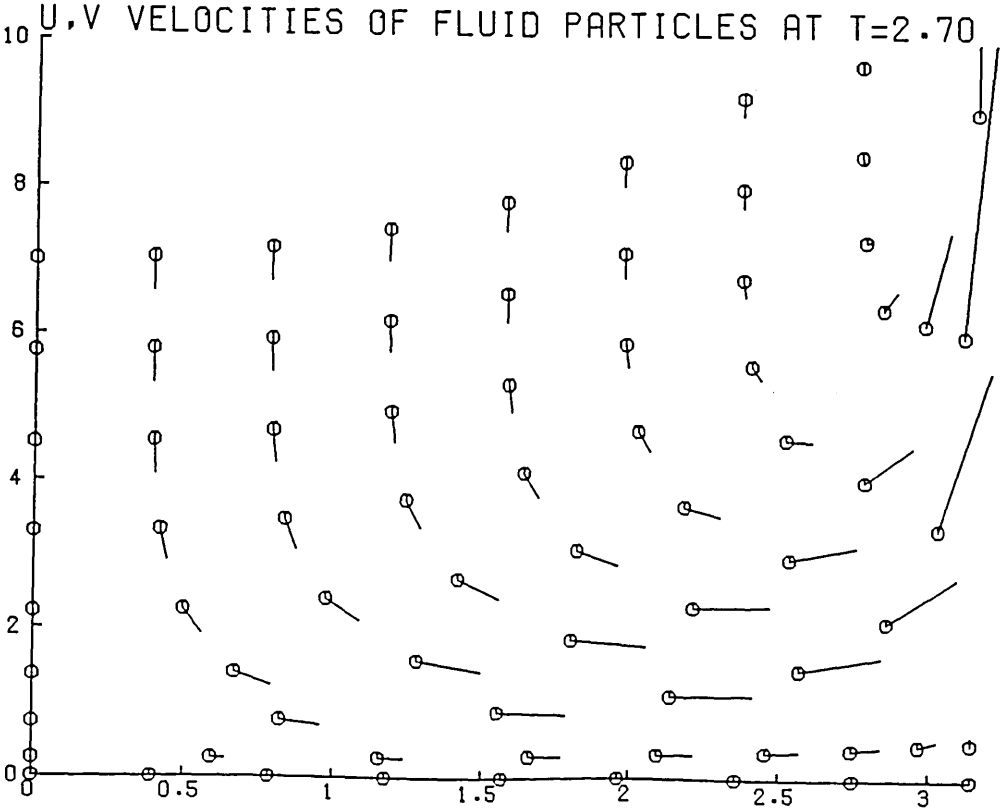


Figure 1.6:5e

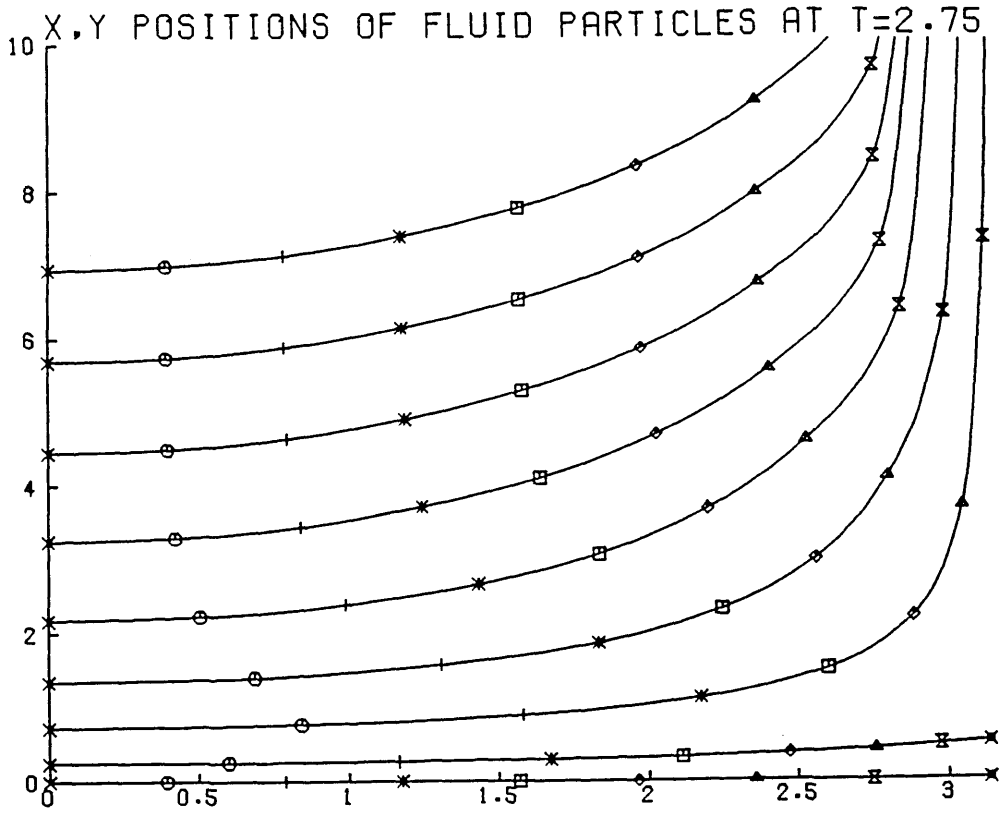


Figure 1.6:6e

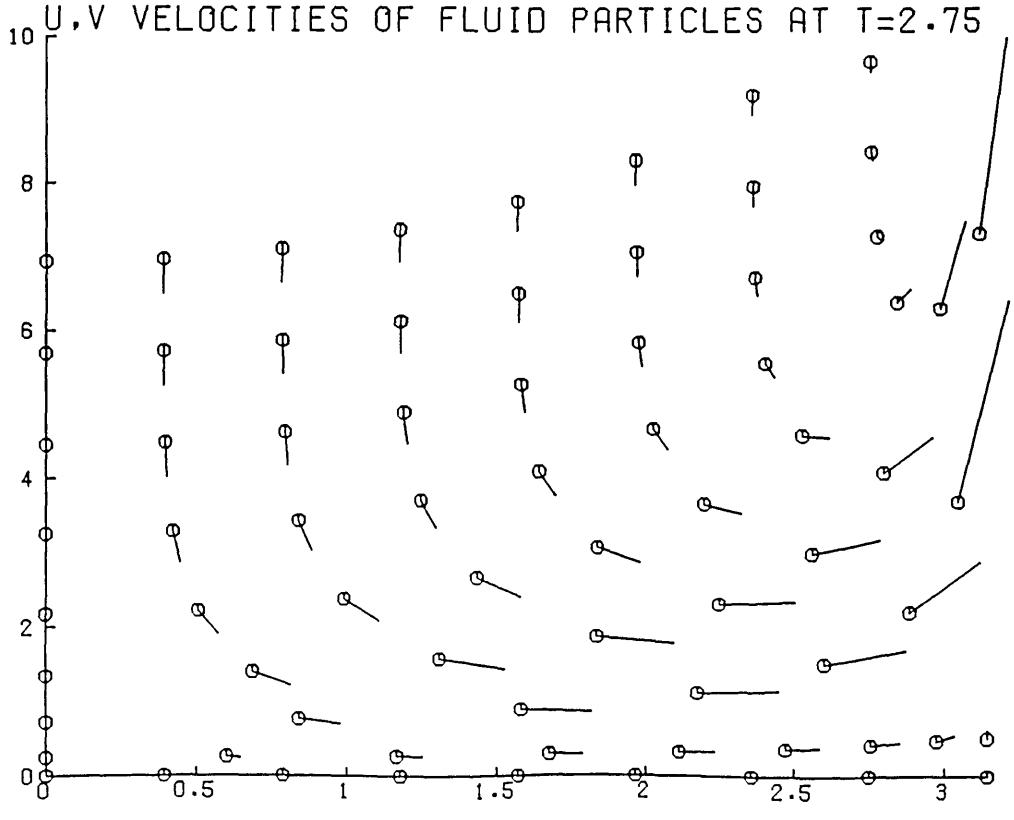


Figure 1.6:5f

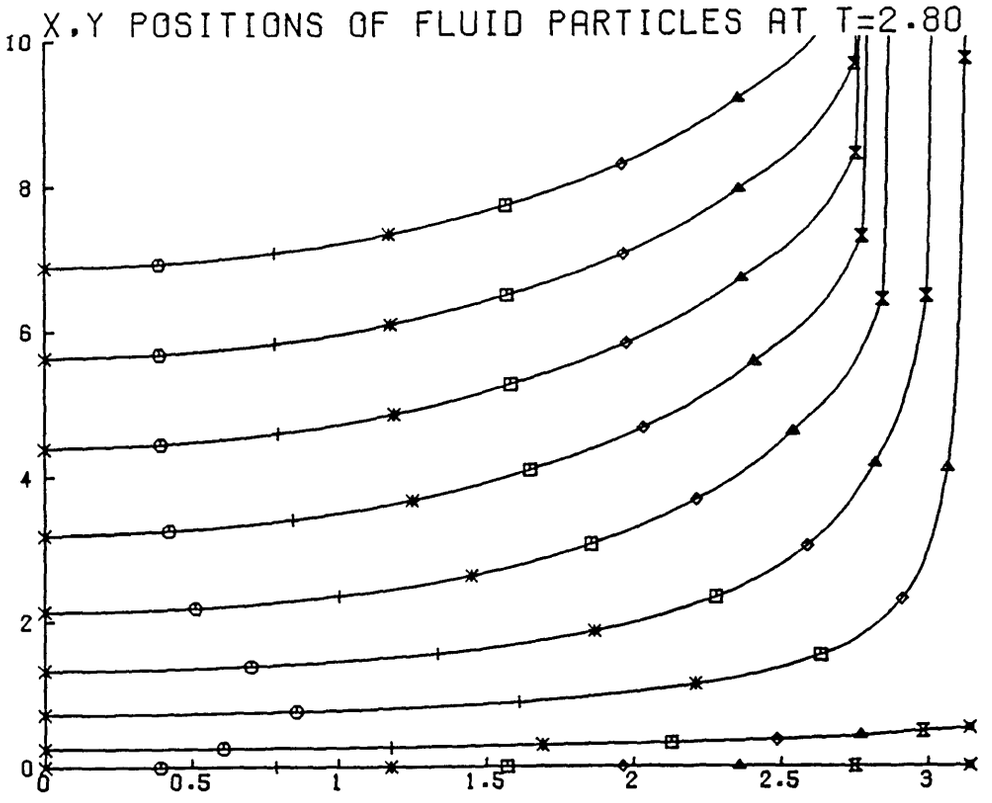


Figure 1.6:6f

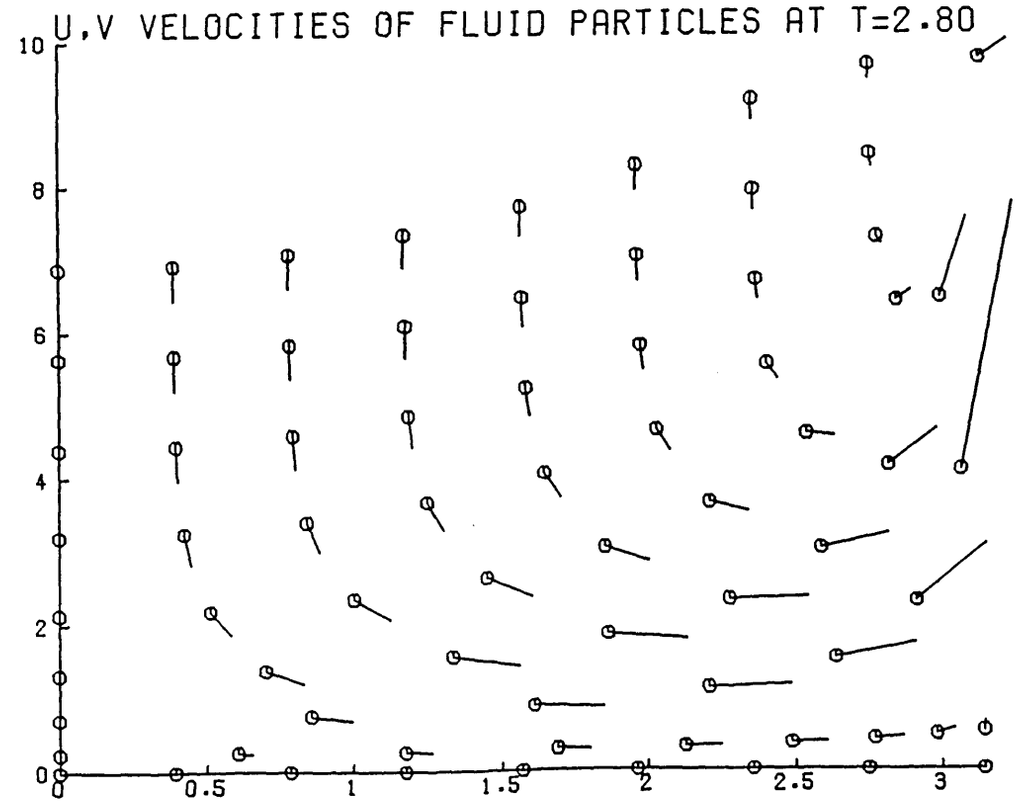


Figure 1.6:7a $W_o = 1$, $\delta = 0$, $\eta = 5$

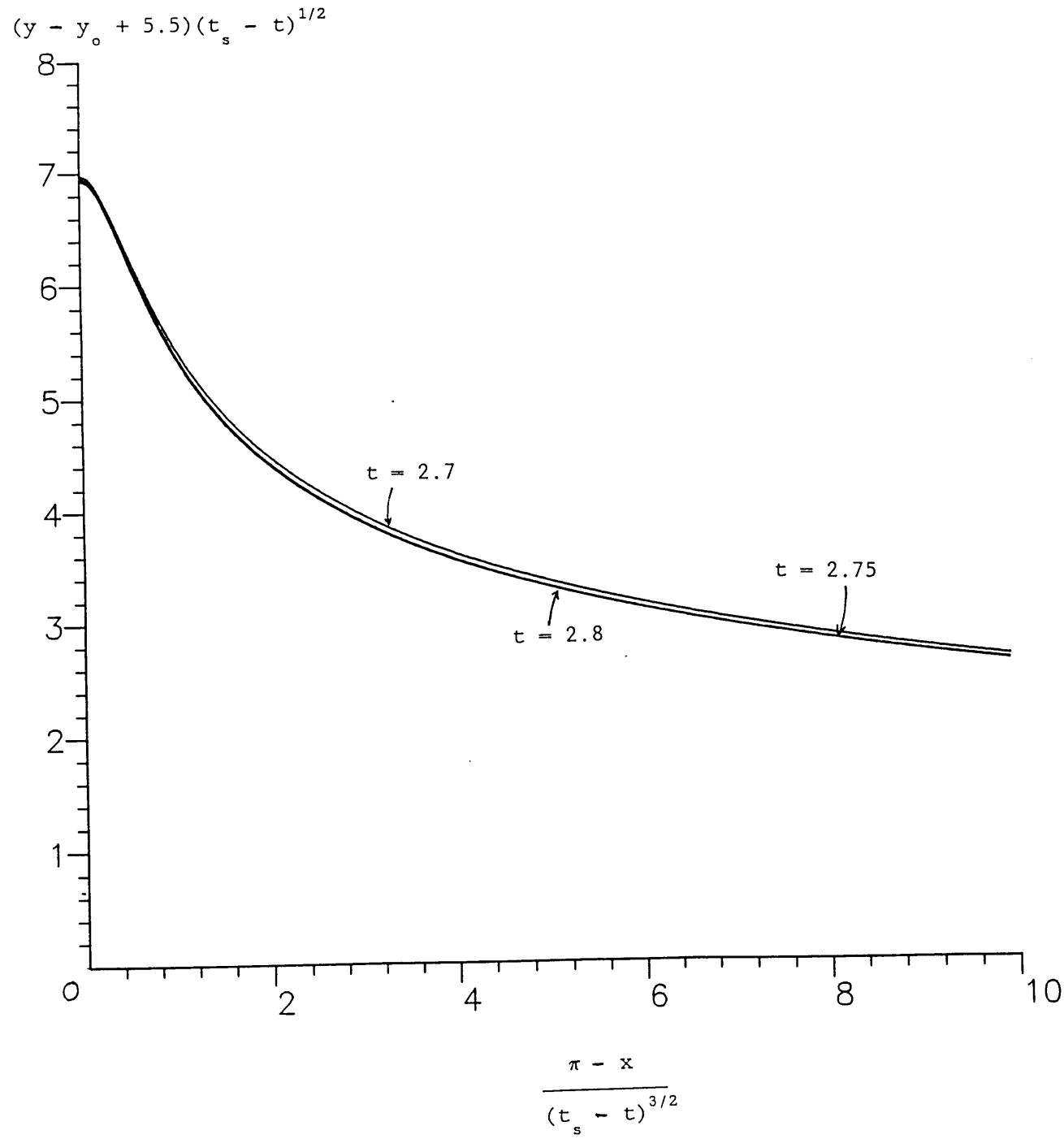


Figure 1.6:7b $W_o = 1$, $\delta = 0$, $\eta = 10$

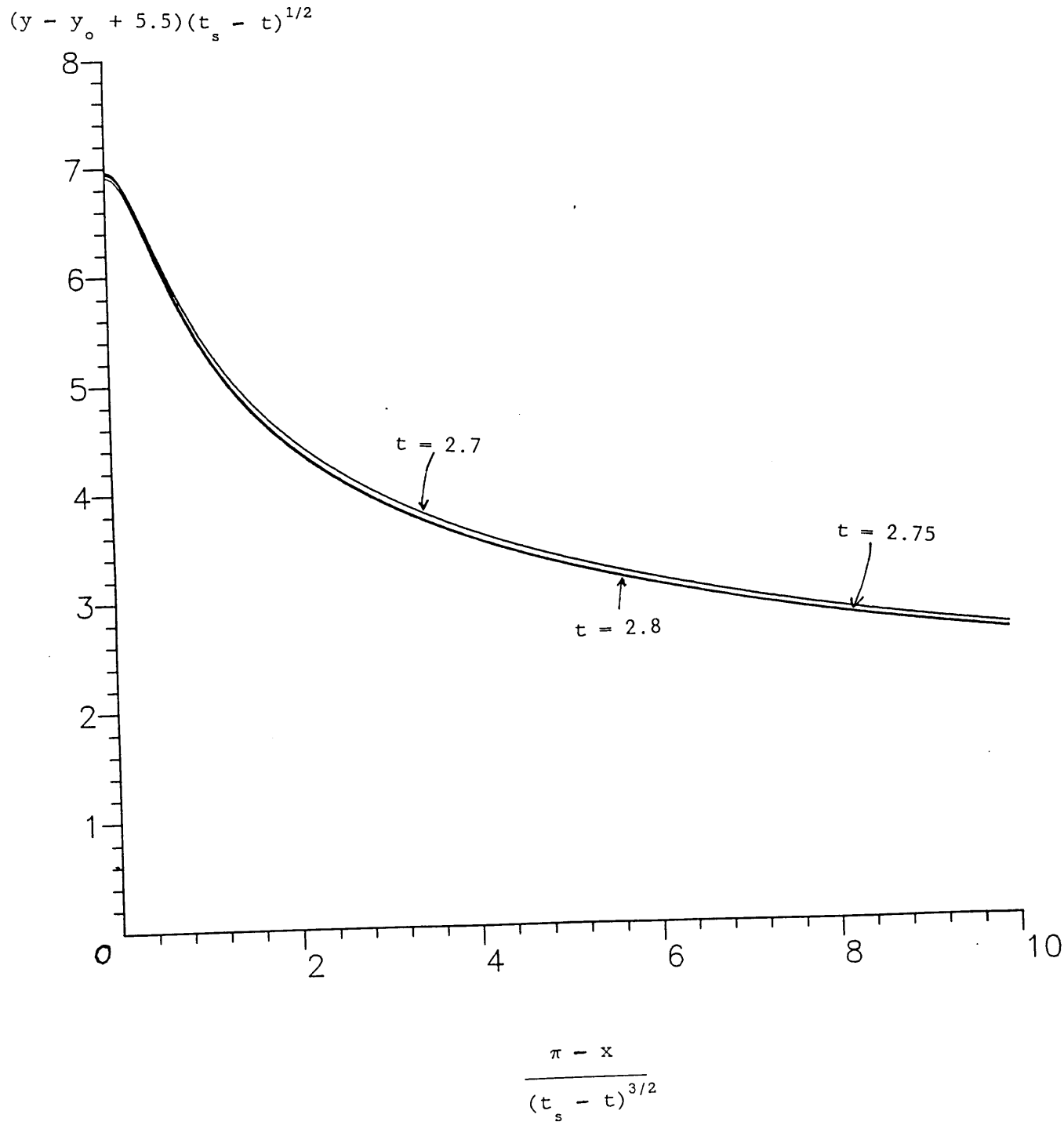


Figure 1.6:8a $W_o = 1$, $\delta = 0$

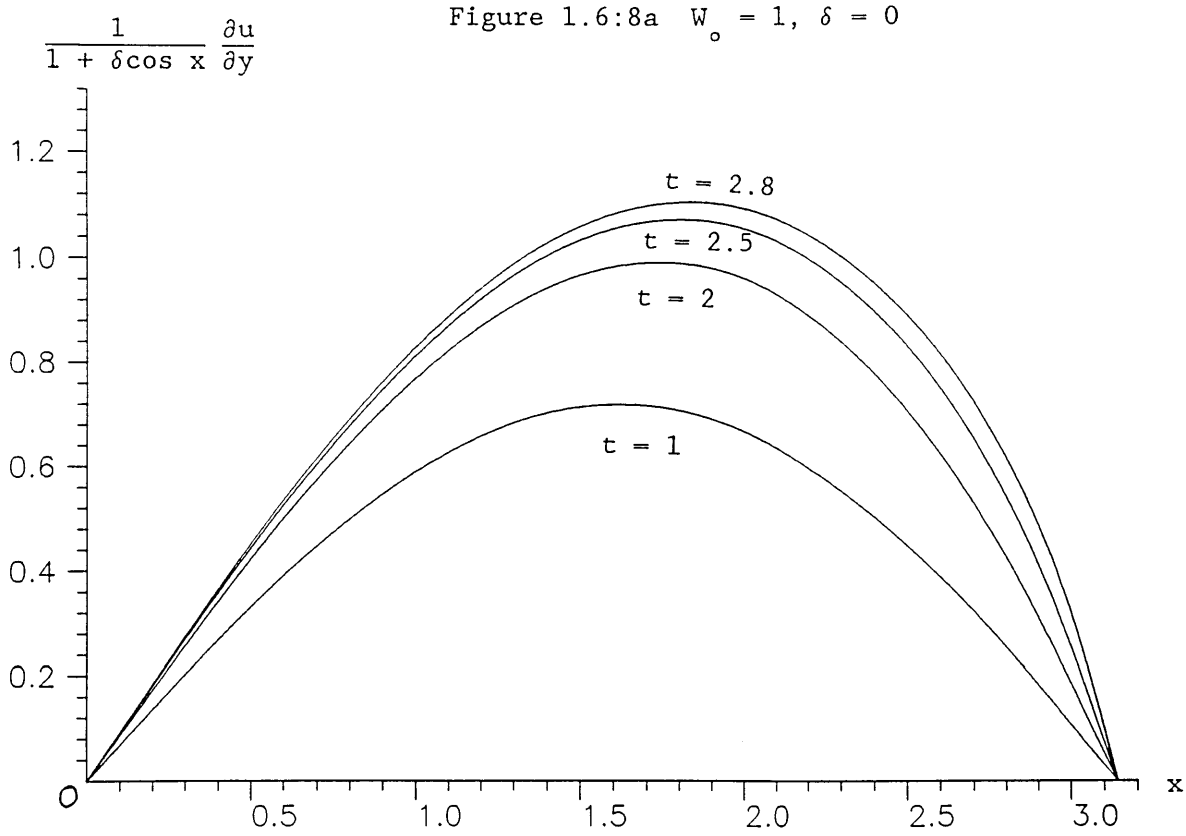


Figure 1.6:8b $W_o = 1$, $\delta = 0$

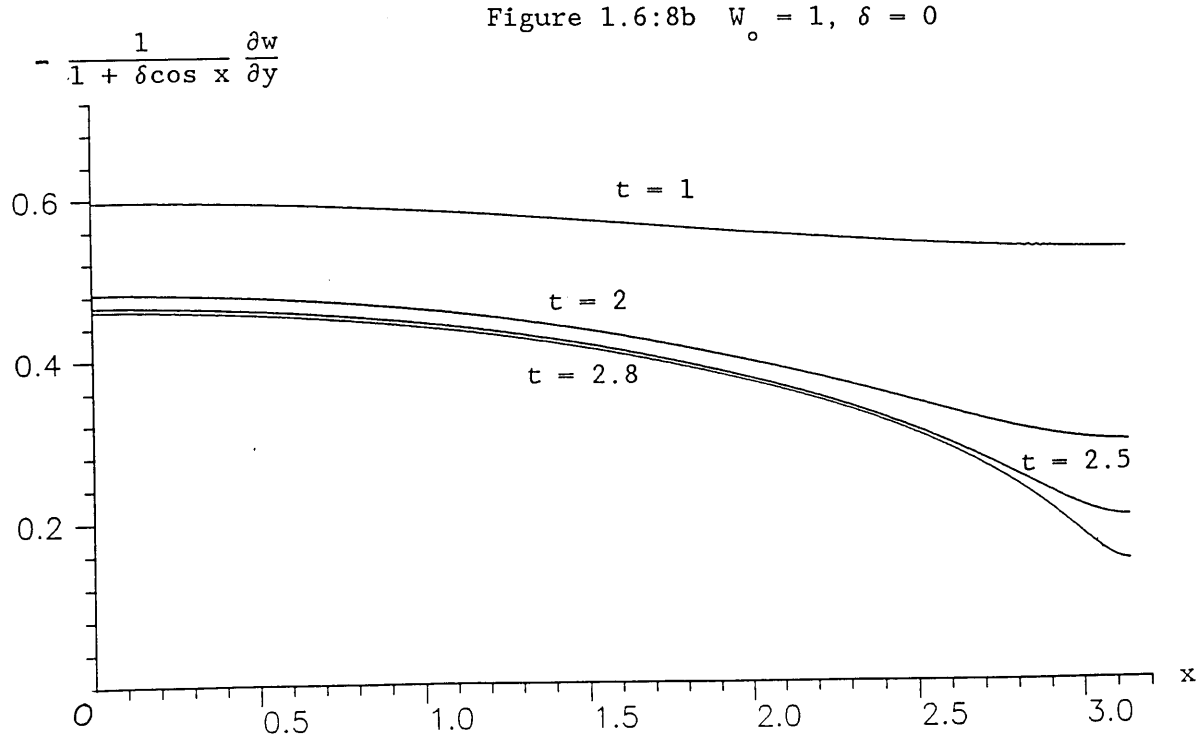


Figure 1.6:9a $W_o = \frac{4t}{t_1}\left[1 - \frac{t}{t_1}\right]$ $0 \le t \le t_1$, $\delta = 0.2$

$t_1 = 11.926$

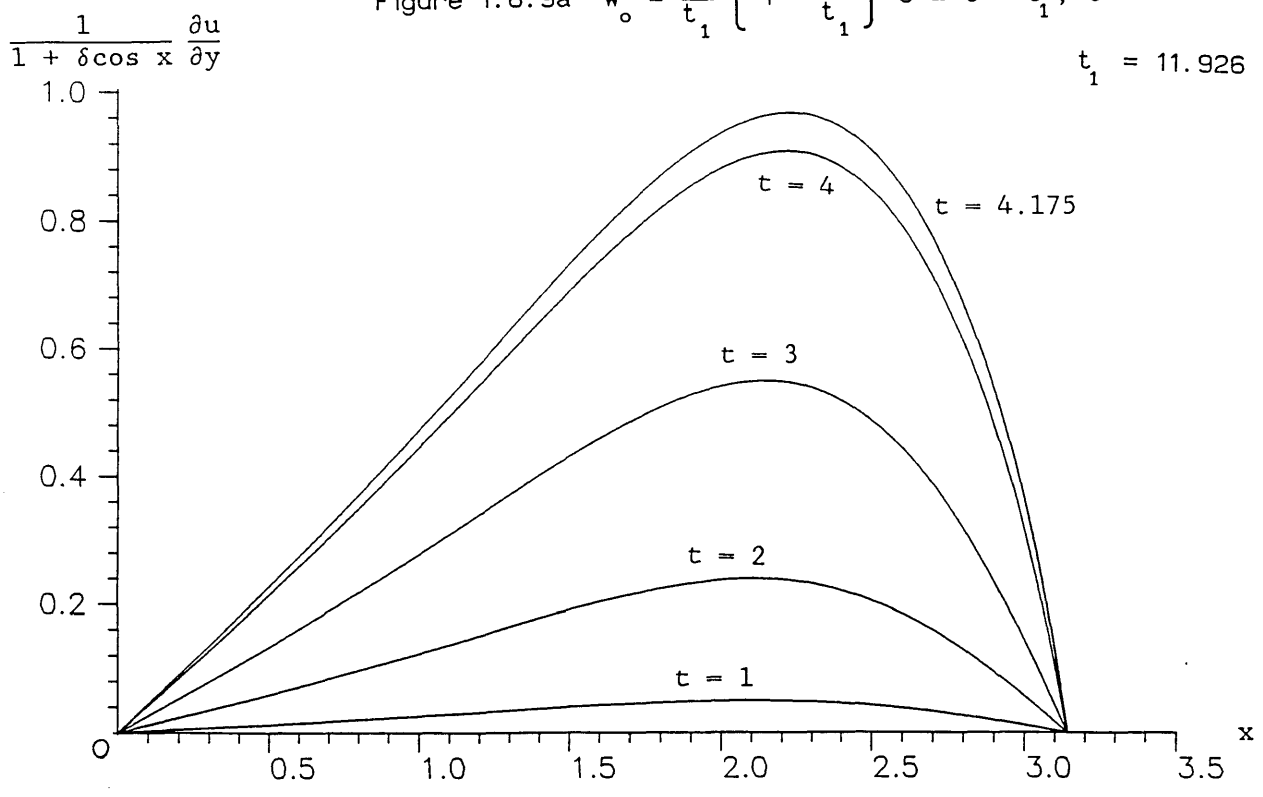
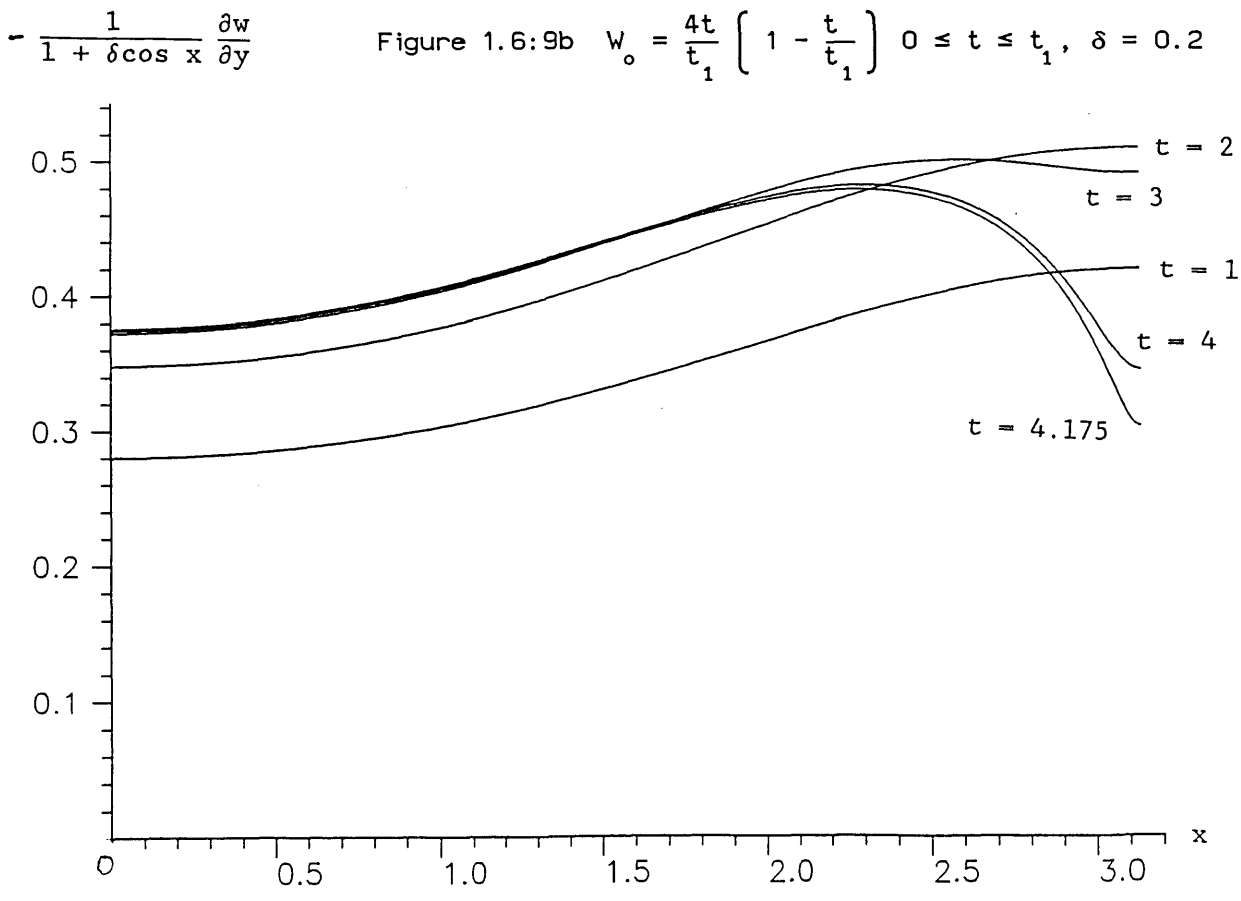


Figure 1.6:9b $W_o = \frac{4t}{t_1}\left[1 - \frac{t}{t_1}\right]$ $0 \le t \le t_1$, $\delta = 0.2$



§ 1.7 Flow inside an Impulsively Rotated Curved Pipe

Experimental results for axially-independent, impulsively started flow through a torus, or part of one, are difficult to obtain because of entrance effects, etc.. For a comparison of our numerical results with experimental data, calculations for a more easily experimentally implemented problem seem appropriate. Here we choose to study starting flow inside a curved pipe which is impulsively rotated. This is possibly an easier experiment to carry out, and we can readily adopt our previous work to perform calculations.

As in previous sections in the chapter, we consider a Newtonian, incompressible laminar fluid inside a loosely curved pipe, which is of the same geometry as that considered before (see figure 1.1:1). The pipe is assumed to rotate uni-directionally about the axis of symmetry through the point C and perpendicular to the symmetry plane of the pipe. In the limit of high Dean number, a boundary layer develops next to the pipe wall, in which the secondary motion forces fluid particles to the *outer* wall for the following reason. A typical axial velocity $\bar{W}$ results in an outward centrifugal/coriolis force of order $\frac{\bar{W}^2}{\bar{L}}$. In the core both the inward centrifugal/coriolis force and the outward pressure gradient are zero. However in the boundary layer, as a consequence of the no-slip condition on the wall of the pipe, the centrifugal/coriolis force is non-zero whereas the pressure gradient is essentially zero. As a result of this inbalance, the excess

centrifugal/coriolis force pushes fluid particles in the boundary layer toward the *outer* wall. As a result of this effect, unsteady boundary-layer separation occurs at the symmetry line of the outer wall.

We next consider the mathematical formulation of this problem which is similar to that in section 1.2. As before, we concentrate on high-Dean-number flow inside a loosely curved pipe. For simplicity, we use the same variables as in section 1.2 unless otherwise defined explicitly. The pipe is impulsively rotated from rest with angular velocity

$$\frac{\bar{W}W_R(t)}{L}$$

i.e. with axial velocity

$$\bar{W}W_R(t)(1 + \delta r\cos\theta) \ , \qquad (1.7:1)$$

and the rotation is confined to planes parallel to the symmetry plane. The governing Navier-Stokes equations are again (1.2:2a-d), but now subject to the boundary conditions

$$U = V = 0, \qquad W = W_R(1 + \delta r\cos\theta) \qquad \text{on} \quad r = 1. \qquad (1.7:2)$$

Defining the local boundary-layer variables x, y and scaled velocites u, v, $\bar{w}$ as in equation (1.2:4), we obtain the boundary-layer equations in Eulerian coordinates

$$(1 + \delta\cos x)v_y + u_x = 0, \tag{1.7:3a}$$

$$u_t + vu_y + \frac{uu_x}{(1 + \delta\cos x)} + \frac{\sin x}{(1 + \delta\cos x)^2}(\delta u^2 + \bar{w}^2)$$

$$= -(1 + \delta\cos x)\frac{\partial p}{\partial x} + u_{yy} , \tag{1.7:3b}$$

$$\frac{\partial p}{\partial y} = 0 , \tag{1.7:3c}$$

and

$$\bar{w}_t + v\bar{w}_y + \frac{u\bar{w}_x}{(1 + \delta\cos x)} = -(1 + \delta\cos x)\frac{\partial p}{\partial z} + \bar{w}_{yy} . \tag{1.7:3d}$$

subject to the boundary conditions

$$\begin{aligned} &u = v = 0 \quad \bar{w} = W_R(t)(1 + \delta\cos x)^2 \qquad \text{on } y = 0, \\ &u \to 0, \qquad \bar{w} \to 0 \qquad\qquad\qquad\quad \text{as } y \to \infty. \end{aligned} \tag{1.7:3e}$$

Since the pipe is impulsively rotated from rest, there is no driving pressure gradient, and we can take

$$\frac{\partial p}{\partial x} = \frac{\partial p}{\partial z} = 0$$

We now examine the flow in Lagrangian coordinates by labelling a fluid particle by its position (ξ, η) at a fixed time, e.g. $t = 0$,

$$\xi = x, \qquad \eta = y \qquad \text{at} \qquad t = 0 .$$

After similar algebraic manipulations to those in (1.2:7-15), we obtain the governing boundary-layer equations in Lagrangian coordinates

$$u = (1 + \delta\cos x)\ x_t, \tag{1.7:4a}$$

$$u_t = \frac{\sin x}{(1 + \delta\cos x)^2} (-W_R^2 + w(2W_R - w) - \delta u^2) + D^2 u \tag{1.7:4b}$$

$$w_t = W_R' + D^2 w . \tag{1.7:4c}$$

subject to the boundary conditions:

$$\begin{aligned} &x = \xi, \quad u = 0, \quad w = W_R(t)[1-(1 + \delta\cos\xi)^2] \quad \text{on } \eta = 0 \quad \text{for } t \geq 0, \\ &x = \xi, \quad u \to 0, \quad w \to W_R(t) \qquad\qquad\quad \text{as } \eta \to \infty \quad \text{for } t \geq 0, \end{aligned} \tag{1.7:4d}$$

where, for consistency with section 1.2

$$w = W_R(t) - \bar{w} ,$$

and the derivative operator D is given by

$$D = \left[\frac{1 + \delta\cos x}{1 + \delta\cos \xi} \right] \left[-x_\eta \frac{\partial}{\partial\xi} + x_\xi \frac{\partial}{\partial\eta} \right] . \tag{1.7:5}$$

Equations (1.7:4) need only to be solved for $0 \leq \xi \leq \pi$ and $0 \leq \eta < \infty$.

To examine the flow at the symmetry lines in detail, we write

$$x - x_f = (\xi - \xi_f)\ x^*, \qquad u - u_f = (\xi - \xi_f)\ u^*,$$

where $x = x_f$, $u = u_f$ at $\xi = \xi_f$.

Hence

$$x_f = 0, \qquad u_f = 0, \qquad \text{at} \quad \xi_f = 0,$$

and

$$x_f = \pi, \qquad u_f = 0, \qquad \text{at} \quad \xi_f = \pi.$$

Then substitution into the governing equations (1.7:4) yields

$$u^* = (1 \pm \delta)x_t^* \qquad (1.7:6a)$$

$$u_t^* = \pm \frac{x^*}{(1\pm\delta)^2}\left[-W_R^2 + w(2W_R - w) \right] + x^{*2}u_{\eta\eta}^* - x^*x_\eta^*u_\eta^* + (x_\eta^{*2} - x^*x_{\eta\eta}^*)u^* \qquad (1.7:6b)$$

$$w_t = W_R' + x^{*2}w_{\eta\eta} + x^*x_\eta^*w_\eta \qquad (1.7:6c)$$

subject to the conditions,

$$x^* = 1 , \quad u^* = 0 , \quad w = W_R(t)[1-(1\pm\delta)^2] \quad \text{at} \quad \eta = 0 ,$$

$$x^* = 1 , \quad u^* = 0 , \quad w = W_R \quad \text{as} \quad \eta \to \infty , \qquad (1.7:6d)$$

$$x^* = 1 , \quad u^* = 0 , \quad w = W_R \quad \text{at} \quad t = 0+, \ \eta \neq 0 .$$

Where there is a choice in sign, the + sign corresponds to the outer wall and the - sign the inner wall.

The numerical procedure to solve equations (1.7:4) and (1.7:6) is similar to that described in section 1.3. Because we are interested in the flow near the outer wall, a stretch function for ξ was used to give refined grid resolution there; the constants λ_1 and λ_2 have been chosen to be 3 and 0.5 respectively by trial runs. The stretch function for η and the convergence criterion were also similar to those in section 1.3. Second-order accuracy has been confirmed.

A full calculation (i.e. yielding solutions for $0 \leq \xi \leq \pi$, $0 \leq \eta < \infty$) was undertaken for $W_R = 1$, $\delta = 0$ using three different grid sizes $N = 37$ $M = 17$ $\Delta t = \frac{1}{20}$, $N = 73$ $M = 33$ $\Delta t = \frac{1}{40}$, and $N = 145$ $M = 65$ $\Delta t = \frac{1}{80}$. The boundary-layer flow develops a zero grad x at the symmetry line of the outer wall after a finite time

t_s. This indicates that unsteady boundary-layer separation occurs after a finite time t_s.

Figure 1.7:1 shows $\min_{\xi,\eta} |\text{grad } x|$ against t for t close to t_s, the linear relationship of which agrees well with equation (1.5:5c). The separation time t_s was approximated by extending this linear relationship down to $|\text{grad } x| = 0$. The results of t_s using different grids are displayed in table 1.7:1a.

Table 1.7:1a $W_R = 1$, $\delta = 0$

grid	t_s	Extrapolated t_s
$\frac{1}{20}$	4.585	
		4.576
$\frac{1}{40}$	4.578	
		4.575
$\frac{1}{80}$	4.576	

Richardson's extrapolation was first applied to the results obtained from grids 37x17 and 73x33, 73x33 and 165x65; these are listed in column 3, yielding $t_s \simeq 4.575$.

With this W_R, the fluid particle (ξ_s, η_s) where $\xi_s = 0$ and $\eta_s \simeq 0.9718$, has travelled approximately a dimensional distance $2.5214a\delta^{-1/2}$ down the pipe along the outer wall by the time that the boundary layer separates after a dimensional time $\frac{4.575a}{\delta^{1/2}\bar{W}}$.

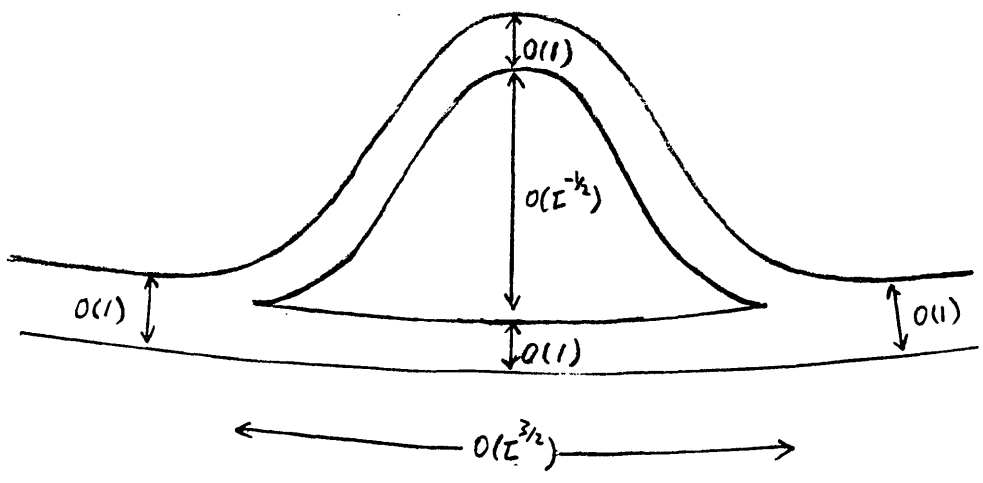
Figure 1.7:2 illustrates the circumferential and axial wall shear,

$$\frac{1}{(1 + \delta\cos x)}\frac{\partial u}{\partial y}, \qquad \frac{1}{(1 + \delta\cos x)}\frac{\partial w}{\partial y},$$

for t = 1.0, 2.0, 3.0, 4.0 and 4.5. Contour plots analogous to figures 1.6:2-6 are not given here since they are qualitatively similar after a refection at $x = \frac{\pi}{2}$.

Finally, to see whether the singularity structure (1.5:5,6) is correct and if our numerical results have adequate resolution, we plot $(y - y_o + c)(t_s - t)^{1/2}$ against $x/(t_s - t)^{3/2}$ for t = 4.4, 4.45 and 4.5 at a constant value of η, e.g. $\eta = 5$ (the behaviour is independent of η for $\eta \geq \eta_s$). Here $y_o = y(t=0)$ and the constant c = 5 is included to take into account the higher-order corrections in y (cf. (1.5:6)). The overlaping lines suggest that the analytical structure and our numerical results agree well.

Having adjusted for the difference in position where unsteady separation occurs, impulsively started flow and the flow due to the impulsive rotation of a pipe are qualitatively similar. Certainly, the separation singularity in section 1.4 applies here since it only assumes that separation occurs on the symmetry line. Hence, as before, the separation singularity is primarily inviscid in a region of width $(t_s - t)^{3/2}$ in the x direction and height $(t_s - t)^{-1/2}$ in the y direction.



A number of other functions have been tried for W_R with $\delta = 0$. Again the boundary-layer flows develop a zero in grad x at the symmetry line of the outer wall after some finite time. Richardson's extrapolation was used on the M = 33, $\Delta t = \frac{1}{80}$ grid and the M = 165, $\Delta t = \frac{1}{160}$ grid to give improved accuracy. The results[1] are listed in table 1.7:1b.

Table 1.7:1b $\delta = 0$

W_R	Extrapolated t_s
$1 + 2\sin t$	2.034
$1 + \sin t$	2.683
$1 + \frac{1}{2}\sin t$	3.343
$1 + \sin 2t$	2.818
$1 + \sin\frac{1}{2}t$	3.066

[1] These are obtained by doing only the symmetry-line calculations.

Figure 1.7:1 $W_R = 1$, $\delta = 0$

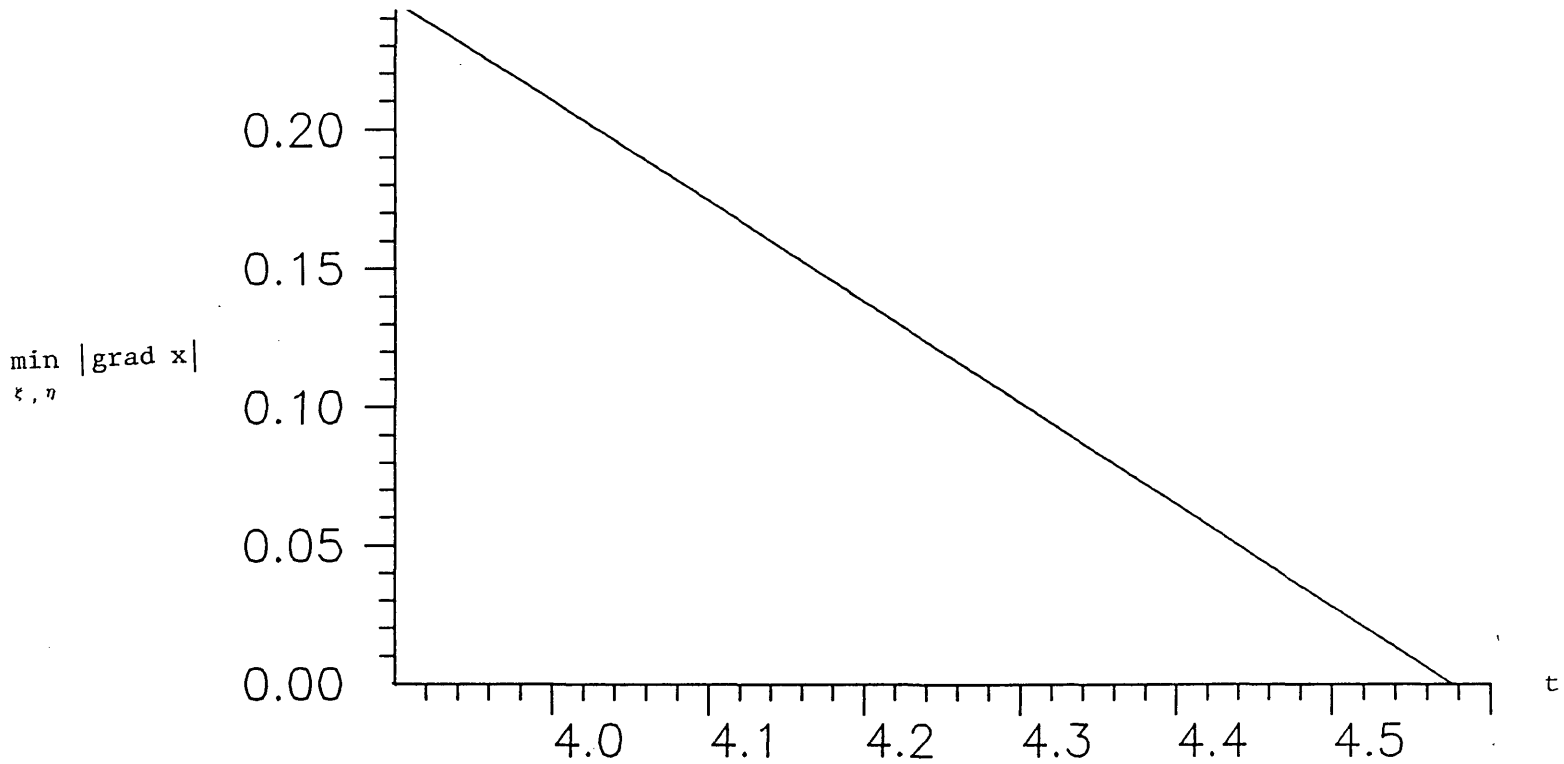


Figure 1.7:2a $W_R = 1,\ \delta = 0$

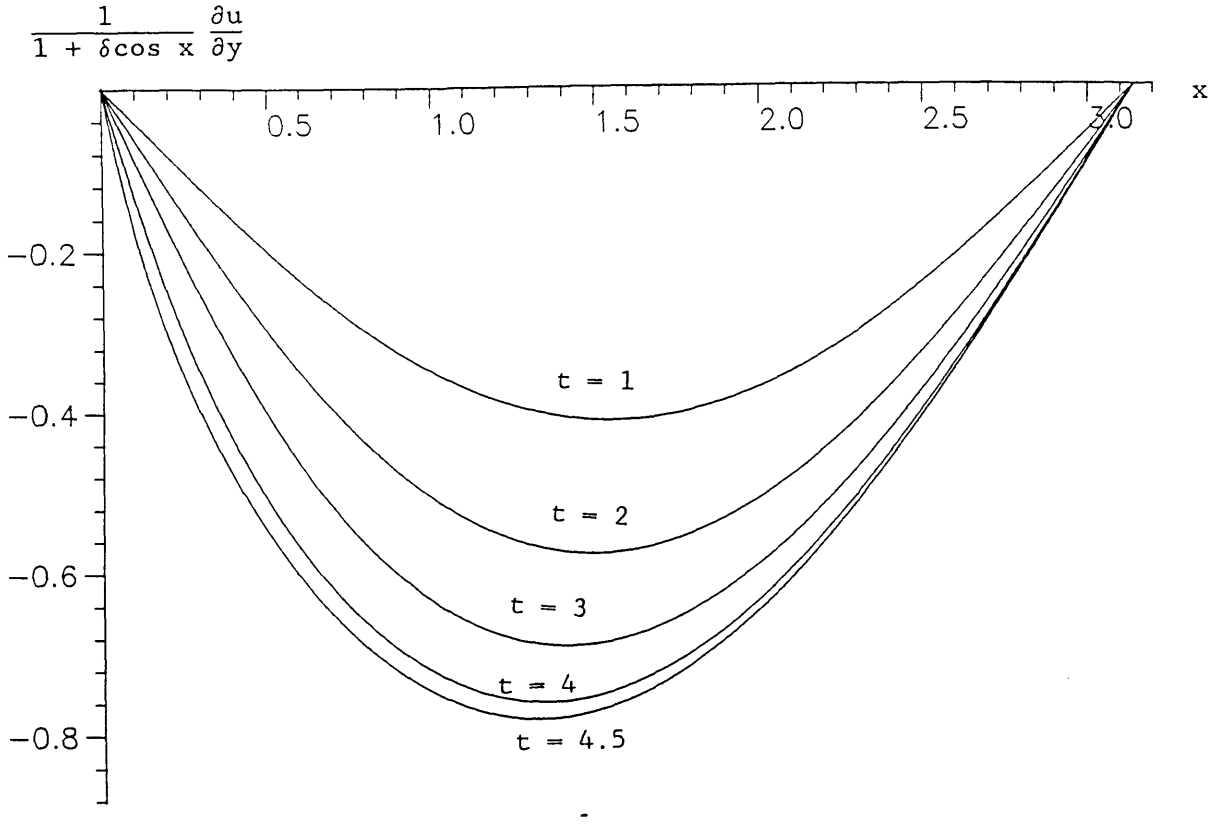


Figure 1.7:2b $W_R = 1,\ \delta = 0$

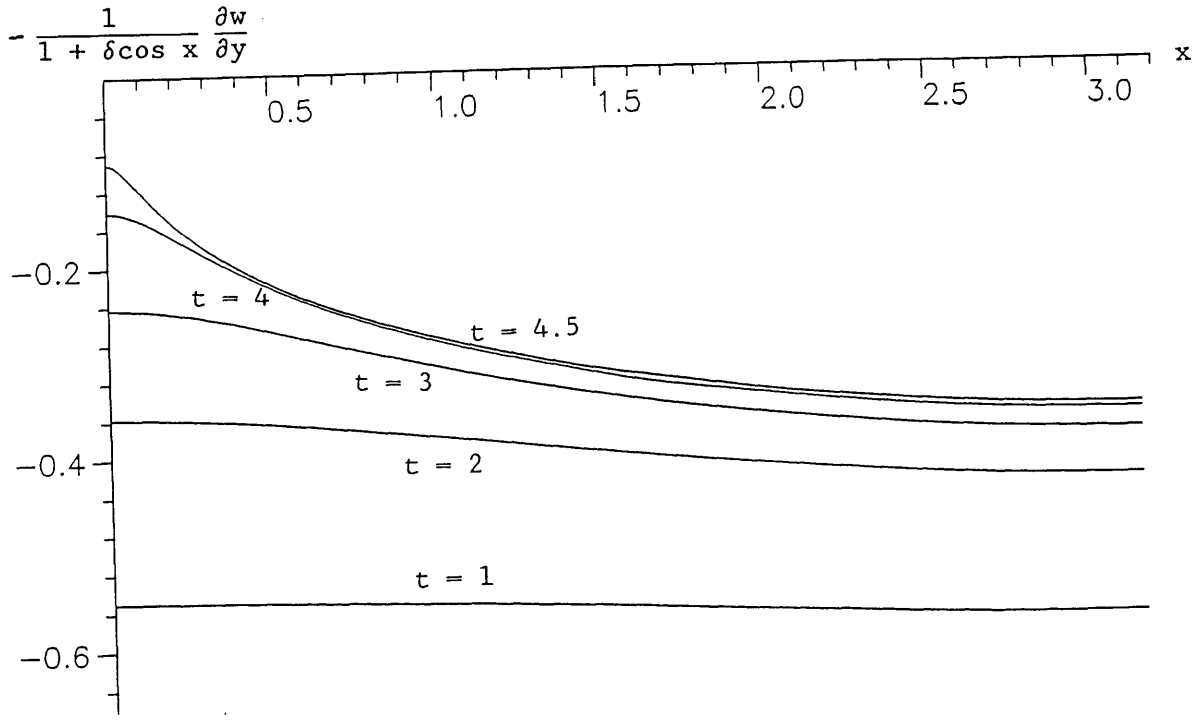
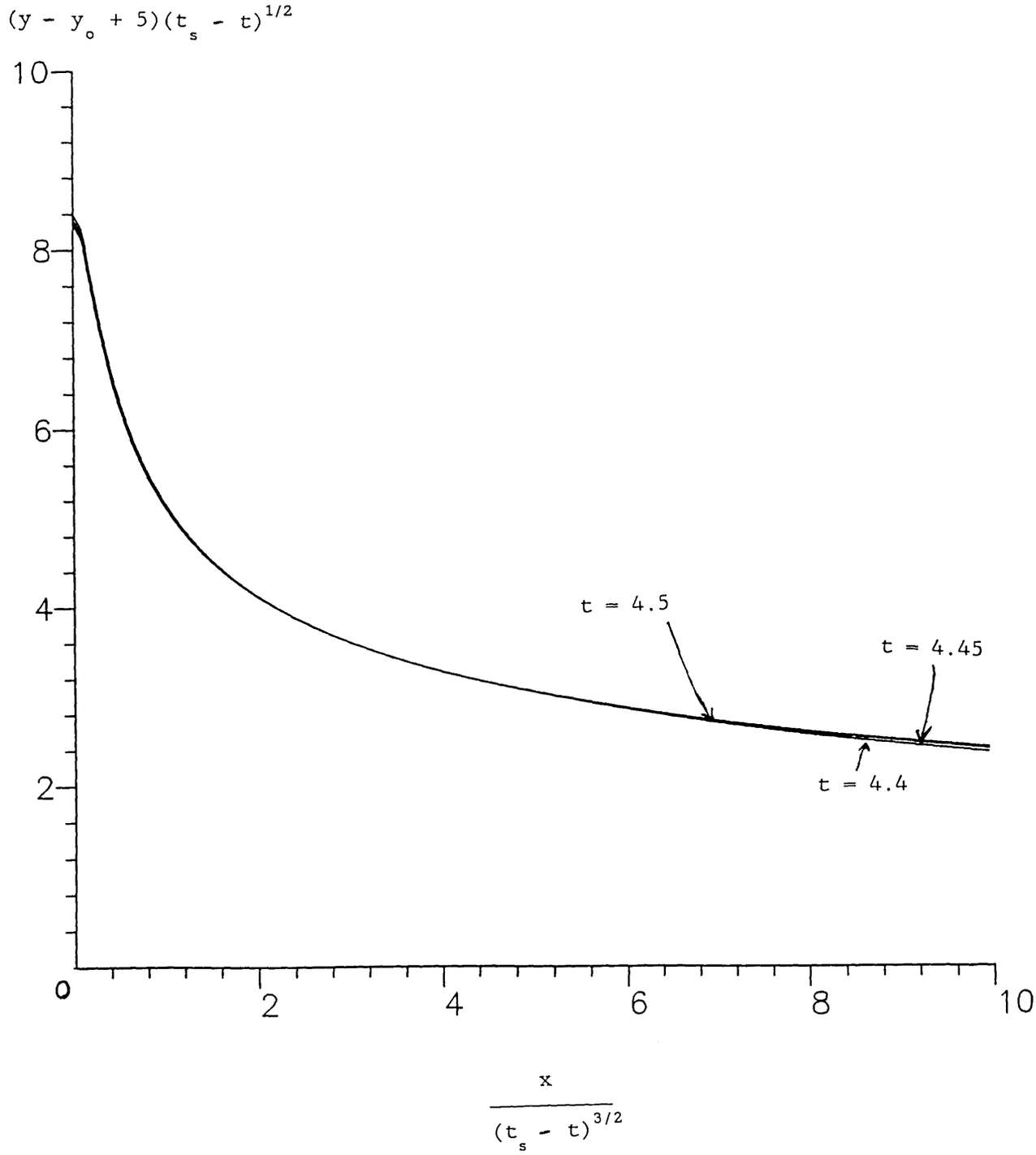


Figure 1.7.3 $W_R = 1$, $\delta = 0$, $\eta = 5$



Appendix 1.A The Unsteady Flow over a Circular Cylinder

High-Reynolds-number impulsively started flow past a two-dimensional circular cylinder has been solved in Lagrangian coordinates (ξ, η) by Van Dommelen and Shen (1980). This two-dimensional boundary-layer problem can be specified by two coupled partial differential equations (see Van Dommelen *et al.* 1980)

$$x_t = u \qquad (1.A:1a)$$

$$u_t = \frac{1}{2}\sin 2x + x_\xi^2 u_{\eta\eta} - 2x_\xi x_\eta u_{\xi\eta} + x_\eta^2 u_{\xi\xi} - x_\xi x_{\eta\eta} u_\xi + (x_\xi u_\eta + x_\eta u_\xi)x_{\xi\eta} - x_\eta x_{\xi\xi} u_\eta \,. \qquad (1.A:1b)$$

subject to the appropriate boundary conditions

$x = \xi, \quad u = \sin x, \quad t = 0, \quad \eta \neq 0,$

$x = 0, \quad u = 0, \quad$ on $\xi = 0,$

$x = \pi, \quad u = 0, \quad$ on $\xi = \pi,$

$x = \xi, \quad u = 0, \quad$ on $\eta = 0,$

$x = 2\arctan(e^t \tan\frac{1}{2}\xi), \quad u \to \sin x \quad$ as $\eta \to \infty$.

The quantity x is the local Eulerian tangential variable and u the velocity in that direction.

In their calculations Van Dommelen *et al.* used a second-order, central-difference, Crank-Nicolson scheme, with a special 'forward and backward' treatment for the first-order u derivatives u_ξ and u_η. The choice of the difference approximations for these derivatives depended on the sign of their coefficients and was such as to maintain diagonal dominance of the resulting difference equations. For example, if the coefficient of u_ξ at

$(\xi_i, \eta_j, (n-\frac{1}{2})\Delta t)$ is positive, the 'forward and backward' treatment approximates u_ξ by a forward difference at $t = n\Delta t$ and a backward difference at $t = (n-1)\Delta t$, i.e.

$$(u_\xi)^{n-1/2}_{i,j} = \frac{1}{2}\left[\frac{u^n_{i+1,j} - u^n_{i,j}}{\Delta\xi} + \frac{u^{n-1}_{i,j} - u^{n-1}_{i-1,j}}{\Delta\xi}\right] \qquad (1.A:2a)$$

where $u^n_{i,j}$ denotes u at the grid point $(\xi_i, \eta_j, n\Delta t)$. When the coefficient is negative the use of the forward and backward approximations is interchanged, i.e.

$$(u_\xi)^{n-1/2}_{i,j} = \frac{1}{2}\left[\frac{u^n_{i,j} - u^n_{i-1,j}}{\Delta\xi} + \frac{u^{n-1}_{i+1,j} - u^{n-1}_{i,j}}{\Delta\xi}\right] . \qquad (1.A:2b)$$

Similar approximations apply to u_η. We note that the choice of the approximations is precisely opposite to that of the 'upwind and downwind' difference approximations for first order equations such as

$$u_t + c\, u_\xi = 0 .$$

Van Dommelen and Shen (1980) solved the implicit difference equations (A.1:1a,b) using point iteration. The iterations proceeded first in the positive η direction towards decreasing ξ, and then in the negative η direction and towards increasing ξ. Also it appears that they completed one iteration sweeping through the whole grid for u, before performing one sweep of x.

As a preliminary exercise to the curved pipe problem, the above calculation for the circular cylinder was repeated using an identical 'forward and backward' treatment for u_ξ and u_η, and point iteration. Similar results to those of Van Dommelen *et al.* were

obtained. Various other iterative procedures were then tried to find the one with the fastest convergence.

The first attempt used the 'forward and backward' treatment based on that of Van Dommelen *et al.*. However, rather than using point iteration, a line iteration technique (cf. section 1.3) was applied to the coupled difference equations for both x and u. The line iterations first proceeded in the direction of decreasing ξ for whole compuational domain, and then in the direction of increasing ξ. This resulted in an increased rate of convergence. However it was found that alternating the directions between ξ and η resulted in even faster convergence.

In addition, as a second method, straight forward second-order central differences were used throughout the discretisation of the coupled partial differential equations. As above a line iteration technique, in which both x and u were updated at the end of each iteration, was used, and the line iterations were alternated between the directions ξ and η. No convergence problems were encountered as the iteration tolerance criterion was reduced (Van Dommelen and Shen reported difficulties with their iteration scheme and central differences). Therefore, it was decided to implement the relatively simpler second-order central difference approximations for the flow through a curved pipe.

Appendix 1.B The Finite Difference Equations

(i) The Leap-frog scheme applied to equations (1.2:7a,8) at $(\xi_i, \eta_j, (n-1)\Delta t)$

$$\frac{x_{i,j}^{n+1} - x_{i,j}^{n-1}}{2\Delta t} + \beta_t \left[\frac{x_{i,j+1}^{n} - x_{i,j-1}^{n}}{2\Delta\beta} \right] = \frac{u_{i,j}^{n}}{1+\delta\cos x_{i,j}^{n}}$$

$$\frac{u_{i,j}^{n+1} - u_{i,j}^{n-1}}{2\Delta t} + \beta_t \left(\frac{u_{i,j+1}^{n} - u_{i,j-1}^{n}}{2\Delta\beta} \right)$$

$$= \frac{\sin x_{i,j}^{n}}{(1+\delta\cos \xi_i)^2} \left[w_{i,j}^{n} \left(2W_o^n - w_{i,j}^{n} \right) - \delta (u_{i,j}^{n})^2 \right]$$

$$+ \left(\frac{1+\delta\cos x_{i,j}^{n}}{1+\delta\cos \xi_i} \right)^2 \alpha_\xi^2 \beta_\eta^2 \left[\left(\frac{x_{i+1,j}^{n} - x_{i-1,j}^{n}}{2\Delta\alpha} \right)^2 \left(\frac{u_{i,j+1}^{n} - 2u_{i,j}^{n} + u_{i,j-1}^{n}}{\Delta\beta^2} \right) \right.$$

$$-2 \left(\frac{x_{i+1,j}^{n} - x_{i-1,j}^{n}}{2\Delta\alpha} \right) \left(\frac{x_{i,j+1}^{n} - x_{i,j-1}^{n}}{2\Delta\beta} \right) \left(\frac{u_{i+1,j+1}^{n} - u_{i+1,j-1}^{n} - u_{i-1,j+1}^{n} + u_{i-1,j-1}^{n}}{4\Delta\alpha\Delta\beta} \right)$$

$$\left. + \left(\frac{x_{i,j+1}^{n} - x_{i,j-1}^{n}}{2\Delta\beta} \right)^2 \left(\frac{u_{i+1,j}^{n} - 2u_{i,j}^{n} + u_{i-1,j}^{n}}{\Delta\alpha^2} \right) \right]$$

$$+\left[\frac{1+\delta\cos x^{n}_{i,j}}{1+\delta\cos \xi_i}\right]^2\left[\frac{u^{n}_{i+1,j}-u^{n}_{i-1,j}}{2\Delta\alpha}\right]\Bigg[-\alpha_\xi^2\beta_\eta^2\left[\frac{x^{n}_{i+1,j}-x^{n}_{i-1,j}}{2\Delta\alpha}\right]\left[\frac{x^{n}_{i,j+1}-2x^{n}_{i,j}+x^{n}_{i,j-1}}{\Delta\beta^2}\right]$$

$$-\alpha_\xi^2\beta_{\eta\eta}\left[\frac{x^{n}_{i+1,j}-x^{n}_{i-1,j}}{2\Delta\alpha}\right]\left[\frac{x^{n}_{i,j+1}-x^{n}_{i,j-1}}{2\Delta\beta}\right]$$

$$+\alpha_\xi^2\beta_\eta^2\left[\frac{x^{n}_{i,j+1}-x^{n}_{i,j-1}}{2\Delta\beta}\right]\left[\frac{x^{n}_{i+1,j+1}-x^{n}_{i+1,j-1}-x^{n}_{i-1,j+1}+x^{n}_{i-1,j-1}}{4\Delta\alpha\Delta\beta}\right]$$

$$+\beta_\eta^2\left[\frac{\alpha_\xi\,\delta\sin\xi_i}{1+\delta\cos\xi_i}+\alpha_{\xi\xi}\right]\left[\frac{x^{n}_{i,j+1}-x^{n}_{i,j-1}}{2\Delta\beta}\right]^2\Bigg]$$

$$+\left[\frac{1+\delta\cos x^{n}_{i,j}}{1+\delta\cos \xi_i}\right]^2\left[\frac{u^{n}_{i,j+1}-u^{n}_{i,j-1}}{2\Delta\beta}\right]\Bigg[-\alpha_\xi^2\beta_\eta^2\left[\frac{x^{n}_{i,j+1}-x^{n}_{i,j-1}}{2\Delta\beta}\right]\left[\frac{x^{n}_{i+1,j}-2x^{n}_{i,j}+x^{n}_{i-1,j}}{\Delta\alpha^2}\right]$$

$$+\alpha_\xi^2\beta_{\eta\eta}\left[\frac{x^{n}_{i+1,j}-x^{n}_{i-1,j}}{2\Delta\alpha}\right]^2$$

$$+\alpha_\xi^2\beta_\eta^2\left[\frac{x^{n}_{i+1,j}-x^{n}_{i-1,j}}{2\Delta\alpha}\right]\left[\frac{x^{n}_{i+1,j+1}-x^{n}_{i+1,j-1}-x^{n}_{i-1,j+1}+x^{n}_{i-1,j-1}}{4\Delta\alpha\Delta\beta}\right]$$

$$-\beta_\eta^2\left[\frac{\alpha_\xi\ \delta\sin\xi_i}{1+\delta\cos\xi_i}+\alpha_{\xi\xi}\right]\left[\frac{x^{n}_{i+1,j}-x^{n}_{i-1,j}}{2\Delta\alpha}\right]\left[\frac{x^{n}_{i,j+1}-x^{n}_{i,j-1}}{2\Delta\beta}\right]\Bigg]$$

$$\frac{w_{i,j}^{n+1} - w_{i,j}^{n-1}}{2\Delta t} + \beta_t \left(\frac{w_{i,j+1}^{n} - w_{i,j-1}^{n}}{2\Delta\beta} \right)$$

$$= \left(\frac{1+\delta\cos x_{i,j}^{n}}{1+\delta\cos \xi_i} \right)^2 \alpha_\xi^2 \beta_\eta^2 \left[\left(\frac{x_{i+1,j}^{n} - x_{i-1,j}^{n}}{2\Delta\alpha} \right)^2 \left(\frac{w_{i,j+1}^{n} - 2w_{i,j}^{n} + w_{i,j-1}^{n}}{\Delta\beta^2} \right) \right.$$

$$-2 \left(\frac{x_{i+1,j}^{n} - x_{i-1,j}^{n}}{2\Delta\alpha} \right) \left(\frac{x_{i,j+1}^{n} - x_{i,j-1}^{n}}{2\Delta\beta} \right) \left(\frac{w_{i+1,j+1}^{n} - w_{i+1,j-1}^{n} - w_{i-1,j+1}^{n} + w_{i-1,j-1}^{n}}{4\Delta\alpha\Delta\beta} \right)$$

$$\left. + \left(\frac{x_{i,j+1}^{n} - x_{i,j-1}^{n}}{2\Delta\beta} \right)^2 \left(\frac{w_{i+1,j}^{n} - 2w_{i,j}^{n} + w_{i-1,j}^{n}}{\Delta\alpha^2} \right) \right]$$

$$+\left[\frac{1+\delta\cos x^{n}_{i,j}}{1+\delta\cos \xi_i}\right]^2\left[\frac{w^{n}_{i+1,j}-w^{n}_{i-1,j}}{2\Delta\alpha}\right]\Bigg[-\alpha_\xi^2\beta_\eta^2\left[\frac{x^{n}_{i+1,j}-x^{n}_{i-1,j}}{2\Delta\alpha}\right]\left[\frac{x^{n}_{i,j+1}-2x^{n}_{i,j}+x^{n}_{i,j-1}}{\Delta\beta^2}\right]$$

$$-\alpha_\xi^2\beta_{\eta\eta}\left[\frac{x^{n}_{i+1,j}-x^{n}_{i-1,j}}{2\Delta\alpha}\right]\left[\frac{x^{n}_{i,j+1}-x^{n}_{i,j-1}}{2\Delta\beta}\right]$$

$$+\alpha_\xi^2\beta_\eta^2\left[\frac{x^{n}_{i,j+1}-x^{n}_{i,j-1}}{2\Delta\beta}\right]\left[\frac{x^{n}_{i+1,j+1}-x^{n}_{i+1,j-1}-x^{n}_{i-1,j+1}+x^{n}_{i-1,j-1}}{4\Delta\alpha\Delta\beta}\right]$$

$$+\beta_\eta^2\left[\frac{\alpha_\xi\,\delta\sin\xi_i}{1+\delta\cos\xi_i}+\alpha_{\xi\xi}\right]\left[\frac{x^{n}_{i,j+1}-x^{n}_{i,j-1}}{2\Delta\beta}\right]^2\Bigg]$$

$$+\left[\frac{1+\delta\cos x^{n}_{i,j}}{1+\delta\cos \xi_i}\right]^2\left[\frac{w^{n}_{i,j+1}-w^{n}_{i,j-1}}{2\Delta\beta}\right]\Bigg[-\alpha_\xi^2\beta_\eta^2\left[\frac{x^{n}_{i,j+1}-x^{n}_{i,j-1}}{2\Delta\beta}\right]\left[\frac{x^{n}_{i+1,j}-2x^{n}_{i,j}+x^{n}_{i-1,j}}{\Delta\alpha^2}\right]$$

$$+\alpha_\xi^2\beta_{\eta\eta}\left[\frac{x^{n}_{i+1,j}-x^{n}_{i-1,j}}{2\Delta\alpha}\right]^2$$

$$+\alpha_\xi^2\beta_\eta^2\left[\frac{x^{n}_{i+1,j}-x^{n}_{i-1,j}}{2\Delta\alpha}\right]\left[\frac{x^{n}_{i+1,j+1}-x^{n}_{i+1,j-1}-x^{n}_{i-1,j+1}+x^{n}_{i-1,j-1}}{4\Delta\alpha\Delta\beta}\right]$$

$$-\beta_\eta^2\left[\frac{\alpha_\xi\,\delta\sin\xi_i}{1+\delta\cos\xi_i}+\alpha_{\xi\xi}\right]\left[\frac{x^{n}_{i+1,j}-x^{n}_{i-1,j}}{2\Delta\alpha}\right]\left[\frac{x^{n}_{i,j+1}-x^{n}_{i,j-1}}{2\Delta\beta}\right]\Bigg]$$

(ii) The Crank-Nicolson scheme applied to equations (1.2:7a,8) at $(\xi_i, \eta_j, (n-\frac{1}{2})\Delta t)$

$$\frac{x^{n}_{i,j} - x^{n-1}_{i,j}}{\Delta t} + \beta_t \left(\frac{x^{n}_{i,j+1} - x^{n}_{i,j-1} + x^{n-1}_{i,j+1} - x^{n-1}_{i,j-1}}{4\Delta\beta} \right) = \frac{\frac{1}{2}(u^{n}_{i,j} + u^{n-1}_{i,j})}{1+\delta\cos\frac{1}{2}(x^{n}_{i,j} + x^{n-1}_{i,j})}$$

$$\frac{u^{n}_{i,j} - u^{n-1}_{i,j}}{\Delta t} + \beta_t \left(\frac{u^{n}_{i,j+1} - u^{n}_{i,j-1} + u^{n-1}_{i,j+1} - u^{n-1}_{i,j-1}}{4\Delta\beta} \right)$$

$$= \frac{\sin \frac{1}{2}(x^{n}_{i,j} + x^{n-1}_{i,j})}{(1+\delta\cos \xi_i)^2} \left[\frac{1}{4}(w^{n}_{i,j} + w^{n-1}_{i,j}) \left(2W^{n}_{o} - w^{n}_{i,j} + 2W^{n-1}_{o} - w^{n-1}_{i,j} \right) - \delta \left(\frac{1}{2}(u^{n}_{i,j} + u^{n-1}_{i,j}) \right)^2 \right]$$

$$+ \left(\frac{1+\delta\cos \frac{1}{2}(x^{n}_{i,j} + x^{n-1}_{i,j})}{1+\delta\cos \xi_i} \right)^2 \alpha_\xi^2 \beta_\eta^2 \left[\left(\frac{x^{n}_{i+1,j} - x^{n}_{i-1,j} + x^{n-1}_{i+1,j} - x^{n-1}_{i-1,j}}{4\Delta\alpha} \right)^2 \left(\frac{u^{n}_{i,j+1} - 2u^{n}_{i,j} + u^{n}_{i,j-1} + u^{n-1}_{i,j+1} - 2u^{n-1}_{i,j} + u^{n-1}_{i,j-1}}{2\Delta\beta^2} \right) \right.$$

$$-2 \left(\frac{x^{n}_{i+1,j} - x^{n}_{i-1,j} + x^{n-1}_{i+1,j} - x^{n-1}_{i-1,j}}{4\Delta\alpha} \right) \left(\frac{x^{n}_{i,j+1} - x^{n}_{i,j-1} + x^{n-1}_{i,j+1} - x^{n-1}_{i,j-1}}{4\Delta\beta} \right) \times$$

$$\left(\frac{u^{n}_{i+1,j+1} - u^{n}_{i+1,j-1} - u^{n}_{i-1,j+1} + u^{n}_{i-1,j-1} + u^{n-1}_{i+1,j+1} - u^{n-1}_{i+1,j-1} - u^{n-1}_{i-1,j+1} + u^{n-1}_{i-1,j-1}}{8\Delta\alpha\Delta\beta} \right)$$

$$\left. + \left(\frac{x^{n}_{i,j+1} - x^{n}_{i,j-1} + x^{n-1}_{i,j+1} - x^{n-1}_{i,j-1}}{4\Delta\beta} \right)^2 \left(\frac{u^{n}_{i+1,j} - 2u^{n}_{i,j} + u^{n}_{i-1,j} + u^{n-1}_{i+1,j} - 2u^{n-1}_{i,j} + u^{n-1}_{i-1,j}}{2\Delta\alpha^2} \right) \right]$$

$$+\left[\frac{1+\delta\cos\frac{1}{2}(x^{n}_{i,j}+x^{n-1}_{i,j})}{1+\delta\cos\xi_i}\right]^2\left[\frac{u^{n}_{i+1,j}-u^{n}_{i-1,j}+u^{n-1}_{i+1,j}-u^{n-1}_{i-1,j}}{4\Delta\alpha}\right]\times$$

$$\left[-\alpha_\xi^2\beta_\eta^2\left[\frac{x^{n}_{i+1,j}-x^{n}_{i-1,j}+x^{n-1}_{i+1,j}-x^{n-1}_{i-1,j}}{4\Delta\alpha}\right]\left[\frac{x^{n}_{i,j+1}-2x^{n}_{i,j}+x^{n}_{i,j-1}+x^{n-1}_{i,j+1}-2x^{n-1}_{i,j}+x^{n-1}_{i,j-1}}{2\Delta\beta^2}\right]\right.$$

$$-\alpha_\xi^2\beta_{\eta\eta}\left[\frac{x^{n}_{i+1,j}-x^{n}_{i-1,j}+x^{n-1}_{i+1,j}-x^{n-1}_{i-1,j}}{4\Delta\alpha}\right]\left[\frac{x^{n}_{i,j+1}-x^{n}_{i,j-1}+x^{n-1}_{i,j+1}-x^{n-1}_{i,j-1}}{4\Delta\beta}\right]$$

$$+\alpha_\xi^2\beta_\eta^2\left[\frac{x^{n}_{i,j+1}-x^{n}_{i,j-1}+x^{n-1}_{i,j+1}-x^{n-1}_{i,j-1}}{4\Delta\beta}\right]\left[\frac{x^{n}_{i+1,j+1}-x^{n}_{i+1,j-1}-x^{n}_{i-1,j+1}+x^{n}_{i-1,j-1}+x^{n-1}_{i+1,j+1}-x^{n-1}_{i+1,j-1}-x^{n-1}_{i-1,j+1}+x^{n-1}_{i-1,j-1}}{8\Delta\alpha\Delta\beta}\right]$$

$$\left.+\beta_\eta^2\left[\frac{\alpha_\xi\,\delta\sin\xi_i}{1+\delta\cos\xi_i}+\alpha_{\xi\xi}\right]\left[\frac{x^{n}_{i,j+1}-x^{n}_{i,j-1}+x^{n-1}_{i,j+1}-x^{n-1}_{i,j-1}}{4\Delta\beta}\right]^2\right]$$

$$+\left[\frac{1+\delta\cos\frac{1}{2}(x^{n}_{i,j}+x^{n-1}_{i,j})}{1+\delta\cos\xi_i}\right]^2\left[\frac{u^{n}_{i,j+1}-u^{n}_{i,j-1}+u^{n-1}_{i,j+1}-u^{n-1}_{i,j-1}}{4\Delta\beta}\right]\times$$

$$\left[-\alpha_\xi^2\beta_\eta^2\left[\frac{x^{n}_{i,j+1}-x^{n}_{i,j-1}+x^{n-1}_{i,j+1}-x^{n-1}_{i,j-1}}{4\Delta\beta}\right]\left[\frac{x^{n}_{i+1,j}-2x^{n}_{i,j}+x^{n}_{i-1,j}+x^{n-1}_{i+1,j}-2x^{n-1}_{i,j}+x^{n-1}_{i-1,j}}{2\Delta\alpha^2}\right]\right.$$

$$+\alpha_\xi^2\beta_{\eta\eta}\left[\frac{x^{n}_{i+1,j}-x^{n}_{i-1,j}+x^{n-1}_{i+1,j}-x^{n-1}_{i-1,j}}{4\Delta\alpha}\right]^2$$

$$+\alpha_\xi^2\beta_\eta^2\left[\frac{x^{n}_{i+1,j}-x^{n}_{i-1,j}+x^{n-1}_{i+1,j}-x^{n-1}_{i-1,j}}{4\Delta\alpha}\right]\left[\frac{x^{n}_{i+1,j+1}-x^{n}_{i+1,j-1}-x^{n}_{i-1,j+1}+x^{n}_{i-1,j-1}+x^{n-1}_{i+1,j+1}-x^{n-1}_{i+1,j-1}-x^{n-1}_{i-1,j+1}+x^{n-1}_{i-1,j-1}}{8\Delta\alpha\Delta\beta}\right]$$

$$\left.-\beta_\eta^2\left[\frac{\alpha_\xi\ \delta\sin\xi_i}{1+\delta\cos\xi_i}+\alpha_{\xi\xi}\right]\left[\frac{x^{n}_{i+1,j}-x^{n}_{i-1,j}+x^{n-1}_{i+1,j}-x^{n-1}_{i-1,j}}{4\Delta\alpha}\right]\left[\frac{x^{n}_{i,j+1}-x^{n}_{i,j-1}+x^{n-1}_{i,j+1}-x^{n-1}_{i,j-1}}{4\Delta\beta}\right]\right]$$

$$\frac{w_{i,j}^{n} - w_{i,j}^{n-1}}{\Delta t} + \beta_t \left(\frac{w_{i,j+1}^{n} - w_{i,j-1}^{n} + w_{i,j+1}^{n-1} - w_{i,j-1}^{n-1}}{4\Delta\beta} \right)$$

$$= \left(\frac{1+\delta\cos\frac{1}{2}(x_{i,j}^{n} + x_{i,j}^{n-1})}{1+\delta\cos\xi_i} \right)^2 \alpha_\xi^2 \beta_\eta^2 \left[\left(\frac{x_{i+1,j}^{n} - x_{i-1,j}^{n} + x_{i+1,j}^{n-1} - x_{i-1,j}^{n-1}}{4\Delta\alpha} \right)^2 \left(\frac{w_{i,j+1}^{n} - 2w_{i,j}^{n} + w_{i,j-1}^{n} + w_{i,j+1}^{n-1} - 2w_{i,j}^{n-1} + w_{i,j-1}^{n-1}}{2\Delta\beta^2} \right) \right.$$

$$-2 \left(\frac{x_{i+1,j}^{n} - x_{i-1,j}^{n} + x_{i+1,j}^{n-1} - x_{i-1,j}^{n-1}}{4\Delta\alpha} \right) \left(\frac{x_{i,j+1}^{n} - x_{i,j-1}^{n} + x_{i,j+1}^{n-1} - x_{i,j-1}^{n-1}}{4\Delta\beta} \right) \times$$

$$\left(\frac{w_{i+1,j+1}^{n} - w_{i+1,j-1}^{n} - w_{i-1,j+1}^{n} + w_{i-1,j-1}^{n} + w_{i+1,j+1}^{n-1} - w_{i+1,j-1}^{n-1} - w_{i-1,j+1}^{n-1} + w_{i-1,j-1}^{n-1}}{8\Delta\alpha\,\Delta\beta} \right)$$

$$\left. + \left(\frac{x_{i,j+1}^{n} - x_{i,j-1}^{n} + x_{i,j+1}^{n-1} - x_{i,j-1}^{n-1}}{4\Delta\beta} \right)^2 \left(\frac{w_{i+1,j}^{n} - 2w_{i,j}^{n} + w_{i-1,j}^{n} + w_{i+1,j}^{n-1} - 2w_{i,j}^{n-1} + w_{i-1,j}^{n-1}}{2\Delta\alpha^2} \right) \right]$$

$$+\left[\frac{1+\delta\cos\frac{1}{2}(x^{n}_{i,j}+x^{n-1}_{i,j})}{1+\delta\cos\xi_i}\right]^2\left[\frac{w^{n}_{i+1,j}-w^{n}_{i-1,j}+w^{n-1}_{i+1,j}-w^{n-1}_{i-1,j}}{4\Delta\alpha}\right]\times$$

$$\left[-\alpha_\xi^2\beta_\eta^2\left[\frac{x^{n}_{i+1,j}-x^{n}_{i-1,j}+x^{n-1}_{i+1,j}-x^{n-1}_{i-1,j}}{4\Delta\alpha}\right]\left[\frac{x^{n}_{i,j+1}-2x^{n}_{i,j}+x^{n}_{i,j-1}+x^{n-1}_{i,j+1}-2x^{n-1}_{i,j}+x^{n-1}_{i,j-1}}{2\Delta\beta^2}\right]\right.$$

$$-\alpha_\xi^2\beta_{\eta\eta}\left[\frac{x^{n}_{i+1,j}-x^{n}_{i-1,j}+x^{n-1}_{i+1,j}-x^{n-1}_{i-1,j}}{4\Delta\alpha}\right]\left[\frac{x^{n}_{i,j+1}-x^{n}_{i,j-1}+x^{n-1}_{i,j+1}-x^{n-1}_{i,j-1}}{4\Delta\beta}\right]$$

$$+\alpha_\xi^2\beta_\eta^2\left[\frac{x^{n}_{i,j+1}-x^{n}_{i,j-1}+x^{n-1}_{i,j+1}-x^{n-1}_{i,j-1}}{4\Delta\beta}\right]\left[\frac{x^{n}_{i+1,j+1}-x^{n}_{i+1,j-1}-x^{n}_{i-1,j+1}+x^{n}_{i-1,j-1}+x^{n-1}_{i+1,j+1}-x^{n-1}_{i+1,j-1}-x^{n-1}_{i-1,j+1}+x^{n-1}_{i-1,j-1}}{8\Delta\alpha\,\Delta\beta}\right]$$

$$\left.+\beta_\eta^2\left[\frac{\alpha_\xi\,\delta\sin\xi_i}{1+\delta\cos\xi_i}+\alpha_{\xi\xi}\right]\left[\frac{x^{n}_{i,j+1}-x^{n}_{i,j-1}+x^{n-1}_{i,j+1}-x^{n-1}_{i,j-1}}{4\Delta\beta}\right]^2\right]$$

$$+\left[\frac{1+\delta\cos\frac{1}{2}(x^{n}_{i,j}+x^{n-1}_{i,j})}{1+\delta\cos\xi_i}\right]^2\left[\frac{w^{n}_{i,j+1}-w^{n}_{i,j-1}+w^{n-1}_{i,j+1}-w^{n-1}_{i,j-1}}{4\Delta\beta}\right]\times$$

$$\left[-\alpha_\xi^2\beta_\eta^2\left[\frac{x^{n}_{i,j+1}-x^{n}_{i,j-1}+x^{n-1}_{i,j+1}-x^{n-1}_{i,j-1}}{4\Delta\beta}\right]\left[\frac{x^{n}_{i+1,j}-2x^{n}_{i,j}+x^{n}_{i-1,j}+x^{n-1}_{i+1,j}-2x^{n-1}_{i,j}+x^{n-1}_{i-1,j}}{2\Delta\alpha^2}\right]\right.$$

$$+\alpha_\xi^2\beta_{\eta\eta}\left[\frac{x^{n}_{i+1,j}-x^{n}_{i-1,j}+x^{n-1}_{i+1,j}-x^{n-1}_{i-1,j}}{4\Delta\alpha}\right]^2$$

$$+\alpha_\xi^2\beta_\eta^2\left[\frac{x^{n}_{i+1,j}-x^{n}_{i-1,j}+x^{n-1}_{i+1,j}-x^{n-1}_{i-1,j}}{4\Delta\alpha}\right]\left[\frac{x^{n}_{i+1,j+1}-x^{n}_{i+1,j-1}-x^{n}_{i-1,j+1}+x^{n}_{i-1,j-1}+x^{n-1}_{i+1,j+1}-x^{n-1}_{i+1,j-1}-x^{n-1}_{i-1,j+1}+x^{n-1}_{i-1,j-1}}{8\Delta\alpha\,\Delta\beta}\right]$$

$$\left.-\beta_\eta^2\left[\frac{\alpha_\xi\,\delta\sin\xi_i}{1+\delta\cos\xi_i}+\alpha_{\xi\xi}\right]\left[\frac{x^{n}_{i+1,j}-x^{n}_{i-1,j}+x^{n-1}_{i+1,j}-x^{n-1}_{i-1,j}}{4\Delta\alpha}\right]\left[\frac{x^{n}_{i,j+1}-x^{n}_{i,j-1}+x^{n-1}_{i,j+1}-x^{n-1}_{i,j-1}}{4\Delta\beta}\right]\right]$$

Appendix 1.C The Evaluation of a Function on a Characteristic in a Two-dimensional Computational Domain

Suppose we want to evaluate a function F along a characteristic of constant x given a two-dimensional computational domain of N points in the ξ direction by M points in the η direction. In general, the paths of constant $x(\xi, \eta)$ do not pass through these discrete points. Suppose we require the value of $F(x_*, \eta_*)$ and that the characteristic $x(\xi, \eta) = x_*$ goes through the position (ξ_*, η_*). At times before the separation singularity develops, the value of ξ_* is uniquely determined by x_* and η_*. For simplicity we consider the case where the neighbouring two grid points in any direction lie in the computational domain, i.e. i and j exist such that (a) ξ_* lies between ξ_i and ξ_{i+1} and η_* between η_j and η_{j+1}, and (b) i and j satisfy the following inequalities

$$1 \le i-1, \qquad i+2 \le N, \qquad 1 \le j-1, \qquad \text{and} \qquad j+2 \le M.$$

When the conditions are not satisfied a slightly modified approach is necessary.

The position (ξ_*, η_*), marked by '*', then lies in the grid as shown in figure 1.C:1.

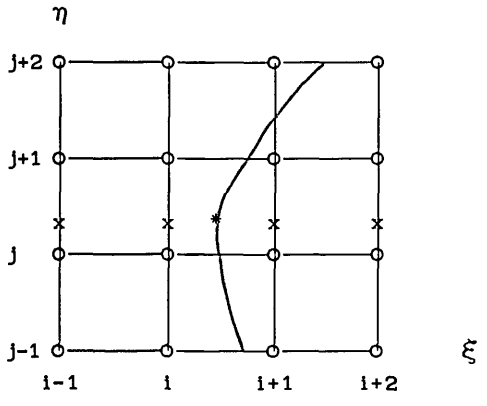


Figure 1.C:1

On the assumption that the function F and the values of $x(\xi, \eta)$ are known at all the discrete grid points (ξ, η) marked by 'o', it is possible to evaluate the function $F(x, \eta)$ at (ξ_*, η_*) by two one-dimensional, cubic Lagrangian interpolations.

Firstly, cubic interpolations are applied in the vertical direction to obtain the values of $x(\xi_k, \eta_*)$ and $F(\xi_k, \eta_*)$ for $i-1 \leq k \leq i+2$, i.e. interpolated values of x and F are found at all points marked 'x'. Given the values of F at four distinct values of x, it is now possible to interpolate directly for the value of $F(x_*, \eta_*)$ using an interpolation formula for a non-uniform grid. Note that the value of ξ_* is not needed and is not calculated.

Appendix 1.D Constants for a Padé Approximant Integration Method

Suppose we approximate a function $f(\eta)$ by

$$f = \frac{A}{\varepsilon+(\eta-\eta_o)^2} + \frac{B(\eta-\eta_o)}{\varepsilon+(\eta-\eta_o)^2} + C \ , \qquad (1.D:1)$$

where A, B, C, ε and η_o are unknown constants. For convenience, the value of the function at η_j is denoted by f_j, i.e.

$$f_j = \frac{A}{\varepsilon+(\eta_j-\eta_o)^2} + \frac{B(\eta_j-\eta_o)}{\varepsilon+(\eta_j-\eta_o)^2} + C \ , \qquad (1.D:2a)$$

and the difference between η_j and η_o by g_j, i.e.

$$g_j = \eta_j - \eta_o \ . \qquad (1.D:2b)$$

Then using the five neighbouring points, $\eta = \eta_{j-2}$, η_{j-1}, η_j, η_{j+1} and η_{j+2}, and defining new constants γ_1, γ_2, γ_3 and γ_4 by

$$\gamma_1 = 2(f_{j+1} - f_{j-1}) - (f_{j+2} - f_{j-2}) \ , \qquad (1.D:3a)$$

$$\gamma_2 = f_{j+1} + f_{j-1} - (f_{j+2} + f_{j-2}) \ , \qquad (1.D:3b)$$

$$\gamma_3 = f_{j+1} - f_{j-1} - 2(f_{j+2} + f_{j-2}) \ , \qquad (1.D:3c)$$

$$\gamma_4 = 4(f_{j+1} + f_{j-1}) - (f_{j+2} + f_{j-2}) - 6f_j \ , \qquad (1.D:3d)$$

we may express the required constants in terms of γ_1, γ_2, γ_3 and γ_4 as

$$\eta_o = \eta_j - \frac{\Delta\eta}{2}\left[\frac{2\gamma_1\gamma_2 - \gamma_3\gamma_4}{\gamma_2\gamma_4 - \gamma_1^2}\right] \ , \qquad (1.D:4a)$$

$$\varepsilon = -4\,\Delta\eta\left[\frac{g_n\gamma_1 + \Delta\eta\,\gamma_2}{\gamma_4}\right] - g_j^{\,2}, \qquad (1.D:4b)$$

$$C = \frac{1}{2(\Delta\eta)^2}\Big[(\varepsilon + g_j^{\,2})\,(f_{j+1} - 2f_j + f_{j-1}) + 2\Delta\eta\, g_j(f_{j+1} - f_{j-1}) + (\Delta\eta)^2(f_{j+1} - f_{j-1})^2\Big], \qquad (1.D:4c)$$

$$B = \frac{1}{\Delta\eta}\Big[(\varepsilon + g_j^{\,2})\,(f_{j+1} - f_j) + \Delta\eta(2g_j + \Delta\beta)\,(f_{j+1} - C)\Big], \qquad (1.D:4d)$$

$$A = (f_j - C)\,(\varepsilon + g_j^{\,2}) - B\,g_j\,. \qquad (1.D:4e)$$

Chapter 2

Stability of Flow through Curved Pipes

§ 2.1 Introduction

Laminar flows tend to be unstable at sufficiently large Reynolds numbers, and therefore, boundary-layer theory, like other large-Reynolds-number asymptotic analysis, often results in unstable solutions (although at moderately large Reynolds numbers the instabilities may not be readily observable). In this chapter we examine the linear stability of unsteady boundary-layer flow down a loosely curved pipe. We concentrate on disturbances with relatively large frequencies, and show that the unsteady, classical boundary-layer formulation includes a linear instability when a skewed velocity profile includes a point of zero shear (i.e. zero vorticity) at some point *above* the boundary.

In the notation of the previous chapter, the Eulerian boundary-layer equations for unsteady flow through a curved pipe of constant curvature ratio δ are (e.g. see Farthing 1977, Pedley 1980)

$$\frac{u_x}{(1 + \delta\cos x)} + v_y - \frac{w_z}{(1 + \delta\cos x)^2} = 0, \qquad (2.1:1a)$$

$$u_t + vu_y + \frac{uu_x}{(1+\delta\cos x)} + \frac{\sin x}{(1+\delta\cos x)^2}(\delta u^2 - w(2W_o - w)) + \frac{(W_o - w)u_z}{(1+\delta\cos x)^2} = u_{yy}\,, \tag{2.1:1b}$$

$$w_t + vw_y + \frac{uw_x}{(1+\delta\cos x)} + \frac{(W_o - w)w_z}{(1+\delta\cos x)^2} = w_{yy}\,, \tag{2.1:1c}$$

subject to the boundary conditions

$$\begin{aligned} &u = v = 0, \quad && w = W_o(t) && \text{on } y = 0, \\ &u \to 0, && w \to 0 && \text{as } y \to \infty. \end{aligned} \tag{2.1:1d}$$

As in Chapter 1, the local Eulerian boundary-layer coordinates are (x, y, z) and the corresponding velocity components are $\left(\frac{u}{1+\delta\cos x}, v, \frac{W_o - w}{1+\delta\cos x} \right)$ respectively.

In section 2.2, we examine the stability of a flow satisfying these equations to high-frequency disturbances similar to those considered by Cowley, Hocking and Tutty (1985) in two-dimensional boundary layers. By focusing attention on disturbances away from the symmetry line the three-dimensional problem is shown to be similar to the previous two-dimensional study. Then, in section 2.3 a stability analysis for flow near (but not on) a symmetry line is given for axially-independent disturbances.

§ 2.2 Instability Analysis for Flow away from a Symmetry Line

In this section we examine the stability of flow away from a symmetry line. As in Cowley, Hocking and Tutty (1985), we denote an exact solution of equations (2.1:1) by (u_o, v_o, w_o) and consider its stability to disturbances of amplitude ε, where $\varepsilon \ll 1$, by writing

$$(u, v, w) = (u_o, v_o, w_o) + \varepsilon(\tilde{u}, \tilde{v}, \tilde{w}) . \qquad (2.2:1)$$

Substitution of the above into the equations (2.1:1) and linearisation with respect to ε yields

$$\frac{\tilde{u}_x}{(1 + \delta\cos x)} + \tilde{v}_y - \frac{\tilde{w}_z}{(1 + \delta\cos x)^2} = 0, \qquad (2.2:2a)$$

$$\tilde{u}_t + (v_o\tilde{u}_y + \tilde{v}u_{oy}) + \frac{1}{(1 + \delta\cos x)}(u_o\tilde{u}_x + \tilde{u}u_{ox}) + \frac{\delta\sin x}{(1 + \delta\cos x)^2}(2u_o\tilde{u}) - \frac{2\sin x}{(1 + \delta\cos x)^2}\tilde{w}(W_o - w_o) + \frac{1}{(1 + \delta\cos x)^2}((W_o - w_o)\tilde{u}_z - \tilde{w}u_{oz}) = \tilde{u}_{yy} , \qquad (2.2:2b)$$

$$\tilde{w}_t + (v_o\tilde{w}_y + \tilde{v}w_{oy}) + \frac{1}{(1 + \delta\cos x)}(u_o\tilde{w}_x + \tilde{u}w_{ox}) + \frac{1}{(1 + \delta\cos x)^2}((W_o - w_o)\tilde{w}_z - \tilde{w}w_{oz}) = \tilde{w}_{yy} , \qquad (2.2:2c)$$

subject to the boundary conditions

$$\begin{aligned} &\tilde{u} = \tilde{v} = \tilde{w} = 0 && \text{on } y = 0 , \\ &\tilde{u} \to 0 , \quad \tilde{w} \to 0 && \text{as } y \to \infty . \end{aligned} \qquad (2.2:2d)$$

We restrict our attention to *short wavelength* and *high frequency* disturbances, and introduce 'fast' length and time scales (X, Z, T), where

$$(X, Z, T) = \alpha(x, z, t) \qquad \text{and} \qquad \alpha >> 1.$$

For convenience, we write

$$h(x) = (1 + \delta \cos x) ,$$

which is constant to leading order on the fast X scale. Similarly the slip velocity $W_o(t)$ is constant to leading order on the fast T scale. A solution for $(\tilde{u}, \tilde{v}, \tilde{w})$ is sought of the form

$$(\tilde{u}, \tilde{v}, \tilde{w}) = \exp \left[i\vartheta(X, Z, T) \right] (\bar{u}, \alpha\bar{v}, \bar{w}) , \qquad (2.2:3)$$

where $\bar{u}$, $\bar{v}$, and $\bar{w}$ are functions of y and the slow variables x, z and t, and

$$\begin{aligned} \vartheta_X &= K(x,z,t) , \\ \vartheta_T &= -\omega(x,z,t) , \\ \vartheta_Z &= L(x,z,t) . \end{aligned} \qquad (2.2:4)$$

Here $\alpha\omega$, αK and αL are the local *complex* frequency, and *real* wavenumbers in the x and z directions respectively. For consistency of the mixed partial derivatives of ϑ

$$\begin{aligned} K_t + \omega_x &= 0 , \\ K_z - L_x &= 0 , \\ L_t + \omega_z &= 0 . \end{aligned} \qquad (2.2:5)$$

We now further expand in powers of the small parameter $\alpha^{-1/2}$:

$$(\bar{u}, \bar{v}, \bar{w}, K, \omega, L) = (\bar{u}_o, \bar{v}_o, \bar{w}_o, K_o, \omega_o, L_o) + \alpha^{-1/2}(\bar{u}_1, \bar{v}_1, \bar{w}_1, K_1, \omega_1, L_1) + \ldots . \tag{2.2:6}$$

Substituting equations (2.2:3-6) into (2.2:2) and equating terms to the leading order we find

$$iK_o\bar{u}_o + h\bar{v}_{oy} - \frac{i}{h}L_o\bar{w}_o = 0 , \tag{2.2:7a}$$

$$-i\omega_o\bar{u}_o + \bar{v}_o u_{oy} + \frac{i}{h}u_o K_o\bar{u}_o + \frac{i}{h^2}(W_o - w_o)L_o\bar{u}_o = 0 , \tag{2.2:7b}$$

$$-i\omega_o\bar{w}_o + \bar{v}_o w_{oy} + \frac{i}{h}u_o K_o\bar{w}_o + \frac{i}{h^2}(W_o - w_o)L_o\bar{w}_o = 0 . \tag{2.2:7c}$$

Note that these equations are inviscid, which is a direct result of studying *high*-frequency disturbances. Because of the three-dimensionality it is convenient to follow Gregory, Stuart and Walker (1955) and introduce skewed velocity components in the direction of the local wavenumber. We therefore define for the basic flow

$$f_o = Ku_o + \frac{L}{h}(W_o - w_o) , \quad f_{oo} = K_o u_o + \frac{L_o}{h}(W_o - w_o) , \tag{2.2:8}$$

and for the disturbance $\tilde{f}$

$$\tilde{f} = \exp\left[i\vartheta(X, Z, T) \right] \bar{f} , \tag{2.2:9a}$$

$$\bar{f} = K\bar{u} - \frac{L}{h}\bar{w} = \bar{f}_o + \alpha^{-1/2}\bar{f}_1 + \ldots . \tag{2.2:9b}$$

Then, after some manipulation, equations (2.2:7) can be simplified to a single equation for $\bar{v}$:

$$\bar{v}_o f_{ooy} - \bar{v}_{oy}(f_{oo} - h\omega_o) = 0 . \qquad (2.2:10)$$

Following Cowley *et al.* (1985), we now suppose that there is a point of zero shear in the leading-order, skewed, basic velocity profile f_{oo} at $y = y_s > 0$, i.e. $f_{ooy}(y_s) = 0$. We then take for the solution of (2.2:10)

$$\bar{v}_o = 0, \qquad \text{for } y < y_s , \qquad (2.2:11a)$$

$$\bar{v}_o = f_o(y) - h\omega_o , \qquad \text{for } y > y_s . \qquad (2.2:11b)$$

The leading-order frequency ω_o is now fixed by requiring that $\bar{v}_o$ is continuous at y_s (note that $\bar{v}_o$ satisfies the appropriate inviscid wall boundary condition of zero normal velocity), i.e.

$$f_o(y_s) = h\omega_o . \qquad (2.2:11c)$$

Substitution of the solution (2.2:11) into equation (2.2:7) gives

$$\frac{i}{h}\bar{w}_o(f_{oo} - h\omega_o) + \gamma(f_{oo} - h\omega_o)w_{oy} = 0 , \qquad (2.2:12a)$$

where $\gamma = 0$ for $y < y_s$ and $\gamma = 1$ for $y > y_s$. A similar equation is satisfied by $\bar{u}_o$. These equations yield

$$\bar{u}_o = 0 \quad , \quad \bar{w}_o = 0 \qquad \text{for } y < y_s , \qquad (2.2:12b)$$

$$\bar{u}_o = ihu_{oy} \quad , \quad \bar{w}_o = ihw_{oy} \qquad \text{for } y > y_s . \qquad (2.2:12c)$$

Note that $\bar{u}_o$ and $\bar{w}_o$ are discontinuous at y_s, although their combination $\bar{f}_o$ is continuous. Substituting (2.2:3-6) into (2.2:2), and equating terms at the next order, we find that

$$i(K_o\bar{u}_1 + K_1\bar{u}_o) + h\bar{v}_{1y} - \frac{i}{h}(L_o\bar{w}_1 + L_1\bar{w}_o) = 0 , \qquad (2.2:13a)$$

$$-i(\omega_o \bar{u}_1 + \omega_1 \bar{u}_o) + \bar{v}_1 u_{oy} + \frac{i}{h} u_o (K_o \bar{u}_1 + K_1 \bar{u}_o) + \frac{i}{h^2}(W_o - w_o)(L_o \bar{u}_1 + L_1 \bar{u}_o) = 0 \quad . \tag{2.2:13b}$$

The equation for $\bar{w}_1$ is similar to (2.2:13b) with u_{oy}, $\bar{u}_o$ and $\bar{u}_1$ replaced by w_{oy}, $\bar{w}_o$ and $\bar{w}_1$, etc.. The solution to (2.2:13) is

$$\left.\begin{aligned} &\bar{v}_1 = \bar{u}_1 = \bar{w}_1 = 0 && \text{for } y < y_s \ , \\ &\bar{v}_1 = \beta(f_{oo} - h\omega_o) - h\omega_1 + K_1 u_o + \frac{L_1}{h}(W_o - w_o), \\ &\bar{u}_1 = i\beta h u_{oy} \quad , \quad \bar{w}_1 = i\beta h w_{oy} && \text{for } y > y_s \end{aligned}\right\} \tag{2.2:14}$$

where β is a function of x, z and t which is determined at higher order.

The discontinuities in $\bar{v}_{oyy}$, $\bar{u}_o$, $\bar{w}_o$, $\bar{v}_1$, etc. at y_s indicate the presence of an asymptotically small critical layer there. As Cowley *et al.* (1985) show, matching the solutions (2.2:11, 14) across this *viscous* critical layer effectively determines the eigenvalue ω_1.

To find the disturbance solution within the critical layer we introduce a scaled y coordinate

$$y - y_s(x,z,t) = \alpha^{-1/4} Y \ , \tag{2.2:15}$$

and expand the basic flow

$$u_o = u_s + \alpha^{-1/4} u_s' Y + \alpha^{-1/2} u_s'' \frac{Y^2}{2!} + \ldots \ , \tag{2.2:16a}$$

$$w_o = w_s + \alpha^{-1/4} w_s' Y + \alpha^{-1/2} w_s'' \frac{Y^2}{2!} + \ldots \ , \tag{2.2:16b}$$

$$f_{oo} = h\omega_o + \quad 0 \quad + \alpha^{-1/2} f_s'' \frac{Y^2}{2!} + \ldots \ , \tag{2.2:16c}$$

where $u_s = u_o(y_s)$, $u_s' = u_{oy}(y_s)$, etc.. Analogous to (2.2:3) the disturbance inside the critical layer is assumed to be of the form

$$\tilde{f} = \alpha^{-1/4} \exp\left[i\vartheta(X, Z, T) \right] F(x, Y, z, t) , \qquad (2.2.17a)$$

$$\tilde{v} = \alpha^{1/2} \exp\left[i\vartheta(X, Z, T) \right] V(x, Y, z, t) , \qquad (2.2:17b)$$

$$\tilde{w} = \exp\left[i\vartheta(X, Z, T) \right] W(x, Y, z, t) . \qquad (2.2:17c)$$

Substituting (2.2:17) into (2.2:2) we obtain, after some manipulation,

$$iF + hV_y = 0 , \qquad (2.2:18a)$$

$$f_s'' YV - \left[f_s'' \frac{Y^2}{2} - h\omega_1 + K_1 u_s + \frac{L_1(W_o - w_s)}{h} \right] V_Y = ihV_{YYY} , \qquad (2.2:18b)$$

$$hw_s' V + i\left[f_s'' \frac{Y^2}{2} - h\omega_1 + K_1 u_s + \frac{L_1(W_o - w_s)}{h} \right] W = hW_{YY} , \qquad (2.2:18c)$$

subject to the boundary conditions,

$$V, W \to 0 \text{ as } Y \to -\infty , \quad W \to ihw_s' \text{ as } Y \to \infty , \qquad (2.2:19a)$$

$$V \to f_s'' \frac{Y^2}{2} - h\omega_1 + K_1 u_s + \frac{L_1(W_o - w_s)}{h} \text{ as } Y \to \infty . \qquad (2.2:19b)$$

Equations (2.2:18a,b) are similar to those solved in Cowley *et al.* (1985), and a tranformation analogous to theirs can be used to simplify them:[1]

---

[1] For simplicity we assume that $f_s'' > 0$. An analogous transformation exists when $f_s'' < 0$.

$$\zeta = \left[\frac{if_s''}{h} \right]^{1/4} Y , \qquad h\omega_1 - K_1 u_s - \frac{L_1(W_o - w_s)}{h} = \left[-if_s'' h \right]^{1/2} G, \quad (2.2:20a)$$

$$2V = \left[-if_s'' h \right]^{1/2} \left[\frac{\zeta^2}{2} - G + \mathcal{v} \right] , \qquad 2W = ihw_s'(1+\mathcal{w}) . \quad (2.2:20b)$$

On substituting into (2.2:18, 19) we obtain

$$\mathcal{v}_{\zeta\zeta\zeta} - \left[\frac{\zeta^2}{2} - G \right] \mathcal{v}_\zeta + \zeta \mathcal{v} = 0 , \qquad (2.2:21a)$$

$$\mathcal{w}_{\zeta\zeta} - \left[\frac{\zeta^2}{2} - G \right] \mathcal{w} = - \mathcal{v} , \qquad (2.2:21b)$$

subject to the boundary conditions

$$\mathcal{v} \to \pm \left[\frac{\zeta^2}{2} - G \right] , \quad \mathcal{w} \to \pm 1 \qquad \text{as } \zeta \to \pm\infty . \qquad (2.2:21c)$$

The above problem for $\mathcal{v}$ effectively reduces to finding appropriate eigenvalues G. Cowley *et al.* (1985) sought solutions for $\mathcal{v}$ of the form

$$\mathcal{v} = \left[\frac{\zeta^2}{2} - G \right] \mathrm{erf}(\mu\zeta) + \exp(-\mu^2\zeta^2) \sum_{r=0}^{n} a_r \zeta^{2r+1} \qquad (2.2:22)$$

where $\mu = 2^{-3/2}$. For each $n \geq 0$ they found solutions with eigenvalues

$$G = (4n+7)2^{-1/2} , \qquad (2.2:23a)$$

together with two further eigensolutions for n = 0 with eigenvalues

$$G = (4N+7)2^{-1/2} \qquad \text{for } N = -2, -1 . \qquad (2.2:23b)$$

Substitution of (2.2:23) into (2.2:20) yields one eigenvalue, that for N = -2, with $\mathrm{Im}(\omega_1) > 0$ (recall that we are assuming that the

wavenumbers are real). This corresponds to an *unstable* mode with a growth rate proportional to $\alpha^{1/2}$.

It remains to check that a solution for w can be found, but it follows from equation (2.2:21) that a solution for w which satisfies the boundary conditions as $\zeta \to \pm\infty$, is

$$w = v_{\zeta\zeta} .$$

Comments

The above analysis demonstrates that the work of Cowley *et al.* (1985) can be extended from two dimensions to three, in that a high-frequency instability can be found in three-dimensional boundary layers if some skewed velocity profile has a point of zero shear away from the wall.[2] For flow through a pipe this is almost always the case. For example, if axially-independent disturbances are examined, the condition reduces to the requirement that the secondary azimuthal velocity, u, has a point of zero shear; but this condition is always satisfied unless u is identically zero because u is zero both at the wall and at the edge of the boundary layer.

As in the case of the two-dimensional instability, the growth rate $\mathrm{Im}(\alpha^{1/2}\omega_1)$ monotonically increases with wavenumber α, and on the boundary-layer scaling has no upper bound. In two-dimensions this led Cowley *et al.* (1985) to tentatively suggest that the

---

[2] Note that the above analysis can be easily extended to almost any other three-dimensional boundary layer, i.e. the curved pipe boundary layer is not a special case.

instability may be connected with the appearance of the unsteady separation singularity (cf. Moore 1979). However, this connection is harder to make for the curved pipe since the separation singularity develops on the symmetry line, and the above instability analysis is not valid there. To be precise the above analysis is based on the assumption that

$$\frac{1}{\alpha K} << d \quad , \tag{2.2:24}$$

where d is the distance to the nearest symmetry line, i.e. it is assumed that a typical wavelength is very much less than a typical length scale in the boundary layer. For given large α this condition is not met sufficiently close to the symmetry lines.

In an attempt to relate the instability to the separation singularity, in the next section we modify the above analysis to relax condition (2.2:24). For simplicity, we will study axially-independent disturbances since (a) the separation singularity can form in an axially-independent formulation, and (b) this assumption simplifies the analysis without losing the essential ingredients (whereas an assumption of azimuthally independent disturbances would be more restrictive since the axial velocity is less likely to have a point of zero shear).

As a preliminary we note that close to a symmetry line (e.g. $x = 0$) it follows from (2.2:8, 11c) that, since $u_o \propto x$,

$$\omega_o \sim xK_o\Omega_o(t) \quad . \tag{2.2:25}$$

Using (2.2:4) we find that

$$\vartheta_o \sim \alpha\Gamma(\log(x) - \int \Omega_o dt) \quad , \tag{2.2:26}$$

where $\Gamma(s)$ is an undetermined function, and we have assumed $x > 0$.

As far as the solution near the symmetry line is concerned, the asymptotic behaviour of $\Gamma(s)$ as $s \to -\infty$ is required. If exponential temporal growth is anticipated, as is the case far from the symmetry line, then $\Gamma(s) \sim \lambda s$, and

$$\tilde{u} \sim x^{i\alpha\lambda} \exp\left[-i\alpha\lambda \int \Omega_o \, dt \right] \bar{u} \quad , \quad \text{etc..} \qquad (2.2:27)$$

This form of disturbance for flow near a stagnation point has been suggested previously by Prof. S.H. Davis (private communication). It is the form adopted in the following section because the temporal growth factor is consistent with the solution away from the symmetry line. The disadvantage of this choice is that as $x \to 0+$, $\tilde{u}$ oscillates increasingly rapidly for real λ, and the disturbance cannot be continued into $x < 0$. However, (i) the continuation into $x < 0$ may be via a Navier-Stokes region, i.e. a region where $x \sim D^{-1/2}$ and the boundary-layer approximation is no longer valid (Prof. S.H. Davis, private communication), and (ii) alternative choices for the asymptotic behaviour of $\Gamma(s)$ appear to have significant drawbacks (e.g. $\Gamma(s) \sim \exp(\lambda s)$ forces us to consider complex wavenumbers and complex frequencies simultaneously, with possible matching difficulties with the disturbances away from the symmetry line).

§ 2.3 Instability Analysis for Flow near a Symmetry Line

As indicated above, we will assume that both the basic flow and the disturbance are axially-independent. For further convenience we will assume that $\delta = 0$ and $W_o = 1$.

The simplified governing equations in Eulerian coordinates are then

$$u_x + v_y = 0 \quad , \tag{2.3:1a}$$

$$u_t + uu_x + vu_y - (2 - w)w \sin(x) = u_{yy} \quad , \tag{2.3:1b}$$

$$w_t + uw_x + vw_y = w_{yy} \quad . \tag{2.3:1c}$$

Close to the inner wall symmetry line we assume that an exact solution to (2.3:1) has the form (cf. (1.3:4))

$$u \sim (\pi - x)u_o(y,t) \quad , \quad v \sim v_o(y,t) \quad , \quad w \sim w_o(y,t) \quad , \tag{2.3:2}$$

and introduce a disturbance of small amplitude, $\varepsilon << 1$, so that

$$(u,\ v,\ w) = (\ (\pi - x)u_o,\ v_o,\ w_o) + \varepsilon(\tilde{u},\ \tilde{v},\ \tilde{w}) + \ldots \quad . \tag{2.3:3a}$$

On the basis of the discussion at the end of section 2.2 we study high frequency disturbances of the form

$$(\tilde{u},\tilde{v},\tilde{w}) = ((\pi - x)\bar{u},\ \alpha\bar{v},\ \bar{w})\ (\pi - x)^{-i\alpha} \exp\left[-i\alpha \int \Omega(t)dt\right] + \ldots, \tag{2.3:3b}$$

with $\alpha >> 1$, where $\bar{u}$, $\bar{v}$, $\bar{w}$ are functions of y, t and α.[1]

---

[1] The following analysis is unchanged to the order that it is taken if the right hand side of (2.3:3b) is slightly generalised by the inclusion of an additional factor of $(\pi - x)^a$, where a is an order one number and $\mathrm{Re}(a) \geq 0$.

Substitution of (2.3:3) into (2.3:1) yields, at leading order in $(\pi-x)$,

$$(i\alpha-1)\bar{u} + \alpha\bar{v}_y = 0 \ , \tag{2.3:4a}$$

$$i\alpha(u_o-\Omega)\bar{u} + \alpha\bar{v}u_{oy} + \bar{u}_t - 2\bar{u}u_o + v_o\bar{u}_y - 2(1 - w_o)\bar{w} = \bar{u}_{yy} \ , \tag{2.3:4b}$$

$$i\alpha(u_o-\Omega)\bar{w} + \alpha\bar{v}w_{oy} + \bar{w}_t + v_o\bar{w}_y = \bar{w}_{yy} \ . \tag{2.3:4c}$$

As before we now expand in inverse powers of $\alpha^{+1/2}$,

$$(\bar{u},\bar{v},\bar{w},\Omega) = (\bar{u}_o,\bar{v}_o,\bar{w}_o,\Omega_o) + \alpha^{-1/2}(\bar{u}_1,\bar{v}_1,\bar{w}_1,\Omega_1) + \ldots \ , \tag{2.3:5}$$

and substitute into (2.3:4) to obtain

$$i\bar{u}_o + \bar{v}_{oy} = 0 \ , \tag{2.3:6a}$$

$$-(u_o-\Omega_o)\bar{v}_{oy} + \bar{v}_o u_{oy} = 0 \ , \tag{2.3:6b}$$

$$i(u_o-\Omega_o)\bar{w}_o + \bar{v}_o w_{oy} = 0 \ , \tag{2.3:6c}$$

and

$$i\bar{u}_1 + \bar{v}_{1y} = 0 \ , \tag{2.3:7a}$$

$$-(u_o-\Omega_o)\bar{v}_{1y} + \bar{v}_1 u_{oy} = -\Omega_1\bar{v}_{oy} \ , \tag{2.3:7b}$$

$$i(u_o-\Omega_o)\bar{w}_1 + \bar{v}_1 w_{oy} = i\Omega_1\bar{w}_o \ . \tag{2.3:7c}$$

Paralleling the theory of the previous section we suppose that there exists a point $y = y_s > 0$ where u_{oy} is zero, i.e.

$$u_s' \equiv u_{oy}(y_s) = 0 \ , \tag{2.3:8}$$

and take as the solutions to (2.3:6, 7)

$$\bar{u}_o = \bar{v}_o = \bar{w}_o = \bar{u}_1 = \bar{v}_1 = \bar{w}_1 = 0 \qquad \text{for } y < y_s$$

$$\left.\begin{aligned} \bar{u}_o &= iu_{oy} \quad , \quad \bar{v}_o = (u_o - \Omega_o) \quad , \quad \bar{w}_o = iw_{oy} \\ \bar{u}_1 &= i\beta_1 u_{oy} \quad , \quad \bar{v}_1 = -\Omega_1 + \beta_1(u_o - \Omega_o) \\ \bar{w}_1 &= i\beta_1 w_{oy} \end{aligned}\right\} \quad \text{for } y > y_s \qquad (2.3:9)$$

where

$$\Omega_o = u_o(y_s) \quad , \qquad (2.3:10)$$

and $\beta_1(t)$ is determined at higher order.

The discontinuities in the solutions (2.3:9) at $y = y_s$ indicate the presence of a critical layer, where a scaled coordinate

$$y - y_s(t) = \alpha^{-1/4} Y \qquad (2.3:11)$$

is appropriate. The above solution suggests that within the critical layer the relevant scalings are

$$(\bar{u}, \bar{v}, \bar{w}) = (\alpha^{-1/4}U, \alpha^{-1/2}V, W) + \ldots \quad . \qquad (2.3.12)$$

Substituting into equation (2.3:4) we find, at leading order,

$$iU + V_Y = 0 \quad , \qquad (2.3:13a)$$

$$-(\tfrac{1}{2}u_s''Y^2 - \Omega_1)V_Y + u_s''YV = iV_{YYY} \quad , \qquad (2.3:13b)$$

$$i(\tfrac{1}{2}u_s''Y^2 - \Omega_1)W + w_s''YV = W_{YY} \quad . \qquad (2.3:13c)$$

Equations (2.3:13b, c) are essentially the same as (2.2:18b, c), and can be shown to have equivalent boundary conditions. They are solved as explained in section 2.2, so yielding one eigenvalue Ω_1 representing a growing mode. We therefore conclude that a similar instability exists to that described in section 2.2. In fact the

discussion at the end of section 2.2 indicates that the instabilities of both this and the previous section can be matched together in the region where they overlap (i.e. $\alpha^{-1} \ll (\pi-x) \ll 1$).

From (2.3:3b) we note that because the $(\pi-x)^{i\alpha}$ factor has a wavelength proportional to $(\pi-x)$, the disturbance oscillates increasingly fast as $x \to \pi$. Despite this, the asymptotic solution appears to be uniformly valid, with a rescaling only becoming necessary when a *Navier-Stokes* region is entered where $(\pi-x) \sim D^{-1/2}$. The correctness of the above description of the disturbance will depend on whether, within the Navier-Stokes region, a solution can be found which matches both with the above boundary-layer solution and with its equivalent form for $(\pi-x) < 0$. We do not pursue the resultant linear, two-dimensional, Navier-Stokes, eigenvalue problem here, although we note that for simple two-dimensional stagnation point flow an analogous eigenvalue problem has been formulated by Prof. S.H. Davis (private communication). However, if our analysis is correct, it appears that the generalisation of the instability identified by Cowley *et al.* (1985) does not exist *on* the symmetry line in a *boundary-layer* (as opposed to Navier-Stokes) formulation. This in turn suggests that there may be *no* link between this type of instability and the

separation singularity.[2]

---

[2] We have also looked for instabilities in the unsteady symmetry line formulation (1.3:4) without success. This supports the view that there is no connection between the instability and the singularity.

CHAPTER 3

Periodic Boundary-Layer Flows

§3.1 Introduction

For the second problem, we study a circular cylinder of radius a, rotating anticlockwise with angular velocity Ω and translating with uniform velocity U to the left through an incompressible Newtonian fluid of denisty ρ and kinematic viscosity ν. This motion is a classical example of a two-dimensional laminar flow with lift. The flow can be characterised by two non-dimensional numbers: (i) the ratio of the uniform flow velocity to the rotational velocity of the cylinder's surface,

$$\delta = U/a\Omega \ , \qquad (3.1:1a)$$

and (ii) the rotational Reynolds number,

$$R = a^2\Omega/\nu \ . \qquad (3.1:1b)$$

A number of authors have worked on this problem experimentally, analytically and numerically. For example, Prandtl and Tietjens (1934) visualised the flow at *large Reynolds numbers* for a range of values of δ, i.e. δ = 1/6, 1/4, 1/3, 1/2, 1 and ∞ (e.g. see Goldstein 1938 plate 17, Batchelor 1967 plate 12). Their results suggest that for δ less than 1/4 the viscous boundary layer which exists on the surface of the cylinder at high-Reynolds-numbers remains smoothly attached. However, for δ greater than 1/3 an attached boundary layer solution does not appear experimentally possible, and eddies develop behind the

cylinder.

While the boundary layer remains attached, inviscid theory should describe the fluid motion away from the cylinder's surface at large Reynolds numbers. If it is assumed that a steady circulation of strength K is generated, then the cylinder will experience a lift of magnitude ρKU perpendicular to the direction of the uniform stream (Kutta 1910). However, the precise dependence of the circulation K on the uniform flow U and the angular velocity Ω can only be determined by the inclusion of viscous effects (these are necessarily present because the inviscid solution predicts a non-zero slip velocity on the cylinder surface).

The boundary-layer equations describing the fluid motion close to the cylinder surface at high Reynolds numbers have been solved by Wood (1957) and Glauert (1957) using a perturbation series expansion for relatively fast angular velocities, i.e. $\delta \ll 1$. The latter author calculated the first three terms of the solution in powers of δ^2, obtaining for the circulation

$$\frac{K}{2\pi\Omega a^2} = 1 - 3\delta^2 - 3.24\delta^4 + \ldots , \quad R \gg 1, \ \delta \ll 1 . \qquad (3.1{:}2)$$

In an alternative approach, Moore (1957) obtained a solution based upon a perturbation series expansion for small δ, but without assuming $R \gg 1$. For R greater than $\sqrt{48}$, he obtained the first two terms for the circulation K. In the limit $R \to \infty$ his result agrees with the boundary-layer solutions of Wood (1957) and Glauert (1957).

Numerical solutions of the full Navier-Stokes equations have been obtained by Ta Phoc Loc (1975), Shkadova (1982) and Ingham

(1983). In terms of a Reynolds number based on the uniform velocity, $\mathcal{R}=2Ua/\nu$, the latter two authors solved the problem for moderate Reynolds numbers up to 100 and 20 respectively. For example, the streamline plots for $\delta = 0.2$, $\mathcal{R}=40$ (Shkadova, 1982) and $\delta=0.2$, $\mathcal{R}=20$ (Ingham, 1983) are qualitatively similar, although a direct comparison between the two sets of results is not possible.

The material in this chapter is an extension of the earlier high-Reynolds-number boundary-layer calulations of Wood (1957) and Glauert (1957) to order one values of δ. For $\delta \ll 1$, it was possible to make analytic progress because the fluid in the boundary layer is dragged around by the cylinder at approximately the speed of the cylinder's surface. However as δ increases, the effect of the adverse pressure gradient generated by the uniform flow significantly slows the boundary-layer flow over half the surface; as a result a stagnation point starts to develop in the boundary layer. One of our aims is to identify the critical value of δ, say δ_s, at which a stagnation point first occurs in the boundary layer.

The significance of the stagnation point is that the boundary-layer solution appears to become singular at this point, suggesting that no attached classical boundary-layer solution will exist for larger δ. Hence for $\delta > \delta_s$ separation eddies, etc. are likely to be observed experimentally.

The central mathematical task consists of solving the classical boundary-layer equations with periodic boundary conditions. Similar boundary-layer problems occur in steady streaming flows (e.g. Riley 1978), driven cavity flows (e.g. Riley

1981), flows over wavy surfaces (Bordner 1978), and flows in a rotating annulus with bottom topography (e.g. Page 1982). The boundary-layers associated with the moderate amplitude Tollmien-Schlicting waves identified by Ryzhov and Zhuk (1982), Stephanoff, Pedley, Lawrence and Secomb (1983), Smith and Burggraf (1985) and Rothmayer and Smith (1987) are also closely analogous (see section 3.5).

§3.2 Formulation

According to inviscid flow theory, a circular cylinder moving with uniform velocity U through a flow with circulation K generates a slip-velocity $U_e(x)$ at its boundary, where

$$U_e(x) = 1 - \frac{4\pi Ua}{K}\cos(x) \ , \qquad (3.2:1a)$$

and x is measured anticlockwise along the surface of the cylinder from its 'highest' point (see figure 3.2:1). Here x and $U_e(x)$ have been non-dimensionalised by the radius a and scaled circulation $\frac{K}{2\pi a}$ respectively, and for future convenience we define

$$\varepsilon = \frac{4\pi Ua}{K}. \qquad (3.2:1b)$$

At large but finite Reynolds numbers, the slip-velocity $U_e(x)$ generates a boundary layer, within which the flow is described by the steady boundary-layer equations (e.g. Schlichting, 1968)

$$\begin{aligned} uu_x + vu_y &= U_e U_{ex} + u_{yy} \ , \\ u_x + v_y &= 0 \ , \end{aligned} \qquad (3.2:2a)$$

subject to the boundary conditions

$$u = U_w \equiv \frac{2\pi\Omega a^2}{K}, \qquad v = 0, \qquad \text{on } y = 0, \qquad (3.2:2b)$$

$$u \to U_e(x), \qquad \text{as } y \to \infty. \qquad (3.2:2c)$$

Here the local normal, y, measured from the cylinder surface, is non-dimensionalised by $aRe^{-1/2}$, where the Reynolds number,

$$Re = \frac{K}{2\pi\nu} \ ,$$

is based on the circulatory component of the slip-velocity. The

velocity components (u,v) in the (x,y) directions are non-dimensionalised by $\frac{K}{2\pi a}$ and $\frac{KRe^{-1/2}}{2\pi a}$ respectively, and U_w is just the scaled velocity of the cylinder's surface.

There are many equivalent formulations of system (3.2:2), a number of which are used in this work. One alternative is to introduce the streamfunction ψ as a dependent variable, where

$$u = \psi_y, \qquad v = -\psi_x .$$

Equation (3.2:2a) then becomes

$$\psi_y\psi_{xy} - \psi_x\psi_{yy} = U_e U_{ex} + \psi_{yyy} \tag{3.2:3a}$$

subject to the boundary conditions

$$\psi = 0, \qquad \psi_y = U_w, \qquad \text{on } y = 0 \tag{3.2:3b}$$

$$\psi_y \to U_e(x), \qquad \text{as } y \to \infty. \tag{3.2:3c}$$

The advantage of this formulation is that there is only one governing equation to be solved.

Another formulation uses the streamfunction as an independent variable. Applying a Von Mises transformation, i.e. $(x,y) \to (x,\psi)$, to equation (3.2:2) yields (Wood, 1957)

$$uu_x = U_e U_{ex} + u(uu_\psi)_\psi, \tag{3.2:4a}$$

subject to the boundary conditions

$$u = U_w , \qquad \text{on } \psi = 0, \tag{3.2:4b}$$

$$u \to U_e(x) , \qquad \text{as } \psi \to \infty. \tag{3.2:4c}$$

The above governing equations are parabolic which means that for a given positive slip velocity $U_e(x)$, the equations may be integrated downstream for positive values of the scaled wall velocity U_w. However, for a specified uniform flow and circulation,

there exists an *unique* angular velocity which generates a *periodic* flow; i.e. given an oncoming flow of relative strength $\varepsilon = \frac{4\pi Ua}{K}$, the periodicity requirement determines a steady, *periodic eigenvalue* problem for the scaled wall velocity $U_w = \frac{2\pi\Omega a^2}{K}$.

Wood (1957) and Glauert (1957) assumed that ε was small and sought a series expansion solution, finding U_w correct to order ε^2 and ε^4 respectively (note that an expansion in terms of ε is essentially equivalent to one in terms of δ since from (3.1:1a), (3.2:1b) and (3.2:2b) $\varepsilon = 2U_w\delta$). One method to extend their results to larger values of ε would be to find higher order terms, and then use series extension techniques (e.g. Van Dyke 1984). An attempt to obtain these terms using the algebraic manipulators REDUCE, MACSYMA and CAMAL was unsuccessful, e.g. after 30 minutes execution time on an AMDAHL 470 mainframe, the REDUCE program had not obtained the solution to the highest order that Glauert (1957) examined! Alternatively, the higher order governing equations could have been solved numerically (cf. Cowley 1983). However, Riley (1978, 1981) has been successful with a purely numerical technique in similar problems, and this is the approach adopted for the most part here.

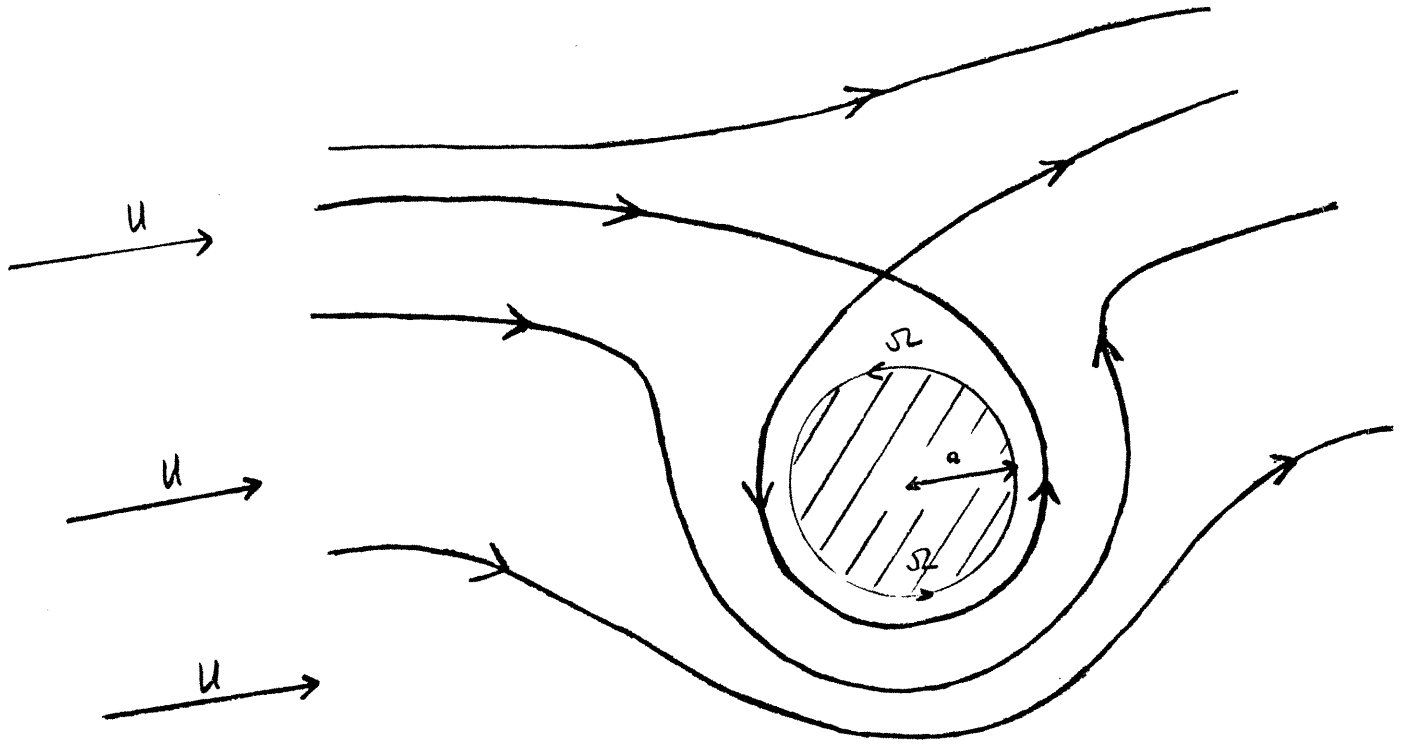


Figure 3.2:1

§3.3 Numerical Methods

In this section, we discuss the different numerical methods used to solve this problem. The first method is similar to that of Riley (1978, 1981) and will be referred to as the FD method. It consists of integrating the boundary-layer equations with a finite difference method through repeated periods of 2π until the solution settles down to a steady, periodic state. The other approaches involve spectral schemes based upon the substitution of truncated Fourier series for the dependent variables into the governing equations, and then numerical solution of the resulting systems of coupled ordinary differential equations by finite-difference methods.

For all the methods, the problem was solved numerically in a finite computational domain, where the asymptotic condition (3.2:2c) was applied in the form $u = U_e(x)$ at $y = y_\infty$ where y_∞ was at the upper edge of the computational domain. Riley (1981) shows that this means that periodic solutions can apparently be found for a range of U_w, although only one of these truly satisfies the condition (3.2:2c) in the limit as $y_\infty \to \infty$. In order to identify this solution it is necessary to examine the solution towards the edge of the boundary layer. We write

$$u(x,\psi) = U_e(x) + \tilde{u}(x,\psi) \ , \qquad (3.3:1a)$$

substitute into (3.2:4a), and retain only linear terms in $\tilde{u}$ on the assumption that $|\tilde{u}|$ is small for $\psi \gg 1$. The resulting equation for $\tilde{u}$ has a separable solution that is periodic in x, (cf. Riley 1981)

$$\tilde{u} = \frac{1}{U_e(x)}\left[A_o + B\psi + \sum_{n=1}^{\infty} \left[A_n \exp\left[in \int \frac{U_e(x)}{\bar{U}_e} dx - (1+i)\sqrt{\frac{n}{2\bar{U}_e}}\,\psi \right] + c.c. \right] \right] \qquad (3.3:1b)$$

where $\bar{U}_e$ is the mean value of $U_e(x)$ and c.c. denotes the complex conjugate. The imposition of $u = U_e(x)$ at $\psi_\infty >> 1$ (or equivalently $y_\infty >> 1$) leads for most choices of U_w to non-zero values of A_o and B (although $A_o + B\psi_\infty \approx 0$). Only by applying an additional condition which forces B, and hence A_o, to zero as $\psi_\infty \to \infty$, e.g.

$$U_e(x)u_\psi = 0 \qquad \text{at } \psi_\infty, \qquad (3.3:2a)$$

or

$$u_y = 0 \qquad \text{at } y_\infty, \qquad (3.3:2b)$$

for $0 \le x \le 2\pi$, do we obtain the correct exponentially decaying behaviour at the edge of the boundary layer and a unique solution for U_w.

With the first numerical method, as summarised in the flow diagram in figure 3.3:1, it proved fastest and most convenient to work in Von Mises coordinates using equation (3.2:4).

A computational domain of NX x NY grid points was used with NX intervals distributed over the period 2π in the x direction (grid points x_i, $1 \le i \le NX$) and NY points distributed over 0 to ψ_∞ in the ψ direction (grid points ψ_j, $1 \le j \le NY$). A non-uniform distribution was implemented using stretch functions - see below, equation (3.3:4). The following procedure was adopted to converge to the unique value of U_w from an initial guess.

To march the parabolic boundary-layer equation (3.2:4a) forward from x_{i-1} to x_i, an implicit Crank-Nicolson scheme (e.g. Roache, 1972) was applied in which the equation was discretized by a second-order, centred, finite-difference approximation at $(x_{i-1/2}, \psi_j)$ for $2 \le j \le NY-1$. The resulting implicit nonlinear difference equations were solved by Newton-Raphson iteration as follows.

Let $\underline{u}_i$ denote the solution vector consisting of $u(x_i, \psi_j)$ for $1 \le j \le NY$, and $\underline{u}_i^k$ the kth iterate of $\underline{u}_i$. The initial guess $\underline{u}_i^o$ was calculated by linear interpolation from $\underline{u}_{i-1}$ and $\underline{u}_{i-2}$. We write

$$\underline{u}_i^{k+1} = \underline{u}_i^k + \delta\underline{u}_i, \qquad (3.3:3a)$$

and substitute $\underline{u}_i^{k+1}$ in place of $\underline{u}_i$ in the difference equations and linearise with respect to $\delta\underline{u}_i$. The resulting linear equations can be represented in matrix form,

$$L\ \delta\underline{u}_i = \underline{b}\ , \qquad (3.3:3b)$$

where L is an NY x NY banded matrix of band width 3, and $\underline{b}$ is a known function vector of length NY. The matrix L is not necessarily diagonally dominant, so $\delta\underline{u}_i$ was solved for using partial pivoting. The solution was then updated and the procedure repeated until each element in $\delta\underline{u}_i$ was reduced to less than a specified small tolerance.

Using this procedure the equation was integrated over a number of periods of 2π until the difference in solutions a period 2π apart was within a given tolerance. This FD method of integrating the governing equations over many periods of 2π has also been applied to equations (3.2:3,4) using a Keller-box scheme. See

appendix 3.A for details.

As mentioned above, the upper boundary condition $u = U_e(x)$ was applied at a finite $\psi = \psi_\infty$. Once the periodic solution has been obtained the value of B in (3.3:1b) was estimated by obtaining the mean of $U_e(x)u_\psi(x, \psi_\infty)$ over 2π assuming the exponental terms were negligible. A better approximation for the eigenvalue U_w was then calculated by a secant iteration with the aim of forcing B to zero. The procedure was repeated with the new U_w, until $|B|$ was less than a specified small tolerance. As a check, the Fourier series of $U_e(x)u_\psi(x, \psi_\infty)$ was then evaluated. It was confirmed that when rounding and truncation errors were negligible, and when ψ_∞ was large enough, the amplitudes of the harmonics were $O(B^2)$, as might be expected from nonlinear interactions.

To initialise the solution procedure, a velocity profile was needed at the starting position, taken to be the position of minimum external velocity, $x = 0$. Such a profile should model the correct oscillatory exponential decay and satisfy the boundary conditions both at $\psi = 0$ and as $\psi \to \infty$. For example, a velocity profile loosely based on Glauert's (1957) solution was used for $\varepsilon < 0.4$

$$u=U_e+(U_w-U_e)\exp(-2^{-1/2}\psi)\cos(\gamma + 2^{-1/2}\psi)/\cos(\gamma)$$

where $\gamma = \frac{1}{2}\sin\left[\dfrac{U_e-U_w}{2U_w-U_e}\right]$ and U_e was evaluated at $x = 0$. The constant γ allowed for a slight phase shift. For $\varepsilon \geq 0.4$, the periodic velocity profile $u(0, \psi)$ for a smaller value of ε was saved, and used as the velocity profile for a next larger ε. With this method, the increment of ε was limited to a maximum of 0.1

when ε was relatively small, and to 0.005 when ε was close to ε_s (see below for definition of ε_s).

In addition, on changing U_w a careful updating of the velocity profile u was necessary in order to avoid introducing thin viscous shear layers at the wall which took many periods to diffuse out of the flow. Specifically, the velocity profile at $x = 0$ for the new U_w was obtained by linear interpolation from the velocity profiles at $x = 0$ for two previous values of U_w.

As explained in the next section, there is a maximum value of ε above which solutions could not be obtained. This value of ε, denoted by ε_s, corresponds to the development of a singularity associated with a *stagnation point* in the boundary layer at $x = x_s$, $\psi = \psi_s$. For ε close to but less than ε_s, we tried to improve convergence by replacing the convective term uu_x in (3.2:4a) with $\max(0.001, |u|)u_x$. This coped with the difficulties associated with negative flow velocities introduced by inappropriately small values of U_w resulting from the secant iteration. This approach is acceptable because by definition of ε_s, the velocity u is necessarily positive for $\varepsilon < \varepsilon_s$, and for all the calculated solutions, $u_{min} = \min_{x,\psi}(u)$ has been shown to be positive for $\varepsilon < \varepsilon_s$. Also, to help resolve the velocity profile near this stagnation point, we refined the mesh there by means of the stretching functions

$$x = \tilde{X} - \left[1 - (\varepsilon_c - \varepsilon)^{1/2} \right] \sin \tilde{X} \qquad (3.3:4a)$$

and

$$\psi = \phi - \frac{1-\delta^*}{\lambda} \left[\tanh (\lambda(\phi-\phi_o)) + \tanh(\lambda\phi_o) \right] . \qquad (3.3:4b)$$

These were introduced in the x- and ψ-directions respectively and an equi-spaced grid in $\tilde{X}$ and ϕ adopted. The constants ε_c, λ, δ^* and ϕ_o were chosen to give fine grid resolution near the position of minumum velocity. In particular, we chose ϕ_o to be close to that value of ϕ at which the velocity has a minimum $u_{min}(x_o,\psi_o)$, and set $\lambda = 0.25$, $\delta^* = 0.005$, $\varepsilon_c = 0.656$ (ε_c is slightly greater than ε_s as calculated later).

A number of different values of ψ_∞ were tried, and for most of the results presented here ψ_∞ was taken to be 28, with grid domains of 40x91, 80x181 and 160x361 points. The solution at each point, $u(x_i, \psi_j)$, was converged to an accuracy of 10^{-12} by Newton-Raphson iteration, and $|B|$ was typically forced down to 10^{-13} by the secant iteration. The number of periods over which the discretized form of (3.2:4) had to be integrated to obtain a periodic solution for a given value of U_w increased with ε and the size of the grid; e.g. it was in the range of 10 for $\varepsilon = 0.1$ and the 40x91 grid, and 70 for $\varepsilon = 0.655$ and the 160x361 grid.

Discretizing equation (3.2:4) directly proved to be approximately 10 times faster than a Keller-box scheme for the primitive variable equation (3.2:2). Test runs confirmed that the scheme is second-order accurate in step size, and improved accuracy was obtained by Richardson extrapolation. The FD method requires little computer storage e.g. typically 15,000 words, but it is sensitive to the velocity profile at $x = 0$ for larger values of ε. For $\varepsilon = 0.653$, the largest grid attempted was 360x721 points which required 3400s CPU time on a Cray 1S.

As an alternative to the above scheme, which required careful

tuning and checking, a spectral method using the streamfunction ψ was adopted. This, referred to as the NRK method, expressed the streamfunction ψ as a Fourier series in x:

$$\psi = f_o(y) + \sum_{n=1}^{\infty} \left[f_c^n(y) \cos(nx) + f_s^n(y) \sin(nx) \right] . \qquad (3.3:5)$$

Note that the superscipt n is used to associate the coefficient with the nth mode of the Fourier series (i.e. f_c^n is not the nth power of f_c nor is it the nth derivative). This series was substituted into the boundary-layer equation (3.2:3a) and the quadratic terms reordered. An example of this reordering is given in appendix 3.B. The series was then truncated after a finite number of N terms, so yielding 2N+1 third-order, coupled, nonlinear ordinary differential equations for the functions $f_o(y)$, $f_c^n(y)$ and $f_s^n(y)$, $1 \le n \le N$ (these are given in appendix 3.B).

The functions f_o etc. were approximated using NY points in the normal direction. Let the vector

$$\underline{f}_j(y_j) = \left[f_o(y_j),\ f_c^n(y_j) \text{ and } f_s^n(y_j) \text{ for } 1 \le n \le N \right]$$

correspond to the solution at each point y_j, $1 \le j \le NY$. As a consequence of the linear term ψ_{yyy} in (3.2:3a), it was possible to express the third derivative of $\underline{f}_j$ explicitly as a nonlinear function of its lower derivatives. This means that at each point y_j for $2 \le j \le NY-1$ the coupled ordinary differential equations, given in appendix 3.B, could be written as

$$\underline{f}_j' = \frac{\partial}{\partial y}(\underline{f}_j) \qquad (3.3:6a)$$

$$\underline{f}_j'' = \frac{\partial}{\partial y}(\underline{f}_j') \qquad (3.3:6b)$$

$$\underline{f}_j''' = G(\underline{f}_j, \underline{f}_j', \underline{f}_j'') \qquad (3.3:6c)$$

where G is a nonlinear function (cf. equation (3.B:4)). The relevant boundary conditions from (3.2:3b,c) are

$$f_o(y_1) = 0, \qquad f_c^n(y_1) = f_s^n(y_1) = 0 \quad \text{for } 1 \le n \le N, \qquad (3.3:7a)$$

$$f_o'(y_1) = U_w, \qquad f_c^{n'}(y_1) = f_s^{n'}(y_1) = 0 \text{ for } 1 \le n \le N, \qquad (3.3:7b)$$

$$f_o'(y_\infty) = 1, \qquad f_c^{1'}(y_\infty) = -\varepsilon, \qquad f_s^{1'}(y_\infty) = 0,$$

$$f_c^{n'}(y_\infty) = f_s^{n'}(y_\infty) = 0 \qquad \text{for } 2 \le n \le N, \qquad (3.3:7c)$$

where, as before the asymptotic boundary condition $\psi_y \to U_e$ has been applied at a finite y_∞. To obtain a unique U_w the correct behaviour at infinity must be imposed, i.e. both A_o and B in (3.3:1b) must be forced to zero. On assuming y_∞ is large enough so that the exponentially small terms are negligible, this is achieved by applying (cf. equation (3.3:2b))

$$f_o''(y_\infty) = 0 . \qquad (3.3:7d)$$

This system of equations was solved by Newton-Raphson iteration using a fourth-order boundary-value package (Cash and Moore 1980). The Jacobian required for the iteration was calculated analytically and is given in appendix 3.B.

A uniform grid in y was used, and because the y position at which u_{min} occurred, say y_o, increased as ε tended to ε_s, y_∞ was increased with ε (e.g. $y_\infty = 36$ for $\varepsilon < 0.6$ and $y_\infty = 45$ for

$\varepsilon \geq 0.6$). The test criterion for convergence was that the update for $\underline{f}_j$, denoted by $\delta\underline{f}_j$, must satisfy

$$\max_j |\delta\underline{f}_j| + \max_j |\delta\underline{f}_j'| + \max_j |\delta\underline{f}_j''| \leq 10^{-8}.$$

Both the fourth-order accuracy and the quadratic convergence have been confirmed. For each ε, the solution $\underline{f}_j$, $\underline{f}_j'$ and $\underline{f}_j''$ for $1 \leq j \leq NY$ was saved and used as an initial guess for the Newton-Raphson iteration at the next larger value of ε. The increment of ε using this method was allowed to be much larger than for the FD method, although an increment of 0.001 was used when ε was close to ε_s due to the need for detailed solutions.

Trial runs showed that accurate results could be obtained with 8 modes for smaller values of ε, but as $\varepsilon \to \varepsilon_s$ successively more modes were needed (e.g. for ε close to ε_s we used up to 20 modes, the maximum that was allowed by our computer storage capacity, i.e. 750,000 words). The results obtained with this method compare well with those from the FD method; see table 3.4:1. This approach requires large computer memory but is moderate in CPU time, for example, with NY=91, N=20, ε=0.655, 600s of Cray 1S CPU were required.

In an attempt to decrease the size of the computational domain, and therefore the storage required, a spectral approach using Von Mises coordinates was tried. The advantage of using ψ as the independent variable over using y is that ψ_o (i.e. the value of ψ at which u_{min} occurs) appears to tend to a finite value as $\varepsilon \to \varepsilon_s$. In this approach, referred to as the VM method, the velocity u was expressed as a Fourier series in x, with

coefficients which are functions of ψ:

$$u = g_o(\psi) + \sum_{n=1}^{\infty} g_c^n(\psi)\cos(nx) + g_s^n(\psi)\sin(nx) \ . \qquad (3.3:8)$$

This series was substituted into (3.2:4), the quadratic and cubic terms reordered and the series then truncated after N terms. This process yielded 2N+1 coupled nonlinear ordinary differential equations for $g_o(\psi)$, $g_c^n(\psi)$ and $g_s^n(\psi)$, $1 \le n \le N$ (these are given in appendix 3.B).

The disadvantage of using Von Mises coordinates is that the highest ψ-derivatives of $g_o(\psi)$, $g_c^n(\psi)$ and $g_s^n(\psi)$, $1 \le n \le N$ are involved in a double summation with the consequence that the equations cannot easily be rewritten in a schematic form similar to that expressed in (3.3:6). The nonlinear equations are therefore not amenable to solution by the Cash and Moore (1980) package, and a tailor-made program had to be written.

Again, NY points were used to represent ψ over the boundary layer, and the stretch (3.3:4b) was used in ψ. The equations were discretized at ψ_j, $2 \le j \le NY-1$ by second-order finite-differences. Let the vector $\underline{G}$ consist of U_w and the (2N+1) x NY variables $g_o(\psi_j)$, $g_c^n(\psi_j)$ and $g_s^n(\psi_j)$ for $1 \le n \le N$, $1 \le j \le NY$, let $\underline{G}_2$ be the second-order accurate solution of $\underline{G}$, and let $\underline{G}_2^k$ be the kth Newton-Raphson iterate to the solution $\underline{G}_2$. From now on, we denote the vectors derived from a second- and fourth-order-accurate approximation by the subscripts 2 and 4 respectively. We write

$$\underline{G}_2^{k+1} = \underline{G}_2^k + \delta\underline{G}_2 \ , \qquad (3.3:9a)$$

and substitute $\underline{G}_2^{k+1}$ in place of $\underline{G}$ in the coupled difference

equations, and linearise them with respect to $\delta\underline{G}_2$, so obtaining

$$A\ \delta\underline{G}_2 = \underline{b}_2 \ . \qquad (3.3:9b)$$

The Jacobian A, which is a banded matrix of band width 8N+3 (see below) and length of 1+(2N+1)NY, was decomposed and inverted by NAG routines F01LBF and F04LDF. Once a second-order-accurate solution had been obtained, a fourth-order-accurate solution was found by defect correction. The fourth-order solution was obtained by Newton-Raphson iteration using the same Jacobian. For details on this scheme see appendix 3.C.

It has been confirmed that the Newton-Raphson iteration converged quadratically, and that the uncorrected solution was second-order accurate. However the quartic accuracy of the defect corrected solution could not be verified for the relatively coarse grid-sizes which we could use. Therefore the method was tested on a similar, but simpler, model problem. It was found that quartic behaviour was recovered only for more refined grids. Nevertheless, in this model problem the corrected solution was more accuate than the uncorrected solution for all grid-sizes, and therefore we believe that the defect correction yielded a more accurate solution in the full problem.

In order to reduce computation time and storage, many attempts were made to model the correct exponentially decaying behaviour at a relatively small value of ψ_∞ by using the expression (3.3:1b). Each x-dependent term of (3.3:1b) was expressed as an infinite Fourier series, i.e.

$$\tilde{u} = \tilde{g}_o(\psi) + \sum_{n=1}^{\infty} \tilde{g}_c^n(\psi)\cos(nx) + \tilde{g}_s^n(\psi)\sin(nx) , \qquad (3.3:10a)$$

$$\frac{1}{U_e(x)} = p_0 + \sum_{m=1}^{\infty} p_m \cos(mx) , \qquad (3.3:10b)$$

$$\frac{\cos\left[n\int_o^x U_e(x)dx \right]}{U_e(x)} = c_{n0} + \sum_{m=1}^{\infty} c_{nm}\cos(mx) , \qquad (3.3:10c)$$

$$\frac{\sin\left[n\int_o^x Ue(x)dx \right]}{U_e(x)} = \sum_{m=1}^{\infty} d_{nm}\sin(mx) \qquad (3.3:10d)$$

where the constants p_0, c_{n0}, p_m, c_{nm} and d_{nm} for $1 \le m \le \infty$ and $1 \le n \le \infty$ could be calculated. Substituting equations (3.3:10) into (3.3:1b), and equating coefficients for cos(nx), etc., we find

$$\tilde{g}_o(\psi) = (A_o + B\psi)p_o + \sum_{m=1}^{\infty} \left[a_m \cos\sqrt{\frac{m}{2}}\psi + b_m \sin\sqrt{\frac{m}{2}}\psi \right] c_{mo} \exp\left[-\sqrt{\frac{m}{2}}\psi \right] \qquad (3.3:11a)$$

$$\tilde{g}_c^n(\psi) = (A_o + B\psi)p_n + \sum_{m=1}^{\infty} \left[a_m \cos\sqrt{\frac{m}{2}}\psi + b_m \sin\sqrt{\frac{m}{2}}\psi \right] c_{mn} \exp\left[-\sqrt{\frac{m}{2}}\psi \right] \qquad (3.3:11b)$$

$$\tilde{g}_s^n(\psi) = \sum_{m=1}^{\infty} \left[a_m \sin\sqrt{\frac{m}{2}}\psi - b_m \cos\sqrt{\frac{m}{2}}\psi \right] d_{mn} \exp\left[-\sqrt{\frac{m}{2}}\psi \right] \qquad (3.3:11c)$$

where $a_m = \mathrm{Re}(A_m)$ and $b_m = \mathrm{Im}(A_m)$ are constants to be determined.

To obtain managable boundary conditions at ψ_∞ we truncated the

series in (3.3:11c) after one term, i.e. we assumed that

$$\exp\left[-\sqrt{\tfrac{1}{2}}\,\psi_\infty\right] \gg \exp\left[-\sqrt{\tfrac{m}{2}}\,\psi_\infty\right] \qquad \text{for } m \geq 2 \ .$$

This left two unknown constants a_1 and b_1 to be determined and two constants, A_o and B to be forced to zero. To do this we used the expressions for $\tilde{g}_o$, $\tilde{g}_c^1$ and their first derivatives (these two Fourier coefficients were chosen since g_o and g_c^1 are forced directly by the boundary condition). Then A_o and B can be forced to zero by imposing the boundary conditions

$$\frac{\tilde{g}_o}{c_{1o}} - \frac{\tilde{g}_c^1}{c_{11}} = 0 \ , \qquad \frac{\tilde{g}_o'}{c_{1o}} - \frac{\tilde{g}_c^{1\prime}}{c_{11}} = 0 \ . \qquad (3.3:12a)$$

The appropriate boundary conditions for the higher modes are then

$$\frac{\sqrt{2}\,\tilde{g}_c^{n\prime}}{c_{1n}} = -\frac{\tilde{g}_c^n}{c_{1n}} - \frac{\tilde{g}_s^n}{d_{1n}} \ , \qquad \frac{\sqrt{2}\,\tilde{g}_s^{n\prime}}{d_{1n}} = \frac{\tilde{g}_c^n}{c_{1n}} - \frac{\tilde{g}_s^n}{d_{1n}} \qquad (3.3:12b)$$

for $1 \leq n \leq N$. Equations (3.3:12) specify 2N+2 boundary conditions, which are sufficient both to resolve the exponentially decaying behaviour at infinity (2N+1 of them are required for this) and to fix U_w.

These boundary conditions were applied midway between the grid points NY - 1 and NY. Test runs showed that they gave more accurate results than just imposing $u = U_e(x)$ at the same value of ψ_∞, although the improvement was not dramatic. This is because the neglected terms A_n, $n \geq 2$, appear to be significant.

In implementing both the modification of the upper boundary conditions and the fourth-order defect correction, care was taken not to increase the band width of the Jacobian matrix, e.g. only

the two points closest to the top and bottom boundaries were used for the boundary conditions. As in the FD method, a stretch (3.3:4b) was used. A number of test runs were tried with different values of the various parameters. For the results presented in the following section, we used NY = 91, ψ_∞ = 19.69, and λ, δ^* as before; the Newton-Raphson iteration convergence criterion was that successive iterates should change by less than 10^{-9} at each point. The parameters required to give consistent results were N = 10 for $\varepsilon < 0.6$, N = 18 for $0.6 \leq \varepsilon < 0.65$ and N = 25 for $\varepsilon \geq 0.65$. See table 3.4:1.

For each $\varepsilon \geq 0.4$, the solution $g_o(\psi_j)$, $g_c^n(\psi_j)$ and $g_s^n(\psi_j)$, for $1 \leq n \leq N$ and $1 \leq j \leq NY$ was saved and used as the initial solution for the next larger value of ε. The increment of ε using this method was similar to the NRK method. This method is very efficient, but requires significant programming effort and large computer memory (eg. for NY=91, N=18, ε=0.65, 800,000 words and 100s CPU time were required on Cray 1S).

In the hope of a further improvement on the boundary conditions, we introduced a transformation of co-ordinates (X, ψ) where

$$X = \int_o^x \frac{U_e(x)}{\bar{U}_e}\, dx, \qquad (3.3:13a)$$

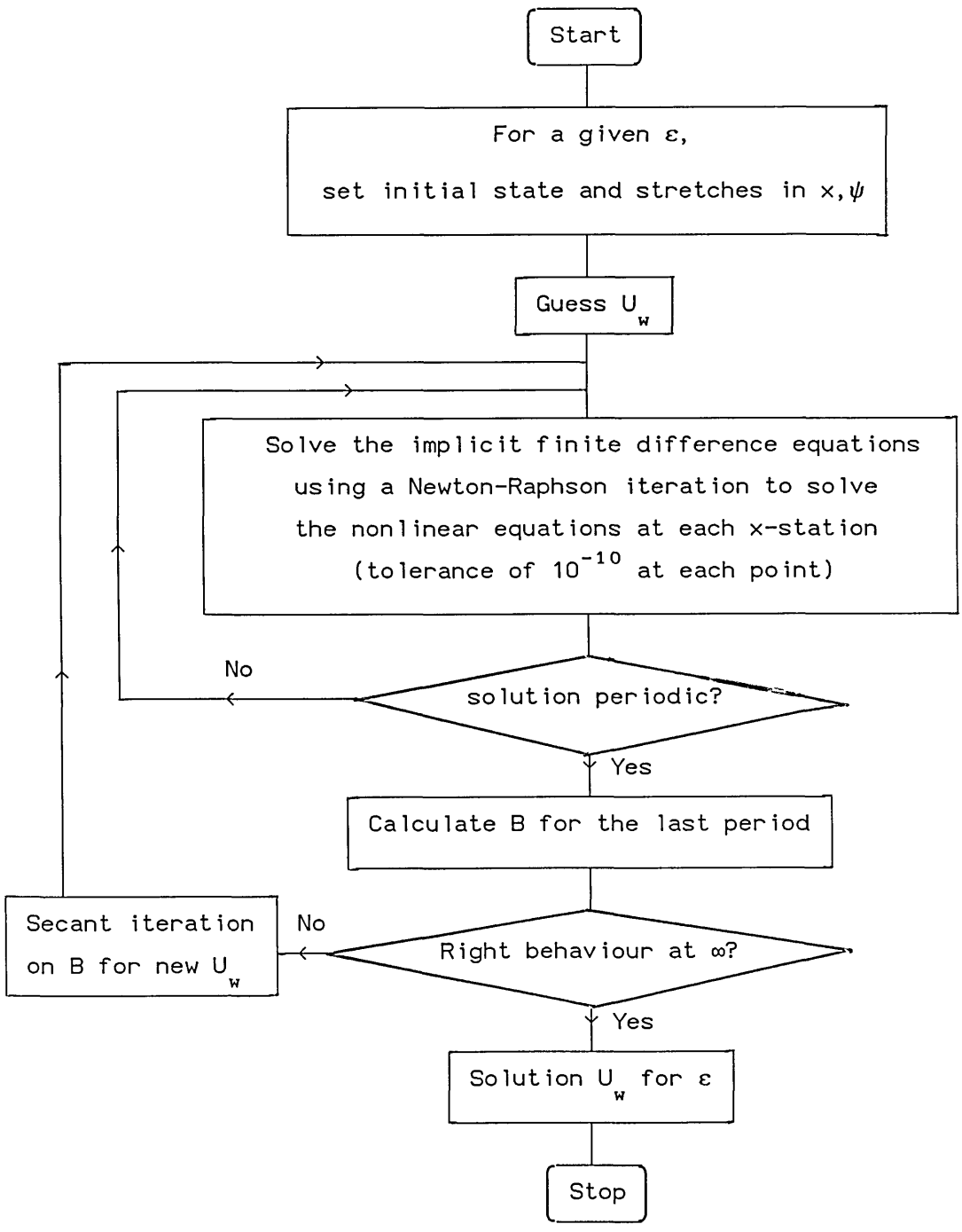
as suggested by equation (3.3:1b). We also defined a velocity-like quantity,

$$\bar{u}(X, \psi) = u(x, \psi)U_e(x) - U_e(x)^2 \qquad (3.3:13b)$$

as the dependent variable. $\bar{u}(X, \psi)$ was then expanded as Fourier

series in X and the resulting equations solved in a similar manner to that for the VM method. However, in these coordinates, the Fourier coefficients of the pressure gradient, $\frac{1}{2}(U_e^2)_x$, decay slowly with wavenumber, with the result that a large value of N is required for accuracy. Consequently, due to computer storage limitations, it was difficult to obtain accurate solutions for ε greater 0.65. This method is discussed in more detail in appendix 3.D.

Figure 3.3:1


Start
For a given ε,
set initial state and stretches in x,ψ
Guess U_w
Solve the implicit finite difference equations
using a Newton-Raphson iteration to solve
the nonlinear equations at each x-station
(tolerance of 10^-10 at each point)
No
solution periodic?
Yes
Calculate B for the last period
Secant iteration
on B for new U_w
No
Right behaviour at ∞?
Yes
Solution U_w for ε
Stop

§3.4 Results

Inviscid theory predicts that a solution exists for all values of ε. For $0 < \varepsilon < 1$ closed streamline exist immediately around the cylinder, and a stagnation point occurs in the inviscid flow somewhere on the line $x = 0$. The stagnation point approaches the surface of the cylinder as $\varepsilon \to 1$. When viscous effects are included the slip velocity generates a thin boundary layer. As ε increases from zero, the flow within the boundary layer is slowed down by the increasingly strong adverse pressure gradient on the rear of the cylinder, and a second stagnation point starts to develop within the boundary layer. Our numerical results show that at a critical value of ε, $\varepsilon_s \approx 0.656 < 1$, the *boundary-layer flow* develops a stagnation point away from the wall close to $x = 0$, i.e. where the minimum external velocity occurs. Beyond this value of ε_s no solution could be obtained using classical boundary-layer theory.

Solutions have been obtained for $0 \le \varepsilon \le 0.655$. A comparison of the three successful methods applied to this problem is given in table 3.4:1. The results are given for the eigenvalue U_w and $\min_{x,\psi}(u) = u_{min}$ for $\varepsilon = 0.6$ to 0.655; note that $u_{min}(\varepsilon)$ is difficult to calculate accurately. To increase the accuracy of the results obtained by the FD scheme, Richardson extrapolation has been applied to the 40x91, 80x181 and the 80x181, 160x361 grids; the results are given only to the number of significant figures to which both extrapolations agree.

In the graphs that follow our numerical results are denoted by solid lines; they are compared with Glauert's (1957) analytical

solutions, represented by broken lines, wherever possible.

Figure 3.4:1 illustrates the dependence of the circulation on the free stream velocity; specifically we plot the nondimensional circulation, $\frac{K}{2\pi\Omega a^2} = \frac{1}{U_w}$ versus the nondimensional free stream velocity $\delta = \frac{U}{\Omega a} = \frac{\varepsilon}{2U_w}$, where both are scaled by the rotation Ω. The agreement between the numerical solutions and Glauert's (1957) expansion is very good for $\delta < 0.15$, although as δ increases the numerical results have a steeper gradient than that predicted by (3.1:2). As a consequence of the development of a stagnation point in the boundary-layer flow, no classical boundary-layer solution can be obtained for $\delta > \delta_s$. The same data is replotted in figure 3.4:2 in the form of a graph of the reciprocal of the lift coefficient, $\frac{1}{C_L} = \frac{\varepsilon}{4\pi}$, versus the scaled free stream velocity δ.

Figure 3.4:3 illustrates the minimum of u over the whole flow field against δ. There is good graphical agreement for small δ between our numerical results and Glauert's analytical solutions; however for $\delta > 0.1$, Glauert's expansion overestimates u_{min}.

We denote by $(x_o(\delta), \psi_o(\delta))$ the position where $u_{min}(\delta)$ occurs. Figure 3.4:4 shows the velocity profile u at $x = x_o$ against ψ for ε close to ε_s. As ε increases, u appears almost linear in $|\psi - \psi_o|$ for ψ close to ψ_o (especially for $\psi < \psi_o$). Both figures (3.4:3) and (3.4:4) suggest that u_{min} is tending to zero at a finite value of $\varepsilon = \varepsilon_s$. This in turn suggests that the solutions may become singular at $\varepsilon = \varepsilon_s$, because the steady classical boundary-layer equation is parabolic with the result that stagnation points are generally associated with singularities (e.g. Goldstein (1948),

Elliott, Smith and Cowley (1983), Williams and Stewartson (1983)).

In an attempt to understand the asymptotic structure of the velocity profile for ε close to ε_s (or equivalently δ close to δ_s), the asymptotic form

$$u_{min} = c(\varepsilon_s - \varepsilon)^n \qquad (3.4:1)$$

is assumed, with unknown constants c, ε_s and n. Equation (3.4:1) is fitted over data for ε close to ε_s; the results of ε_s and n are listed in table 3.4:2. The power n seems to be close to 0.5 and $\varepsilon_s \simeq 0.656$ ($\delta \simeq 0.256$). This relationship is supported by figure 3.4:5 where u_{min} is plotted against $(\varepsilon_s - \varepsilon)^{1/2}$ although there may of course be $\log(\varepsilon_s - \varepsilon)$ terms etc. in the relationship.

Further evidence of a singularity comes from examining the displacement thickness β,

$$\beta = \int_o^\infty \left(1 - \frac{u}{U_e} \right) dy \, , \qquad (3.4:2)$$

and the blowing velocity v_∞,

$$v_\infty = \lim_{y\to\infty} (v + U_{ex} y) \, , \qquad (3.4:3)$$

which usually become singular when a stagnation point develops in a classical boundary layer. Note that the blowing velocity can be alternatively expressed as

$$v_\infty = \int_o^\infty \left[\frac{U_e}{u} \right]_x d\psi \, , \qquad (3.4:4)$$

which has the advantage over other equivalent forms of being numerically well behaved as $\psi \to \infty$.

Figures 3.4:6a,b illustrate β and v_∞ as functions of x for representative values of ε close to ε_s. Evidence of a singularity

is given in figures (3.4:7a,b). In figure 3.4:7a we plot the maximum of the displacement thickness of the boundary layer against $-\ln(\varepsilon_s - \varepsilon)$, and in figure 3.4:7b we plot $\frac{1}{\max_{x,\varphi}(v_\infty) - \min_{x,\varphi}(v_\infty)}$ against $(\varepsilon_s - \varepsilon)^{+1/2}$. Both of the curves are reasonably straight for ε greater than 0.63 (although figure 3.4:7b is less so). This suggests that both the quantities tend to infinity rather like the respective functions of ε.

The numerical solutions of (3.2:2-4) thus seem to predict that at large Reynolds numbers a singularity develops in the classical boundary-layer formulation for $\delta = \delta_s$, making it likely that solutions with attached boundary layers can only be found for $\frac{U}{\Omega a} \leq 0.256$. This result is in fair agreement with Prandtl *et. al.*'s (1934) experiments which 'for values $\Omega a/U$ greater than 4' show 'a ring of fluid around the cylinder rotating about it permanently' (Prandtl and Tietjens, 1934).

Direct quantitative comparison between our results and experiment is not possible, mainly due to a lack of experiments. For reference we include a table and three more plots. Table 3.3:3 displays the quantitive result of U_w for $\varepsilon \leq 0.655$ ($\delta \leq 0.256$) and the minimum of u over the resulting flow field.

Figure 3.4:8 shows the wall shear $u_y|_{y=0}$ over the period of 2π for various values of ε, namely $\varepsilon = 0.1,\ 0.4,\ 0.5,\ 0.6$ and 0.655. The torque exerted by this wall shear is given in non-dimensional form by

$$T = \frac{1}{2\pi} \int_0^{2\pi} u_y(x,\ 0)\ dx\ . \qquad (3.4:5)$$

In an experiment this should be a measurable quantity. It has been plotted in figure 3.4:9. Our numerical results are not very different from Glauert's small ε analysis. Therefore the comparison between Glauert's (1957) solution and Reid's (1924) experimental results is similar to that of ours with Reid's[1]. Moreover, our solution terminates at $\delta \simeq 0.256$, wherease Reid's result is displayed for $\delta \geq 0.28$ in Glauert's (1957) paper.

Finally in figure 3.4:10 the streamlines over the whole flow field for $\varepsilon = 0.4$, 0.6 and 0.655 have been plotted. As expected, as $y \to \infty$ the distance between streamlines at constant x is proportional to the change in streamfunction.

Discussion

The boundary-layer flow over a rotating and translating circular cylinder has been solved numerically up to a finite value of the ratio ε. A number of different methods have been used, all of which give consistent results. These codes can be easily adapted to solve general two-dimensional, steady, classical boundary-layer problems for periodic slip velocities (e.g. see section 3.5).

Inviscid theory predicts that a stagnation point develops in the flow for $0 < \varepsilon < 1$. However, the introduction of viscosity

---

1 Our copy of Reid's (1924) paper does not display any quantitive results for a rotating and translating cylinder. This makes a direct comparison between our results and his impossible.

shows that at $\varepsilon = \varepsilon_s$ a second stagnation point develops within the boundary layer near the minimum of the external velocity. Our calculation terminates at this value of ε due to steady boundary-layer separation as a result of the second stagnation point in the boundary layer. With $\varepsilon_s \simeq 0.656$ determined, $\delta_s \simeq 0.256$ can be calculated which agrees well with Prandtl *et al.*'s (1934) experiments in which the flow is separation free for δ less than 0.25.

For ε greater than but close to ε_s, i.e. $0 < \varepsilon - \varepsilon_s \ll 1$ an interactive theory is required to examine the flow structure. Therefore, it is necessary to find the asymptotic structure of the separation singularity. Although many attempts have been tried (for details, see appendix 3.E), the exact structure is not clear. Thus, more work is required to fully understand the singularity structure, and to formulate an interactive problem. Anyhow, the inviscid flow is expected to be significantly influenced by the boundary-layer separation.

The mathematical problem resulting for this flow is similar to that of an interactive formulation of high-frequency Tollmien-Schlicting waves generated in the viscous boundary layers of a plane channel. This is discussed in detail in section 3.5.

Table 3.4:1

ε	U_w	u_{min}
0.6	1.237 6	0.238
	1.237 5	0.237
	1.237 6	0.238
0.65	1.276 3	0.076
	1.276 2	0.076
	1.276 3	0.076
0.653	1.278 8	0.05
	1.278 8	0.052
	1.278 9	0.051
0.654	1.279 7	0.04
	1.279 7	0.041
	1.279 7	0.040
0.655	1.280 6	0.02
	1.280 5	0.027
	1.280 5	0.023

A comparison between the three successful methods for various ε. The result for each ε are given in the order of FD, NRK, VM.

FD = the finite-difference scheme
NRK = the spectral method in the primary variables
VM = the spectral method in the Von Mises coordinates

Table 3.4:2

ε			ε_s	n
0.600	0.630	0.650	0.655 6	0.492 6
0.630	0.650	0.653	0.655 3	0.477 0
0.650	0.653	0.654	0.655 5	0.512 4
0.653	0.654	0.655	0.655 5	0.502 8

The approximated values of ε_s and n are obtained by assuming, close to ε_s,

$$u_{min} = c\ (\varepsilon_s - \varepsilon\ )^n$$

with unknown constants c, ε_s and n. The first column lists the 3 values of ε used to predict the constants, of which only ε_s and n are shown.

Table 3.4:3 A summary of results

ε	δ	U_w	u_{min}
0.1	0.049 63	1.007 46	0.892 05
0.2	0.097 14	1.029 45	0.781 47
0.3	0.140 87	1.064 84	0.666 80
0.4	0.179 83	1.112 14	0.545 2
0.5	0.213 69	1.169 91	0.410 1
0.55	0.228 70	1.202 46	0.332 0
0.6	0.242 41	1.237 57	0.238
0.63	0.249 97	1.260 16	0.161
0.65	0.254 65	1.276 28	0.076
0.653	0.255 31	1.278 85	0.051
0.654	0.255 52	1.279 73	0.040
0.655	0.255 73	1.280 63	0.023

For each value of $0.1 \leq \varepsilon = \frac{4\pi Ua}{K} \leq 0.655$, the eigenvalue $U_w = \frac{2\pi\Omega a^2}{K}$ and $U_{min}(\varepsilon)$ from the resulting flow field are shown; the corresponding $\delta = \frac{U}{\Omega a}$ is thus calculated.

Figure 3.4:1

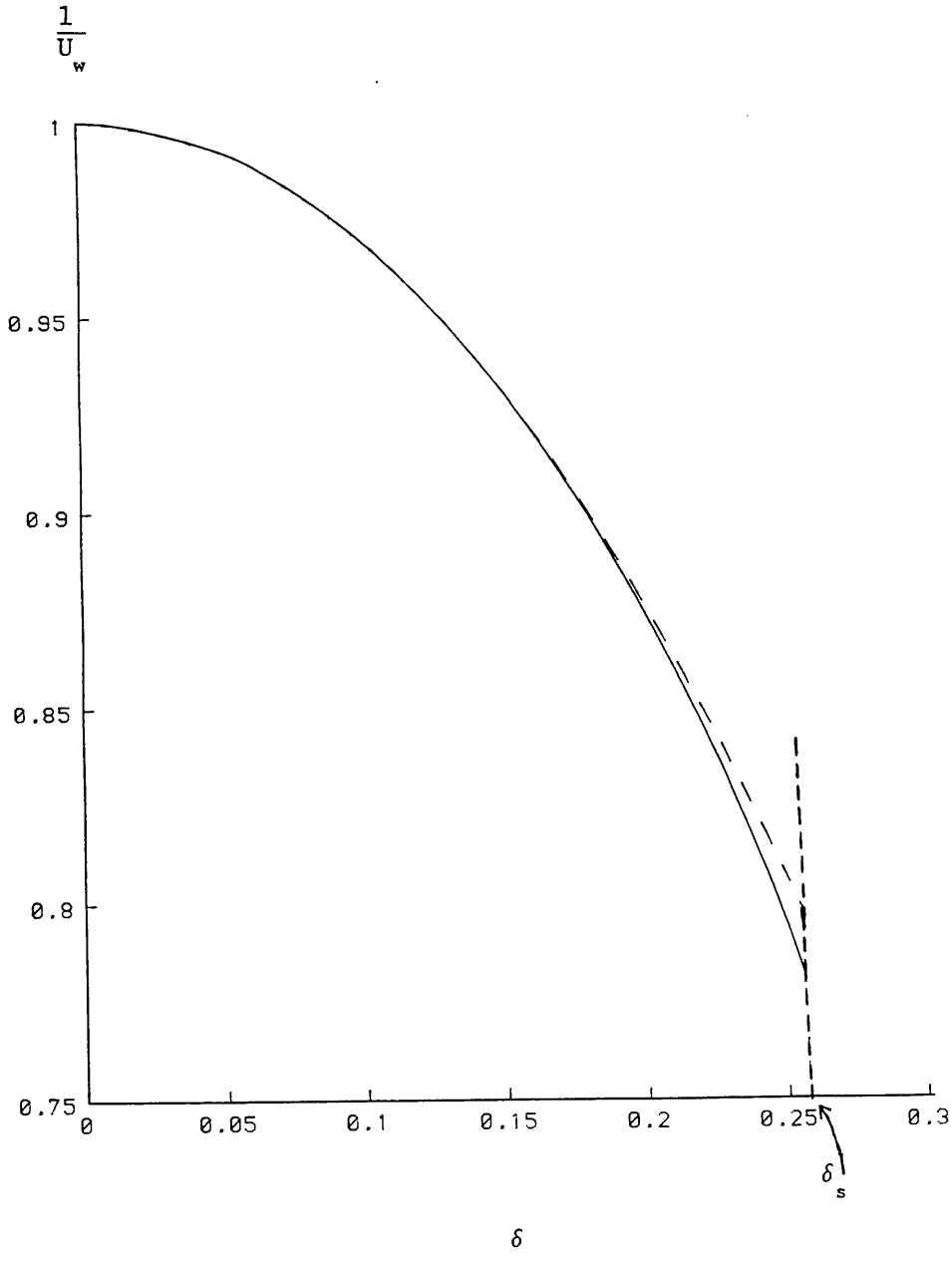


Figure 3.4:2

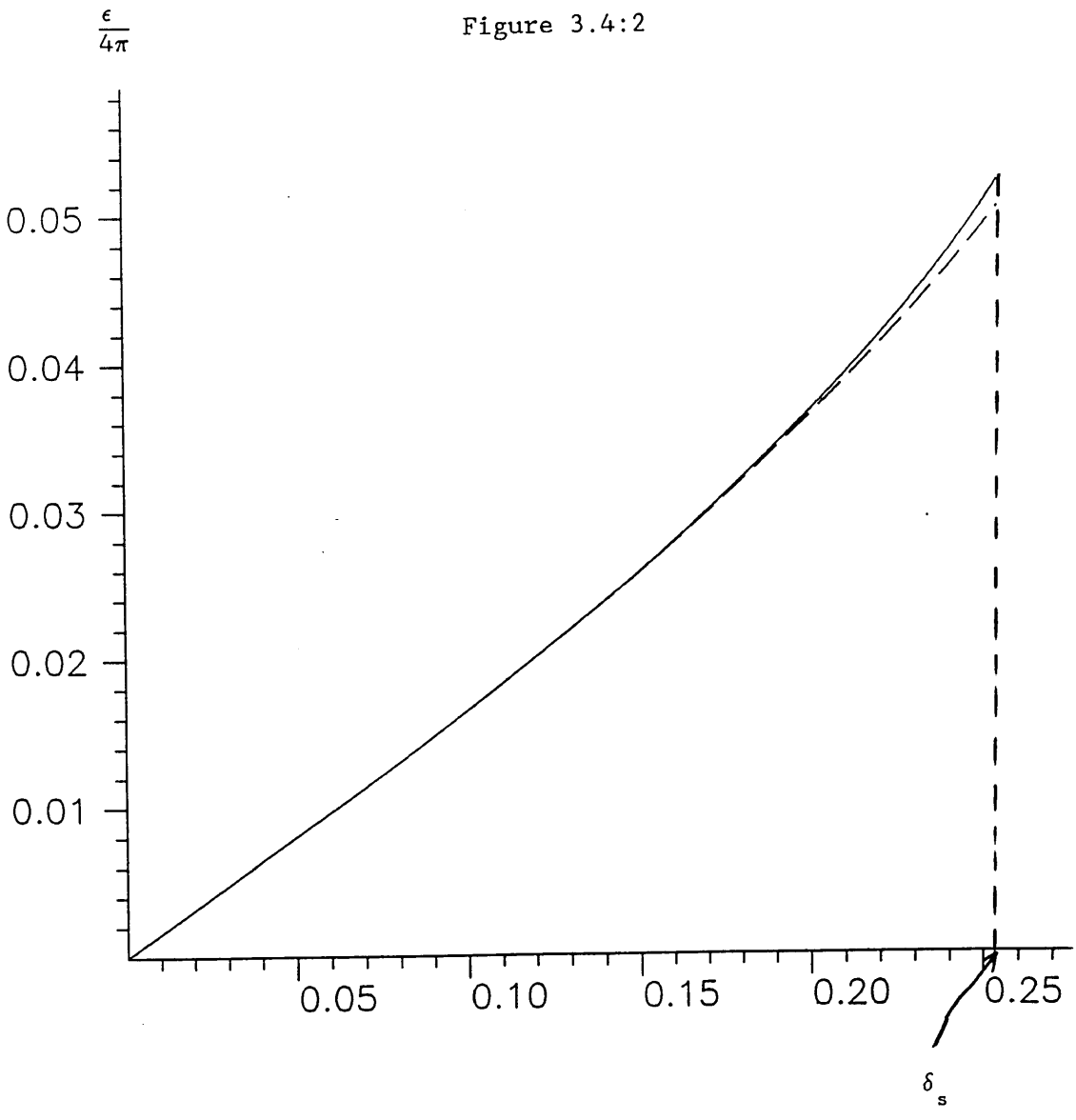

$\frac{\epsilon}{4\pi}$
0.05
0.04
0.03
0.02
0.01
0.05
0.10
0.15
0.20
0.25
δ_s
δ

Figure 3.4:3

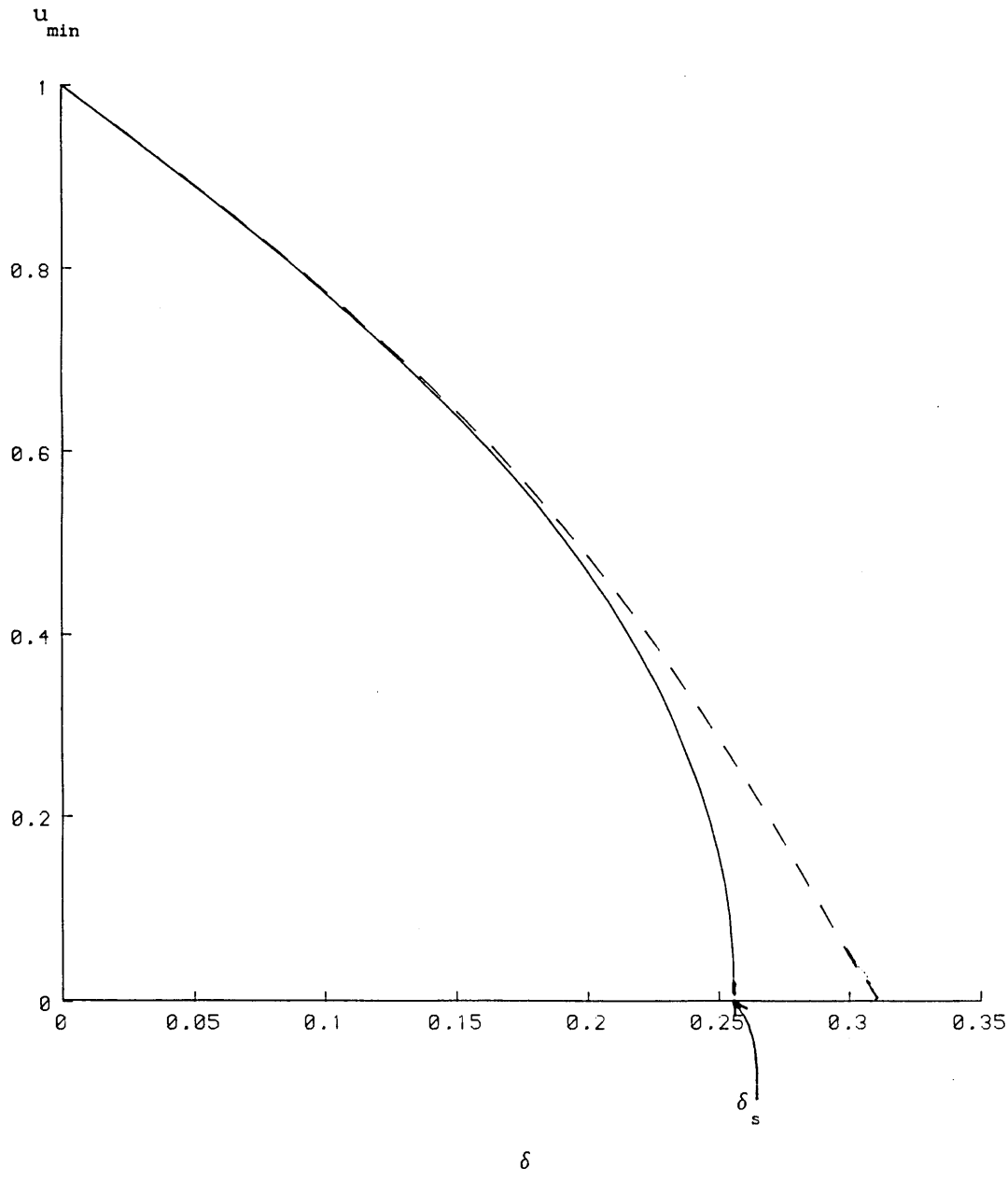


Figure 3.4:4

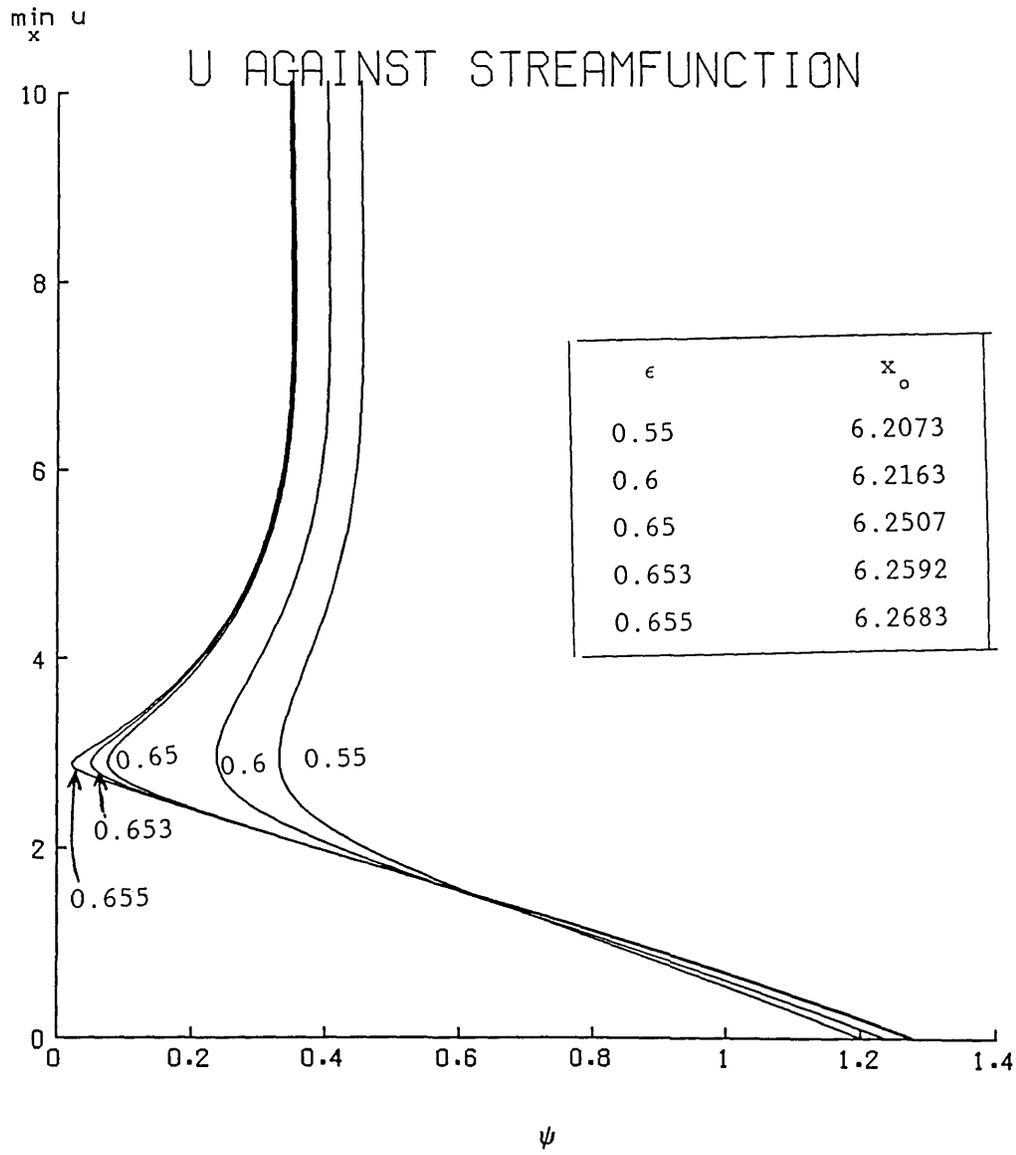

min u
x
U AGAINST STREAMFUNCTION
10
8
6
4
2
0
0
0.2
0.4
0.6
0.8
1
1.2
1.4
ψ
0.65
0.6
0.55
0.653
0.655
ε
x
o
0.55
6.2073
0.6
6.2163
0.65
6.2507
0.653
6.2592
0.655
6.2683

Figure 3.4:5

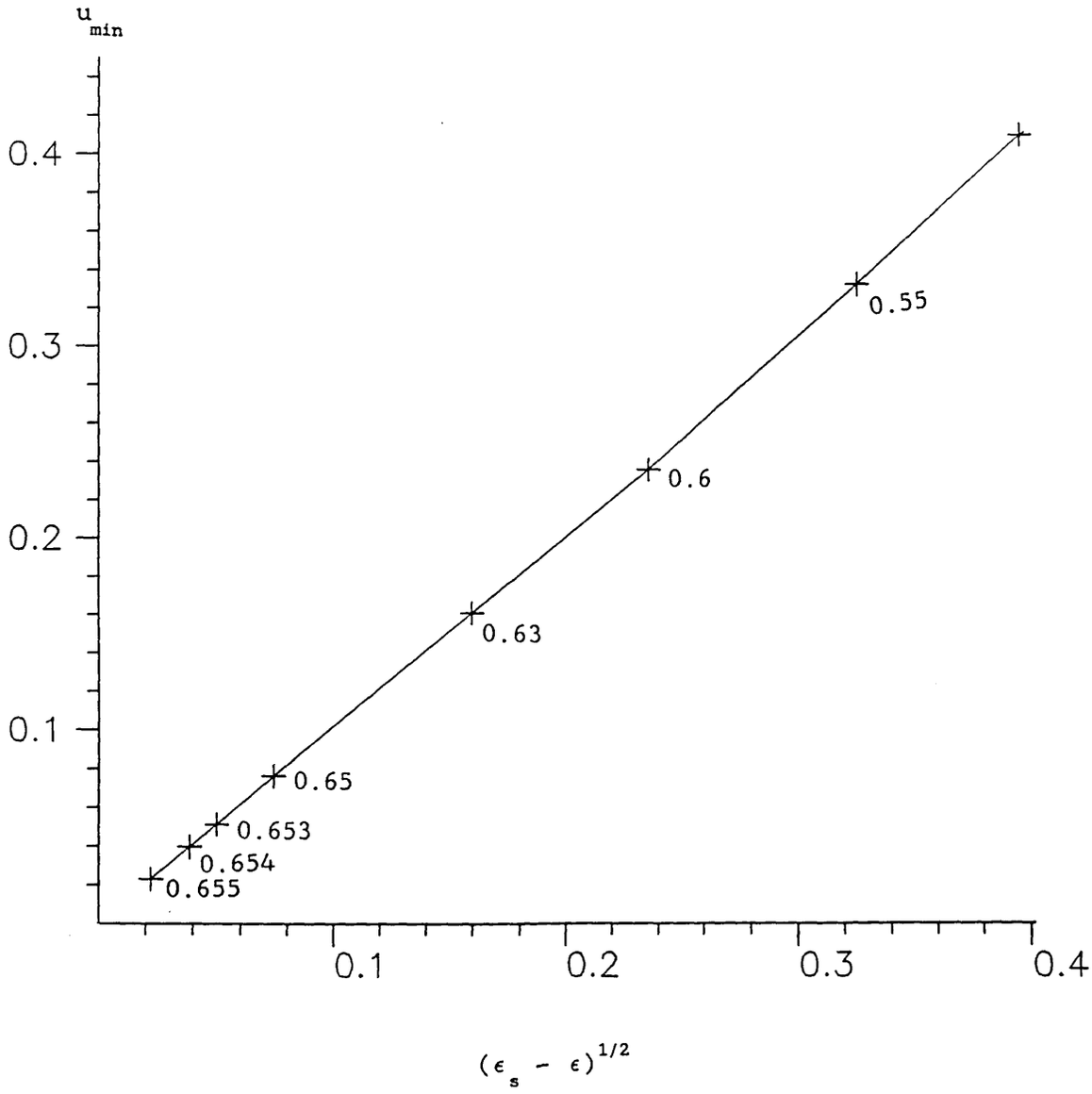


Figure 3.4:6a

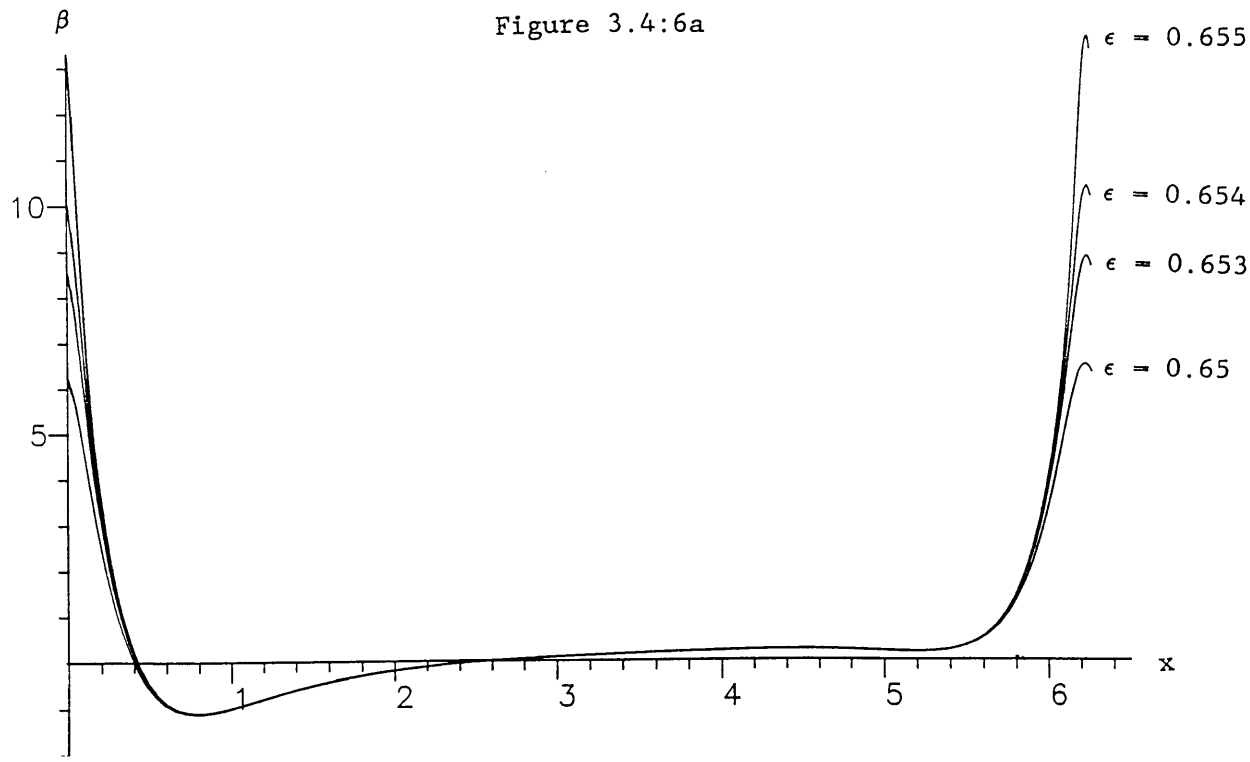


Figure 3.4:6b

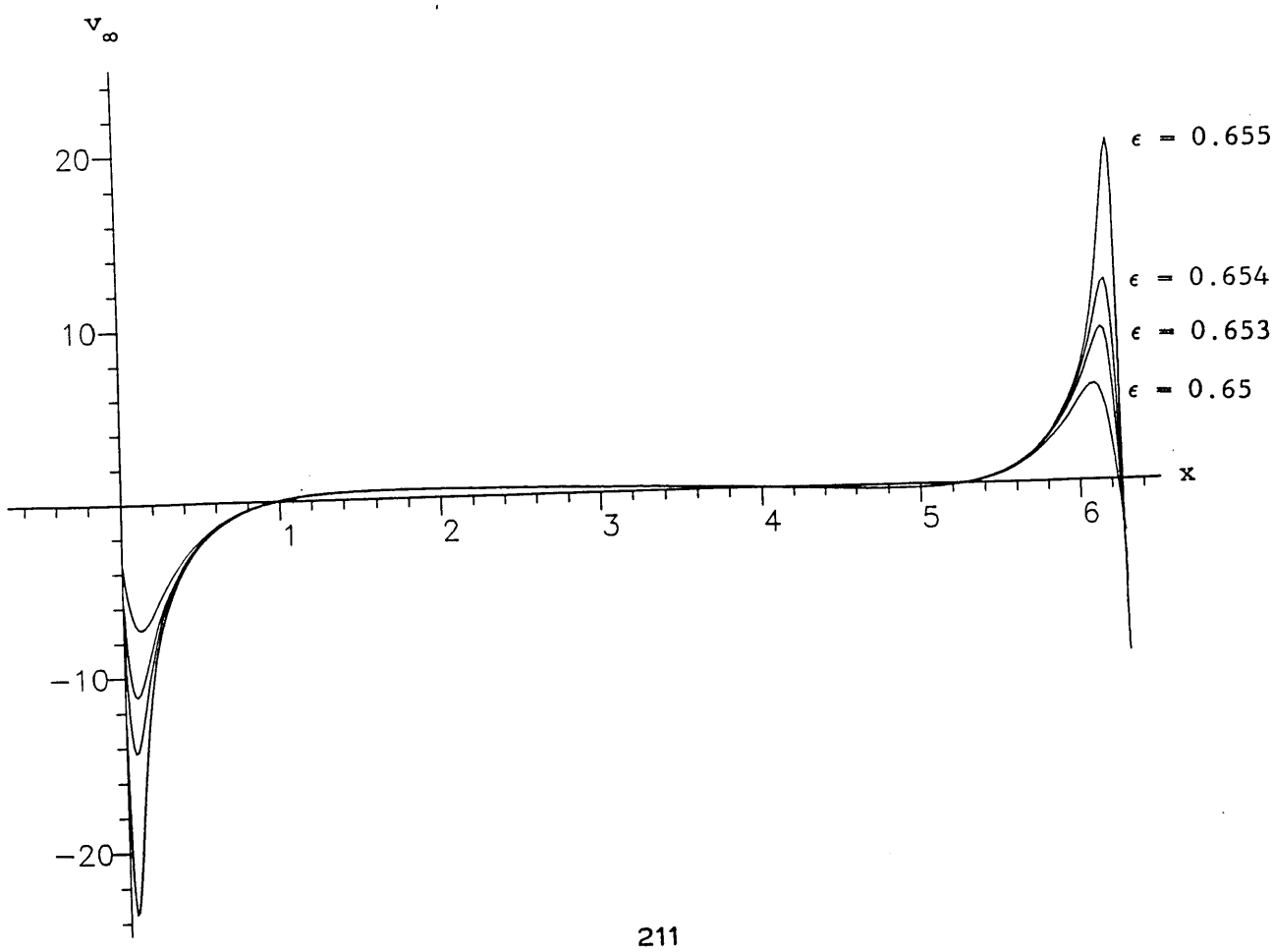
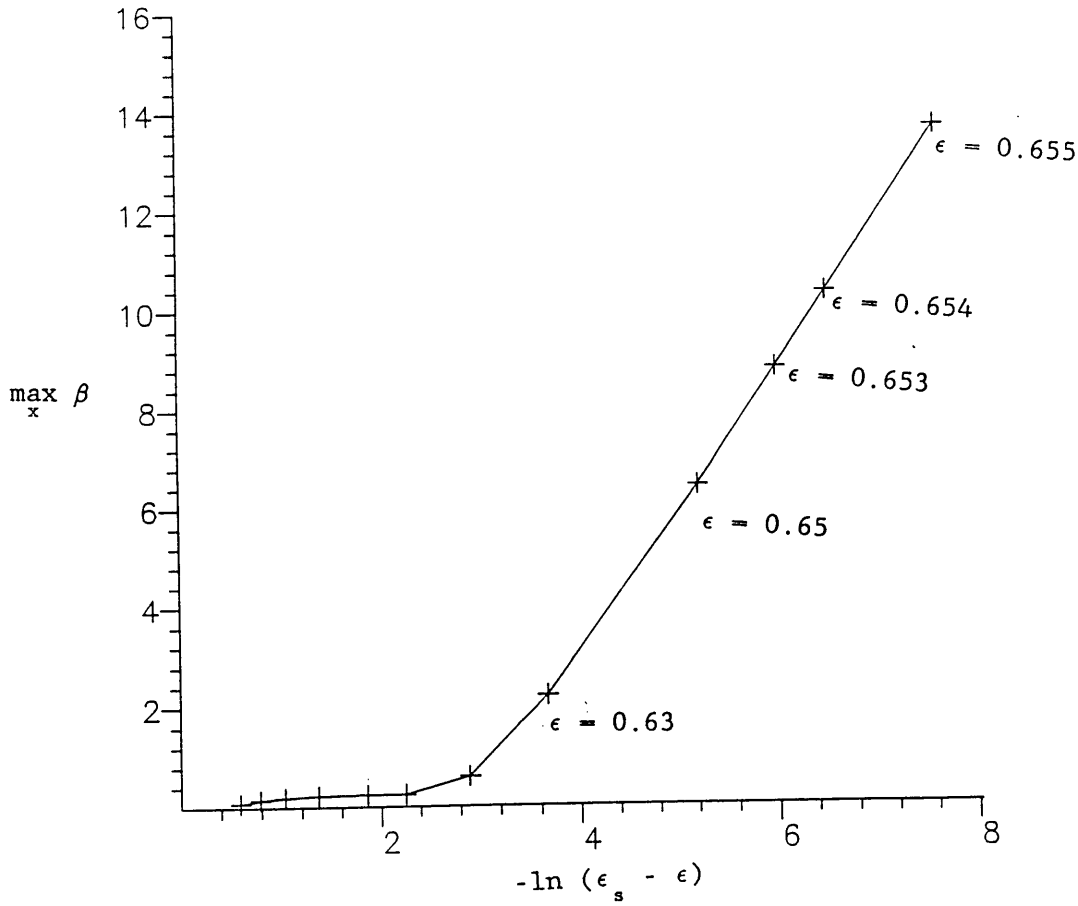


Figure 3.4:7a



$$\frac{1}{\max_x(v_\infty) - \min_x(v_\infty)}$$

Figure 3.4:7b

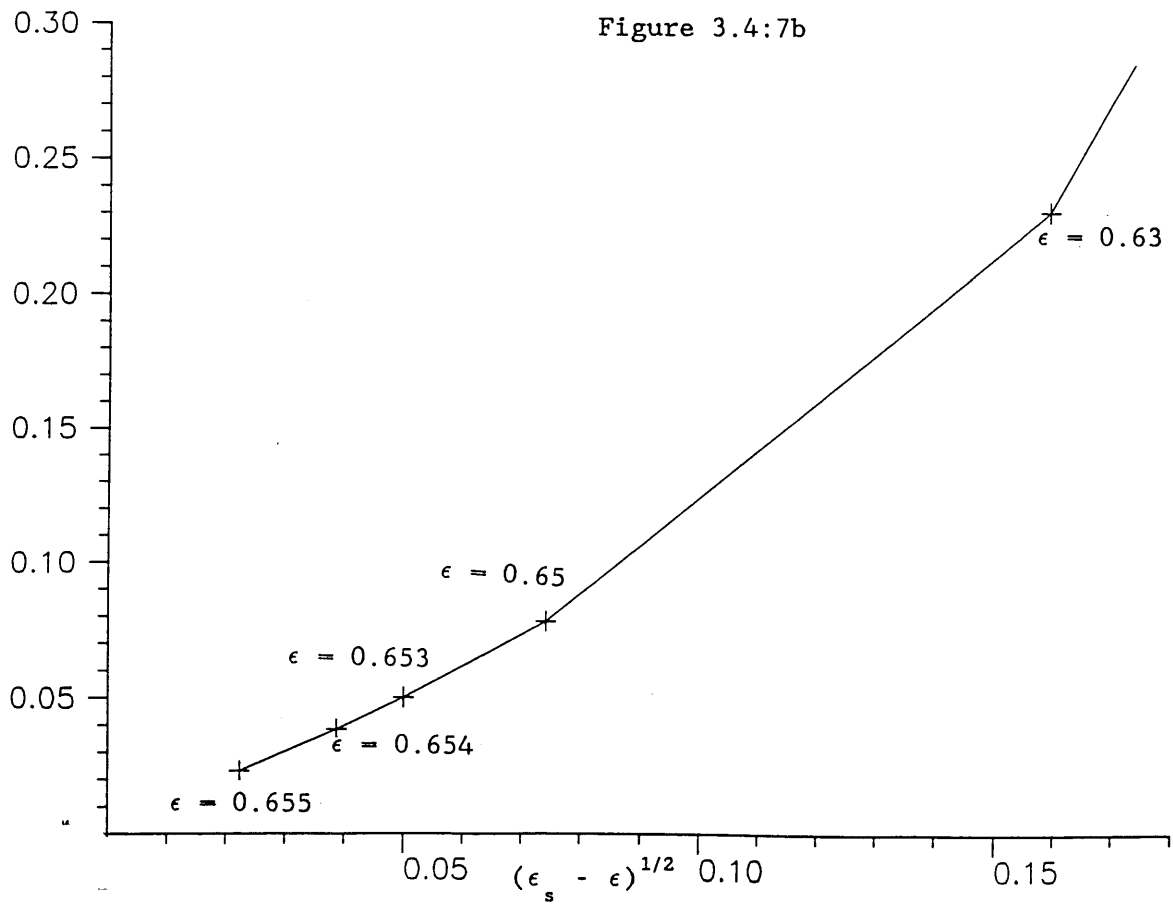


Figure 3.4:8

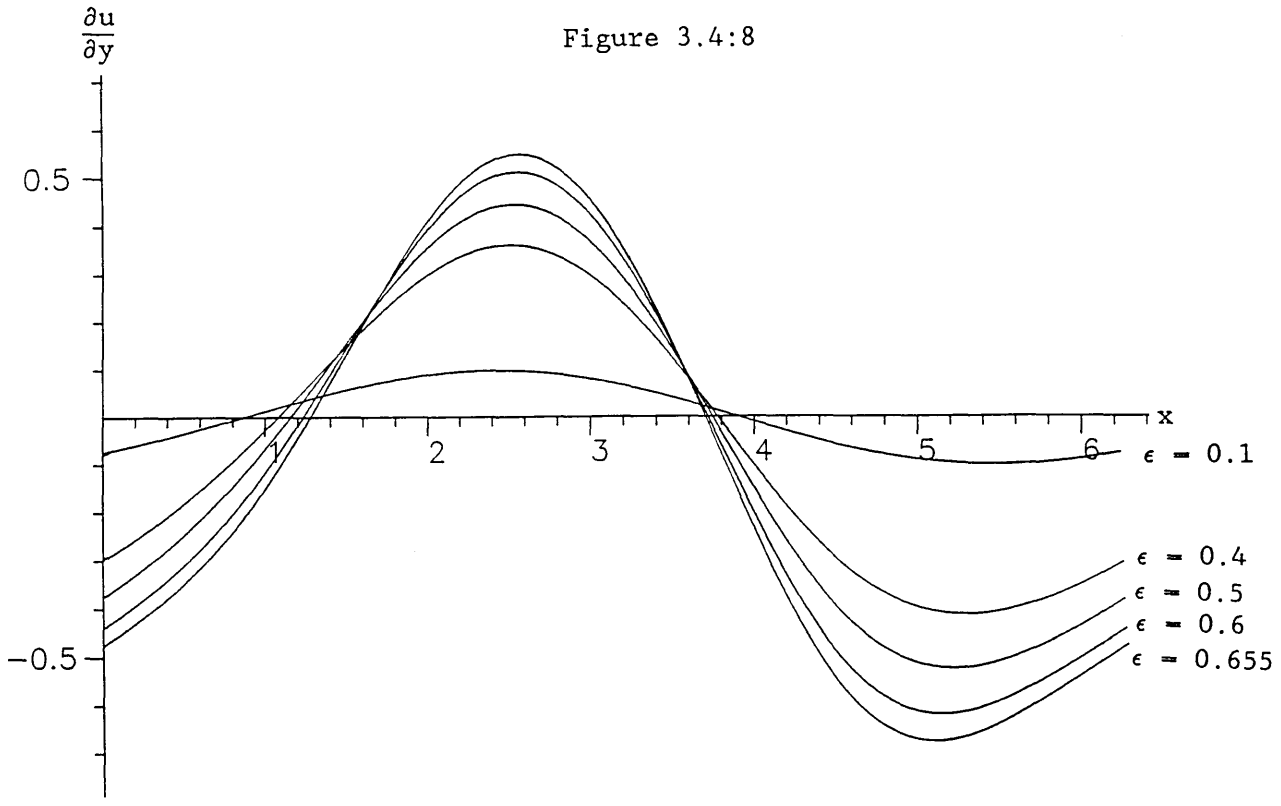


Figure 3.4:9

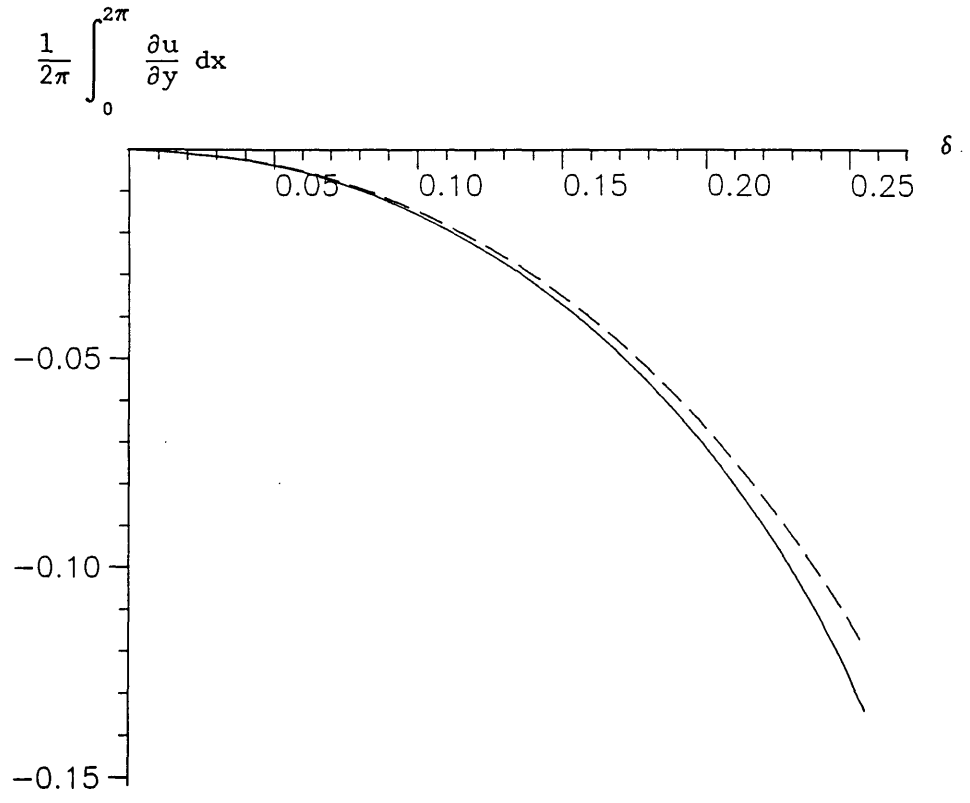


Figure 3.4:10a

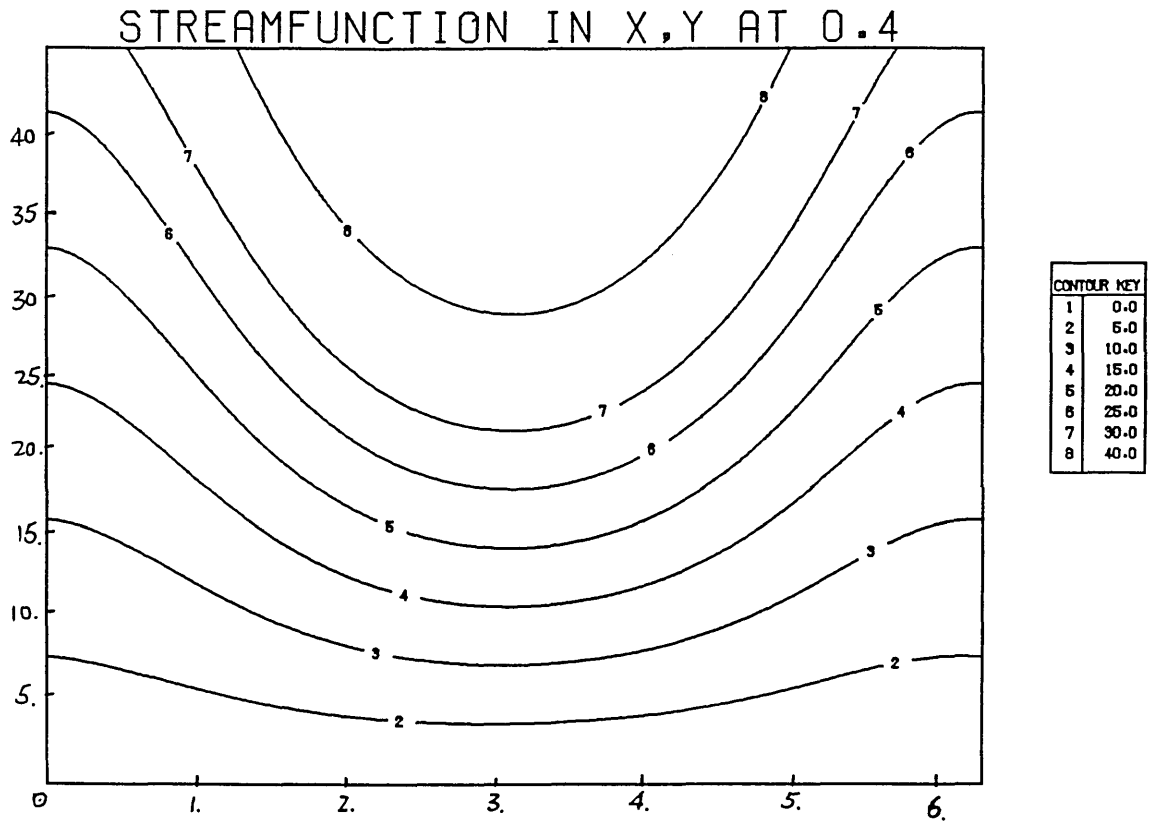


Figure 3.4:10b

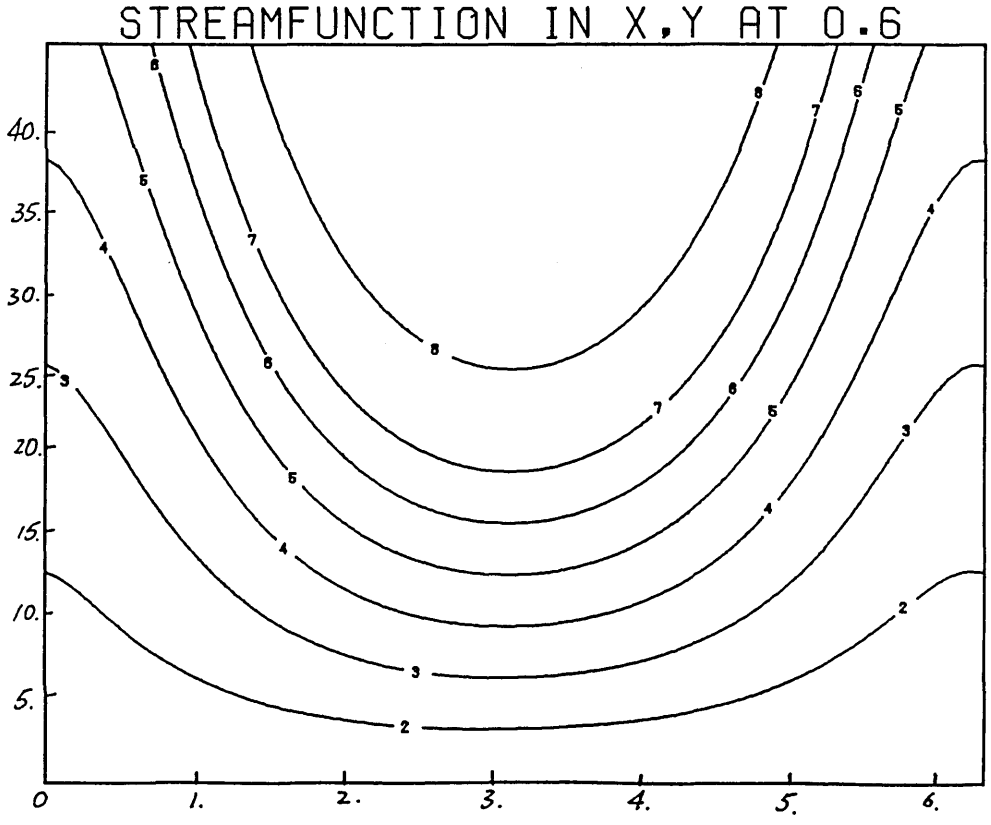
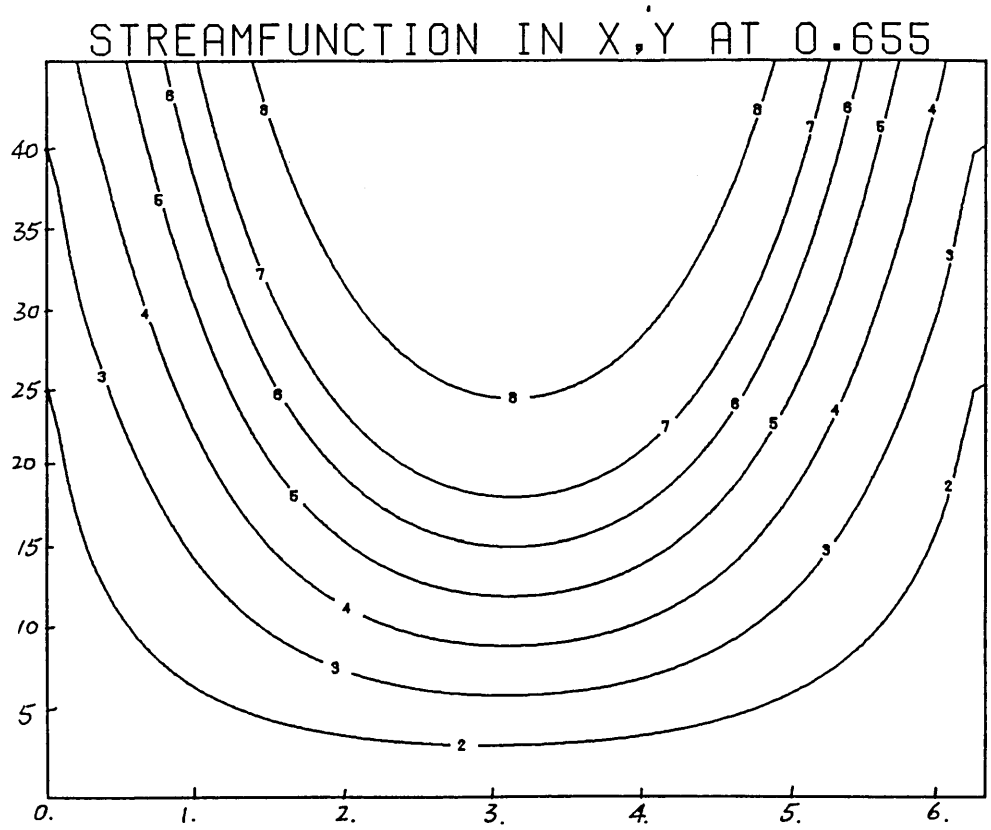


Figure 3.4:10c



§3.5 Nonlinear Tollmien-Schlichting Waves

In this section we describe how our numerical calculations for the circular cylinder also relate to progressive (or at least 'almost' progressive) Tollmien-Schlichting waves in channels and boundary layers.

We begin by considering flow driven through a channel of width a by a mean pressure gradient of strength -G. The fluid is assumed to have density ρ and viscosity ν, and we define a Reynolds number, $R = \frac{Ga^3}{\rho\nu^2}$, which is assumed to be large. Lengths, velocities, pressure and time are non-dimensionalised by a, $Ga^2/(\rho\nu)$, Ga and $\rho\nu/(Ga)$ respectively. $\hat{x}$ and $\hat{y}$ are used to denote the (non-dimensional) distances along and across the channel respectively (see figure 3.5:1), $\hat{u}$ and $\hat{v}$ denote the corresponding velocity components, and $\hat{p}$ and $\hat{t}$ are the pressure and time respectively. The solution for Poiseuille flow through such a channel is given by

$$\hat{u} = \hat{u}_o \equiv \hat{y}(1-\hat{y})/2 \ .$$

Waves can be generated in such channels by, for example, distorting the walls of the channel. Smith (1976d,e, 1979a,b) and Secomb (1979) showed that there was a distinguished scaling for asymmetric disturbances, given by the wavelength and frequency of 'lower-branch', Tollmien-Schlichting (T-S) waves, viz. $\hat{x}\sim R^{1/7}$, $\hat{t}\sim R^{3/7}$. Zhuk and Ryzhov (1982), Stephanoff, Pedley, Lawrence and Secomb (1983), Smith and Burggraf (1985), and Rothmayer and Smith (1987) then indicated how the governing equations for this distinguished scaling could themselves be rescaled to yield

equations which describe nonlinear, high-frequency, T-S waves.

Below, we outline the scalings and arguments leading to the governing equations for nonlinear T-S waves (see the above papers for more details); to fix ideas we allow for the walls to be slightly distorted by an $O(R^{-2/7})$ amplitude. At the end of this derivation we show that the periodic, classical boundary-layer problem which was solved for the rotating cylinder problem plays an important role in this theory.

Wall distortions of typical length $R^{1/7}$ and amplitude $R^{-2/7}$, generate cross-channel velocity disturbances of amplitude $R^{-3/7}$ in the centre of the channel. Here, the flow is expected to be approximately inviscid at high Reynolds numbers, and the appropriate scaling is then ($\alpha=R^{-1/7}$)

$$x = \alpha\hat{x}, \quad t = \alpha^3\hat{t},$$

$$\hat{u} = \left[\hat{u}_o(\hat{y}) + \alpha^2\hat{u}_1(x,\hat{y},t) + ... \right] , \qquad (3.5:1a)$$

$$\hat{v} = \left[\qquad \alpha^3\hat{v}_1(x,\hat{y},t) + ... \right] , \qquad (3.5:1b)$$

$$\hat{p} = \alpha^{-3} \left[\hat{p}_1(x,\hat{y},t) + ... \right] . \qquad (3.5:1c)$$

The solutions for $\hat{u}_1$, $\hat{v}_1$ and $\hat{p}_1$ are:

$$\hat{u}_1 = W(\hat{y},t) + A(x,t)\hat{u}_o'(\hat{y}) , \quad \hat{v}_1 = -A'(x,t)\hat{u}_o(\hat{y}), \qquad (3.5:1e)$$

$$\hat{p}_1(x,\hat{y},t) = \hat{p}_1(x,0,t) + A''(x,t) \int_o^{\hat{y}} \hat{u}_o^2(y)dy . \qquad (3.5:1f)$$

Here $A(x,t)$ is known as the displacement function, and allows for an interaction between the boundary-layers on either channel wall (see below). For an isolated distortion, the condition of no

disturbance far upstream fixes $W\equiv 0$, and $A\to 0$ as $x\to-\infty$. However, for periodic flow W cannot be determined at leading order, although without loss of generality we impose $\langle A\rangle=0$, where $\langle A\rangle$ is the average of A over a period.

The inviscid solution in general leads to slip velocities at the walls, and hence boundary layers. The flow within the boundary layer on the lower wall, $\hat{y}=\alpha^2 f(x,t)$, is specified by the scaling,

$$\hat{y} = \alpha^2(\tilde{y} + f(x,t)) , \qquad \hat{p} = \alpha^{-3}\tilde{p}(x,\tilde{y},t) + \ldots ,$$

$$\hat{u} = \alpha^2\tilde{u}(x,\tilde{y},t) + \ldots , \quad \hat{v} = \alpha^5(\tilde{v}(x,\tilde{y},t)+\tilde{u}f_x+f_t) + \ldots ,$$

the boundary-layer equations

$$\tilde{u}_x + \tilde{v}_{\tilde{y}} = 0, \quad \tilde{u}_t + \tilde{u}\tilde{u}_x + \tilde{v}\tilde{u}_{\tilde{y}} = -\tilde{p}_x + \tilde{u}_{\tilde{y}\tilde{y}}, \quad \tilde{p}_{\tilde{y}} = 0, \quad (3.5{:}2a,b,c)$$

and the boundary conditions,

$$\tilde{u} = \tilde{v} = 0 \text{ on } \tilde{y} = 0, \quad \tilde{u} \sim \tfrac{1}{2}(\tilde{y} + A(x,t) + f(x,t)) + W(0,t) \text{ as } \tilde{y} \to \infty. \quad (3.5{:}2d,e)$$

On the upper wall, $\hat{y}=1+\alpha^2 g(x,t)$, the corresponding equations are

$$1-\hat{y} = \alpha^2(\tilde{\tilde{y}} - g(x,t)) , \qquad \hat{p} = \alpha^{-3}\tilde{\tilde{p}}(x,\tilde{\tilde{y}},t) + \ldots ,$$

$$\hat{u} = \alpha^2\tilde{\tilde{u}}(x,\tilde{\tilde{y}},t) + \ldots , \quad \hat{v} = -\alpha^5(\tilde{\tilde{v}}(x,\tilde{\tilde{y}},t) - \tilde{\tilde{u}}g_x - g_t) + \ldots ,$$

$$\tilde{\tilde{u}}_x + \tilde{\tilde{v}}_{\tilde{\tilde{y}}} = 0, \quad \tilde{\tilde{u}}_t + \tilde{\tilde{u}}\tilde{\tilde{u}}_x + \tilde{\tilde{v}}\tilde{\tilde{u}}_{\tilde{\tilde{y}}} = -\tilde{\tilde{p}}_x + \tilde{\tilde{u}}_{\tilde{\tilde{y}}\tilde{\tilde{y}}} , \quad \tilde{\tilde{p}}_{\tilde{\tilde{y}}} = 0 , \quad (3.5{:}3a,b,c)$$

$$\tilde{\tilde{u}} = \tilde{\tilde{v}} = 0 \text{ on } \tilde{\tilde{y}} = 0, \quad \tilde{\tilde{u}} \sim \tfrac{1}{2}(\tilde{\tilde{y}} - A(x,t) - g(x,t)) + W(1,t) \text{ as } \tilde{\tilde{y}} \to \infty. \quad (3.5{:}3d,e)$$

From (3.5:1) the pressure in the two layers is related by:

$$\tilde{\tilde{p}} - \tilde{p} = \frac{1}{120} A_{xx} . \qquad (3.5{:}4)$$

The mathematical problem we wish to solve is specified by (3.5:2-4). Following Zhuk and Ryzhov (1982), Stephanoff *et al.*

(1983), Smith and Burggraf (1985) and Rothmayer and Smith (1987) we seek short-wavelength nonlinear T-S wave solutions to these equations when there are no wall distortions (i.e. we now assume that f=g=0). The assumption of high frequency divides each of the two boundary layers into two asymptotic regions, namely viscous layers immediately adjacent to the walls and inviscid layers lying between the viscous layers and the original inviscid core flow.

Let us assume that $\lambda \ll 1$ is a typical wavelength of the waves, and introduce the scaled coordinate $\lambda\xi = x$. We also assume that T-S waves have a slowly varying form of solution, with a fast time scale $\tau = \lambda^{-3}t$, and a slow time scale $T = \lambda^{1/2}t$. Then as has been shown by previous authors, the appropriate scalings, etc. are:

Lower inviscid layer

$$\tilde{y} = \frac{\eta}{\lambda^2}\,, \quad \tilde{u} = \frac{U}{\lambda^2}\,, \quad \tilde{v} = \frac{V}{\lambda^5}\,, \quad \tilde{p} = \frac{P}{\lambda^4}\,, \quad A = \frac{\mathcal{A}}{\lambda^2}\,, \quad W = \frac{\mathcal{W}}{\lambda^2}, \tag{3.5:5a}$$

$$U_\xi + V_\eta = 0, \quad U_\tau + \lambda^{7/2}U_T + UU_\xi + VU_\eta = -P_\xi + \lambda^7 U_{\eta\eta}, \tag{3.5:5b}$$

$$V = 0 \quad \text{on} \quad \eta = 0, \quad U \sim \tfrac{1}{2}(\eta + \mathcal{A}(\xi,\tau,T)) + \mathcal{W}(0,\tau,T)\,, \quad \text{as} \quad \eta \to \infty\,; \tag{3.5:5c}$$

Upper inviscid layer

$$\bar{\tilde{y}} = \frac{\bar{\eta}}{\lambda^2}\,, \quad \bar{\tilde{u}} = \frac{\bar{U}}{\lambda^2}\,, \quad \bar{\tilde{v}} = \frac{\bar{V}}{\lambda^5}\,, \quad \bar{\tilde{p}} = \frac{\bar{P}}{\lambda^4}\,, \tag{3.5:5d}$$

$$\bar{U}_\xi + \bar{V}_{\bar{\eta}} = 0, \quad \bar{U}_\tau + \lambda^{7/2}\bar{U}_T + \bar{U}\bar{U}_\xi + \bar{V}\bar{U}_{\bar{\eta}} = -\bar{P}_\xi + \lambda^7 \bar{U}_{\bar{\eta}\bar{\eta}}, \tag{3.5:5e}$$

$$\bar{V} = 0 \quad \text{on} \quad \bar{\eta} = 0, \quad \bar{U} \sim \tfrac{1}{2}(\bar{\eta} - \mathcal{A}(\xi,\tau,T)) + \mathcal{W}(1,\tau,T)\,, \quad \text{as} \quad \bar{\eta} \to \infty\,; \tag{3.5:5f}$$

Pressure-displacement law

$$\bar{P} - P = \frac{1}{120}\mathcal{A}_{\xi\xi} \ . \qquad (3.5:5g)$$

Before giving the equations for the viscous layers we find that it is convenient to simplify these equations. We will assume that to leading order in λ the solutions are progressive waves, i.e. the variables ξ and τ are assumed to occur only in the combination

$$\sigma = \xi - \int_0^\tau c(T)dT = \xi - \lambda^{-7/2}\int_0^T c(T)dT \ , \qquad (3.5:6a)$$

where c is the local wave speed, and for this definition τ and T are not regarded as independent variables. Note that if the solution depends only on σ, then $\mathcal{W}$ must be independent of τ.

We now seek a solution to (3.5:5) as a series in $\lambda^{7/2}$:

$$(U,V,P,\bar{U},\bar{V},\bar{P},\mathcal{A},\mathcal{W},c) = (U_o,V_o,P_o,\bar{U}_o,\bar{V}_o,\bar{P}_o,\mathcal{A}_o,\mathcal{W}_o,c_o) \qquad (3.5:6b)$$
$$+ \lambda^{7/2}(U_1,V_1,P_1,\bar{U}_1,\bar{V}_1,\bar{P}_1,\mathcal{A}_1,\mathcal{W}_1,c_1) + \ldots \ .$$

Subsituting into (3.5:5) we obtain:

$$U_{o\sigma} + V_{o\eta} = 0, \quad (U_o - c_o)U_{o\sigma} + V_o U_{o\eta} = -P_{o\sigma} \ , \qquad (3.5:7a,b)$$

$$\bar{U}_{o\sigma} + \bar{V}_{o\eta} = 0, \quad (\bar{U}_o - c_o)\bar{U}_{o\sigma} + \bar{V}_o \bar{U}_{o\eta} = -\bar{P}_{o\sigma} \ , \qquad (3.5:7c,d)$$

$$U_{1\sigma} + V_{1\eta} = 0, \quad \bar{U}_{1\sigma} + \bar{V}_{1\eta} = 0 \ , \qquad (3.5:7e,f)$$

$$U_{oT} + (U_o - c_o)U_{1\sigma} + (U_1 - c_1)U_{o\sigma} + V_1 U_{o\eta} + V_o U_{1\eta} = -P_{1\sigma} \ , \qquad (3.5:7g)$$

$$\bar{U}_{oT} + (\bar{U}_o - c_o)\bar{U}_{1\sigma} + (\bar{U}_1 - c_1)\bar{U}_{o\sigma} + \bar{V}_1 \bar{U}_{o\eta} + \bar{V}_o \bar{U}_{1\eta} = -\bar{P}_{1\sigma} \ . \qquad (3.5:7h)$$

The leading-order problem (3.5:7a-d) is nonlinear, but fortunately

there are simple solutions which satisfy boundary conditions (3.5:5c,f):

$$U_o = \frac{1}{2}(\eta + \mathcal{A}_o) + W_o(0,T) \ , \quad V_0 = -\frac{1}{2}\mathcal{A}_{o\sigma}\eta \ , \tag{3.5:8a}$$

$$-P_{o\sigma} = \frac{1}{2}\mathcal{A}_{o\sigma}\left[\frac{1}{2}\mathcal{A}_o + W_o(0,T) - c_o\right] \ , \tag{3.5:8b}$$

$$\bar{U}_o = \frac{1}{2}(\bar{\eta} - \mathcal{A}_o) + W_o(1,T) \ , \quad \bar{V}_0 = \frac{1}{2}\mathcal{A}_{o\sigma}\bar{\eta} \ , \tag{3.5:8c}$$

$$-\bar{P}_{o\sigma} = \frac{1}{2}\mathcal{A}_{o\sigma}\left[\frac{1}{2}\mathcal{A}_o - W_o(1,T) + c_o\right] \ . \tag{3.5:8d}$$

The solutions to (3.5:7e-h) are then

$$U_1 = \frac{1}{2}\mathcal{A}_1 + W_1(0,T) \ , \quad V_1 = -\frac{1}{2}\mathcal{A}_{1\sigma}\eta + \mathcal{V}_1(\sigma,T) \ , \tag{3.5:8e}$$

$$\begin{aligned} -P_{1\sigma} = {} & \frac{1}{2}\mathcal{A}_{oT} + W_{oT}(0,T) + \frac{1}{2}\mathcal{A}_{1\sigma}\left[\frac{1}{2}\mathcal{A}_o + W_o(0,T) - c_o\right] \\ & + \frac{1}{2}\mathcal{V}_1(\sigma,T) + \frac{1}{2}\mathcal{A}_{o\sigma}\left[\frac{1}{2}\mathcal{A}_1 + W_1(0,T) - c_1\right] \ , \end{aligned} \tag{3.5:8f}$$

$$\bar{U}_1 = -\frac{1}{2}\mathcal{A}_1 + W_1(1,T) \ , \quad \bar{V}_1 = +\frac{1}{2}\mathcal{A}_{1\sigma}\bar{\eta} + \bar{\mathcal{V}}_1(\sigma,T) \ , \tag{3.5:8g}$$

$$\begin{aligned} -\bar{P}_{1\sigma} = {} & -\frac{1}{2}\mathcal{A}_{oT} + W_{oT}(1,T) + \frac{1}{2}\mathcal{A}_{1\sigma}\left[\frac{1}{2}\mathcal{A}_o - W_o(1,T) + c_o\right] \\ & + \frac{1}{2}\bar{\mathcal{V}}_1(\sigma,T) + \frac{1}{2}\mathcal{A}_{o\sigma}\left[\frac{1}{2}\mathcal{A}_1 - W_1(1,T) + c_1\right] \ , \end{aligned} \tag{3.5:8h}$$

where $\mathcal{V}_1(\sigma,T)$ and $\bar{\mathcal{V}}_1(\sigma,T)$ are the values of V_1 and $\bar{V}_1$ on $\eta=0$ and $\bar{\eta}=0$ respectively. Note that there is no guarantee that these solutions are unique, and hence there may be other progressive wave solutions which we do not identify by this approach. Also, from averaging (3.5:8f,h) over a period, and using $\langle\mathcal{A}\rangle=0$, we find that

$$\langle P_{1\sigma}\rangle = \langle -W_{oT}(0,T)\rangle \ , \qquad \langle \bar{P}_{1\sigma}\rangle = \langle -W_{oT}(1,T)\rangle \ ,$$

i.e. over the slow time scale *the mean pressure gradient changes* if $W_{oT}\neq 0$. (Dr. P. A. Stewart points out that this pressure gradient is

much larger than the original pressure gradient. However it can be forced to zero if another slow time scale, and another asymptotic layer, are introduced.)

Combining (3.5:5g) and (3.5:8b,d,f,h) we conclude that $\mathcal{A}_0$ and $\mathcal{A}_1$ satisfy the equations

$$\frac{1}{120}\mathcal{A}_{0\sigma\sigma\sigma} - (\tfrac{1}{2}(W_0(1,T)+W_0(0,T)) - c_0)\mathcal{A}_{0\sigma} = 0 , \qquad (3.5:9a)$$

$$\frac{1}{120}\mathcal{A}_{1\sigma\sigma\sigma} - (\tfrac{1}{2}(W_0(1,T)+W_0(0,T)) - c_0)\mathcal{A}_{1\sigma} = \mathcal{A}_{0T} + W_{0T}(0,T) - W_{0T}(1,T)$$

$$+ (\tfrac{1}{2}(W_1(1,T)+W_1(0,T)) - c_1)\mathcal{A}_{0\sigma} + \tfrac{1}{2}(V_1(\sigma,T) - \bar{V}_1(\sigma,T)) . \qquad (3.5:9b)$$

Equation (3.5:9a) has the zero-mean solution

$$\mathcal{A}_0 = 2a_0(T)\cos(\Lambda_0(T)(\sigma+\phi_0(T))) , \qquad (3.5:10a)$$

$$c_0 = \frac{\Lambda_0^2(T)}{120} + \tfrac{1}{2}(W_0(1,T)+W_0(0,T)) . \qquad (3.5:10b)$$

Here a_0, Λ_0 and ϕ_0 are slowly varying functions which are determined at higher order. From the arbitrariness in defining the typical lengthscale λ, we may take $\Lambda_0(0)=1$ without loss of generality, and from a translation of coordinates at T=0 we can assume $\phi(0)=0$.

Before finding the solution for $\mathcal{A}_1$, it is convenient to determine V_1 and $\bar{V}_1$ by obtaining solutions in the boundary layers which are driven by the inviscid slip velocity specified by (3.5:8e,g). As previous authors have shown, the relevant governing equations, etc. in these layers are:

Lower viscous layer:

$$\tilde{y} = \lambda^{3/2} y \tag{3.5:11a}$$

$$(\lambda^2\tilde{u},\ \lambda^{3/2}\tilde{v},\ \lambda^4\tilde{p}) = (u_o, v_o, P_o) + \lambda^{7/2}(u_1, v_1, P_1) + \ldots \ .$$

$$u_{o\sigma} + v_{oy} = 0, \quad (u_o - c_o)u_{o\sigma} + v_o u_{oy} = -P_{o\sigma} + u_{oyy}, \quad P_{oy} = 0 \ , \tag{3.5:11b}$$

$$\begin{aligned} u_o = v_o = 0 \quad &\text{on} \quad y = 0 \ , \\ u_o \sim a_o \cos(\Lambda_o(\sigma + \phi_o)) + W_o(0,T) \quad &\text{as} \quad y \to \infty \ , \end{aligned} \tag{3.5:11c}$$

$$\begin{aligned} u_{1\sigma} + v_{1y} = 0, \quad P_{1y} = 0 \ , \\ (u_o - c_o)u_{1\sigma} + (u_1 - c_1)u_{o\sigma} + u_{oT} + v_o u_{1y} + v_1 u_{oy} = -P_{1\sigma} + u_{1yy}, \end{aligned} \tag{3.5:11d}$$

$$\begin{aligned} u_1 = v_1 = 0 \quad &\text{on} \quad y = 0 \ , \\ u_1 \sim \tfrac{1}{2}(y + \mathcal{A}_1) + W_1(0,T) \quad &\text{as} \quad y \to \infty \ ; \end{aligned} \tag{3.5:11e}$$

Upper viscous layer:

$$\bar{\tilde{y}} = \lambda^{3/2} \bar{y} \tag{3.5:12a}$$

$$(\lambda^2\bar{\tilde{u}},\ \lambda^{3/2}\bar{\tilde{v}},\ \lambda^4\bar{\tilde{p}}) = (\bar{u}_o, \bar{v}_o, \bar{P}_o) + \lambda^{7/2}(\bar{u}_1, \bar{v}_1, \bar{P}_1) + \ldots \ .$$

$$\bar{u}_{o\sigma} + \bar{v}_{oy} = 0, \quad (\bar{u}_o - \bar{c}_o)\bar{u}_{o\sigma} + \bar{v}_o \bar{u}_{oy} = -\bar{P}_{o\sigma} + \bar{u}_{oyy}, \quad \bar{P}_{oy} = 0 \ , \tag{3.5:12b}$$

$$\begin{aligned} \bar{u}_o = \bar{v}_o = 0 \quad &\text{on} \quad \bar{y} = 0 \ , \\ \bar{u}_o \sim -a_o \cos(\Lambda_o(\sigma + \phi_o)) + W_o(1,T) \quad &\text{as} \quad y \to \infty \ , \end{aligned} \tag{3.5:12c}$$

$$\begin{aligned} \bar{u}_{1\sigma} + \bar{v}_{1y} = 0, \quad \bar{P}_{1y} = 0 \ , \\ (\bar{u}_o - \bar{c}_o)\bar{u}_{1\sigma} + (\bar{u}_1 - \bar{c}_1)\bar{u}_{o\sigma} + \bar{u}_{oT} + \bar{v}_o \bar{u}_{1y} + \bar{v}_1 \bar{u}_{oy} = -\bar{P}_{1\sigma} + \bar{u}_{1yy}, \end{aligned} \tag{3.5:12d}$$

$$\begin{aligned} \bar{u}_1 = \bar{v}_1 = 0 \quad &\text{on} \quad \bar{y} = 0 \ , \\ \bar{u}_1 \sim \tfrac{1}{2}(\bar{y} - \mathcal{A}_1) + W_1(1,T) \quad &\text{as} \quad \bar{y} \to \infty \ . \end{aligned} \tag{3.5:12e}$$

By comparison with our equation (3.2:2) for the rotating

cylinder problem (see also below), we see that if a periodic solution is sought (3.5:11b,c) specify an eigenvalue problem for $W_o(0,T)$ given a_o, Λ_o, ϕ_o and c_o. Using the transformation $\sigma \to \sigma + \pi/\Lambda_o$ we see also that (3.5:12b,c) specifies the same problem for $W_o(1,T)$, and hence, since the solution is unique (see section 3.4),

$$u_o(\sigma,y) = \bar{u}_o(\sigma+\pi/\Lambda_o,y), \quad W_o(0,T) = W_o(1,T) \equiv W_o(T) \ . \qquad (3.5:13a)$$

It follows from matching with the inviscid layer that

$$v_{o\infty} = \lim_{y\to\infty} (v_o + u_{o\sigma} y) = V_1(\sigma,T) = \bar{V}_1(\sigma+\pi/\Lambda_o,T) \ . \qquad (3.5:13b)$$

Further, using the transformation (see also (3.5:10b))

$$x = -\Lambda_o(\sigma+\phi_o) \ , \quad z = (\Lambda_o^3/120)^{1/2} y \ , \quad u = 120(c_o - u_o)/\Lambda_o^2 \ ,$$

$$v = (120/\Lambda_o^3)^{1/2} v_o \ , \quad p = (120)^2 p_o/\Lambda_o^4 \ , \quad \varepsilon = 120a_o/\Lambda_o^2 \ , \qquad (3.5:14)$$

$$w = 120W_o/\Lambda_o^2 = 120c_o/\Lambda_o^2 - 1 \ ,$$

we note that equation (3.5:11b,c) can be rewritten as

$$u_x + v_z = 0 \ , \quad uu_x + vu_z = -U_e U_{ex} + u_{zz} \ , \qquad (3.5:15a)$$

$$u=1+w, \ v=0 \ \text{ on } \ z=0 \ , \quad u \to U_e = 1-\varepsilon\cos(x) \ \text{ as } \ z \to \infty \ . \qquad (3.5:15b)$$

This is the same problem as specified by (3.2:2), the solution of which is given in section 3.4. Thus w is a known function of ε, i.e. from (3.5:14) c_o *is a known function of* a_o *and* Λ_o.

In section 3.4, $v_\infty(x;\varepsilon) = \lim_{z\to\infty} (v_o + u_{ox} z)$ was calculated, which for convenience we express as a Fourier series (note that $\langle v \rangle = 0$):

$$v_\infty = \sum_{n=1}^{\infty} (\alpha_n \cos(nx) + \beta_n \sin(nx)) \ . \qquad (3.5:16)$$

Then from (3.5:9b, 13, 15, 16) we obtain

$$\frac{1}{120}(\mathcal{A}_{1\sigma\sigma\sigma} + \Lambda_o^2\mathcal{A}_{1\sigma}) = 2a_{oT}\cos(\Lambda_o(\sigma+\phi_o))$$

$$- 2a_o\left\{\Lambda_{oT}(\sigma+\phi_o)+\Lambda_o[\phi_{oT} + \frac{1}{2}(W_1(1,T)+W_1(0,T)) - c_1]\right\}\sin(\Lambda_o(\sigma+\phi_o))$$

$$+ \left[\frac{\Lambda_o^3}{120}\right]^{1/2} \sum_{m=0}^{\infty}\left\{\begin{array}{l} \alpha_{2m+1}\cos((2m+1)(\Lambda_o(\sigma+\phi_o))) \\ - \beta_{2m+1}\sin((2m+1)(\Lambda_o(\sigma+\phi_o))) \end{array}\right\} . \qquad (3.5:17)$$

If the asymptotic series (3.5:6b) is to remain valid as $|\sigma| \to \infty$, then (3.5:17) must yield solutions $\mathcal{A}_1$ which are bounded as $|\sigma| \to \infty$ (this is just the statement of a secularity condition). Hence we conclude from (3.5:17) that

$$\Lambda_{oT} = 0 \quad \Rightarrow \quad \Lambda_o = 1 , \qquad (3.5:18a)$$

$$2a_o(\tfrac{1}{2}(W_1(1,T)+W_1(0,T))+\phi_{oT}-c_1) + (120)^{-1/2}\beta_1 = 0 , \qquad (3.5:18b)$$

$$2a_{oT} + (120)^{-1/2}\alpha_1 = 0 . \qquad (3.5:18c)$$

Equation (3.5:18a) implies that the wavelength is invariant as time evolves on the slow scale. Also for given a_o, and hence β_1, (3.5:18b) relates W_1 to $(c_1-\phi_{oT})$ - cf. (3.5:10b) which relates W_o to c_o. Further, for fixed W_1 we see that an increase in c_1 must be balanced by an increase in ϕ_{oT}. From (3.5:6a, 13a) it follows that this makes no physical difference to the answer, because the only physical quantity is $(c_1-\phi_{oT})$, or its integral. Thus without loss of generality we can take $\phi_o=0$.

Equation (3.5:18c) determines the evolution of the leading order amplitude, a_o (recall that α_1 is a function of $\varepsilon = 120a_o$). A graph of α_1 against a_o is given in figure 3.5:2. As can be seen, α_1 is negative for $a_o \leq \varepsilon_s/120$, and hence the amplitude increases

monotonically until a finite time T_s when $a_o = \varepsilon_s/120$. At this time the boundary-layer solution breaks down due to the formulation of a singularity. For small a_o, the relationship between a_o and α_1 is approximately linear, therefore for small initial amplitudes $a_o = \hat{a}_o \ll 1$ at $t = 0$, the finite time T_s has the form (cf. (3.5:18b))

$$T_s \simeq \gamma_o \ln |\hat{a}_o| + \gamma_1 .$$

Numerical solutions of equation (3.5:18c) with small a_o, and Glauert's small a_o solution (i.e. small ε solution), yield

$$\gamma_o = -\frac{1}{\sqrt{15}}, \qquad \gamma_1 = \frac{1}{\sqrt{15}} \ln \left|\frac{0.656}{120}\right| .$$

How the T-S wave evolves after this time requires further investigation; however we note that at no point does the T-S wave equilibriate at a finite amplitude, i.e. no 'nonlinear' neutral curve is encountered.

The above solution is only valid if higher order terms to the solution can be found. Clearly we cannot do this to arbitrarily high order, and it will have to be assumed that such solutions can be found. However, we note that the solution to (3.5:17) is (i.e. $\langle \mathcal{A}_1 \rangle = 0$)

$$\mathcal{A}_1 = 2a_1(T)\cos(\sigma+\phi_1(T)) - (120)^{1/2} \sum_{m=1}^{\infty} \frac{1}{(2m+1)4m(m+1)} \left\{ \begin{matrix} \beta_{2m+1}\cos((2m+1)\sigma) \\ + \alpha_{2m+1}\sin((2m+1)\sigma) \end{matrix} \right\}, \tag{3.5:19}$$

where a_1 and ϕ_1 are functions of T determined at higher order; thus

$$\mathcal{A}_1(\sigma+\pi) = -\mathcal{A}_1(\sigma) . \tag{3.5:20}$$

For given a_o, a_1, c_1 and ϕ_1, the next order boundary-layer problems (3.5:11d,e) and (3.5:12d,e) can be viewed as eigenvalue

problems for $W_1(0,T)$ and $W_1(1,T)$ respectively. By again considering the transformation $\sigma \to \sigma+\pi$, we conclude, using (3.5:6) and (3.5:20), that

$$u_1(\sigma,y) = \bar{u}_1(\sigma+\pi,y), \quad W_1(0,T) = W_1(1,T) \equiv W_1(T) , \qquad (3.5:21)$$

and so from (3.5:18c) the second order boundary-layer problem fixes c_1 as a function of a_o and a_1 (cf. the leading-order boundary-layer problem which fixes c_o as a function of a_o). We do not solve this linear, but numerical, boundary-layer problem here, although it appears reasonable to expect a solution to exist.

We conclude that nonlinear T-S waves with an 'almost' progressive-wave form do exist in a channel, and that their amplitude slowly increases in time, until boundary-layer separation disrupts their simple harmonic structure.

With the above formulation, an interesting aspect of the solution is that both the mean pressure gradient and mass flux must change slowly in time in a specified manner. However this is a rather artificial restriction and it is more natural to fix one or the other. This can be done by introducing another slow time scale and a further asymptotic layer (Dr. P. A. Stewart, private communication, 1988).

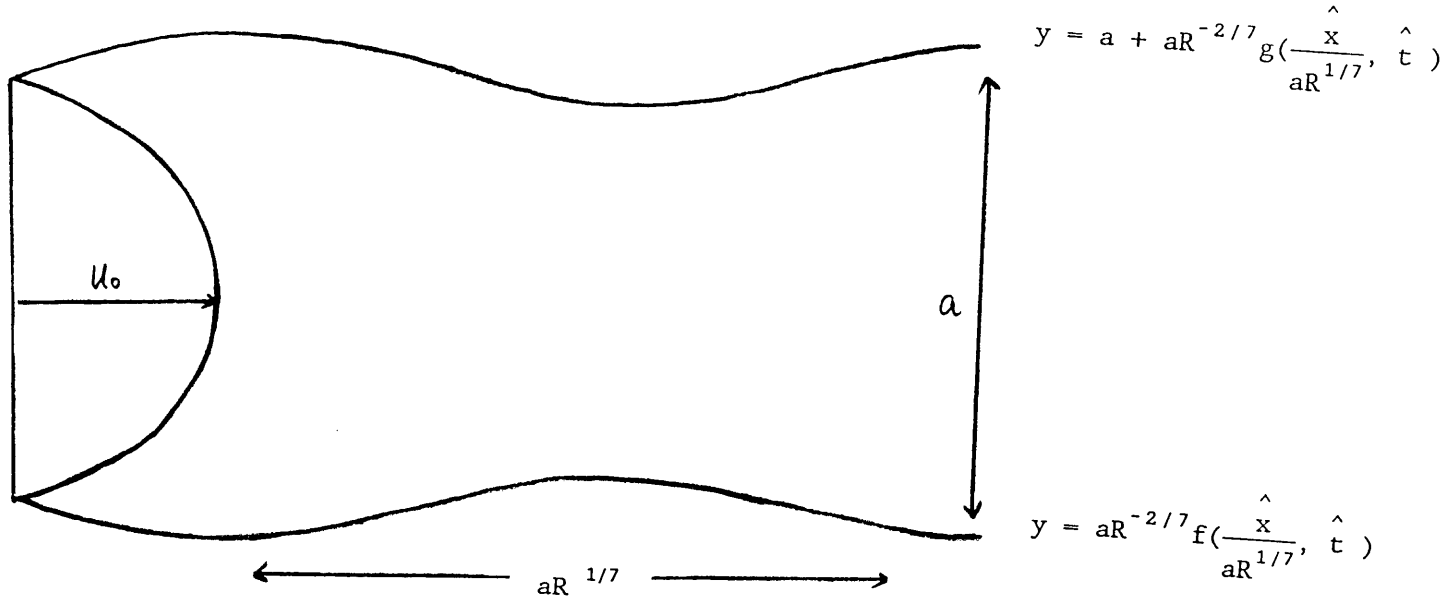
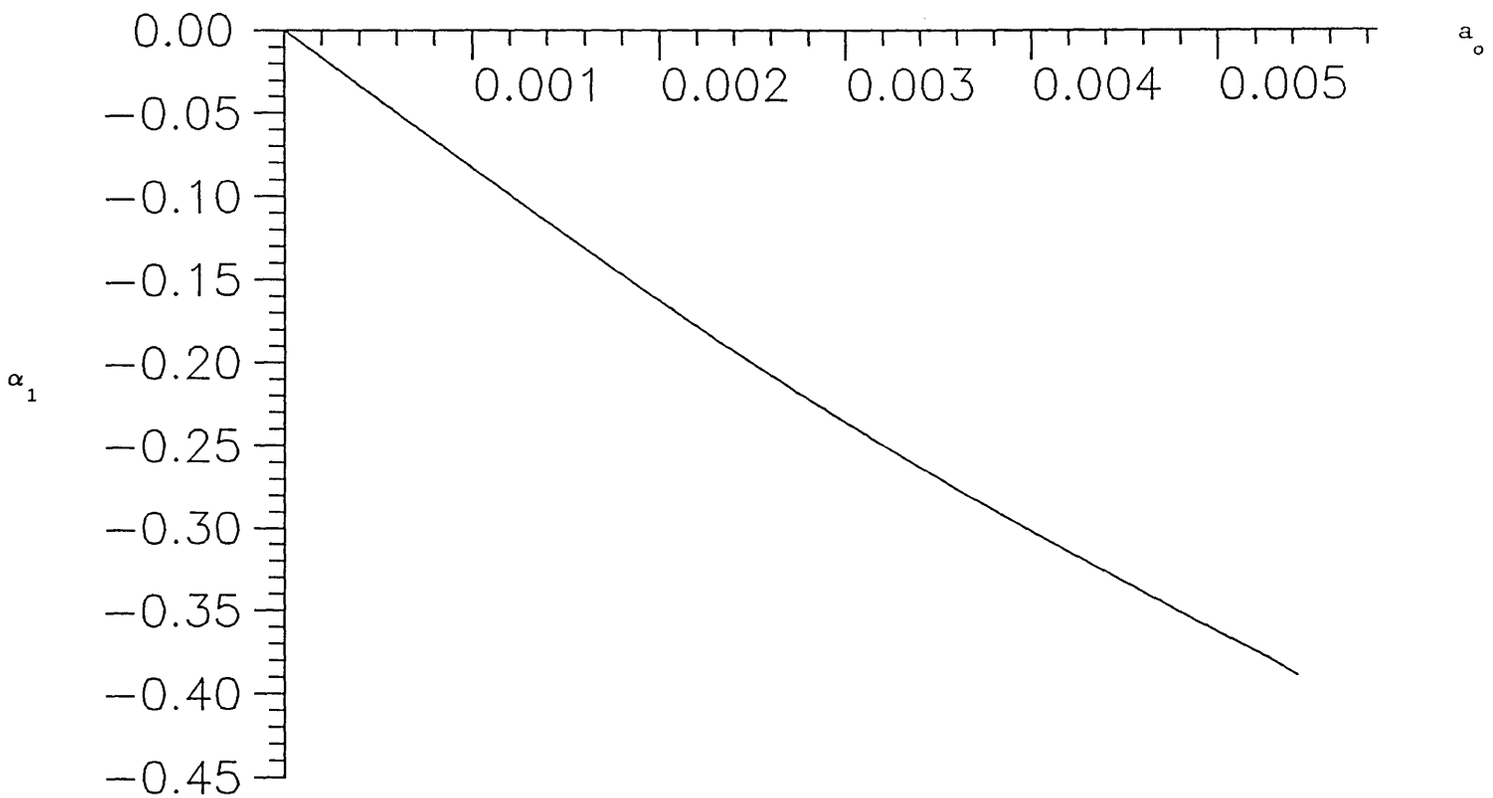

$y = a + aR^{-2/7} g(\frac{\hat{x}}{aR^{1/7}}, \hat{t})$
U_o
a
$y = aR^{-2/7} f(\frac{\hat{x}}{aR^{1/7}}, \hat{t})$
$aR^{1/7}$

Figure 3.5:1

Figure 3.5:2


0.00
−0.05
−0.10
−0.15
−0.20
−0.25
−0.30
−0.35
−0.40
−0.45
0.001
0.002
0.003
0.004
0.005
a_o
α_1

Appendix 3.A Keller-box Schemes

Our first attempt to solve the rotating cylinder problem used a Keller-box scheme. This is based on splitting a kth order differential equation into k first order equations. We therefore write

$$G = \psi, \qquad E = \psi_y = u = G_y, \qquad C = \psi_{yy} = u_y = E_y \ . \quad (3.A.1a,b,c)$$

On expressing equation (3.2:3) in the variables G, E and C, we obtain three first-order partial differential equations. These equations are discretised using second-order finite-difference approximations about $(x_{i-1/2}, y_{j-1/2})$ where x_i, y_j $1 \le i \le NX$, $1 \le j \le NY$ are the grid points. Given the solution at x_{i-1}, the resulting nonlinear equations are solved simultaneously for $G_{i,j}$, $E_{i,j}$, $C_{i,j}$ $(1 \le j \le NY)$ by Newton-Raphson iteration in a similar manner as in the FD method. The Jacobian matrix L is a 9 x NY x NY banded matrix with a band width of 9 (cf. (3.3:3b)). This scheme is more time-consumming than the FD code, because of the increased size of the matrix.

In addition to using the Keller-box scheme on the boundary-layer equation in primitive variable, we also wrote a Keller-box code for equation (3.2:4). Here we wrote

$$C = u, \qquad E = u_y = C_y \ ,$$

and substituted into (3.2:4) to obtain two first-order partial differential equations. These were discretised as above, and the resulting equations again solved by Newton-Raphson iteration. The computational time of this method was intermediate between that for

the Keller-box method for (3.2:3) and the FD method. This reflects the size of the Jacobian matrix. The answers for all three codes were consistent, but the FD code was approximately an order of magnitude faster.

Appendix 3.B Spectral Methods

In this appendix we give more details of the spectral method schemes used in section 3.3.

The quadratic multiplication of two Fourier series

At a number of points in secion 3.3 there is a need to multiply two finite Fourier series to form quadratic terms, viz.

$$\left[q_o + \sum_{n=1}^{N}\left[q_c^n \cos nx + q_s^n \sin nx\right]\right]\left[r_o + \sum_{m=1}^{N}\left[r_c^m \cos mx + r_s^m \sin mx\right]\right] . \tag{3.B:1a}$$

On expanding out the above two series and using the trigonometric multiple-angle formulae, we obtain for the multiple shown in equation (3.B:1a), after truncating the result to N terms,

$$\begin{aligned} & q_o r_o + \frac{1}{2}\sum_{n=1}^{N}\left[q_c^n r_c^n + q_s^n r_s^n\right] \\ & + \sum_{n=1}^{N} \cos nx \left[q_o r_c^n + q_c^n r_o + \frac{1}{2}\sum_{m=1}^{n-1}\left[q_c^m r_c^{n-m} - q_s^m r_s^{n-m}\right]\right. \\ & \qquad + \frac{1}{2}\sum_{m=n+1}^{N}\left[q_c^m r_c^{m-n} + q_s^m r_s^{m-n}\right] \\ & \qquad \left. + \frac{1}{2}\sum_{m=1}^{N-n}\left[q_c^m r_c^{m+n} + q_s^m r_s^{m+n}\right]\right] \end{aligned}$$

$$+ \sum_{n=1}^{N} \sin nx \left[q_o r_s^n + q_s^n r_o + \frac{1}{2} \sum_{m=1}^{n-1} \left(q_c^m r_s^{n-m} + q_s^m r_c^{n-m} \right) \right.$$

$$+ \frac{1}{2} \sum_{m=n+1}^{N} \left(-q_c^m r_s^{m-n} + q_s^m r_c^{m-n} \right)$$

$$\left. - \frac{1}{2} \sum_{m=1}^{N-n} \left(-q_c^m r_s^{m+n} + q_s^m r_c^{m+n} \right) \right] . \qquad (3.B:1b)$$

The governing equations for the NRK method

In deriving the governing equations for the NRK method we express the streamfunction ψ and the *square* of the external velocity, U_e^2, in terms of Fourier series as

$$\psi(x, y) = f_o(y) + \sum_{n=1}^{N} \left[f_c^n(y) \cos(nx) + f_s^n(y) \sin(nx) \right] , \qquad (3.B:2a)$$

and

$$U_e(x)^2 = U_o + \sum_{n=1}^{N} \left[U_c^n \cos(nx) + U_s^n \sin(nx) \right] . \qquad (3.B:2b)$$

Note that the superscript n denotes the coefficients associated with the nth mode of the Fourier series and <u>not</u> the power n or the nth derivative. Equations (3.B:2) are substituted into

$$\psi_y \psi_{xy} - \psi_x \psi_{yy} = \frac{1}{2} (U_e^2)_x + \psi_{yyy} \qquad (3.B:3)$$

to give the following system of coupled ordinary differential

equations; a prime denotes differentiation with respect to y, and (3.B:1) has been used repeatedly. The equation for the x-independent term is

$$f_o''' = \sum_{m=1}^{N} \frac{m}{2} \left[f_c^m f_s^{m''} - f_s^m f_c^{m''} \right] ; \qquad (3.B:4a)$$

the equations for the cos(nx) coefficients for $1 \le n \le N$ are

$$f_c^{n'''} - n f_s^{n'} f_o' + n f_s^n f_o'' + \frac{1}{2} n U_s^n$$

$$= \sum_{m=1}^{n-1} \frac{m}{2} \left[f_s^{m'} f_c^{n-m'} + f_c^{m'} f_s^{n-m'} - f_c^m f_s^{n-m''} - f_s^m f_c^{n-m''} \right]$$

$$+ \sum_{m=n+1}^{N} \frac{m}{2} \left[f_s^{m'} f_c^{m-n'} - f_c^{m'} f_s^{m-n'} + f_c^m f_s^{m-n''} - f_s^m f_c^{m-n''} \right]$$

$$+ \sum_{m=1}^{N-n} \frac{m}{2} \left[f_s^{m'} f_c^{m+n'} - f_c^{m'} f_s^{m+n'} + f_c^m f_s^{m+n''} - f_s^m f_c^{m+n''} \right] ; \qquad (3.B:4b)$$

the equations for the sin(nx) coefficients for $1 \le n \le N$ are

$$f_s^{n'''} + n\, f_c^{n'}\, f_o' - n\, f_c^{n}\, f_o'' - \frac{1}{2} n\, U_c^n$$

$$= \sum_{m=1}^{n-1} \frac{m}{2} \left[- f_c^{m'}\, f_c^{n-m'} + f_s^{m'}\, f_s^{n-m'} + f_c^{m}\, f_c^{n-m''} - f_s^{m}\, f_s^{n-m''} \right]$$

$$+ \sum_{m=n+1}^{N} \frac{m}{2} \left[- f_c^{m'}\, f_c^{m-n'} - f_s^{m'}\, f_s^{m-n'} + f_c^{m}\, f_c^{m-n''} + f_s^{m}\, f_s^{m-n''} \right]$$

$$- \sum_{m=1}^{N-n} \frac{m}{2} \left[- f_c^{m'}\, f_c^{m+n'} - f_s^{m'}\, f_s^{m+n'} + f_c^{m}\, f_c^{m+n''} + f_s^{m}\, f_s^{m+n''} \right] .$$

(3.B:4c)

To solve this system of 2N+1 coupled nonlinear, third-order, ordinary differential equations, they are rewritten as (6N+3) first-order equations as explained in section 3.3 - see equation (3.3:7).

Let the solution vector $\underline{s}$ be

$$\underline{s} = (U_w,\ f_o,\ f_1^c,\ f_1^s,\ \ldots\ ,\ f_o'',\ f_1^{c''},\ f_1^{s''},\ \ldots\ ) .$$

Then the governing equations can be written as

$$\underline{s}' = \underline{H}(\underline{s})$$

where $\underline{H}$ is a nonlinear vector function. The Cash and Moore (1980) NRK code requires the Jacobian $\left[\frac{\partial H_i}{\partial s_j} \right]$. The non-zero elements of the Jacobian matrix associated with (3.3:6a,b) are straightforward, and are all unity. Those associated with the third derivatives are more complex. From equation (3.B:4a), we have, for $1 \le n \le N$,

$$\frac{\partial(f_o''')}{\partial(f_o)} = 0 , \qquad \frac{\partial(f_o''')}{\partial(f_o')} = 0 , \qquad \frac{\partial(f_o''')}{\partial(f_o'')} = 0 ,$$

$$\frac{\partial(f_o''')}{\partial(f_c^n)} = \frac{n}{2} f_s^{n''} , \qquad \frac{\partial(f_o''')}{\partial(f_c^{n'})} = 0 , \qquad \frac{\partial(f_o''')}{\partial(f_c^{n''})} = - \frac{n}{2} f_s^n ,$$

$$\frac{\partial(f_o''')}{\partial(f_s^n)} = - \frac{n}{2} f_c^{n''} , \qquad \frac{\partial(f_o''')}{\partial(f_s^{n'})} = 0 , \qquad \frac{\partial(f_o''')}{\partial(f_s^{n''})} = \frac{n}{2} f_c^n ,$$

(3.B:7)

while differentiating (3.B:4b) and (3.B:4c) with respect to the derivatives of f_o, f_o', f_o'' yields, for $1 \le n \le N$,

$$\frac{\partial(f_c^{n'''})}{\partial(f_o)} = 0 , \qquad \frac{\partial(f_c^{n'''})}{\partial(f_o')} = n f_s^{n'} , \qquad \frac{\partial(f_c^{n'''})}{\partial(f_o'')} = - n f_s^n ,$$

and

$$\frac{\partial(f_s^{n'''})}{\partial(f_o)} = 0 , \qquad \frac{\partial(f_s^{n'''})}{\partial(f_o')} = - n f_c^{n'} , \qquad \frac{\partial(f_s^{n'''})}{\partial(f_o'')} = n f_c^n .$$

(3.B:8)

The matrix elements of the general form $\frac{\partial(f_c^{n'''})}{\partial(f_c^m)}$, etc., are more complicated. They are listed in tables (3.B:1,2) below in the following manner. Column 1 shows the elements of the Jacobian, for example $\frac{\partial(f_c^{n'''})}{\partial(f_c^m)}$, for $1 \le n, m \le N$. The entries in column 2, 3 and 4 should be included in this element if the inequalities $1 \le m \le n-1$, $1 \le m \le N-n$, and $n+1 \le m \le N$ are satisfied respectively. Table (3.B:1) is calculated from equation (3.B:4b) and Table (3.B:2) from equation (3.B:4c). $\delta_{n,m}$ is the delta

function. The Jacobian entries associated with the boundary conditions are straightforward and are omitted.

Table 3.B:1

	$1 \le m \le n-1$	$1 \le m \le N-n$	$n+1 \le m \le N$
$\frac{\partial(f_c^{n'''})}{\partial(f_c^{m})}$	$-\frac{m}{2} f_s^{n-m''}$	$\frac{m}{2} f_s^{m+n''}$	$\frac{m}{2} f_s^{m-n''}$
$\frac{\partial(f_c^{n'''})}{\partial(f_s^{m})}$	$-\frac{m}{2} f_c^{n-m''}$	$-\frac{m}{2} f_c^{m+n''}$ $- n f_o^{''} \delta_{n,m}$	$-\frac{m}{2} f_c^{m-n''}$
$\frac{\partial(f_c^{n'''})}{\partial(f_c^{m'})}$	$\frac{n}{2} f_s^{n-m'}$	$\frac{n}{2} f_s^{m+n'}$	$-\frac{n}{2} f_s^{m-n'}$
$\frac{\partial(f_c^{n'''})}{\partial(f_s^{m'})}$	$\frac{n}{2} f_c^{n-m'}$	$-\frac{n}{2} f_c^{m+n'}$ $+ n f_o^{'} \delta_{n,m}$	$\frac{n}{2} f_c^{m-n'}$
$\frac{\partial(f_c^{n'''})}{\partial(f_c^{m''})}$	$-\frac{(n-m)}{2} f_s^{n-m}$	$-\frac{(m+n)}{2} f_s^{m+n}$	$-\frac{(m-n)}{2} f_s^{m-n}$
$\frac{\partial(f_c^{n'''})}{\partial(f_s^{m''})}$	$-\frac{(n-m)}{2} f_c^{n-m}$	$\frac{(m+n)}{2} f_c^{m+n}$	$\frac{(m-n)}{2} f_c^{m-n}$

Table 3.B:2

	$1 \le m \le n-1$	$1 \le m \le N-n$	$n+1 \le m \le N$
$\frac{\partial(f_s^{n'''})}{\partial(f_c^{m})}$	$\frac{m}{2} f_c^{n-m''}$	$-\frac{m}{2} f_c^{m+n''}$ $+ n f_o^{''} \delta_{n,m}$	$\frac{m}{2} f_c^{m-n''}$
$\frac{\partial(f_s^{n'''})}{\partial(f_s^{m})}$	$-\frac{m}{2} f_s^{n-m''}$	$-\frac{m}{2} f_s^{m+n''}$	$\frac{m}{2} f_s^{m-n''}$
$\frac{\partial(f_s^{n'''})}{\partial(f_c^{m'})}$	$-\frac{n}{2} f_c^{n-m'}$	$-\frac{n}{2} f_c^{m+n'}$ $- n f_o^{'} \delta_{n,m}$	$-\frac{n}{2} f_c^{m-n'}$
$\frac{\partial(f_s^{n'''})}{\partial(f_s^{m'})}$	$\frac{n}{2} f_s^{n-m'}$	$-\frac{n}{2} f_s^{m+n'}$	$-\frac{n}{2} f_s^{m-n'}$
$\frac{\partial(f_s^{n'''})}{\partial(f_c^{m''})}$	$\frac{(n-m)}{2} f_c^{n-m}$	$\frac{(m+n)}{2} f_c^{m+n}$	$-\frac{(m-n)}{2} f_c^{m-n}$
$\frac{\partial(f_s^{n'''})}{\partial(f_s^{m''})}$	$-\frac{(n-m)}{2} f_s^{n-m}$	$\frac{(m+n)}{2} f_s^{m+n}$	$-\frac{(m-n)}{2} f_s^{m-n}$

The governing equations for the VM method

The derivation of the governing equations for the VM method is similar to that for the NRK method. First, u, u^2 and U_e^2 are expressed in terms of Fourier series in x as

$$u(x, \psi) = g_o(\psi) + \sum_{n=1}^{N} \left[g_c^n(\psi) \cos(nx) + g_s^n(\psi) \sin(nx) \right] , \tag{3.B:9a}$$

$$u^2(x, \psi) = G_o(\psi) + \sum_{n=1}^{N} \left[G_c^n(\psi) \cos(nx) + G_s^n(\psi) \sin(nx) \right] , \tag{3.B:9b}$$

and

$$U_e(x)^2 = U_o + \sum_{n=1}^{N} \left[U_c^n \cos(nx) + U_s^n \sin(nx) \right] . \tag{3.B:9c}$$

From (3.B:1), G_o, G_c^n and G_s^n are related to g_o, g_c^n and g_s^n for $1 \le n \le N$ by

$$G_o = g_o g_o + \frac{1}{2} \sum_{m=1}^{N} \left[g_c^m g_c^m + g_s^n g_s^n \right] , \tag{3.B:10a}$$

$$\begin{aligned} G_c^n = 2\, g_o g_c^n &+ \frac{1}{2} \sum_{m=1}^{n-1} \left[g_c^m g_c^{n-m} - g_s^m g_s^{n-m} \right] \\ &+ \frac{1}{2} \sum_{m=n+1}^{N} \left[g_c^m g_c^{m-n} + g_s^m g_s^{m-n} \right] \\ &+ \frac{1}{2} \sum_{m=1}^{N-n} \left[g_c^m g_c^{m+n} + g_s^m g_s^{m+n} \right] , \end{aligned} \tag{3.B:10b}$$

and

$$G_s^n = 2\, g_o g_s^n + \frac{1}{2} \sum_{m=1}^{n-1} \left[\; g_c^m \, g_s^{n-m} + g_s^m \, g_c^{n-m} \; \right]$$

$$+ \frac{1}{2} \sum_{m=n+1}^{N} \left[- g_c^m \, g_s^{m-n} + g_s^m \, g_c^{m-n} \right]$$

$$- \frac{1}{2} \sum_{m=1}^{N-n} \left[- g_c^m \, g_s^{m+n} + g_s^m \, g_c^{m+n} \right] . \qquad (3.B:10c)$$

Equations (3.B:9) are substituted into

$$(u^2)_x = (U_e^{\,2})_x + u(u^2)_{\psi\psi} \qquad (3.B:11)$$

to give the following system of coupled ordinary differential equations. A prime now denotes differentiation with respect to ψ. The equation for the x-independent coefficient is

$$g_o \, G_o'' + \frac{1}{2} \sum_{m=1}^{N} \left[\; g_c^m \, G_c^{m\prime\prime} + g_s^m \, G_s^{m\prime\prime} \; \right] = 0 . \qquad (3.B:12a)$$

The equations for the cos(nx) coefficients, for $1 \le n \le N$, are

$$n \, G_s^n = g_o \, G_c^{n\prime\prime} + G_o'' \, g_c^n + n \, U_s^n$$

$$+ \frac{1}{2} \sum_{m=1}^{n-1} \left[\; g_c^m \, G_c^{n-m\prime\prime} - g_s^m \, G_s^{n-m\prime\prime} \; \right]$$

$$+ \frac{1}{2} \sum_{m=n+1}^{N} \left[\; g_c^m \, G_c^{m-n\prime\prime} + g_s^m \, G_s^{m-n\prime\prime} \; \right]$$

$$+ \frac{1}{2} \sum_{m=1}^{N-n} \left[\; g_c^m \, G_c^{m+n\prime\prime} + g_s^m \, G_s^{m+n\prime\prime} \; \right] ,$$

(3.B:12b)

and the equations for the sin(nx) coefficients, for $1 \le n \le N$, are

$$
\begin{aligned}
- n\, G_c^n = {} & g_o\, G_s^{n\prime\prime} + G_o^{\prime\prime}\, g_s^n - n\, U_c^n \\
& + \frac{1}{2} \sum_{m=1}^{n-1} \left[\; g_c^m\, G_s^{n-m\prime\prime} + g_s^m\, G_c^{n-m\prime\prime} \; \right] \\
& + \frac{1}{2} \sum_{m=n+1}^{N} \left[- g_c^m\, G_s^{m-n\prime\prime} + g_s^m\, G_c^{m-n\prime\prime} \right] \\
& - \frac{1}{2} \sum_{m=1}^{N-n} \left[- g_c^m\, G_s^{m+n\prime\prime} + g_s^m\, G_c^{m+n\prime\prime} \right] .
\end{aligned}
$$

(3.B:12c)

Newton-Raphson iteration was used to solve this system of coupled ordinary differential equations, and therefore the appropriate Jacobian was required. For a solution vector $\underline{g}$ consisting of U_w, g_o, g_c^n and g_s^n for $1 \le n \le N$, we denote the kth Newton iterate by $\underline{g}^k$,

$$\underline{g}^{k+1} = \underline{g}^k + \delta\underline{g} \; .$$

On substituting into the governing equations, and linearising with respect to $\delta\underline{g}$, we obtain (cf. (3.3:9))

$$A\, \delta\underline{g} = b.$$

The derivatives of $\delta\underline{g}$ were approximated by second-order finite-differences. To minimize the band width of A, the elements, $\delta g^c_{n,j}$, $\delta g^s_{n,j}$ $1 \le n \le N$, and $\delta g_{o,j}$ for $1 \le j \le NY$, of the vector $\delta\underline{g}$ are arranged as follows,

$$
\delta\underline{g} = \left\{ \begin{array}{ll}
\delta U_w & \\
\left.\begin{array}{l} \delta g^c_{n,1} \\ \delta g^s_{n,1} \end{array}\right\} & 1 \le n \le N \\
\delta g_{o,1} & \\
\vdots & \\
\left.\begin{array}{l} \delta g^c_{n,j} \\ \delta g^s_{n,j} \end{array}\right\} & 1 \le n \le N \\
\delta g_{o,j} & \\
\vdots & \\
\left.\begin{array}{l} \delta g^c_{n,NY} \\ \delta g^s_{n,NY} \end{array}\right\} & 1 \le n \le N \\
\delta g_{o,NY} &
\end{array} \right\} .
$$

We now proceed to describe how the matrix elements for the Jacobian matrix are stored. For convenience, we will concentrate on the governing equations in the interior of the computational domain since the lower and upper boundary conditions are relatively straightforward. For each j, $2 \le j \le NY-1$, there are 2N+1 rows in the Jacobian matrix corresponding to the 2N+1 equations (3.B:12) - the cos(nx) equations occupy the first N rows, the sin(nx) equations the next N rows and finally the cos(0x) equation the $2N+1^{th}$ row. Each group of 2N+1 rows is placed one below the other in the direction of increasing j, $1 \le j \le NY$. Therefore, the cos(nx) equation at the point j is in row (2N+1)(j-1)+n+1 (the extra 1 being the boundary condition for the constant eigenvalue U_w). The coefficients of $\delta g^c_{n,j}$, $\delta g^s_{n,j}$, $1 \le n \le N$, and $\delta g_{o,j}$ are

tabulated in a similar way to above. Each column of the matrix A is identified by the corresponding row in the vector $\delta\underline{g}$, hence the (2N+1)(j-1)+n+1 column is identified by $\delta g^{c}_{n,j}$. This arrangment is illustrated for part of the matrix A in figure 3.B:1. Therefore a typical equation involving $\delta g^{c}_{n,k}$, $\delta g^{s}_{n,k}$, $1 \leq n \leq N$, and $\delta g_{o,k}$ for $j-1 \leq k \leq j+1$ has 6N+3 non-zero elements in the associated row[1].

The entries in tables (3.B:3), (3.B:4) and (3.B:5) correspond to the contributions from the cos(0x) equation (3.B:12a), the cos(nx) equations (3.B:12b) and the sin(nx) equations (3.B:12c) respectively. In tables (3.B:4) and (3.B:5) the integer n can take any value between 1 and N thus corresponding to the different cos(nx) and sin(nx) equations. The entries in the first column of all the tables indicate the $\delta\underline{g}$ element; the remaining columns list the contributions to those elements. Note that a table entry with a superscript other than n, e.g. $\delta g^{m}_{c,j}$ or $\delta g^{k}_{c,j}$, is valid for a range of m or k which is stated at the top of the relevant table or column.

The functions A_1, A_2 and A_3 are defined as

$$A_1(g) = \frac{g}{h^2} - \frac{g'}{h},$$

$$A_2(g) = g'' - \frac{2g}{h},$$

$$A_3(g) = \frac{g}{h^2} - \frac{g'}{h},$$

---

[1] We note that the band width of A is 8N+3 because the band width is the sum of two maximum distances from the principle diagonal in the two opposite directions.

where h is the step size in ψ, and the derivatives are approximated using second- or fourth-order centred finite-differences.

Figure 3.B:1

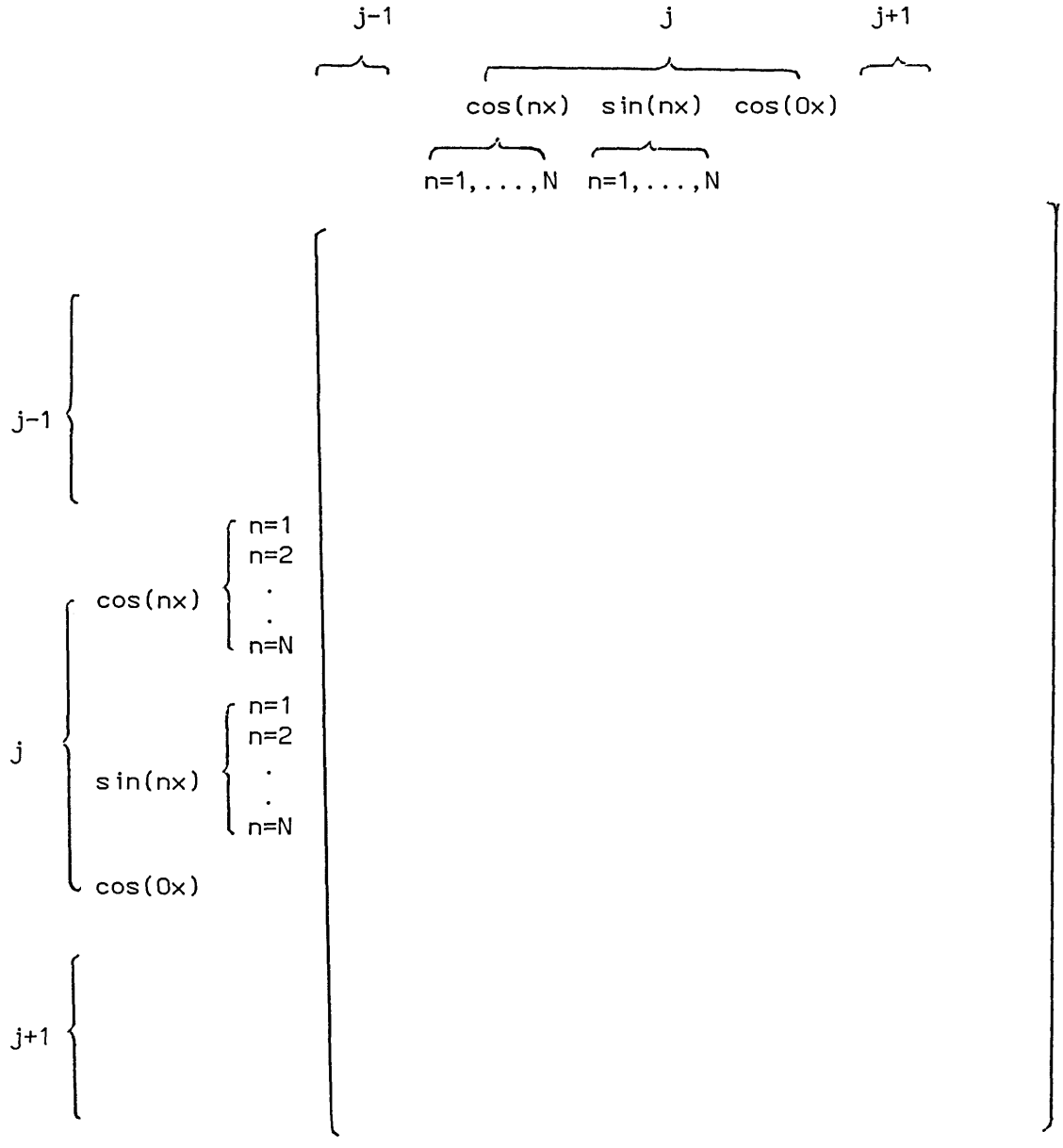


Table 3.B:3a

$\delta g_{o,j+1}$	$2g_o A_1(g_o) + \sum_{m=1}^{N} \left[g_c^m A_1(g_c^m) + g_s^m A_1(g_s^m) \right]$
$\delta g_{o,j}$	$2g_o A_2(g_o) + G_o'' + \sum_{m=1}^{N} \left[g_c^m A_2(g_c^m) + g_s^m A_2(g_s^m) \right]$
$\delta g_{o,j-1}$	$2g_o A_3(g_o) + \sum_{m=1}^{N} \left[g_c^m A_3(g_c^m) + g_s^m A_3(g_s^m) \right]$

Table 3.B:3b

$\delta g^n_{c,\,j+1}$	$g_o A_1(g^n_c) + g^n_c A_1(g_o)$
$\delta g^n_{c,\,j}$	$g_o A_2(g^n_c) + g^n_c A_2(g_o) + \frac{1}{2} G^{n''}_c$
$\delta g^n_{c,\,j-1}$	$g_o A_3(g^n_c) + g^n_c A_3(g_o)$
$\delta g^n_{s,\,j+1}$	$g_o A_1(g^n_s) + g^n_s A_1(g_o)$
$\delta g^n_{c,\,j}$	$g_o A_2(g^n_s) + g^n_s A_2(g_o) + \frac{1}{2} G^{n''}_s$
$\delta g^n_{c,\,j-1}$	$g_o A_3(g^n_s) + g^n_s A_3(g_o)$

Table 3.B:3c

	$\frac{1}{2}\sum_{m=1}^{n-1}$	$\frac{1}{2}\sum_{m=n+1}^{N}$	$\frac{1}{2}\sum_{m=1}^{N-n}$
$\delta g^m_{c,j+1}$	$g_c^n A_1 (g_c^{n-m})$	$g_c^n A_1 (g_c^{m-n})$	$g_c^n A_1 (g_c^{m+n})$
	$+ g_s^n A_1 (g_s^{n-m})$	$- g_s^n A_1 (g_s^{m-n})$	$+ g_s^n A_1 (g_s^{m+n})$
$\delta g^m_{c,j}$	$g_c^n A_2 (g_c^{n-m})$	$g_c^n A_2 (g_c^{m-n})$	$g_c^n A_2 (g_c^{m+n})$
	$+ g_s^n A_2 (g_s^{n-m})$	$- g_s^n A_2 (g_s^{m-n})$	$+ g_s^n A_2 (g_s^{m+n})$
$\delta g^m_{c,j-1}$	$g_c^n A_3 (g_c^{n-m})$	$g_c^n A_3 (g_c^{m-n})$	$g_c^n A_3 (g_c^{m+n})$
	$+ g_s^n A_3 (g_s^{n-m})$	$- g_s^n A_3 (g_s^{m-n})$	$+ g_s^n A_3 (g_s^{m+n})$
$\delta g^m_{s,j+1}$	$- g_c^n A_1 (g_s^{n-m})$	$g_c^n A_1 (g_s^{m-n})$	$g_c^n A_1 (g_s^{m+n})$
	$+ g_s^n A_1 (g_c^{n-m})$	$+ g_s^n A_1 (g_c^{m-n})$	$- g_s^n A_1 (g_c^{m+n})$
$\delta g^m_{s,j}$	$- g_c^n A_2 (g_s^{n-m})$	$g_c^n A_2 (g_s^{m-n})$	$g_c^n A_2 (g_s^{m+n})$
	$+ g_s^n A_2 (g_c^{n-m})$	$+ g_s^n A_2 (g_c^{m-n})$	$- g_s^n A_2 (g_c^{m+n})$
$\delta g^m_{s,j-1}$	$- g_c^n A_3 (g_s^{n-m})$	$g_c^n A_3 (g_s^{m-n})$	$g_c^n A_3 (g_s^{m+n})$
	$+ g_s^n A_3 (g_c^{n-m})$	$+ g_s^n A_3 (g_c^{m-n})$	$- g_s^n A_3 (g_c^{m+n})$

Table 3.B:4a

$$\delta g_{o,j+1} \qquad 2g_o A_1(g_c^n) + 2g_c^n A_1(g_o)$$

$$+ \sum_{m=1}^{n-1} \left[g_c^{n-m} A_1(g_c^m) - g_s^{n-m} A_1(g_s^m) \right]$$

$$+ \sum_{m=n+1}^{N} \left[g_c^{m-n} A_1(g_c^m) + g_s^{m-n} A_1(g_s^m) \right]$$

$$+ \sum_{m=1}^{N-n} \left[g_c^{m+n} A_1(g_c^m) + g_s^{m+n} A_1(g_s^m) \right]$$

$$\delta g_{o,j} \qquad 2g_o A_2(g_c^n) + 2g_c^n A_2(g_o) + G_c^{n''} - 2ng_s^n$$

$$+ \sum_{m=1}^{n-1} \left[g_c^{n-m} A_2(g_c^m) - g_s^{n-m} A_2(g_s^m) \right]$$

$$+ \sum_{m=n+1}^{N} \left[g_c^{m-n} A_2(g_c^m) + g_s^{m-n} A_2(g_s^m) \right]$$

$$+ \sum_{m=1}^{N-n} \left[g_c^{m+n} A_2(g_c^m) + g_s^{m+n} A_2(g_s^m) \right]$$

$$\delta g_{o,j-1} \qquad 2g_o A_3(g_c^n) + 2g_c^n A_3(g_o)$$

$$+ \sum_{m=1}^{n-1} \left[g_c^{n-m} A_3(g_c^m) - g_s^{n-m} A_3(g_s^m) \right]$$

$$+ \sum_{m=n+1}^{N} \left[g_c^{m-n} A_3(g_c^m) + g_s^{m-n} A_3(g_s^m) \right]$$

$$+ \sum_{m=1}^{N-n} \left[g_c^{m+n} A_3(g_c^m) + g_s^{m+n} A_3(g_s^m) \right]$$

Table 3.B:4b

$\delta g^n_{c,j+1}$	$2g_o A_1(g_o)$
$\delta g^n_{c,j}$	$2g_o A_2(g_o) + G''_o$
$\delta g^n_{c,j-1}$	$2g_o A_3(g_o)$
$\delta g^n_{s,j}$	$- 2ng_o$

Table 3.B:4c for $\underline{1 \leq m \leq N}$

$\delta g^m_{c,j+1}$	$g^n_c A_1(g^m_c)$
$\delta g^m_{c,j}$	$g^n_c A_2(g^m_c)$
$\delta g^m_{c,j-1}$	$g^n_c A_3(g^m_c)$
$\delta g^m_{s,j+1}$	$g^n_c A_1(g^m_s)$
$\delta g^m_{s,j}$	$g^n_c A_2(g^m_s)$
$\delta g^m_{s,j-1}$	$g^n_c A_3(g^m_s)$

Table 3.B:4d

	$1 \le m \le n-1$	$n+1 \le m \le N$	$1 \le m \le N-n$
$\delta g^m_{c,j+1}$	$g_o A_1(g_c^{n-m})$	$g_o A_1(g_c^{m-n})$	$g_o A_1(g_c^{m+n})$
	$+ g_c^{n-m} A_1(g_o)$	$+ g_c^{m-n} A_1(g_o)$	$+ g_c^{m+n} A_1(g_o)$
$\delta g^m_{c,j}$	$g_o A_2(g_c^{n-m})$	$g_o A_2(g_c^{m-n})$	$g_o A_2(g_c^{m+n})$
	$+ g_c^{n-m} A_2(g_o)$	$+ g_c^{m-n} A_2(g_o)$	$+ g_c^{m+n} A_2(g_o)$
	$- n g_s^{n-m}$	$+ n g_s^{m-n}$	$- n g_s^{m+n}$
	$+ \frac{1}{2} G_c^{n-m''}$	$+ \frac{1}{2} G_c^{m-n''}$	$+ \frac{1}{2} G_c^{m+n''}$
$\delta g^m_{c,j-1}$	$g_o A_3(g_c^{n-m})$	$g_o A_3(g_c^{m-n})$	$g_o A_3(g_c^{m+n})$
	$+ g_c^{n-m} A_3(g_o)$	$+ g_c^{m-n} A_3(g_o)$	$+ g_c^{m+n} A_3(g_o)$
$\delta g^m_{s,j+1}$	$- g_o A_1(g_s^{n-m})$	$g_o A_1(g_s^{m-n})$	$g_o A_1(g_s^{m+n})$
	$- g_s^{n-m} A_1(g_o)$	$+ g_s^{m-n} A_1(g_o)$	$+ g_s^{m+n} A_1(g_o)$
$\delta g^m_{s,j}$	$- g_o A_2(g_s^{n-m})$	$g_o A_2(g_s^{m-n})$	$g_o A_2(g_s^{m+n})$
	$- g_s^{n-m} A_2(g_o)$	$+ g_s^{m-n} A_2(g_o)$	$+ g_s^{m+n} A_2(g_o)$
	$- n g_c^{n-m}$	$- n g_c^{m-n}$	$+ n g_c^{m+n}$
	$- \frac{1}{2} G_s^{n-m''}$	$+ \frac{1}{2} G_s^{m-n''}$	$+ \frac{1}{2} G_s^{m+n''}$
$\delta g^m_{s,j-1}$	$- g_o A_3(g_s^{n-m})$	$g_o A_3(g_s^{m-n})$	$g_o A_3(g_s^{m+n})$
	$- g_s^{n-m} A_3(g_o)$	$+ g_s^{m-n} A_3(g_o)$	$+ g_s^{m+n} A_3(g_o)$

Table 3.B:4e for $1 \le k \le m-1$

	$\frac{1}{2}\sum_{m=1}^{n-1}$	$\frac{1}{2}\sum_{m=n+1}^{N}$	$\frac{1}{2}\sum_{m=1}^{N-n}$
$\delta g^{k}_{c,j+1}$	$g_c^{n-m}A_1(g_c^{m-k})$	$g_c^{m-n}A_1(g_c^{m-k})$	$g_c^{m+n}A_1(g_c^{m-k})$
	$- g_s^{n-m}A_1(g_s^{m-k})$	$+ g_s^{m-n}A_1(g_s^{m-k})$	$+ g_s^{m+n}A_1(g_s^{m-k})$
$\delta g^{k}_{c,j}$	$g_c^{n-m}A_2(g_c^{m-k})$	$g_c^{m-n}A_2(g_c^{m-k})$	$g_c^{m+n}A_2(g_c^{m-k})$
	$- g_s^{n-m}A_2(g_s^{m-k})$	$+ g_s^{m-n}A_2(g_s^{m-k})$	$+ g_s^{m+n}A_2(g_s^{m-k})$
$\delta g^{k}_{c,j-1}$	$g_c^{n-m}A_3(g_c^{m-k})$	$g_c^{m-n}A_3(g_c^{m-k})$	$g_c^{m+n}A_3(g_c^{m-k})$
	$- g_s^{n-m}A_3(g_s^{m-k})$	$+ g_s^{m-n}A_3(g_s^{m-k})$	$+ g_s^{m+n}A_3(g_s^{m-k})$
$\delta g^{k}_{s,j+1}$	$- g_c^{n-m}A_1(g_s^{m-k})$	$- g_c^{m-n}A_1(g_s^{m-k})$	$- g_c^{m+n}A_1(g_s^{m-k})$
	$- g_s^{n-m}A_1(g_c^{m-k})$	$+ g_s^{m-n}A_1(g_c^{m-k})$	$+ g_s^{m+n}A_1(g_c^{m-k})$
$\delta g^{k}_{s,j}$	$- g_c^{n-m}A_2(g_s^{m-k})$	$- g_c^{m-n}A_2(g_s^{m-k})$	$- g_c^{m+n}A_2(g_s^{m-k})$
	$- g_s^{n-m}A_2(g_c^{m-k})$	$+ g_s^{m-n}A_2(g_c^{m-k})$	$+ g_s^{m+n}A_2(g_c^{m-k})$
$\delta g^{k}_{s,j-1}$	$- g_c^{n-m}A_3(g_s^{m-k})$	$- g_c^{m-n}A_3(g_s^{m-k})$	$- g_c^{m+n}A_3(g_s^{m-k})$
	$- g_s^{n-m}A_3(g_c^{m-k})$	$+ g_s^{m-n}A_3(g_c^{m-k})$	$+ g_s^{m+n}A_3(g_c^{m-k})$

Table 3.B:4f for $m+1 \le k \le N$

	$\frac{1}{2}\sum_{m=1}^{n-1}$	$\frac{1}{2}\sum_{m=n+1}^{N}$	$\frac{1}{2}\sum_{m=1}^{N-n}$
$\delta g^k_{c,j+1}$	$g_c^{n-m}A_1(g_c^{k-m})$	$g_c^{m-n}A_1(g_c^{k-m})$	$g_c^{m+n}A_1(g_c^{k-m})$
	$+ g_s^{n-m}A_1(g_s^{k-m})$	$- g_s^{m-n}A_1(g_s^{k-m})$	$- g_s^{m+n}A_1(g_s^{k-m})$
$\delta g^k_{c,j}$	$g_c^{n-m}A_2(g_c^{k-m})$	$g_c^{m-n}A_2(g_c^{k-m})$	$g_c^{m+n}A_2(g_c^{k-m})$
	$+ g_s^{n-m}A_2(g_s^{k-m})$	$- g_s^{m-n}A_2(g_s^{k-m})$	$- g_s^{m+n}A_2(g_s^{k-m})$
$\delta g^k_{c,j-1}$	$g_c^{n-m}A_3(g_c^{k-m})$	$g_c^{m-n}A_3(g_c^{k-m})$	$g_c^{m+n}A_3(g_c^{k-m})$
	$+ g_s^{n-m}A_3(g_s^{k-m})$	$- g_s^{m-n}A_3(g_s^{k-m})$	$- g_s^{m+n}A_3(g_s^{k-m})$
$\delta g^k_{s,j+1}$	$g_c^{n-m}A_1(g_s^{k-m})$	$g_c^{m-n}A_1(g_s^{k-m})$	$g_c^{m+n}A_1(g_s^{k-m})$
	$- g_s^{n-m}A_1(g_c^{k-m})$	$+ g_s^{m-n}A_1(g_c^{k-m})$	$+ g_s^{m+n}A_1(g_c^{k-m})$
$\delta g^k_{s,j}$	$g_c^{n-m}A_2(g_s^{k-m})$	$g_c^{m-n}A_2(g_s^{k-m})$	$g_c^{m+n}A_2(g_s^{k-m})$
	$- g_s^{n-m}A_2(g_c^{k-m})$	$+ g_s^{m-n}A_2(g_c^{k-m})$	$+ g_s^{m+n}A_2(g_c^{k-m})$
$\delta g^k_{s,j-1}$	$g_c^{n-m}A_3(g_s^{k-m})$	$g_c^{m-n}A_3(g_s^{k-m})$	$g_c^{m+n}A_3(g_s^{k-m})$
	$- g_s^{n-m}A_3(g_c^{k-m})$	$+ g_s^{m-n}A_3(g_c^{k-m})$	$+ g_s^{m+n}A_3(g_c^{k-m})$

Table 3.B:4h for $1 \le k \le N-m$

	$\frac{1}{2}\sum_{m=1}^{n-1}$	$\frac{1}{2}\sum_{m=n+1}^{N}$	$\frac{1}{2}\sum_{m=1}^{N-n}$
$\delta g^{k}_{c,\,j+1}$	$g_c^{n-m}A_1(g_c^{k+m})$	$g_c^{m-n}A_1(g_c^{k+m})$	$g_c^{m+n}A_1(g_c^{k+m})$
	$- g_s^{n-m}A_1(g_s^{k+m})$	$+ g_s^{m-n}A_1(g_s^{k+m})$	$+ g_s^{m+n}A_1(g_s^{k+m})$
$\delta g^{k}_{c,\,j}$	$g_c^{n-m}A_2(g_c^{k+m})$	$g_c^{m-n}A_2(g_c^{k+m})$	$g_c^{m+n}A_2(g_c^{k+m})$
	$- g_s^{n-m}A_2(g_s^{k+m})$	$+ g_s^{m-n}A_2(g_s^{k+m})$	$+ g_s^{m+n}A_2(g_s^{k+m})$
$\delta g^{k}_{c,\,j-1}$	$g_c^{n-m}A_3(g_c^{k+m})$	$g_c^{m-n}A_3(g_c^{k+m})$	$g_c^{m+n}A_3(g_c^{k+m})$
	$- g_s^{n-m}A_3(g_s^{k+m})$	$+ g_s^{m-n}A_3(g_s^{k+m})$	$+ g_s^{m+n}A_3(g_s^{k+m})$
$\delta g^{k}_{s,\,j+1}$	$g_c^{n-m}A_1(g_s^{k+m})$	$g_c^{m-n}A_1(g_s^{k+m})$	$g_c^{m+n}A_1(g_s^{k+m})$
	$+ g_s^{n-m}A_1(g_c^{k+m})$	$- g_s^{m-n}A_1(g_c^{k+m})$	$- g_s^{m+n}A_1(g_c^{k+m})$
$\delta g^{k}_{s,\,j}$	$g_c^{n-m}A_2(g_s^{k+m})$	$g_c^{m-n}A_2(g_s^{k+m})$	$g_c^{m+n}A_2(g_s^{k+m})$
	$+ g_s^{n-m}A_2(g_c^{k+m})$	$- g_s^{m-n}A_2(g_c^{k+m})$	$- g_s^{m+n}A_2(g_c^{k+m})$
$\delta g^{k}_{s,\,j-1}$	$g_c^{n-m}A_3(g_s^{k+m})$	$g_c^{m-n}A_3(g_s^{k+m})$	$g_c^{m+n}A_3(g_s^{k+m})$
	$+ g_s^{n-m}A_3(g_c^{k+m})$	$- g_s^{m-n}A_3(g_c^{k+m})$	$- g_s^{m+n}A_3(g_c^{k+m})$

Table 3.B:5a

$$\delta g_{o,j+1} \qquad 2g_o A_1(g_s^n) + 2g_s^n A_1(g_o)$$

$$+ \sum_{m=1}^{n-1} \left[g_c^{n-m} A_1(g_s^m) + g_s^{n-m} A_1(g_c^m) \right]$$

$$+ \sum_{m=n+1}^{N} \left[g_c^{m-n} A_1(g_s^m) - g_s^{m-n} A_1(g_c^m) \right]$$

$$+ \sum_{m=1}^{N-n} \left[-g_c^{m+n} A_1(g_s^m) + g_s^{m+n} A_1(g_c^m) \right]$$

$$\delta g_{o,j} \qquad 2g_o A_2(g_s^n) + 2g_s^n A_2(g_o) + G_s^{n''} + 2ng_c^n$$

$$+ \sum_{m=1}^{n-1} \left[g_c^{n-m} A_2(g_s^m) + g_s^{n-m} A_2(g_c^m) \right]$$

$$+ \sum_{m=n+1}^{N} \left[g_c^{m-n} A_2(g_s^m) - g_s^{m-n} A_2(g_c^m) \right]$$

$$+ \sum_{m=1}^{N-n} \left[-g_c^{m+n} A_2(g_s^m) + g_s^{m+n} A_2(g_c^m) \right]$$

$$\delta g_{o,j-1} \qquad 2g_o A_3(g_s^n) + 2g_s^n A_3(g_o)$$

$$+ \sum_{m=1}^{n-1} \left[g_c^{n-m} A_3(g_s^m) + g_s^{n-m} A_3(g_c^m) \right]$$

$$+ \sum_{m=n+1}^{N} \left[g_c^{m-n} A_3(g_s^m) - g_s^{m-n} A_3(g_c^m) \right]$$

$$+ \sum_{m=1}^{N-n} \left[-g_c^{m+n} A_3(g_s^m) + g_s^{m+n} A_3(g_c^m) \right]$$

Table 3.B:5b

$\delta g^{n}_{c,j}$	$2ng_o$
$\delta g^{n}_{s,j+1}$	$2g_o A_1(g_o)$
$\delta g^{n}_{s,j}$	$2g_o A_2(g_o) + G_o''$
$\delta g^{n}_{s,j-1}$	$2g_o A_3(g_o)$

Table 3.B:5c for $\underline{1 \leq m \leq N}$

$\delta g^{m}_{c,j+1}$	$g^{n}_{s} A_1(g^{m}_{c})$
$\delta g^{m}_{c,j}$	$g^{n}_{s} A_2(g^{m}_{c})$
$\delta g^{m}_{c,j-1}$	$g^{n}_{s} A_3(g^{m}_{c})$
$\delta g^{m}_{s,j+1}$	$g^{n}_{s} A_1(g^{m}_{s})$
$\delta g^{m}_{s,j}$	$g^{n}_{s} A_2(g^{m}_{s})$
$\delta g^{m}_{s,j-1}$	$g^{n}_{s} A_3(g^{m}_{s})$

Table 3.B:5d

	$1 \le m \le n-1$	$n+1 \le m \le N$	$1 \le m \le N-n$
$\delta g^m_{c,j+1}$	$g_o A_1(g_s^{n-m})$	$-\, g_o A_1(g_s^{m-n})$	$g_o A_1(g_s^{m+n})$
	$+\, g_s^{n-m} A_1(g_o)$	$-\, g_s^{m-n} A_1(g_o)$	$g_s^{m+n} A_1(g_o)$
$\delta g^m_{c,j}$	$g_o A_2(g_s^{n-m})$	$-\, g_o A_2(g_s^{m-n})$	$g_o A_2(g_s^{m+n})$
	$+\, g_s^{n-m} A_2(g_o)$	$-\, g_s^{m-n} A_2(g_o)$	$+\, g_s^{m+n} A_2(g_o)$
	$+\, n g_c^{n-m}$	$+\, n g_c^{m-n}$	$+\, n g_c^{m+n}$
	$+\, \frac{1}{2} G_s^{n-m''}$	$-\, \frac{1}{2} G_s^{m-n''}$	$+\, \frac{1}{2} G_s^{m+n''}$
$\delta g^m_{c,j-1}$	$g_o A_3(g_s^{n-m})$	$-\, g_o A_3(g_s^{m-n})$	$g_o A_3(g_s^{m+n})$
	$g_s^{n-m} A_3(g_o)$	$-\, g_s^{m-n} A_3(g_o)$	$g_s^{m+n} A_3(g_o)$
$\delta g^m_{s,j+1}$	$g_o A_1(g_c^{n-m})$	$g_o A_1(g_c^{m-n})$	$-\, g_o A_1(g_c^{m+n})$
	$+\, g_c^{n-m} A_1(g_o)$	$+\, g_c^{m-n} A_1(g_o)$	$-\, g_c^{m+n} A_1(g_o)$
$\delta g^m_{s,j}$	$g_o A_2(g_c^{n-m})$	$g_o A_2(g_c^{m-n})$	$-\, g_o A_2(g_c^{m+n})$
	$+\, g_c^{n-m} A_2(g_o)$	$+\, g_c^{m-n} A_2(g_o)$	$-\, g_c^{m+n} A_2(g_o)$
	$-\, n g_s^{n-m}$	$+\, n g_s^{m-n}$	$+\, n g_s^{m+n}$
	$+\, \frac{1}{2} G_c^{n-m''}$	$+\, \frac{1}{2} G_c^{m-n''}$	$-\, \frac{1}{2} G_c^{m+n''}$
$\delta g^m_{s,j-1}$	$g_o A_3(g_c^{n-m})$	$g_o A_3(g_c^{m-n})$	$-\, g_o A_3(g_c^{m+n})$
	$+\, g_c^{n-m} A_3(g_o)$	$+\, g_c^{m-n} A_3(g_o)$	$-\, g_c^{m+n} A_3(g_o)$

Table 3.B:5e for $1 \le k \le m-1$

	$\frac{1}{2}\sum_{m=1}^{n-1}$	$\frac{1}{2}\sum_{m=n+1}^{N}$	$\frac{1}{2}\sum_{m=1}^{N-n}$
$\delta g^{k}_{c,\,j+1}$	$g_c^{n-m}A_1(g_s^{m-k})$	$g_c^{m-n}A_1(g_s^{m-k})$	$-\,g_c^{m+n}A_1(g_s^{m-k})$
	$+\,g_s^{n-m}A_1(g_c^{m-k})$	$-\,g_s^{m-n}A_1(g_c^{m-k})$	$+\,g_s^{m+n}A_1(g_c^{m-k})$
$\delta g^{k}_{c,\,j}$	$g_c^{n-m}A_2(g_s^{m-k})$	$g_c^{m-n}A_2(g_s^{m-k})$	$-\,g_c^{m+n}A_2(g_s^{m-k})$
	$+\,g_s^{n-m}A_2(g_c^{m-k})$	$-\,g_s^{m-n}A_2(g_c^{m-k})$	$+\,g_s^{m+n}A_2(g_c^{m-k})$
$\delta g^{k}_{c,\,j-1}$	$g_c^{n-m}A_3(g_s^{m-k})$	$g_c^{m-n}A_3(g_s^{m-k})$	$-\,g_c^{m+n}A_3(g_s^{m-k})$
	$+\,g_s^{n-m}A_3(g_c^{m-k})$	$-\,g_s^{m-n}A_3(g_c^{m-k})$	$+\,g_s^{m+n}A_3(g_c^{m-k})$
$\delta g^{k}_{s,\,j+1}$	$g_c^{n-m}A_1(g_c^{m-k})$	$g_c^{m-n}A_1(g_c^{m-k})$	$-\,g_c^{m+n}A_1(g_c^{m-k})$
	$-\,g_s^{n-m}A_1(g_s^{m-k})$	$+\,g_s^{m-n}A_1(g_s^{m-k})$	$-\,g_s^{m+n}A_1(g_s^{m-k})$
$\delta g^{k}_{s,\,j}$	$g_c^{n-m}A_2(g_c^{m-k})$	$g_c^{m-n}A_2(g_c^{m-k})$	$-\,g_c^{m+n}A_2(g_c^{m-k})$
	$-\,g_s^{n-m}A_2(g_s^{m-k})$	$+\,g_s^{m-n}A_2(g_s^{m-k})$	$-\,g_s^{m+n}A_2(g_s^{m-k})$
$\delta g^{k}_{s,\,j-1}$	$g_c^{n-m}A_3(g_c^{m-k})$	$g_c^{m-n}A_3(g_c^{m-k})$	$-\,g_c^{m+n}A_3(g_c^{m-k})$
	$-\,g_s^{n-m}A_3(g_s^{m-k})$	$+\,g_s^{m-n}A_3(g_s^{m-k})$	$-\,g_s^{m+n}A_3(g_s^{m-k})$

Table 3.B:5f for $m+1 \le k \le N$

	$\frac{1}{2}\sum_{m=1}^{n-1}$	$\frac{1}{2}\sum_{m=n+1}^{N}$	$\frac{1}{2}\sum_{m=1}^{N-n}$
$\delta g^k_{c,j+1}$	$- g_c^{n-m} A_1(g_s^{k-m})$	$- g_c^{m-n} A_1(g_s^{k-m})$	$g_c^{m+n} A_1(g_s^{k-m})$
	$+ g_s^{n-m} A_1(g_c^{k-m})$	$- g_s^{m-n} A_1(g_c^{k-m})$	$+ g_s^{m+n} A_1(g_c^{k-m})$
$\delta g^k_{c,j}$	$- g_c^{n-m} A_2(g_s^{k-m})$	$- g_c^{m-n} A_2(g_s^{k-m})$	$g_c^{m+n} A_2(g_s^{k-m})$
	$+ g_s^{n-m} A_2(g_c^{k-m})$	$- g_s^{m-n} A_2(g_c^{k-m})$	$+ g_s^{m+n} A_2(g_c^{k-m})$
$\delta g^k_{c,j-1}$	$- g_c^{n-m} A_3(g_s^{k-m})$	$- g_c^{m-n} A_3(g_s^{k-m})$	$g_c^{m+n} A_3(g_s^{k-m})$
	$+ g_s^{n-m} A_3(g_c^{k-m})$	$- g_s^{m-n} A_3(g_c^{k-m})$	$+ g_s^{m+n} A_3(g_c^{k-m})$
$\delta g^k_{s,j+1}$	$g_c^{n-m} A_1(g_c^{k-m})$	$g_c^{m-n} A_1(g_c^{k-m})$	$- g_c^{m+n} A_1(g_c^{k-m})$
	$+ g_s^{n-m} A_1(g_s^{k-m})$	$- g_s^{m-n} A_1(g_s^{k-m})$	$+ g_s^{m+n} A_1(g_s^{k-m})$
$\delta g^k_{s,j}$	$g_c^{n-m} A_2(g_c^{k-m})$	$g_c^{m-n} A_2(g_c^{k-m})$	$- g_c^{m+n} A_2(g_c^{k-m})$
	$+ g_s^{n-m} A_2(g_s^{k-m})$	$- g_s^{m-n} A_2(g_s^{k-m})$	$+ g_s^{m+n} A_2(g_s^{k-m})$
$\delta g^k_{s,j-1}$	$g_c^{n-m} A_3(g_c^{k-m})$	$g_c^{m-n} A_3(g_c^{k-m})$	$- g_c^{m+n} A_3(g_c^{k-m})$
	$+ g_s^{n-m} A_3(g_s^{k-m})$	$- g_s^{m-n} A_3(g_s^{k-m})$	$+ g_s^{m+n} A_3(g_s^{k-m})$

Table 3.B:5h for $1 \le k \le N-m$

	$\frac{1}{2}\sum_{m=1}^{n-1}\sum_{k=1}^{N-m}$	$\frac{1}{2}\sum_{m=n+1}^{N}\sum_{k=1}^{N-m}$	$\frac{1}{2}\sum_{m=1}^{N-n}\sum_{k=1}^{N-m}$
$\delta g^{k}_{c,j+1}$	$g_c^{n-m}A_1(g_s^{k+m})$	$g_c^{m-n}A_1(g_s^{k+m})$	$-\,g_c^{m+n}A_1(g_s^{k+m})$
	$+\,g_s^{n-m}A_1(g_c^{k+m})$	$-\,g_s^{m-n}A_1(g_c^{k+m})$	$+\,g_s^{m+n}A_1(g_c^{k+m})$
$\delta g^{k}_{c,j}$	$g_c^{n-m}A_2(g_s^{k+m})$	$g_c^{m-n}A_2(g_s^{k+m})$	$-\,g_c^{m+n}A_2(g_s^{k+m})$
	$+\,g_s^{n-m}A_2(g_c^{k+m})$	$-\,g_s^{m-n}A_2(g_c^{k+m})$	$+\,g_s^{m+n}A_2(g_c^{k+m})$
$\delta g^{k}_{c,j-1}$	$g_c^{n-m}A_3(g_s^{k+m})$	$g_c^{m-n}A_3(g_s^{k+m})$	$-\,g_c^{m+n}A_3(g_s^{k+m})$
	$+\,g_s^{n-m}A_3(g_c^{k+m})$	$-\,g_s^{m-n}A_3(g_c^{k+m})$	$+\,g_s^{m+n}A_3(g_c^{k+m})$
$\delta g^{k}_{s,j+1}$	$-\,g_c^{n-m}A_1(g_c^{k+m})$	$-\,g_c^{m-n}A_1(g_c^{k+m})$	$g_c^{m+n}A_1(g_c^{k+m})$
	$+\,g_s^{n-m}A_1(g_s^{k+m})$	$-\,g_s^{m-n}A_1(g_s^{k+m})$	$+\,g_s^{m+n}A_1(g_s^{k+m})$
$\delta g^{k}_{s,j}$	$-\,g_c^{n-m}A_2(g_c^{k+m})$	$-\,g_c^{m-n}A_2(g_c^{k+m})$	$g_c^{m+n}A_2(g_c^{k+m})$
	$+\,g_s^{n-m}A_2(g_s^{k+m})$	$-\,g_s^{m-n}A_2(g_s^{k+m})$	$+\,g_s^{m+n}A_2(g_s^{k+m})$
$\delta g^{k}_{s,j-1}$	$-\,g_c^{n-m}A_3(g_c^{k+m})$	$-\,g_c^{m-n}A_3(g_c^{k+m})$	$g_c^{m+n}A_3(g_c^{k+m})$
	$+\,g_s^{n-m}A_3(g_s^{k+m})$	$-\,g_s^{m-n}A_3(g_s^{k+m})$	$+\,g_s^{m+n}A_3(g_s^{k+m})$

Appendix 3.C Fourth-order Defect Correction

In this appendix we will outline how defect correction was implemented to increase the accuracy of our solutions from second order to fourth order.

We suppose that the nonlinear differential equations of interest can be discretised by a second-order-accurate finite-difference scheme to obtain a vector of nonlinear algebraic equations

$$\underline{b}_2(\underline{x}) = 0 \ , \tag{3.C:1}$$

where the subscript 2 indicates a second-order-accurate approximation. We suppose that the solution, $\underline{x}$, to this system of equations can be obtained by Newton-Raphson iteration. Specifically we write, (cf (3.3:9))

$$\underline{x}^{k+1} = \underline{x}^{k} + \delta\underline{x} \ , \tag{3.C:2}$$

substitute $\underline{x}^{k}$ into the discretised equaitons, and linearise with respect to $\delta\underline{x}$ to obtain,

$$A\ (\underline{x}^{k})\delta\underline{x} = \underline{b}_2(\underline{x}^{k}) \tag{3.C:3}$$

where A is a Jacobian matrix. By repeated iteration, the second-order-accurate solution $\underline{x}_2$ can be obtained within a given error.

To obtain a fourth-order-accurate solution, a fourth-order discretisation could be employed, and the resulting equation

$$\underline{b}_4(\underline{x}) = 0 \tag{3.C:4}$$

could be solved directly. However this method has the disadvantage that the Jacobian matrix will in genreal involve more non-zero

elements, and the inversion of the Jacobian matrix is the most time-consuming part of the solution process.

As an alternative we write the fourth-order-accurate discretisations in the form

$$\underline{b}_2(\underline{x}) + h^2\underline{d}_4(\underline{x}) = 0 \ . \qquad (3.C:5)$$

Once a second-order-accurate solution, $\underline{x}_2$, has been found, a consistent fourth-order-accurate solution can be obtained by solving

$$\underline{b}_2(\underline{x}) + h^2\underline{d}_4(\underline{x}_2) = 0 \ . \qquad (3.C:6)$$

The advantage of this two stage process is that a Newton-Raphson iteration to solve (3.C:6), i.e.

$$A\ (\underline{x}^k)\delta\underline{x} = \underline{b}_2(\underline{x}^k) + h^2\underline{d}_4(\underline{x}_2) \ , \qquad (3.C:7)$$

uses the same Jacobian matrix A, and hence the Newton-Raphson scheme needs only to be programmed once. Once the fourth-order-accurate solution $\underline{x}_4$ is obtained, a slight improvement in accuracy was achieved by solving

$$\underline{b}_2(\underline{x}) + h^2\underline{d}_4(\underline{x}_4) = 0 \ . \qquad (3.C:8)$$

Appentix 3.D The (X, ψ) coordinate Method

In a further attempt to reduce the value of ψ_∞, at which the correct exponential decaying behaviour can be maintained, we tried a new coordinate system. An inspection of equation (3.2:3) suggested X as an independent variable,

$$X = \int_0^x \frac{U_e(x)}{\bar{U}_e}\, dx \ ,$$

where $\bar{U}_e$ is the mean of $U_e(x)$, and $\bar{u}$ as the dependent variable, where

$$\bar{u} = uU_e - U_e^2 \ .$$

Transforming (x, ψ) to (X, ψ), the governing equations (3.2:2) become,

$$\begin{aligned} &U_e^2(\bar{u}^2)_X + 2U_e^4\bar{u}_X - (U_e^4)\bar{u}^2 \\ &= 2U_e^4\bar{u}_{\psi\psi} + 2U_e^2(\bar{u})_{\psi\psi} - 2U_e^2(u\bar{}_\psi) + {}^2u(\bar{u})^2_{\psi\psi} \end{aligned} \qquad (3.D:1a)$$

with boundary conditions

$$\bar{u} = U_w U_e - U_e^2 \qquad \text{on } \psi = 0, \qquad (3.D:1b)$$

$$\bar{u} \to \tilde{u}U_e(x) \qquad \text{as } \psi \to \infty, \qquad (3.D:1c)$$

with $\tilde{u}$ as defined in (3.3:1). A spectral method was adopted by writing

$$\bar{u} = h_o(\psi) + \sum_{n=0}^{\infty} h_c^n(\psi)\cos(nX) + h_s^n(\psi)\sin(nX) \ . \qquad (3.D:2)$$

The series (3.D:2) was substituted into (3.D:1), the quadratic terms reordered and the series truncated to N terms. The resulting coupled differential equations were solved by the VM method

described in section 3.3.

The governing equations were more complicated than before but the simplicity of application of the upper boundary conditions introducing the proper exponential decaying behaviour made the approach appear attractive. Using equations (3.D:2), (3.D:1c) and (3.3:1b), we obtain

$$h_o(\psi) = A_o + B\psi \ , \qquad (3.D:3a)$$

$$h_c^m(\psi) = \left[a_n \cos\sqrt{\frac{n}{2}}\psi + b_n \sin\sqrt{\frac{n}{2}}\psi \right] \exp\left[-\sqrt{\frac{n}{2}}\psi \right] \ , \qquad (3.D:3b)$$

$$h_s^m(\psi) = \left[a_n \cos\sqrt{\frac{n}{2}}\psi - b_n \sin\sqrt{\frac{n}{2}}\psi \right] \exp\left[-\sqrt{\frac{n}{2}}\psi \right] \ , \qquad (3.D:3c)$$

for $1 \le n \le N$. The constants A_o and B were forced to zero by using the conditions

$$h_o(\psi) = h_o'(\psi) = 0, \qquad (3.D:4a)$$

and the a_n, b_n were eliminated by differentiating (3.D:3b,c) and then substituting back, so to obtain the 2N boundary conditions:

$$h_c^{n\prime} = \sqrt{\frac{n}{2}}\,(-h_n^c - h_n^s), \text{ and } \qquad h_s^{n\prime} = \sqrt{\frac{n}{2}}\,(h_n^c - h_n^s), \qquad (3.D:4b,c)$$

for $1 \le n \le N$. These boundary conditions were applied at $\psi_{NY-\frac{1}{2}}$.

Again, defect correction was applied to the second-order-accurate solutions to yield a fourth-order-accuate results. The same stretch (3.3:2b) was employed in ψ with $\lambda = 0.25$, $\delta^* = 0.05$ as before. With NY = 91 and HY = 0.2, ψ_∞ was reduced to 10.7 - this gave consistent results for $\varepsilon \le 0.6$. However, for $\varepsilon \ge 0.6$, the

forcing term U_e could not be accurately resolved in the X coordinate system with the limited number of Fourier modes, e.g. N = 18, which were available to us before computer memory requirements became a critical factor. With the boundary condition inadequately modeled, there was no point in finding solutions for $\varepsilon \geq 0.6$.

Appendix 3.E Attempts to find the Separation Singularity Structure

This appendix describes a number of unsuccessful attempts to find an asymptotic description for the separation singularity that our numerical results suggest develops at $\varepsilon = \varepsilon_s$. An analytic singularity structure for the classical boundary-layer equations is a necessary preliminary to developing an interactive theory for the marginally separated flow which is likely to exist for $0 < \varepsilon - \varepsilon_s \ll 1$.

Attempted Inviscid Structure with $u \sim X \sim \Psi$

The numerical results of section 3.4 suggest that as $\varepsilon \to \varepsilon_s$ a stagnation point develops away from the wall, close to the location where the pressure gradient is zero, i.e. where $(U_e^2)_x \sim 0$. Other types of separation singularities that develop away from the wall are known to be inviscid. For example, the MRS singularity caused by a stagnation point above a downstream moving wall at a point with a *non-zero* pressure gradient has been shown to be an inviscid singularity (Sychev (1980), Elliott, Cowley and Smith (1983), van Dommelen and Shen (1983), Williams and Stewartson (1983)).

The singularity of section 3.4 does not appear to be a standard MRS singularity because the numerical results suggest that it develops at a point where the pressure gradient is zero. Further, when the minimum velocity is small but positive, i.e. when $0 < \varepsilon_s - \varepsilon \ll 1$, it should be possible to derive an asymptotic solution which describes the flow in the region where the velocity

is small, i.e. where $|x-x_s| \ll 1$. Attempts to derive such a description based on the MRS singularity structure at a point of non-zero pressure gradient were even less successful than the following conjectures.

As a first attempt, we therefore seek an inviscid singularity structure close to a point of zero pressure gradient. For convenience, we denote the stagnation point by the subscript s, and write

$$X = x - x_s, \qquad \Psi = \psi - \psi_s, \qquad Y = y - y_s, \tag{3.E:1a}$$

and for $X \ll 1$, we write the pressure gradient as

$$\frac{1}{2}\left(U_e^{\,2} \right)_x = \mu_1 + \mu_2 X + \frac{1}{2}\mu_3 X^2 + \ldots . \tag{3.E:1b}$$

In Von Mises coordinates, the *inviscid* boundary-layer equation is

$$(u^2)_x = (U_e^{\,2})_x , \tag{3.E:2}$$

which has a solution

$$u = \left[U_e^{\,2}(x) + g(\psi) \right]^{1/2} , \tag{3.E:3}$$

where g is an undetermined function of ψ. At the stagnation point, u must have a minimum in ψ; hence $g'(\psi_s) = 0$, $g''(\psi_s) > 0$, and we are assuming that the pressure gradient is zero there, i.e. $\mu_1 = 0$. Hence a Taylor expansion of (3.E:3) about the stagnation point yields

$$u = \left[\gamma_1 + \mu_2 X^2 + g''(\psi_s)\, \frac{\Psi^2}{2!} + \ldots . \right]^{1/2} , \tag{3.E:4}$$

where $\gamma_1 = U_e^{\,2}(x_s) + g(\psi_s)$. When $\varepsilon = \varepsilon_s$ a singularity structure of this form would have $\gamma_1 = 0$, while for $0 < \varepsilon_s - \varepsilon \ll 1$, γ_1 should be small, positive and some function of $\varepsilon - \varepsilon_s$.

Solution (3.E:4) suggests that in the neighbourhood of the stagnation point, the appropriate asymptotic scaling is

$$u \sim X \sim \Psi \ . \qquad (3.E:5)$$

However the viscous term, $u(uu_{\psi})_{\psi} \sim X$, is then found to be of the same order of magnitude as the inertia terms, $uu_x \sim X$. Hence the proposed inviscid singularity structure is incorrect, and for the scaling (3.E:5) viscous terms must be retained.

We note at this point that, rather than working in Von Mises coordinates (x,ψ), we could have used the primitive variables (x,y) and come to the same conclusion. Specifically, for $|X| \ll 1$, the leading-order, inviscid, boundary-layer equation in primitive variables is

$$uu_X + Vu_Y = X \ , \quad u_X + V_Y = 0 \qquad (3.E:6a)$$

where, $y = g(X) + Y$, $v = ug_X + V$, $g(X)$ is any function of X, and for simplicity we have assumed $\mu_2 = 1$. The solution is

$$u = \sqrt{\frac{X^2}{2} + \gamma_2}\ \cosh(\beta Y) \ , \qquad (3.E:6b)$$

where β and γ_2 are undetermined constants, and $\gamma_2 \to 0$ as $\varepsilon \to \varepsilon_s$. This solution suggests that in the vicinity of the stagnation point $u \sim X$, $Y \sim 1$ and $y \sim -\log(X)/\beta$, which agrees with (3.E:5).

Model problem of a moving wall

Before proceeding to describe other candidates for the singularity structure, we describe first a model problem which has the same singularity, but for which more accurate numerical results

can be obtained. The chosen problem consists of flow over a semi-infinite flat plate (leading edge at x=0), with both the inviscid slip velocity and the wall velocity being non-zero. This flow is not periodic, and no eigenvalue needs to be found.

As before the boundary-layer flow is described by the steady boundary-layer equations in Von Mises coordinates,

$$uu_x = U_e(U_e)_x + u(uu_\psi)_\psi \ , \qquad (3.E:7a)$$

and we choose as boundary conditions,

$$u = U_w > 0 \qquad \text{on } \psi = 0, \qquad (3.E:7b)$$

$$u \to U_e(x) = 1 - x + \lambda x^2 \qquad \text{as } \psi \to \infty, \qquad (3.E:7c)$$

i.e. a constant positive wall velocity, and an external velocity which decelerates at the start of the plate, but then accelerates further downstream ($\lambda > 0$). This model problem is similar to one considered by Elliott, Cowley and Smith (1983) when they were studying the MRS singularity over a downstream-moving wall. Indeed, if λ is zero or sufficiently small (and $U_w < 1$) then an MRS singularity develops at the finite location downstream where a stagnation point develops within the boundary layer. However, if λ is sufficiently large, there is only a small region of adverse pressure gradient, $0 \le x \le x_d(\lambda) = \frac{1}{2\lambda}$, and a solution can be found for all x. Hence there is an intermediate value of λ, say λ_s, above which no singularity forms, but beneath which one does. We are interested in the structure of the singularity (assuming that there is one) for $\lambda = \lambda_s$.

The problem specified by (3.E:7) was solved for various values of λ, using a numerical scheme which was based on the FD method

discussed in section 3.3 (the various modifications included different stretching functions). The numerical results showed that for large λ the velocity u was positive for all x. However, as λ was decreased towards the critical value $\lambda_s \simeq 0.4259$, a stagnation point began to develop away from the wall at a finite distance downstream, $x = x_s$. It was confirmed that solutions obtained for $\lambda < \lambda_s$ developed into inviscid MRS singularities at points of *non-zero* pressure gradient (Elliott *et. al.* 1983, Williams *et al.* 1983).

Figures 3.E:1-3 display, at discrete points of x and for various values of λ close to but greater than λ_s, the velocity u verses both the streamfunction ψ and the local boundary-layer normal y. The lines with decreasing minima in u represent increasing values of x. Figure 3.E:4 displays the minimum velocity u over ψ, i.e. $\min_{\psi}(u)$, against x for $\lambda = 0.4259$ and $\lambda = 0.42595$ (represented by the solid line and the dotted line respectively). This graph indicates that at $\lambda = 0.4259$, $\min_{\psi} u$ is linear in x except when u gets very small, where the accuracy of the calculations is in some doubt. If we denote the position of $u_{min} = \min_{x,\psi}(u)$ by (x_o, ψ_o), this suggests that for $0 < \lambda - \lambda_s \ll 1$ and $u_{min} \ll |x - x_o| \ll 1$,

$$\min_{\psi}(u) \propto (x_o - x) , \qquad (3.E:8)$$

although there may of course be logarithms, etc. in this relationship. Figure 3.E:5a displays u_{min} against λ, from which we conclude that $u_{min} = 0$ at a finite value of λ_s. Further, as $\lambda \to \lambda_s$, the numerical results also tentatively suggest that the stagnation

point develops at the point of zero pressure gradient, i.e. that $x_o \to x_d$ (see figure 3.E:5b). However the results (obtained with the finest grid of 9601x4801 points) given in table 3.E:1 are not conclusive.

Table 3.E:1

λ	u_{min}	x_o	x_d
0.6	0.349533	0.661799	0.833333
0.5	0.269337	0.838702	1.000000
0.45	0.180545	0.969653	1.111111
0.43	0.095157	1.058913	1.162791
0.427	0.061591	1.090158	1.170960
0.4265	0.049041	1.100089	1.172333
0.426	0.027655	1.120239	1.173709
0.42595	0.022452	1.125586	1.173847

In an attempt to obtain the asymptotic behaviour of $u_{min}(\lambda)$ as $\lambda \to \lambda_s$, we tried fitting the numerical results to

$$u_{min}(\lambda) = k_1(\lambda_s - \lambda)^{n_1}, \qquad (3.E:9a)$$

and

$$u_{min}(\lambda) = k_2(\lambda_s - \lambda)^{n_2}\left[\log(\lambda_s - \lambda)\right]^m, \qquad (3.E:9b)$$

where λ_s, k_1, k_2, n_1, n_2 and m are empirical constants. The solutions for λ_s from both fits agreed well, giving $\lambda_s \simeq 0.4259$. However the other constants did not converge to consistent values as λ decreased towards λ_s (e.g. n_1 decreased from 0.4 to 0.26, and n_2 from 0.4 to 0.28 respectively with λ in the range of 0.45 to 0.42595).

In an attempt to understand the numerical results for

$0 < \lambda_s - \lambda \ll 1$, we have also examined the form of the MRS singularity structure in the limit of the pressure gradient at the stagnation point becoming small.

As Sychev (1980), Elliott, Cowley and Smith (1983) and Williams and Stewartson (1983) have shown, the MRS singularity has the scaling

$$\Psi \sim X^{1/2}, \qquad u \sim X^{1/2} \sim \Psi ,$$

and a *non-zero* pressure gradient in the vicinity of the stagnation point. This singularity consists of three asymptotic regions: (i) a region where $y = O(1)$ at the wall, (ii) a region $O(\log(-X))$ away from the wall, where the velocity is small, and (iii) a region $O(2\log(-X))$ away from the boundary where the velocity is $O(1)$ again.

For convenience we briefly outline the asymptotic structure of this singularity. First, we examine the middle layer where

$$y = g(X) + Y . \qquad (3.E:10)$$

Substituting

$$\Psi(Y) = B_0 + |X|^{1/2} f_0 + |X| f_1 + ... \qquad (3.E:11a)$$

where B_0 is a constant, into the steady boundary-layer equations, and equating coefficients of powers of X, etc. we obtain

$$f_0 = \frac{(-2\mu_1)^{1/2}}{\beta} \sinh z , \qquad (3.E:11b)$$

$$f_1 = 2\sigma_1 (1 + \cosh^2 z) + \sigma_2 \cosh z - \frac{1}{3}\beta \sinh 2z , \qquad (3.E:11c)$$

where $z = \beta(Y - Y_0)$, and β, Y_0, σ_1 and σ_2 are constants. If f_1 is to match with the $y = O(1)$ wall layer, etc., then it turns out that $\sigma_2 = 0$, and because of the transformation (3.E:10) we can take $Y_0 = 0$

without loss of generality.

In the lower layer where $y = O(1)$

$$\Psi(y) = \Psi_0(y) + |X|\Psi_1(y) + \ldots , \qquad (3.E:12a)$$

where $\Psi_0(y)$ is a function determined by the upstream solution ($\Psi_0(0)=0$, $\Psi_{0y}(0)=U_w$ to satisfy the wall boundary conditions), and

$$\Psi_1 = \Psi_0' \int_0^y \left[\frac{-\mu_1 - \Psi_0'''}{\Psi_0'^2} \right] dy . \qquad (3.E:12b)$$

We suppose that

$$\Psi_0 \sim B_0 - c_0 e^{-\beta y} - c_1 e^{-\beta 2y} - \ldots \text{ as } y \to \infty, \qquad (3.E:12c)$$

and then,

$$\Psi_1 \sim \frac{-\mu_1}{\beta^2 c_0} \left[\frac{1}{2} e^{\beta y} - \left[\frac{3c_1}{c_0} + \frac{\beta^2 c_0}{\mu_1} \right] + \ldots \right] \quad \text{as } y \to \infty. \qquad (3.7:12d)$$

Before a match between the two layers can be made, $g(x)$ needs to be specified. The appropriate expansion is

$$g(x) = -\bar{g}_o \log|X| + g_o + \ldots . \qquad (3.E:13a)$$

Matching between the two layers shows that

$$\bar{g}_0 = \frac{1}{2\beta} , \qquad g_o = -\frac{1}{\beta} \log \left[\frac{(-2\mu_1)^{1/2}}{2\beta c_0} \right] , \qquad (3.E:13b,c)$$

$$\sigma_1 = - \left[\frac{-c_1 \mu_1}{\beta^2 c_0^{\,2}} + \frac{\beta}{3} \right] . \qquad (3.E:13d)$$

There is another layer like the wall layer with the scaling $y = 2G(X) + \bar{y}$. Details of this layer are omitted for brevity, although we note that $G \sim g$ to leading order.

In our attempt to understand the marginal MRS singularity, we are interested in the behaviour of the constants β, c_0, c_1, etc. as

$\mu_1 \to 0$. Here β and c_0 were estimated from the numerical results using the fact that for small X,

$$\beta \sim \frac{-U_e(0)}{v_\infty X} \qquad \text{and} \qquad c_0^2 \sim \frac{\mu_1 X \exp(2\beta y_{min})}{2\beta^2} ,$$

where v_∞ is the blowing velocity and y_{min} is the position where u_{min} occurs. The calculations suggest that both β and c_0 increase as $\lambda \to \lambda_s$, but sufficient accuracy could not be obtained to demonstrate a definitive parametric dependence on $\lambda - \lambda_s$. A comparison of the inertia and viscous terms showed that they are of the same order of magnitude near $\psi = \psi_o$ as $x \to x_o$ for $\lambda - \lambda_s \ll 1$.

We have also considered a number of other solution methods in order to obtain improved numerical results. For instance, previous authors have had success in identifying singularities using series extension techniques (e.g. Van Dyke 1984).

As a first attempt we assumed that

$$U_e = \sum_{n=1}^{\infty} U_n(y)\, x^n , \quad U_w = \sum_{n=1}^{\infty} W_n(y)\, x^n , \quad U_1 = W_1 = 1 , \qquad (3.E:14a)$$

and sought a solution of the form

$$\psi = \sum_{n=1}^{\infty} \phi_n(y)\, x^n \qquad \text{where} \qquad \phi_1 = y . \qquad (3.E:14b)$$

The coefficients U_n, W_n were chosen so that the pressure gradient was favourable for small x (to accelerate the flow), adverse for larger x (to decelerate the flow towards a stagnation point), and then favourable again (so that a stagnation point would only just form). On substituing into the boundary-layer equations, and equating powers of x, we obtain for $n \geq 2$,

$$\phi_n''' + y\,\phi_n'' - (n+1)\,\phi_n' = -p_n + \sum_{m=2}^{n-1} m\left[\phi_m'\,\phi_{n+1-m}' - \phi_m\,\phi_{n+1-m}''\right] , \qquad (3.E:15a)$$

where

$$U_e\Big[\,U_e\,\Big]_x = x + \sum_{n=2}^{\infty} p_n\,x^n . \qquad (3.E:15b)$$

A disadvantage of this formulation if fast, highly accurate, numerical solutions to the ordinary differential equations are to be obtained, is the presence of the $y\,\phi_n''$ term in (3.E:15a).

In order to eliminate this or similar terms, we considered a model problem where flow originates from $x = -\infty$, and, for example,

$$U_e = 1 - \exp(x) + \lambda\exp(2x), \qquad U_w = \exp(\,-2\exp(x)\,) + \lambda\exp(2x) .$$

To simplify the series expansions a new coordinate $\xi = e^x$ was introduced. Solutions were then sought of the form

$$\psi = \sum_{n=0}^{\infty} \phi_n(y)\;\xi^n , \qquad U_e = \sum_{n=0}^{\infty} U_n\,\xi^n , \qquad U_w = \sum_{n=0}^{\infty} W_n\,\xi^n , \qquad (3.E:16)$$

where $\phi_0 = y$ and $U_0 = W_0 = 1$. On substituting into the boundary-layer equations we obtain for $n \geq 1$

$$\phi_n''' - n\phi_n' = -nU_n + \sum_{m=1}^{n-1} m\left[\phi_m'\,\phi_{n-m}' - \phi_m\,\phi_{n-m}'' - U_m\,U_{n-m}\right] \equiv R_n , \qquad (3.E:17a)$$

$$\phi_n(0) = 0, \qquad \phi_n'(0) = W_n, \qquad \phi_n'(\infty) = U_n . \qquad (3.E:17b)$$

Note that the operator on the left-hand side of (3.E:17a) is just the harmonic operator, which made it simple to use a fourth-order, finite-difference discretisation (sixth-order accuracy was obtained by Richardson extrapolation).

The solution procedure was to first obtain ϕ_n' and ϕ_n''' by solution of

$$(\phi_n')'' - n\phi_n' = R_n \ , \quad \phi_n'(0) = W_n, \quad \phi_n'(y_\infty) = U_n \ , \qquad (3.E:18a)$$

and then ϕ_n'' and ϕ_n from

$$(\phi_n'')'' - n\phi_n'' = R_n' \ , \quad \phi_n''(0) = -\int_0^{y_\infty} \phi_n''' dy, \quad \phi_n''(y_\infty) = 0 \ , \qquad (3.E:18b)$$

$$(\phi_n)'' = \phi_n'' \ , \quad \phi_n(0) = 0, \quad \phi_n(y_\infty) = \int_0^{y_\infty} \phi_n' dy \ , \qquad (3.E:18c)$$

respectively. Note that a bad choice of boundary conditions at y_∞ (the approximation to infinity) can significantly affect the accuracy of the solutions at large n. The above specification was found to be optimal.

To check the accuracy of our results y_∞ was varied over 45, 60, 120 and 180, and uniform grid-sizes of $H = \frac{15}{256}$, $\frac{15}{512}$ and $\frac{15}{1024}$ were used. For $\lambda = 0.5$, it was adequate to use $y_\infty = 45$ and $H = \frac{15}{512}$ to obtain a solution up to 300 modes. As a check on the accuracy of our solution we monitored $| \phi_n^{iv}(y_\infty) |$, which, from above, should be zero. Only modes for which this was less than, say, 10^{-5} were assumed to be reliable.

In order to examine the singularity structure we constructed the series for v_∞, i.e.

$$v_\infty = \sum_{n=1}^{\infty} n \, (U_n y - \phi_n) \, \xi^n \ , \qquad (3.E:19)$$

and then using Padé approximants tried to identify the position of the singularities in the ξ plane for different choices of λ. When a strong MRS singularity formed, the position of the singularity on the real, positive ξ axis could be identified from the poles of the

denominator of the Padé approximant. However, when the MRS singularity was marginal the position of the poles could not be reliably identified. Thus an attempt to find the dependence of the poles on $\lambda - \lambda_s$ was not successful (indeed it was hard to identify λ_s by this method). Further, for a given value of λ, we attempted to calculate $\max_{\xi}(v_\infty)$, in order to identify its dependence on $\lambda - \lambda_s$. However, the results were again not reliable enough to be of use in our quest for the singularity structure. In particular, it was difficult to recognise the x position where $\max_{\xi}(v_\infty)$ occurred.

Attempted Viscous Structure with $u \sim X \sim \Psi$

The numerical results of the previous sub-section for λ close to λ_s, suggest that in the vicinity of the stagnation point, $u \sim \Psi \sim X$ (i.e. scaling (3.E:5)), and that the stagnation point develops at/near the point of zero pressure gradient. In an attempt to find a singularity structure we therefore assume $\mu_1 = 0$, substitute

$$u = Xw, \qquad \Psi = X\zeta \qquad (3.E:20a,b)$$

into the viscous boundary-layer equation, expand in powers of X, and obtain at leading order in X

$$w(w - \zeta w_\zeta) = \mu_2 + w(ww_\zeta)_\zeta . \qquad (3.E:21a)$$

By rescaling we can take $\mu_2 = 1$ without loss of generality ($\mu_2 > 0$), and the appropriate boundary conditions for matching with $\Psi = O(1)$ are

$$w \to \pm B_{\pm}\zeta \text{ as } \zeta \to \pm\infty, \qquad (3.E:21b)$$

where $B_{\pm}$ are positive or negative constants depending on whether X is greater or less than zero (see (3.E:20) and recall that u must be positive).

In order to check whether boundary conditions (3.E:21b) can be satisfied, one possibility would be to use a numerical 'shooting' technique starting from $\zeta=+\infty$ with a given value of B_+. For positive B_+ (i.e. $X > 0$), it is also necessary to specify the magnitude of an exponentially small term present as $\zeta \to \infty$. Alternatively for $B_+ > 0$, a shooting technique can be used where $w(0)$ and $w_\zeta(0)$ are varied until the asymptotic conditions (3.E:21b) are satisfied. For example, by use of the latter technique symmetric solutions were found for a range of values of $w(0) > 1$, each with a corresponding $B_+ = B_-$; the relationship between the two is illustrated in figure 3.E:6a. This indicates that for $X > 0$, a symmetric solution can be found for all $w(0) > 1$, which yields a unique $B_{\pm}$ satisfying (3.E:21b).

For negative $B_{\pm}$, one of the boundary conditions (3.E:21b), say the one as $\zeta \to +\infty$, completely specifies the solution because there are no exponentially small terms present as $|\zeta| \to \infty$. We therefore denote the solution by $w(\zeta;B_+)$. Note also, that since (3.E:21a) is symmetric in ζ, then if a solution, w, with boundary conditions (3.E:21b) exists then so does one, $\omega(\zeta) = w(-\zeta)$, with boundary conditions

$$\omega \to \pm B_{\mp}\zeta \text{ as } \zeta \to \pm\infty \text{ ;} \qquad (3.E:22a)$$

hence $\omega(\zeta)=w(\zeta;B_-)$. If a solution to (3.E:21) is to be found for $X < 0$, it follows that

$$w(0;B_+)=w(0)=w(0;B_-) \quad \text{and} \quad w_\zeta(0;B_+)=-w_\zeta(0)=-w_\zeta(0;B_-). \quad (3.E:22b)$$

Using a numerical shooting method starting from $\zeta = \zeta_\infty$, we calculated $w(0;B)$ and $w_\zeta(0;B)$; figure 3.E:6b displays $w(0)$ against B and figure 3.E:6c $w_\zeta(0)$ against B. No two values of B_+, B_- could be found satisfying (3.E:22b) - note that asymptotic analysis shows that $w \to -1$, $w_\zeta \to 0$ both as $B \to 0-$ and as $B \to -\infty$ (see below). Hence we conclude that the proposed asymptotic structure based on (3.E:20) does not exist, despite the fact the numerical results of section 3.4 and the previous subsection appear to be consistent with this scaling.

In order to confirm this conclusion, we have also examined the singularity structure in primitive variables. Specifically, on substituting

$$y = g(X) + Y, \quad \Psi \sim Xf(Y) , \quad (3.E:23)$$

where $g(X)$ is any function of X, into the boundary-layer equation, and expanding in powers of X, we obtain at leading order in $|X|$,

$$f'^2 - ff'' = 1 + f''' . \quad (3.E:24a)$$

A prime denotes differentiation with respect to Y, $\mu_2 = 1$ has again been assumed, and the appropriate boundary conditions (deduced either from the inviscid solution or from (3.E:21b)) are [1]

---

[1] Note that $\beta_+=B_+$, $\beta_-=B_-$ if $X > 0$, and $\beta_+=-B_-$, $\beta_-=-B_+$ if $X < 0$.

$$f \sim \frac{1}{2}\alpha_+ \exp(\beta_+ Y) \qquad \text{as } Y \to +\infty , \qquad (3.E:24b)$$

$$f \sim -\frac{1}{2}\alpha_- \exp(-\beta_- Y) \qquad \text{as } Y \to -\infty , \qquad (3.E:24c)$$

where $\alpha_\pm$, $\beta_\pm$ are constants ($\alpha_\pm$, $\beta_\pm > 0$ for $X > 0$; $\alpha_\pm < 0$, $\beta_\pm > 0$ for $X < 0$). The transformation $Y \to Y - \log(|\alpha_+|)/\beta_+$, allows us to take, without loss of generality, $\alpha_+ = \sigma$, where $\sigma = 1$ if $X > 0$ and $\sigma = -1$ if $X < 0$.

Numerical solutions of (3.E:24) confirmed that for $X > 0$ (3.E:24b,c) could be satisfied for any β_+, but that for $X < 0$ no regular solution for any β_+ could be found which had the required exponential growth both as $Y \to +\infty$ and as $Y \to -\infty$.

It might be argued that accurate numerical results are hard to obtain at very small or very large values of β_+, and that at one of these extremes a solution for $X < 0$ might exist. However, as the following analysis indicates, this is not the case.

First, we consider the case of *small* β and write

$$z = \beta Y, \qquad f(Y) = \frac{1}{\beta} F(z) \; ; \qquad (3.E:25a)$$

then equation (3.E:24a) becomes

$$F'^2 - FF'' = 1 + \beta^2 F'''' . \qquad (3.E:25b)$$

At leading order in β the equation is inviscid with solution

$$F \sim \frac{\sigma}{b} \sinh bz , \qquad (3.E:26a)$$

where, σ is a constant, and by slightly modifying (3.E:25a), we can take $b = 1$ without loss of generality. Higher-order corrections can be obtained by performing an expansion in powers of β:

$$F = \sigma \sinh(z) + \beta^2 F_1 + \ldots . \qquad (3.E:26b)$$

Substitution into equation (3.E:25b) yields

$$2\cosh(z)\, F_1' - \sinh(z)(F_1 + F_1'') = \cosh z, \qquad (3.E:27a)$$

a solution of which is

$$F_1 = c_2 \cosh z + c_1 \cosh z \int_0^z \tanh^2 z\, dz$$

$$+ \frac{1}{2} \cosh z \int_0^z \frac{1}{\cosh z}\, dz \qquad (3.E:27b)$$

$$- \frac{1}{2} \cosh z \int_0^z \tanh^2 z \log\left[\tanh \frac{1}{2} z \right] dz \, .$$

For the solution to have the correct asymtpotic behaviour as $|z| \to \infty$, it follows that $c_1 = 0$. Then as $z \to 0$,

$$F_1 \sim c_2 \left[1 + \frac{1}{2} z^2 + \ldots \right] + \frac{z}{2} + \frac{1}{6} z^3 + \ldots$$

$$- \frac{1}{2} \left[\frac{1}{3} z^3 \ln \left(\frac{1}{2} z \right) - \frac{1}{9} z^3 + \ldots \right] . \qquad (3.E:28)$$

The logarithmic term suggests the existence of a 'critical layer' near $z = 0$, where viscous forces cannot be neglected. The distinguished scaling for the critical layer is $Y \sim 1$, and matching with (3.E:28) suggests the expansion

$$f = \sigma Y + \beta c_2 + \beta^2 f_2 + \beta^3 f_3 + \beta^4 \ln(\beta) \bar{f}_4 + \beta^4 f_4 + \ldots \, . \qquad (3.E:29)$$

Substitution of (3.E:29) into (3.E:24a), yields after a little manipulation,

$$f_2 = \frac{1}{2} Y + \frac{1}{6} \sigma Y^3 \, , \quad f_3 = \frac{1}{2} c_2 Y^2 \, , \quad \bar{f}_4 = -\frac{1}{6} Y^3 - \frac{1}{2\sigma} Y \, , \qquad (3.E:30a)$$

$$f_4' = \frac{1}{24} Y^4 + \frac{1}{2\sigma} \left(c_2^2 - \frac{1}{4} \right) + g_4 \qquad (3.E:30b)$$

where

$$g_4'' + \sigma Y g_4' - 2\sigma g_4 = -\frac{1}{2}\sigma Y^2 , \qquad (3.E:31a)$$

and $$g_4 \to -\frac{1}{2}Y^2 \log(|Y|) \quad \text{as} \quad |Y| \to \infty . \qquad (3.E:31b)$$

For a successful match to be made with $z = 0-$ and $z = 0+$, $g_4(Y)$ must be a symmetric function of Y. For $\sigma = 1$, the symmetric particular solution to (3.E:31a) will satisfy (3.E:31b) because the complementary functions (i.e. Y^2 and an antisymmetric one which behaves like $\exp(-\sigma Y^2/2)$ as $|Y| \to \infty$), grow less fast as $|Y| \to \infty$ than the particular solution. However, for $\sigma = -1$, a solution to (3.E:31a) does not exist which satisfies (3.E:31b) both as $Y \to +\infty$ and as $Y \to -\infty$.

Asymptotic solutions for *large* β have also been sought. The most obvious scaling in this case is

$$Y = \frac{z}{\beta} , \qquad f(Y) \sim \beta \tilde{f}(z) , \qquad (3.E:32a,b)$$

which yields on substitution into (3.E:24a)

$$\tilde{f}'^2 - \tilde{f}\tilde{f}''' = \tilde{f}''' . \qquad (3.E:32c)$$

This equation has solutions

$$\tilde{f} = c \exp(bz) - b , \qquad (3.E:32d)$$

where b and c are constants. However, for no choice of b or c do these satisfy the boundary conditions (3.E:24b,c) both as $z \to \infty$ and as $z \to -\infty$.

Other candidates for the singularity structure

The above arguments seem to rule out a singularity structure based on the scaling $u \sim \Psi \sim X$, $Y \sim 1$. Next we concentrate on $X < 0$,

and try a more general scaling

$$\eta = \mu(X)Y \ , \qquad \Psi = - \frac{X}{\mu} f(\eta, X) \ . \tag{3.E:33a,b}$$

The boundary-layer equation then becomes

$$f_\eta^{\,2} - f f_{\eta\eta} - X(f_{\eta\eta} f_X - f_\eta f_{\eta X}) + \frac{\mu_X X}{\mu} f f_{\eta\eta} = 1 - \mu^2 f_{\eta\eta\eta} \ . \tag{3.E:33c}$$

We will make the hypothesis that to leading order the singularity is inviscid (this seems to be suggested by some 'continuation' model problems - see below), which imples that $\mu \ll 1$. For maximum interaction at the correction term, we will also assume that

$$\frac{\mu_X X}{\mu} \sim \mu^2, \qquad \text{i.e. that} \qquad \mu = [-\log(-X)]^{-1/2} \ . \tag{3.E:34}$$

Substitution of

$$f = f_0(\eta) + \mu f_1(\eta) + \mu^2 f_2(\eta) + \ldots \tag{3.E:35}$$

into equation (3.E:33c) yields after some algebra (recall $X < 0$ and $u > 0$)

$$f_0 = \frac{1}{\beta} \sinh \beta\eta \ , \tag{3.E:36a}$$

$$f_1 = a_1 \cosh \beta\eta + a_2 \cosh \beta\eta \int_0^\eta \tanh^2 \beta\eta \, d\eta \ . \tag{3.E:36b}$$

In order that f_0 and f_1 maintain their asymptotic ordering as $\eta \to \infty$, we require $a_2 = 0$. The solution for f_2 is then given by

$$\left[\frac{f_2}{\cosh \beta\eta}\right]' = \beta \tanh^2 \beta\eta \int \frac{\cosh \beta\eta}{\sinh^3 \beta\eta} \left[a_1^2 \beta^2 - \beta^2 \cosh \beta\eta - \sinh^2 \beta\eta\right] d\eta \ . \tag{3.E:36c}$$

For all $\beta > 0$, this solution leads to logarithmic terms as $\eta \to 0$ whatever the choice of a_1 (the $O(\mu)$ term was included in (3.E:35) in the hope that a_1 could be chosen to remove the logarithm). For

the same reasons as for $u \sim \Psi \sim X$, $\beta \ll 1$, these logarithmic terms cannot be smoothed out by a critical layer, and hence the above asymptotic structure is incorrect. Further, it does not appear to be possible to add other terms into (3.E:35) to rectify the problem. Obviously the same conclusions can be reached using Von Mises coordinates rather than primitive variables.

A slight variation on the above is to allow the $-X\mu_X/\mu$ term in (3.E:33c) to occur at leading order by choosing $\mu = (-X)^n$ for $n > 0$. In Von Mises coordinates this corresponds to a scaling

$$u = (-X)v(X, \zeta) , \quad \Psi = (-X)^{1-n}\zeta . \qquad (3.E:37a,b)$$

Substitution of a perturbation expansion,

$$v = v_0(\zeta) + (-X)v_1(\zeta) + \ldots + (-X)^{2n}v_v(\zeta) + \ldots \qquad (3.E:37c)$$

into the boundary-layer equation demonstrates that at leading order

$$v_0 = (\mu_2 + c\,\zeta^{2/(1-n)})^{1/2} , \qquad (3.E:38a)$$

where μ_2 is as defined beneath (3.E:1b), and c is a constant. Hence, the leading-order solution is regular only for certain values of n, e.g. $n = 1/2$.

For illustration, the calculation for $n = 1/2$ has been taken to next order. The governing equation for v_1 is (note that for $n = 1/2$ we can take $v_v = 0$)

$$v_0\left[\, 2v_1 - \frac{\zeta}{2}v_{1\zeta} \,\right] + v_1\left(v_0 - \frac{\zeta}{2}v_{0\zeta}\right) = v_0\left(v_0 v_{0\zeta}\right)_\zeta - \frac{\mu_3}{2} . \qquad (3.B:38b)$$

A series solution about $\zeta = 0$ demonstrates that again logarithmic terms are present as $\zeta \to 0$ (these are a consequence of the viscous forcing in the above equation). Therefore a critical layer must be present, and it turns out to be essentially the same as that

considered earlier. Because this critical layer cannot successfully match to logarithmic terms in both $\zeta > 0$ and $\zeta < 0$, we are forced to conclude that this singularity structure is ruled out.

A singularity structure has also been sought with (cf. (3.E:33a,b))

$$\eta = \mu(X)Y \ , \qquad \Psi = -X\ \mu\ \tilde{f}(\eta,\ X) \ , \qquad \text{(3.E:39a,b)}$$

$\mu \gg 1$, and $|X\mu_X/\mu| \ll 1$. The leading order equation of an expansion in powers of μ^{-1} is essentially (3.E:32c), which consists of a balance between inviscid and inertia terms (no pressure gradient term is present). However, solutions to this equation which satisfy the appropriate boundary condition as $Y \to \infty$ [$Y \to -\infty$], cannot be matched onto a suitable flow for $Y \to -\infty$ [$Y \to \infty$] either directly *or* by an intermediate region where the pressure gradient is significant (the different asymptotic behaviours of (3.E:32d) at ∞ and $-\infty$ suggest the presence of an intermediate layer in one direction).

We have also considered scalings where $\mu = (-X)^{-n}$, i.e.

$$\eta = (-X)^{-n}Y \ , \qquad \Psi = (-X)^{1-n}\tilde{f}(\eta) \ . \qquad \text{(3.E:40a,b)}$$

These scalings have $|X\mu_X/\mu| = O(1)$, and for $n > 0$ lead to a modified form of (3.E:32c), viz.

$$\tilde{f}''' - (1-n)\ \tilde{f}\tilde{f}'' + (1-2n)\tilde{f}'^2 = 0 \ , \qquad \text{(3.E:40c)}$$

where $n < 1/2$ is assumed so that a stagnation point develops in u. However, suitable solutions which match as η becomes large (i.e. $f \to \beta\eta^{(1-n)/n}$), and for which u is everywhere positive, do not exist, thus ruling this singularity structure out as well. An important case is $n = 1/4$. This corresponds to a velocity profile

that is regular in the neighbourhood of the stagnation point, i.e. $u \sim \Lambda(y-y_s)^2$ for $|y-y_s| \ll 1$ and $|X| \ll 1$, where Λ is an order one constant.

A related possibilty is that u is regular to leading order at the stagnation point, but that the pressure gradient is non-zero (although this assumption appears to be inconsistent with the numerical results). The scaling $\eta = (-X)^{-1/4}y$, then leads at leading order to (3.E:40c) modified by the addition of a constant on the right-hand side (the constant can be normalised to 1 without loss of generality). The solution to this eqation is just $\tilde{f} = \eta^3/6$. Given this leading order solution, higher order corrections in powers of $(-X)^{1/4}$ can be calculated. They suggest that the displacement thickness and the blowing velocity remain finite for $|X| \ll 1$. This is in disagreement with the numerical results, as is the fact that this singularity structure predicts that $\min_y u \propto (-X)^{1/2}$ for $0 < -X \ll 1$. Further, it is not clear how such a singularity structure is continued into $X > 0$, a consideration which is necessary for $\lambda - \lambda_s$ small but positive. Our conclusion is that this is not the correct singularity structure.

We have also considered a number of other more 'exotic' singularity structures; for example one was based on a behaviour $u \sim [-\log(-\Psi)]$ for u close to u_{min} (although this type of behaviour is of course in disagreement with our numerical results). Unfortunately, none of them has been followed to a successful conclusion.

A continuation approach

Finally, we attempt to obtain some insight into the singularity structure by introducing a new parameter into the problem, say n, and then letting n tend to a value, here n = 1, at which point the original problem is recovered. Specifically, we consider the boundary-layer problem where the pressure gradient is given by $(-X)^n$, and the singularity is assumed to develop at X = 0 (by suitable choice of initial conditions, etc.).

The governing boundary-layer equations are then, for X < 0,

$$\begin{aligned} u_x + v_y &= 0 \ , \\ uu_X + vu_Y &= -(-X)^n + u_{YY} \ . \end{aligned} \qquad (3.E:41)$$

When n = 0 we might expect a standard MRS singularity to occur at X = 0, (or possibly a Goldstein singularity if the stagnation point develops 'at the wall'), and when n = 1 a marginal MRS singularity of the type of present interest should develop.

First, we sought a singularity structure to (3.E:39) which was based on the MRS singularity. On substitution of

$$\begin{aligned} \Psi &= (-X)^{(n+1)/2}\,\zeta \\ u &= (-X)^{(n+1)/2}(w_0(\zeta) + (-X)^{(1-n)/2}w_1(\zeta) + \ldots) \ , \end{aligned} \qquad (3.E:42a)$$

into the Von Mises boundary-layer equations, regular solutions for w_0 and w_1 could be found for $0 \le n < 1$. However, their limiting form as $n \to 1$ was unclear, primarily because there were a number of unknown constants whose magnitude, and dependence on (1-n), would be fixed by the upstream solution. This approach is not pursued further here.

Instead, we assume a singularity structure for $0 < n < 1$ in which the inertia, viscous and pressure gradient terms all balance. The appropriate scaling is then

$$u \sim (-X)^{(n+1)/2} w(\zeta) \ , \quad \Psi = (-X)^{(n+3)/4} \zeta \ . \qquad (3.E:43)$$

On substituting into the boundary-layer equation in Von Mises coordinates, we obtain

$$\frac{(n+3)w}{4} \left[\zeta \, w_\zeta - q \, w \right] = -1 + w \left(w w_\zeta \right)_\zeta \ , \qquad (3.E:44a)$$

where $q = 2(n+1)/(n+3)$. In order that the solution match with a velocity profile that has $u = O(1)$ for $\Psi = O(1)$, the appropriate boundary conditions are

$$w \to B_\pm |\zeta|^q \text{ as } \zeta \to \pm\infty \ , \qquad (3.E:44b)$$

where $B_\pm$ are positive constants. As in the solution of (3.E:21) for $X < 0$, the solution for (3.E:44) can be characterised by its asymptotic behaviour at infinity, i.e. $w \equiv w(\zeta; B_+)$. Similarly, a solution satisfying (3.E:44b) can be found if

$$w(0; B_+) = w(0; B_-) \quad \text{and} \quad w_\zeta(0; B_+) = -w_\zeta(0; B_-) \ . \qquad (3.E:45)$$

Numerical integration demonstrates that such solutions exist for $0 < n < 1$, and that they are symmetric about $\zeta = 0$. The numerical solutions also suggest that $B_+ = B_- \sim 2(1-n)/(n+3)$ as $n \to 1$, and an asymptotic solution for $0 < 1-n \ll 1$ can be found confirming this (also see below). Hence, this model problem suggests that for $n = 1$, we should be looking for a singularity structure which is almost inviscid. However, as indicated above, asymptotic solutions based on this assumption have yet to prove

successful. Further, we consider next a slight modification to (3.E:41) which suggests that there may be other significant difficulties.

Specifically, we consider the boundary-layer equation

$$uu_X = -(-X)(-\log(-X))^{2m} + u(uu_\Psi)_\Psi \ , \qquad (3.E:46)$$

and assume that a singularity develops at $X = 0$. On the basis of the previous example, we might expect to be able to find a singularity structure for $m > 0$ ($m = 0$ corresponds to the main problem of interest). The numerical solutions to (3.E:44a) for $0 < 1-n \ll 1$ suggest an asymptotic expansion of the form

$$\begin{aligned} \Psi &\sim (-X)\left[-\log|X|\right]^{(m+1)/2}\eta \ , \\ u &\sim (-X)\left[-\log|X|\right]^{m}\left(\hat{u}_o + \frac{1}{[-\log(-X)]}\hat{u}_1 + \ldots\right) . \end{aligned} \qquad (3.E:47)$$

Substitution into the governing equations, expansion, matching, etc., yields

$$\hat{u}_o = (1+B^2\eta^2)^{1/2} \ , \quad \hat{u}_1 = \eta^2(1+B^2\eta^2)^{-1/2}\left(\alpha + \int^\eta \eta^{-3}F(\eta)\,d\eta\right) \qquad (3.E:48a)$$

where B and α are constants, and

$$F(\eta) = -m + (1-m)B^2\eta^2/2 + B^2(1+B^2\eta^2)^{1/2} \ . \qquad (3.E:48b)$$

If there are to be no logarithmic terms in $\hat{u}_1(\eta)$ (these need to be avoided since a critical layer cannot seem to be found which smoothes them out), then the coefficient of η^2 in the Taylor expansion of (3.E:48b) about $\eta = 0$ must be zero, i.e.

$$B = (m-1)^{1/2} \ . \qquad (3.E:49)$$

Note that this fixes the asymptotic behaviour of $\hat{u}_o$, and is an

analytic derivation of what we have done numerically in the previous model problem.

The disappointing aspect of this solution is that it is not valid for $0 < m \leq 1$. Thus we cannot get asymptotically close to $m = 0$, i.e. the problem we are really interested in. This suggests that the $m = 0$ problem may have a significantly different singularity structure. We conclude that a singularity structure which looked very straightforward at first, and for which the numerical results suggest the most obvious asymptotic scaling, is in fact far from simple.

Figure 3.E:1a $\lambda = 0.426$

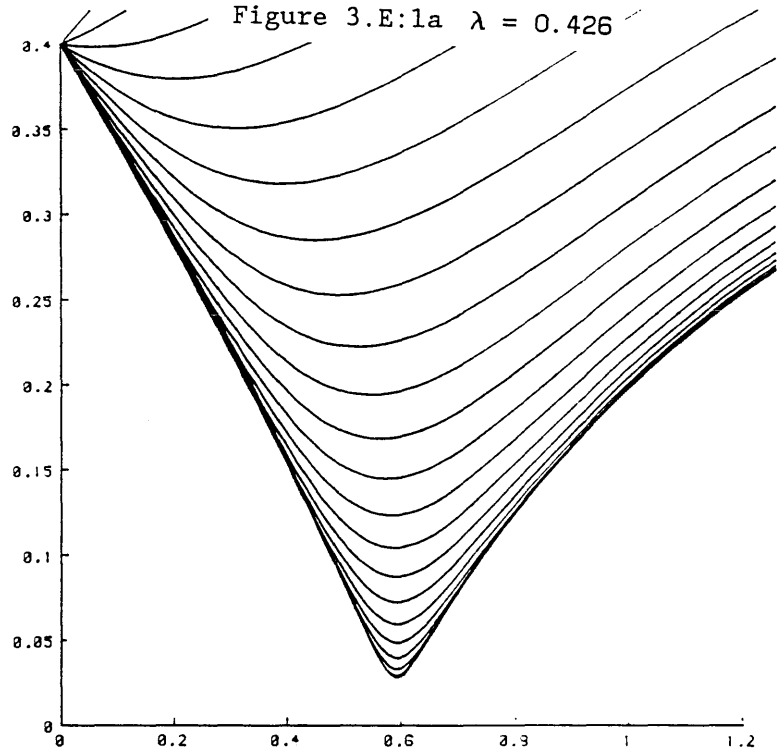


Figure 3.E:1b $\lambda = 0.426$

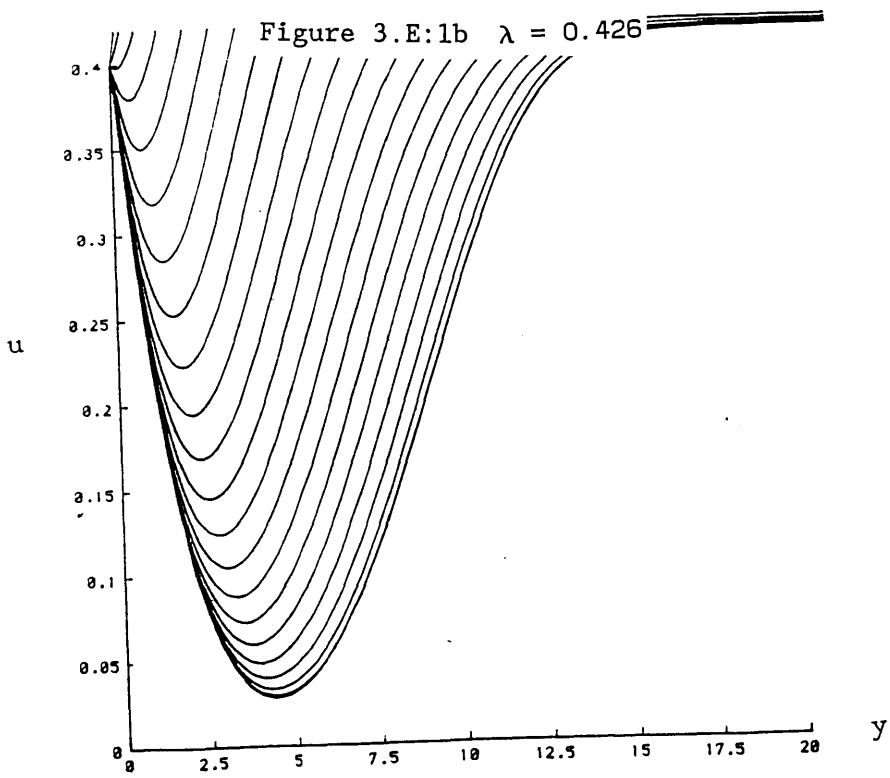


Figure 3.E:2a $\lambda = 0.42595$

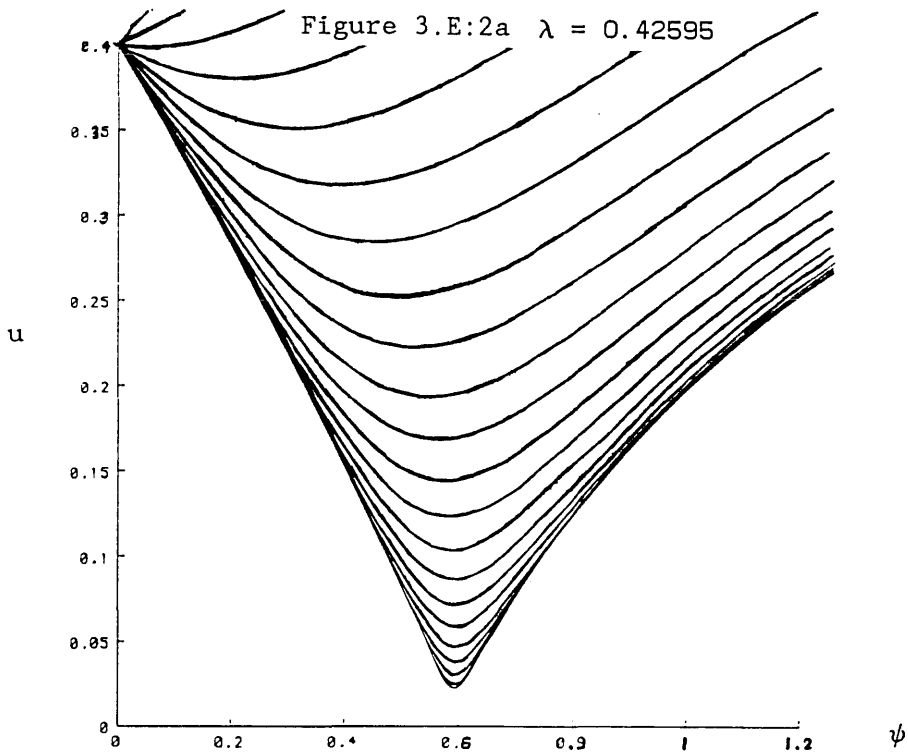
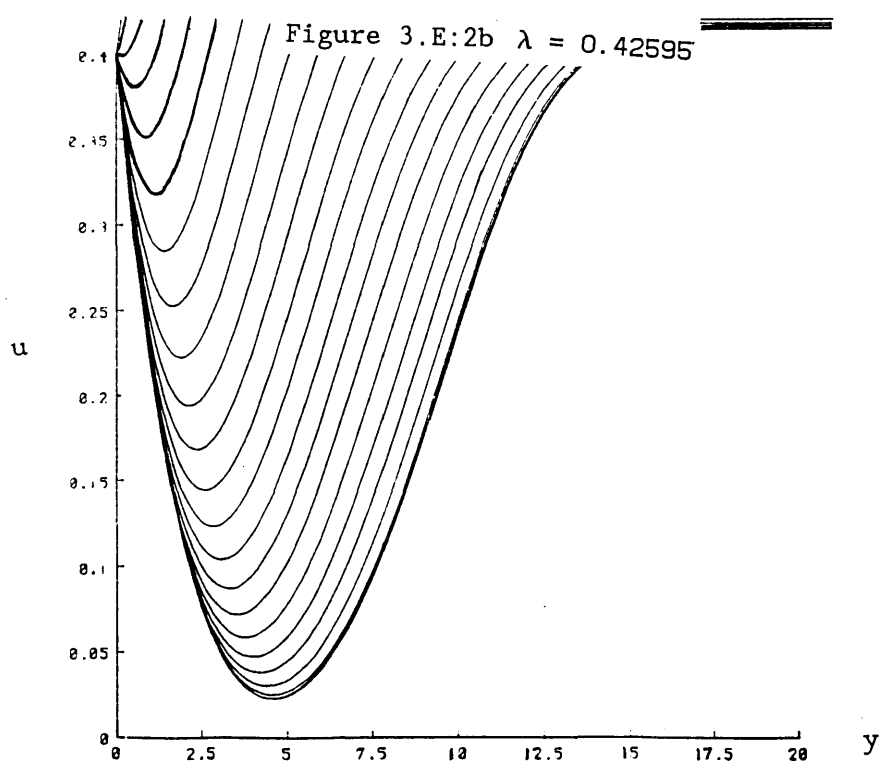


Figure 3.E:2b $\lambda = 0.42595$



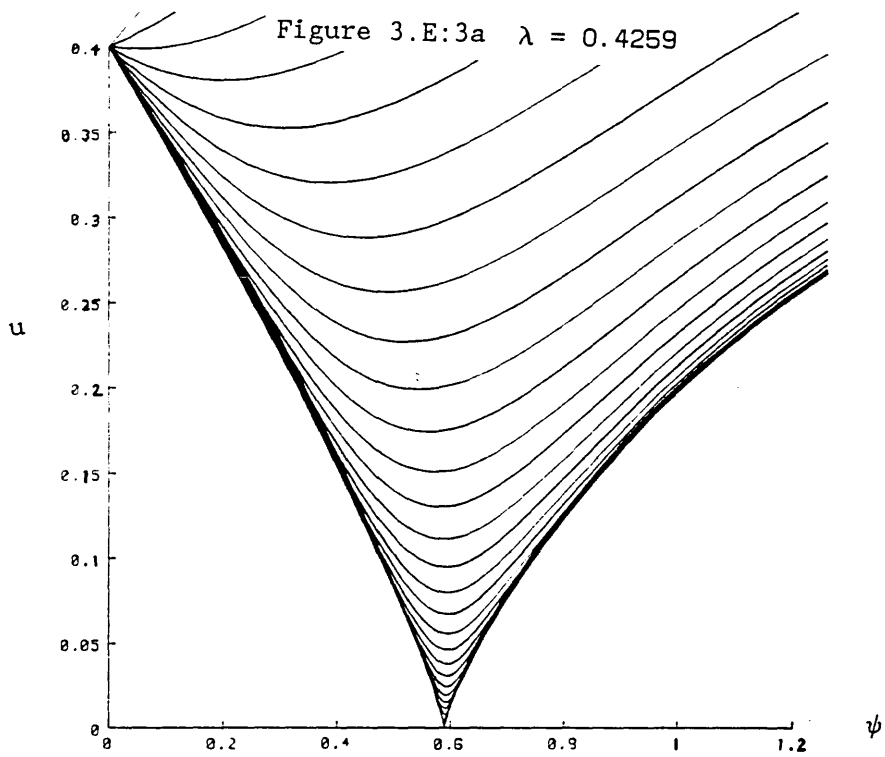


Figure 3.E:3a $\lambda = 0.4259$

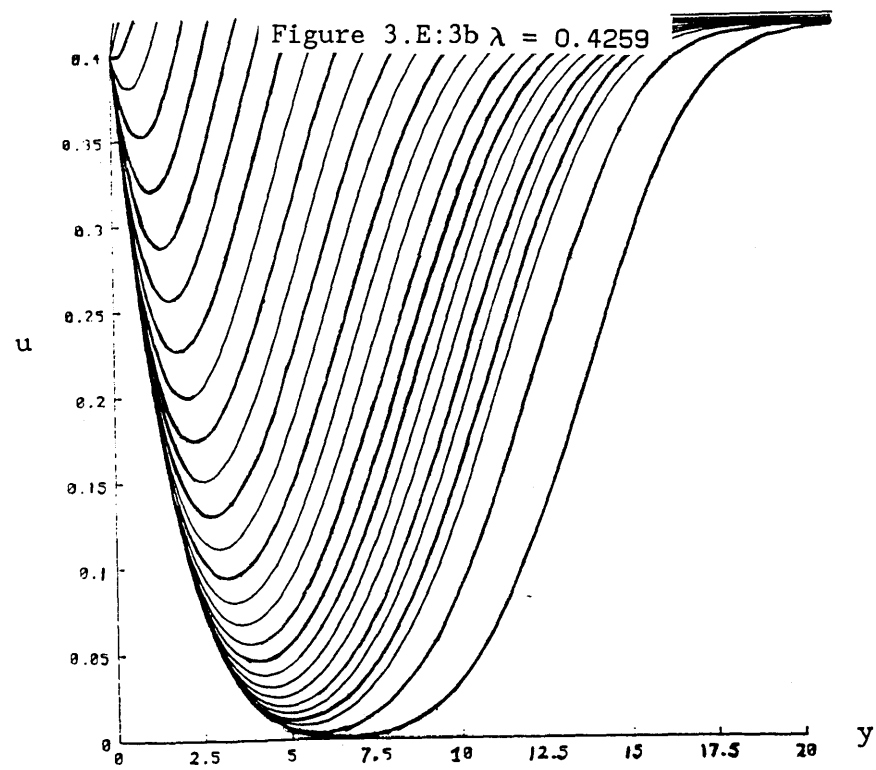


Figure 3.E:3b $\lambda = 0.4259$

Figure 3.E:4

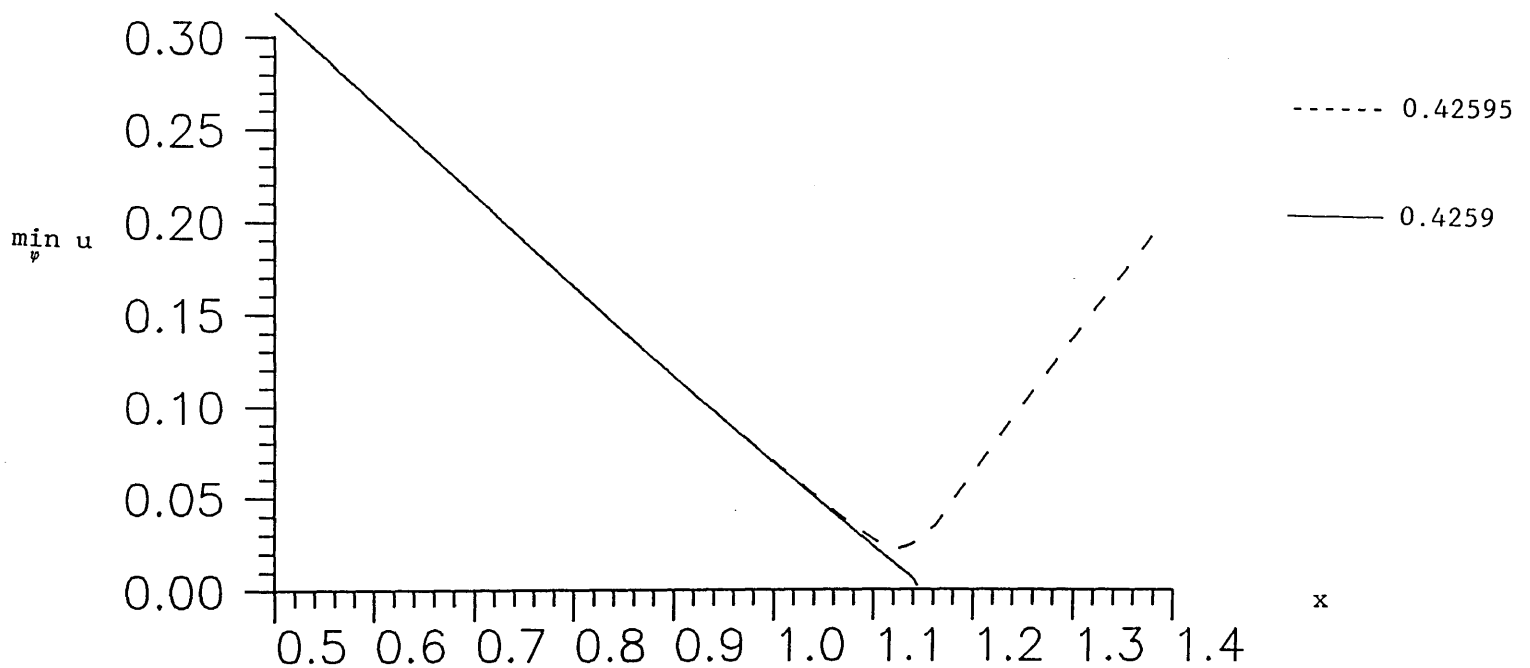

0.30
0.25
0.20
0.15
0.10
0.05
0.00
min u
ψ
0.5 0.6 0.7 0.8 0.9 1.0 1.1 1.2 1.3 1.4
x
------ 0.42595
——— 0.4259

Figure 3.E:5a

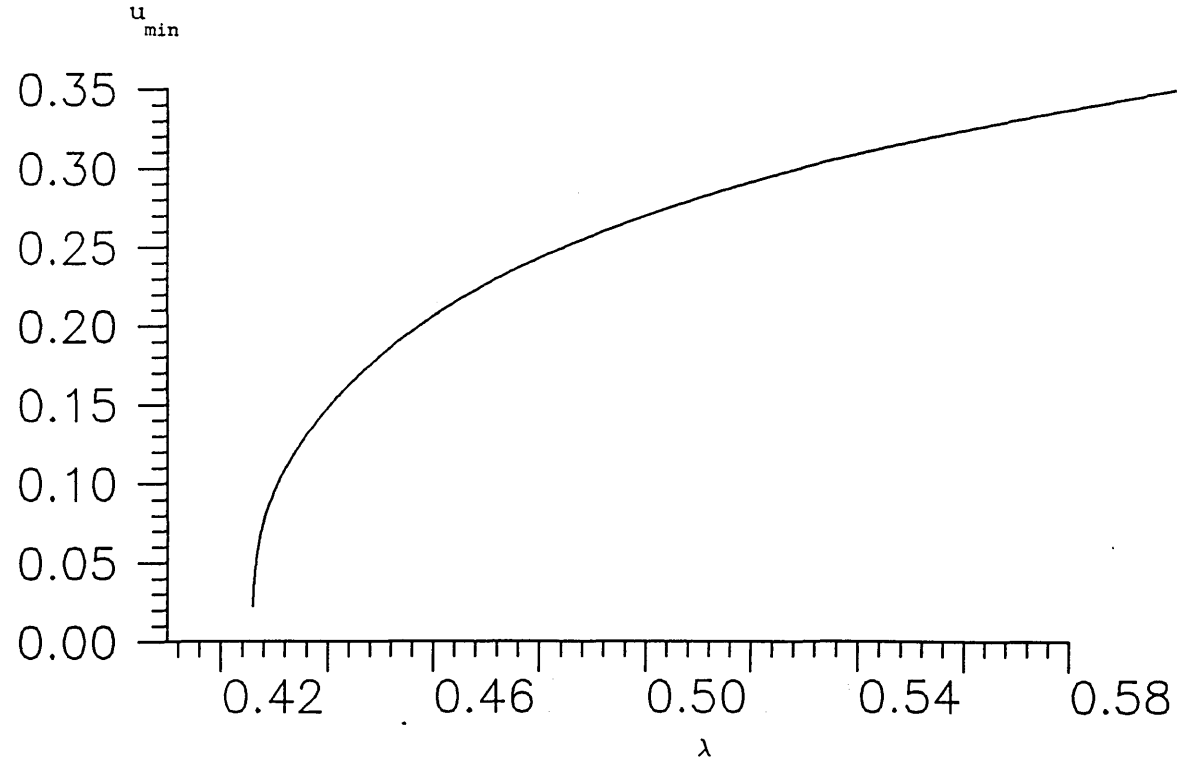


Figure 3.E:5b

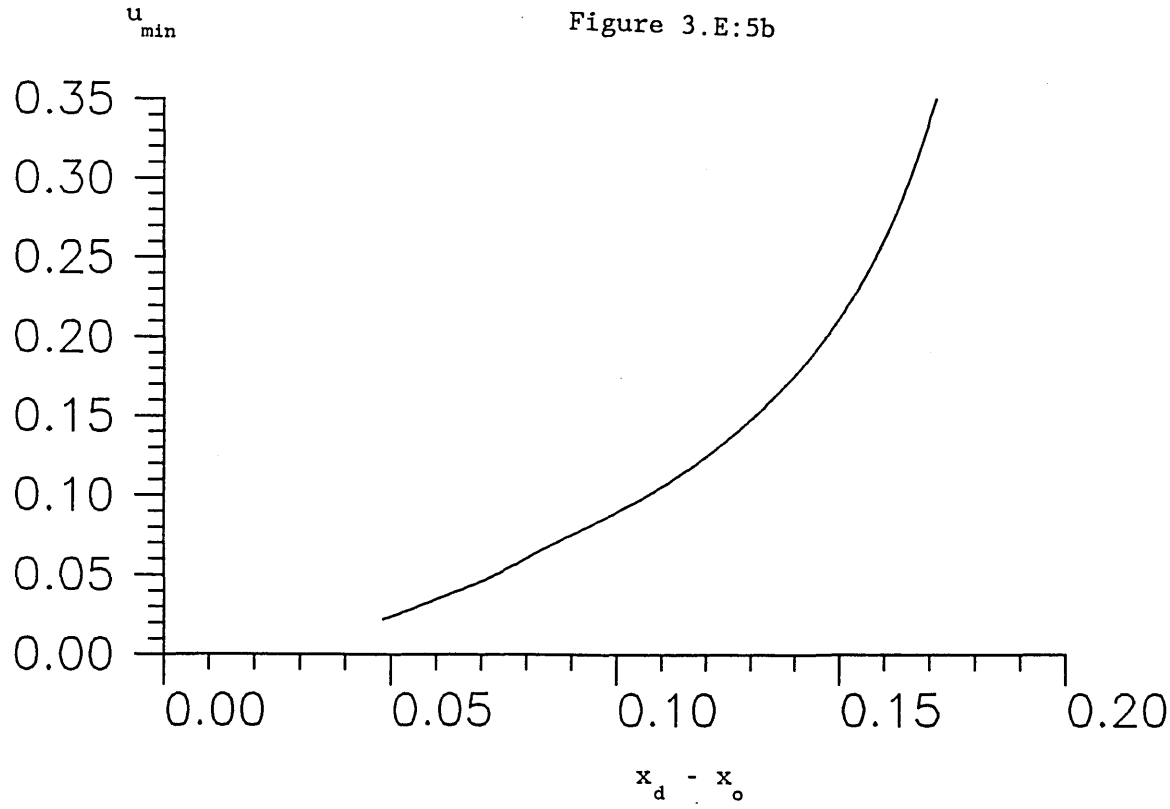


Figure 3.E:6a X > 0

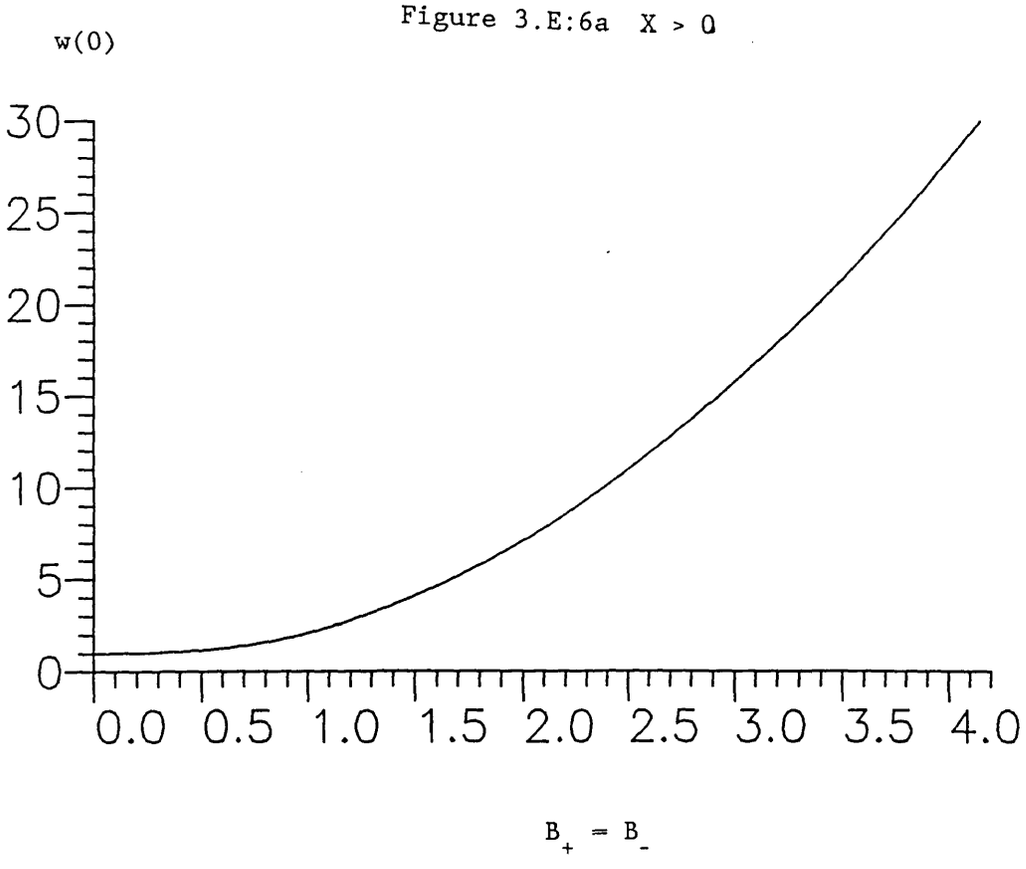


Figure 3.E:6b X < 0

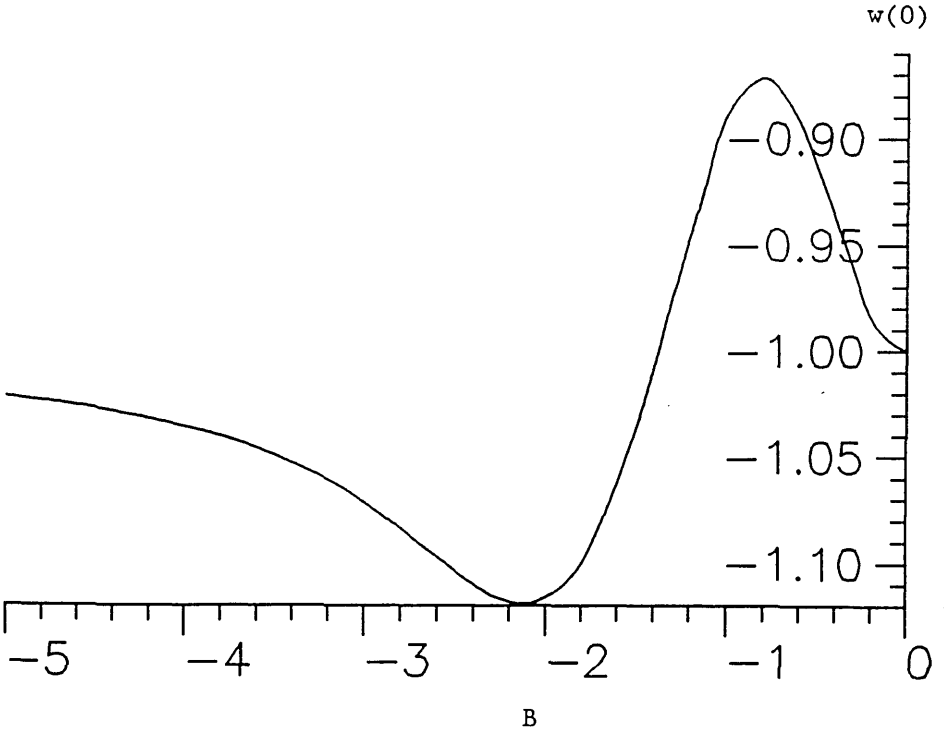
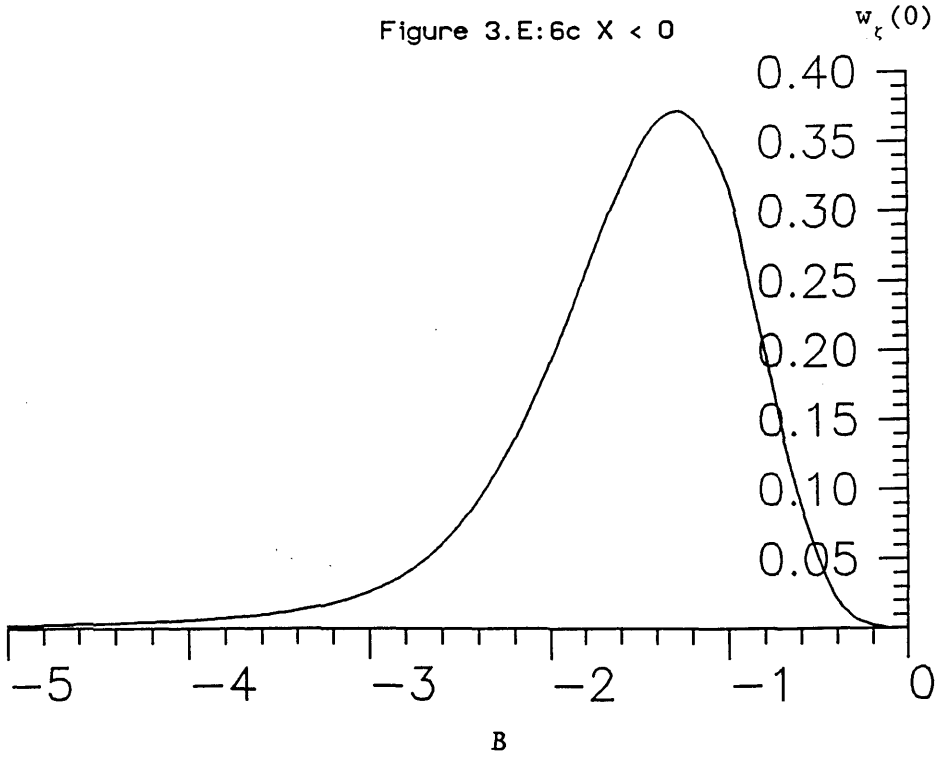


Figure 3.E:6c X < 0



References

Agrawal Y., Talbot L., Gong K. (1978) Laser anemometer study of flow development in curved pipes. *J. Fluid Mech.* 85:497-518.

Austin L.R., Seader J.D. (1973) Fully developed viscous flow in coiled circular pipes. *AIChE J.* 19:85-94.

Banks W.H.H., Zaturska M.B. (1979) The collision of unsteady laminar boundary layers. *J. Eng. Maths.* 13:193-212.

Batchelor G.K. (1967) *An introduction to Fluid Dynamics.* Cambridge Univ. Press.

Bennett J. (1987) PhD thesis. Univ. of London.

Berger S.A., Talbot L., Yao L.-S. (1983) Flow in curved pipes. *Ann. Rev. Fluid Mech.* 15:461-512.

Blennerhassett P. (1976) *Secondary motion and diffusion in unsteady flow in a curved pipe.* Ph.D Thesis. Imperial Coll., London.

Bornder G.L. (1978) Nonlinear analysis of laminar boundary-layer flow over a periodic wavy surface. *Phys. Fluids* 21(9): 1471-4.

Bovendeerd P.H.M., van Steenhoven A.A., van de Vosse F.N., Vossers G. (1987) Steady entry flow in a curved pipe. *J. Fluid Mech.*

177:233-46.

Caro C.G., Fitz-Gerald J.M., Schroter R.C. (1971) Atheroma and arterial wall shear: observation, correlation and proposal of a shear dependent mass transfer mechanism for atherogenesis. *Proc. R. Soc. London Ser. B* 177:109-59.

Cash J.R., Moore D.R. (1980) A high order method for the numerical solution of two-point boundary value problems. *BIT* 20: 44-52.

Chang L.-J., Tarbell J.M. (1985) Numerical simulation of fully developed sinusoidal and pulsatile (physiological) flow in curved tubes. *J. Fluid Mech.* 161:175-98.

Chandran K.B., Yearwood T.L. (1981) Experimental study of physiological pulsatile flow in a curved tube. *J. Fluid Mech.* 111:57-85.

Collins W.M., Dennis S.C.R. (1975) The steady motion of a viscous fluid in a curved tube. *Q. Jl. Mech. Appl. Math.* 28:133-56.

Collins W.M., Dennis S.C.R. (1976a) Steady flow in a curved tube of triangular cross-section. *Proc. R. Soc. London Ser. A* 352:189-211.

Collins W.M., Dennis S.C.R. (1976b) Viscous eddies near a 90° and 45° corner in flow through a curved tube of triangular cross-section. *J. Fluid Mech.* 76:417-32.

Cornhill J.F., Roach M.R. (1976) A quantitative study of the localization of atherosclerotic lesions in the rabbit aorta. *Atherosclerosis* 23:489-501.

Cowley S.J. (1983) Computer extension and analytic continuation of Blasius' expansion for impulsive flow past a circular cylinder. *J. Fluid Mech.* 135: 389-405.

Cowley S.J., Hocking L.M., Tutty O.R. (1985) The stability of solutions of the classical unsteady boundary-layer equation. *Phys. Fluids* 28:441-3.

Dean W.R. (1927) Note on the motion of fluid in a curved pipe. *Philos. Mag.* 20:208-23.

Dean W.R. (1928) The streamline motion of fluid in a curved pipe. *Philos. Mag.* 30:673-93.

Dennis S.C.R. (1980) Calculation of the steady flow through a curved tube using a new finite-difference method. *J. Fluid Mech.* 99:449-67.

Dennis S.C.R., Ng M. (1982) Dual solutions for steady laminar flow through a curved pipe. *Q. Jl. Mech. Appl. Math.* 35:305-24.

Elliott J.W., Cowley S.J., Smith F.T. (1983) Breakdown of boundary

layers: (i) on moving surfaces; (ii) in semi-similar unsteady flow; (iii) in fully unsteady flow. *Geophys. Astrophys. Fluid Dynamics* 25:77-138.

Farthing S.P. (1977) *Flow in the thoracic aorta and its relation to atherogenesis.* Ph.D. Theses. Cambridge Univ.

Fox L., Mayers D.F. (1968) *Computing Methods for Scientists and Engineers.* Clarendon Press, Oxford.

Fry D. L. (1968) Acute vascular endothelial changes associated with increased blood velocity gradients. *Circ. Res.* 22:165-97.

Germano M. (1982) On the efffect of torsion on a helical pipe flow. *J. Fluid Mech.* 125:1-8.

Glauert M.B. (1957) The flow past a rapidly rotating circular cylinder. *PRSA* 242: 108-15.

Goldstein S. (1938) *Modern development in fluid mechanics.* Oxford University Press.

Goldstein S. (1948) On laminar boundary-layer flow near a position of separation. *Q. Jl. Mech. Appl. Math.* 1:43-69.

Gregory, N., Stuart J.T., Walker W.S. (1955) On the stability of three-dimensional boundary layers with application to the flow due

to a rotating disk. *Phil. Trans. R. Soc. Lond. A* 248:155-99.

Grindley J.H., Gibson A.H. (1908) On the frictional resistance to the flow of air through a pipe. *Proc. R. Soc. London Ser. A* 80:114-39.

Humphrey J.A.C., Iacovides H., Launder B.E. (1985) Some numerical experiments on developing laminar flow in circular-sectioned bends. *J. Fluid Mech.* 154:357-75.

Ingham D.B. (1983) Steady flow past a rotating cylinder. *Computers and Fluids* 11(4): 351-66.

Itō H. (1969) Laminar flow in curved pipes. *Z. Angew. Math. Mech.* 49:653-63.

Itō H. (1987) Flow in curved pipes. *JSME* 30(262):543-52.

Kao H.C. (1987) Torsion effect on fully developed flow in a helical pipe. *J. Fluid Mech.* 184:335-56.

Kitoh O. (1987) Swirling flow through a bend. *J. Fluid Mech.* 175:429-46.

Kluwick A., Wohlfahrt H. (1986) Hot-wire-anemometer study of the entry flow in a curved duct. *J. Fluid Mech.* 165:335-53.

Kutta W.M. (1910) Über eine mit den grundlagen des flugproblems in beziehung stehende zweidimensionale strömung. *Sitzungsberichte der Königlich Bayerischen Akademie der Wissenschaften Mathematisch-physikalische Klasse* (Abh. 2): 1-58.

Lin J.Y., Tarbell J.M. (1980) An experimental and numerical study of periodic flow in a curved pipe. *J. Fluid Mech.* 100(3):623-38.

Lyne W.H. (1971) Unsteady viscous flow in a curved pipe. *J. Fluid Mech.* 45:13-31.

McConalogue D.J., Srivastava R.S. (1968) Motion of fluid in a curved tube. *Proc. R. Soc. London Ser. A* 307:37-53.

Moore D.W. (1957) The flow past a rapidly rotating circular cylinder in a uniform stream. *J. Fluid Mech.* 2(6), 541-50.

Moore D.W. (1979) The spontaneous appearence of a singularity in the shape of an evolving vortex sheet. *Proc. R. Soc. Lond. A* 365:105-19.

Moore D.W., Saffman P.G. (1972) The motion of a vortex filament with axial flow. *Phil. Trans. Roy. Soc.* 272:403-29.

Moore F.K. (1958) On the separation of the unsteady laminar boundary layer. *Symp. on boundary layer research.* IUTAM, Springer-Velag.

Mullin T., Greated C.A. (1980a) Oscillatory flow in curved pipes. Part II. The fully developed case. *J. Fluid Mech.* 98:397-416.

Mullin T., Greated C.A. (1980b) Oscillatory flow in curved pipes. Part I. The fully developed case. *J. Fluid Mech.* 98:383-95.

Munson B.R. (1975) Experimental results for oscillating flow in a curved pipe. *Phys. Fluids* 18:1607-9.

Nandakumar K. Masliyah J.H. (1982) Bifurcation in steady laminar flow through curved tubes. *J. Fluid Mech.* 119:475-90.

Page M.A. (1982) Flow separation in a rotating annulus with bottom topography. *J. Fluid Mech.* 123: 303-13.

Papageorgiou D. (1987) Stability of the unsteady viscous flow in a curved pipe. *J. Fluid Mech.* 182:209-33.

Papanu J.S., Alder R.J., Gorensek M.B., Menon M.M. (1986) Separation of fine particle dispersions using periodic flows in a spinning coiled tube. *AIChE* 32(5):798-808.

Pedley T.J. (1980) *The Fluid Mechanics of Large Blood Vessels.* Cambridge Univ. Press.

Prandtl L. (1904) Über Flüssigkeitsbewegung bei sehr kleiner

Reibung. *Proc. of the Third Intern. Math. Congr.*

Prandtl L., Tietjens O.G. (1934) *Fundamentals of Hydro- and Aeromechanics.* Engineering Societies Monographs, McGraw-Hill Book Company.

Pratap Vanka S. (1985) Block-implicit calculations of three-dimensional laminar flow in stronly curved ducts. *Technical Notes.* 1989-91.

Rabadi N.J., Simon H.A., Chow J.C.F. (1980) Numerical solution for fully developed, laminar pulsating flow in curved tubes. *Numer. Heat Transfer* 3:225-39.

Reid E.G. (1924) Tests of rotating cylinders. *Tech. Notes Nat. Adv. Comm. Aero.*, Wash., no 209.

Riley N. (1978) Circular oscillations of a cylinder in a viscous fluid. *ZAMP* 29: 439-49.

Riley N. (1981) High Reynolds number flows with closed streamlines. *J. Eng. Maths.* 15(1): 15-27.

Roache P.J. (1976) *Computational Fluid Dynamics.* Modern Press.

Rott N. (1956) Unsteady viscous flow in the vicinity of a stagnation point. *Q. Jl. Appl. Math.* 13:444-51.

Rothmayer A.P., Smith F.T. (1987) Strongly nonlinear wave-packets in boundary-layers. *ASME* 5:67-79.

Schlichting H. *Boundary-layer Theory.* McGraw-Hill Series in Mechanical Engineering, McGraw-Hill Book Company.

Sears W.R. (1956) Some recent development in airfoil theory. *J. Aeronaut. Sci.* 23:490-9.

Sears W.R., Telionis D.P. (1975) Boundary-layer separation in unsteady flow. *SIAM J. Applied Math.* 28(1):215-35.

Secomb T.W. (1979) *Flows in tubes and channels with indented and moving walls.* Ph.D. Thesis. Cambridge Univ. Press.

Shirayama S., Kuwahara K. (1986) Computational study of flow in curved pipes with circular cross-section. *AIAA/ASME 4th Fluid Mech., Plasma Dynamics and Lasers Conf. AIAA* 1043:1-13.

Shkadova V.P. (1982) Rotating Cylinder in a flowing viscous incompressible fluid. Izvestiya Akademii Nauk SSSR, *Mekhanika Zhidkosti i Gaza*, 1: 12-16.

Simpson C.J., Stewartson K. (1982a) A note on a boundary-layer collision on a rotating sphere. *ZAMP* 33:370-78.

Simpson C.J., Stewartson K. (1982b) A singularity in an unsteady free-convection boundary layer. *Q. Jl. Mech. Appl. Math.* 35.3:291-304.

Singh M.P. (1974) Entry flow in a curved pipe. *J. Fluid Mech.* 65:517-39.

Singh M.P., Sinha P.C., Aggarwal M. (1978) Flow in the entrance of the aorta. *J. Fluid Mech.* 87(1):97-120.

Smith F.T. (1975) Pulsatile flow in curved pipes. *J. Fluid Mech.* 71:15-42.

Smith F.T. (1976a) Steady motion within a curved pipe. *Proc. R. Soc. London Ser. A* 347:345-70.

Smith F.T. (1976b) Fluid flow into a curved pipe. *Proc. R. Soc. London A* 351:71-87.

Smith F.T. (1976d) Flow through constricted or dilated pipes and channels, part 1. *Q. Jl. Mech. Appl. Math.* 29:343-64.

Smith F.T. (1976e) Flow through constricted or dilated pipes and channels, part 2. *Q. Jl. Mech. Appl. Math.* 29:365-76.

Smith F.T. (1979a) Instability of flow through pipes of gerneral cross section, part 1. *Mathematika* 26:187-210.

Smith F.T. (1979b) Instability of flow through pipes of gerneral cross section, part 2. *Mathematika* 26:211-23.

Smith F.T., Burggraf O.R. (1985) On the development of large-sized short-scaled disturbances in boundary layers. *Proc. R. Soc. Lond. A* 339, 25-55.

Snyder B., Hammersley J.R., Olson D.E. (1985) The axial skew of flow in curved pipes. *J. Fluid Mech.* 161:281-94.

Soh W.Y., Berger S.A. (1984) Laminar entrance flow in a curved pipe. *J. Fluid Mech.* 148:109-35.

Stephanoff K.D., Pedley T.J., Lawrence C.J., Secomb T.W. (1983) Fluid flow along a channel with an asymmetric oscillating constriction. *Nature, Lond.* 305: 692-5.

Stewartson K., Cebeci T., Chang K.C. (1980) A boundary-layer collison in a curved duct. *Q. Jl. Mech. Appl. Math.* 33.1:59-75.

Stewartson K., Simpson C.J. (1982) On a singularity initiating a boundary-layer collision. *Q. Jl. Mech. Appl. Math.* 35.1:1-16.

Sychev Vik. V. (1980) On certain singularities in solutions of equations of boundary layer on a moving surface. *Prikl. Matem. Mekhan.* 44(5):831-8.

Ta Phoc Loc (1975) Étude numerique de l'écoulement d'un fluide visqueux incompressible autor d'un cylindre fixe ou en rotation. Effet Magnus. *J. Mec.* 14:109-.

Talbot L., Gong K.O. (1983) Pulsatile entrance flow in a curved pipe. *J. Fluid Mech.* 127:1-25.

Talbot L., Wong S.J. (1982) A note on boundary layer collision in a curved pipe. *J. Fluid Mech.* 122:505-10.

Thomson J. (1876) On the origin of windings of rivers in alluvial plains, with remarks on the flow of water round bends in pipes. *Proc. R. Soc. London Ser. A* 25:5-8.

Truesdell L.C., Alder R.J. (1970) Numerical Treatment of fully developed laminar flow in helically coiled tubes. *AIChE J.* 16(6):1010-5.

Van Dommelen L.L. (1986) Computation of unsteady separation using Lagrangian procedures. *Boundary-Layer separation.* IUTAM, Springer-Verlag.

Van Dommelen L.L., Shen S.F. (1980) The spontaneous generation of the singularity in a separating laminar boundary layer. *J. Comp. Phys.* 38:125-40.

Van Dommelen L.L., Shen S.F. (1982) The genesis of separation. *Proc. Symp. Num. Phys. Aspects Aerod. Flow.* pp 293-311. Springer-Verlag.

Van Dommelen L.L., Shen S.F. (1983) An unsteady interactive separation process. *AIAA. J.* 21(3):358-62.

Van Dyke M. (1978) Extended Stokes series: laminar flow through a loosely coiled pipe. *J. Fluid Mech.* 86(1):129-45.

Van Dyke M. (1984) Computer-extended series. *Ann. Rev. Fluid Mech.* 16: 287-309.

Williams J.C., Stewartson K. (1983) Flow development in the vicinity of the sharp trailing edge on bodies impulsively set to motion, part 2. *J. Fluid Mech.* 131:177-94.

Winters K.H. (1987) A bifurcation study of laminar flow in a curved tube of rectangular cross-section. *J. Fluid Mech.* 180:343-69.

Wood W.W. (1957) Boundary layers whose streamlines are closed. *J. Fluid Mech.* 2: 77-87.

Yang Z., Keller H.B. (1986) *Appl. Numer. Math* 2:257-.

Yao L.S., Berger S.A. (1988) The three-dimensional boundary layer in the entry region of curved pipes with finite curvature ratio.

Phys. Fluids 31(3):486-94.

Yearwood T. L., Chandran K.B. (1982) Physiological pulsatile flow experiments in a model of the human aortic arch. *J. Biomech.* 15:683-704.

Zalosh R.G., Nelson W.G. (1973) Pulsating flow in a curved tube. *J. Fluid Mech.* 59:693-705.

Zhuk V.I., Ryzhov O.S. (1982) Locally nonviscous perturbations in boundary layers with self-induced pressure. *Sov. Phys. Dokl.* 27(3):177-179.